

**DIRECT SHEAR TESTING OF A
HONG KONG SOIL
UNDER VARIOUS
APPLIED MATRIC SUCTIONS**

GEO REPORT No. 11

J.K. Gan & D.G. Fredlund

**GEOTECHNICAL ENGINEERING OFFICE
CIVIL ENGINEERING DEPARTMENT
HONG KONG**

**DIRECT SHEAR TESTING OF A
HONG KONG SOIL
UNDER VARIOUS
APPLIED MATRIC SUCTIONS**

GEO REPORT No. 11

J.K. Gan & D.G. Fredlund

This report was originally produced under Consultancy Agreement CE 21/89

© Hong Kong Government

First published, September 1992
First Reprint, April 1995

Prepared by:

Geotechnical Engineering Office,
Civil Engineering Department,
Civil Engineering Building,
101 Princess Margaret Road,
Homantin, Kowloon,
Hong Kong.

This publication is available from:

Government Publications Centre,
Ground Floor, Low Block,
Queensway Government Offices,
66 Queensway,
Hong Kong.

Overseas orders should be placed with:

Publications (Sales) Office,
Information Services Department,
28th Floor, Siu On Centre,
188 Lockhart Road, Wan Chai,
Hong Kong.

Price in Hong Kong: HK\$136

Price overseas: US\$21.5 (including surface postage)

An additional bank charge of **HK\$50** or **US\$6.50** is required per cheque made in currencies other than Hong Kong dollars.

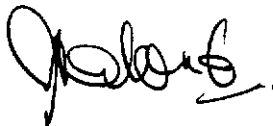
Cheques, bank drafts or money orders
must be made payable to **HONG KONG GOVERNMENT**

PREFACE

In keeping with our policy of releasing information of general technical interest, we make available some of our internal reports in a series of publications termed the GEO Report series. The reports in this series, of which this is one, are selected from a wide range of reports produced by the staff of the Office and our consultants.

Copies of GEO Reports have previously been made available free of charge in limited numbers. The demand for the reports in this series has increased greatly, necessitating new arrangements for supply. In future a charge will be made to cover the cost of printing.

The Geotechnical Engineering Office also publishes guidance documents and presents the results of research work of general interest in GEO Publications. These publications and the GEO Reports are disseminated through the Government's Information Services Department. Information on how to purchase them is given on the last page of this report.



A. W. Malone
Principal Government Geotechnical Engineer
April 1995

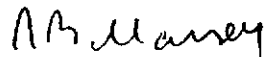
FOREWORD

This report presents the results of research into the direct shear properties of a saprolitic soil under various applied matric suctions. The soil tested was a completely decomposed fine ash tuff from Tseung Kwan O.

The study was carried out by Mr. J.K. Gan and Professor D.G. Fredlund at the University of Saskatchewan as Consultants to the Geotechnical Engineering Office (GEO) of the Civil Engineering Department. It forms part of the GEO research programme on the shear strength of Hong Kong soils.

The draft report was reviewed by Dr T.Y. Irfan, Dr R.P. Martin and Mr. J.M. Shen of the GEO, who also contributed to the finalization of the details of the research. The report incorporates contributions from Dr Irfan regarding the effect of soil microfabric on the shear behaviour of the volcanic soil. He also supervised sampling on site and provided the sample descriptions.

Volume 2 of the study report incorporating detailed test results is available for viewing in the Civil Engineering Library.



J.B. Massey
Government Geotechnical Engineer/Development
September 1992

CONTENTS

	Page No.
TITLE PAGE	1
FOREWORD	4
CONTENTS	5
1. INTRODUCTION	7
2. LITERATURE REVIEW AND THEORY ON THE SHEAR STRENGTH OF UNSATURATED SOILS	9
2.1 THEORY	9
2.2 HISTORY OF SHEAR STRENGTH TESTING OF UNSATURATED SOILS	12
3. EQUIPMENT	21
3.1 DESCRIPTION OF THE MODIFIED DIRECT SHEAR BOX APPARATUS OF THE GEOTECHNICAL ENGINEERING LABORATORY AT THE UNIVERSITY OF SASKATCHEWAN	21 21
3.1.1 Shear Box Base Design	21
3.1.2 Air Pressure Chamber Design	22
3.1.3 Suction Control	23
3.2 TESTING PROCEDURE USING THE MODIFIED DIRECT SHEAR EQUIPMENT	23
4. SPECIMEN PREPARATION	25
5. TESTING PROGRAMS	26
5.1 PILOT TEST PROGRAM	26
5.1.1 Results and Discussion	26
5.1.1.1 Results from Conventional Shear Box (First Test)	26
5.1.1.2 Results from the Modified Shear Box	27
5.1.1.3 Comparison of the Two Pilot Tests	28
5.1.1.4 Results from Conventional Shear Box (Second Test)	28
5.1.2 Recommendation	28

	Page No.
5.2 PRELIMINARY TEST PROGRAM	30
5.2.1 Results and Discussion	30
5.2.2 Suggested Modification to the Main Test Program	32
5.3 MAIN TEST PROGRAM	33
5.3.1 Test Program and Presentation of Results	33
5.3.2 Interpretation of the Results	35
6. CONCLUSIONS	39
7. RECOMMENDATION FOR FURTHER RESEARCH	41
7.1 LABORATORIES STUDIES	41
7.1.1 Alternative No. 1	41
7.1.2 Alternative No. 2	41
7.1.3 Alternative No. 3	42
7.1.4 Other Suggestions	42
7.2 ANALYTICAL STUDIES	42
7.2.1 Integrated Slope Stability-Seepage Modelling	43
7.2.2 Stress Path Dependency	43
8. REFERENCES	44
LIST OF TABLES	48
LIST OF FIGURES	58
APPENDIX A : SAMPLING SITE AND DESCRIPTION OF SAMPLE (T.Y. Irfan)	220

1. INTRODUCTION

In a letter dated 20 February 1989, Dr. A.W. Malone of the Geotechnical Control Office (GCO), Hong Kong, informed us of their desire to embark on a study on the direct shear testing of weathered rocks and residual soils. One area of interest was the shear strength of soils under applied suctions. We were requested to submit a research proposal on this subject. A first draft of the proposal was submitted on March 2, 1989. Further information exchanges and discussions ensued. Some of the concerns raised at that time were as follows:

- a) There was a concern that the 50mm x 50mm specimen size may be difficult for testing saprolites, particularly the coarser grained soils.
- b) There was a concern that the multistage shearing procedure may not be satisfactory as inhouse tests by GCO showed that the structure of the soil becomes disturbed during a second stage of loading.
- c) There was a request to look into the possibility of conducting a parallel set of comparative triaxial tests

We responded that a larger shear box to accommodate 100 mm x 100 mm x 40 mm specimen could be fabricated. The cost of building equipment was quite high and it was deemed more appropriate to consider this option as a future study. It was also concluded that possibly an appropriate, finer grained saprolites could be found for this study. Both parties agreed that there was considerable sample variability with saprolitic soils. However, it was decided that the best course of action was to proceed with an immediate program on smaller specimens. Both parties also agreed that the comparative triaxial tests should be left for a future study.

The final proposal was submitted to GCO on April 13, 1989. In a letter dated 26 May, 1989, we were informed that the proposal was satisfactory and GCO asked us to proceed with the project. The agreement for the research contract was signed on October 16, 1989.

The research program was to quantify the effects of matric suction on the shear strength of a selected Hong Kong Soil. The samples were received in early October, 1989 and the study commenced in November, 1989. Most of the shear strength tests were to be conducted using a Modified Direct Shear Box developed at the University of Saskatchewan, Saskatoon, Canada.

The material selected by the Geotechnical Control Office (GCO) for testing was a fine ash tuff. Three block samples, each of dimensions approximately 300 mm x 300 mm x 300 mm were received. The sampling site was located at an elevation of about 130 mPD on the midslopes of Tai Shung Tok Hill, west of Tseung Kwan O (Junk Bay) new town in the New Territories, Hong Kong. Details on the material and the site as described by Dr Irfan of GCO are presented in Appendix A.

The research program can be divided into three stages as follows:

- i) a pilot program
- ii) a preliminary program
- iii) main program

The purpose of the pilot program was to obtain an understanding of the complete shear stress versus displacement characteristics for the fine ash tuff. This information was necessary for determining the appropriate testing procedures to be adopted for the tests in the preliminary program and the main program. The purpose of the preliminary program was to establish the effective shear strength parameters, c' and ϕ' (i.e., the effective cohesion and the effective friction angle). The purpose of the main program was to determine the effect of soil matric suction on shear strength. Previous research programs have shown that the shear strength of a soil increases as the matric suction was increased. The present research program is to be performed on a relatively coarse grained soil and one of the concerns being investigated relates to whether or not the proposed shear strength equation applies for this soil.

2. LITERATURE REVIEW AND THEORY ON THE SHEAR STRENGTH OF UNSATURATED SOILS

As part of the Contract, the researchers at the University of Saskatchewan were asked to provide a brief literature review of the research work performed to-date by other researchers. The literature review is mainly with respect to test data presented by other research workers testing unsaturated soils. It is, however, appropriate to first briefly present the theory related to the shear strength of an unsaturated soil.

2.1 THEORY

Numerous shear strength equations have been formulated for unsaturated soils in terms of a single effective stress variables, σ' . A summary of proposed effective stress equations for unsaturated soils is presented in Table 1. Of these equations the best known is that of Bishop (1959). The shear strength equation formulated using Bishop's effective stress variable, σ' , can be written as:

$$\tau = c' + [\sigma - u_a + \chi (u_a - u_w)] \tan \phi' \quad \dots \dots [1]$$

where τ = shear strength

c' = effective cohesion

ϕ' = effective friction angle

u_a = pore air pressure

u_w = pore water pressure

σ = total stress

χ = coefficient having values ranging from zero to one, and is a function of the degree of saturation and soil type.

Fredlund and Morgenstern (1977) found that the stress state in an unsaturated soil is more appropriately described in terms of two independent stress state variables. Although any two of the three possible stress state variables ($\sigma - u_a$), ($u_a - u_w$) and ($\sigma - u_w$) can be used, the most advantageous combination in practice is the combination, ($\sigma - u_a$) and ($u_a - u_w$). Using these stress variables, Fredlund, Morgenstern and Widger (1978) formulated the following shear strength equation for an unsaturated soil.

$$\tau_{ff} = c' + (\sigma_{ff} - u_{af}) \tan \phi' + (u_a - u_w)_f \tan \phi^b \quad \dots \dots [2]$$

where: c' = intercept of the "extended" Mohr-Coulomb failure envelope on the shear stress axis when the net normal stress and the matric suction at failure are equal to zero. It is also referred to as "effective cohesion".

$(\sigma_{ff} - u_{af})$ = net normal stress variable on the failure plane at failure

u_{af} = pore-air pressure at failure

ϕ' = angle of internal friction associated with the net normal stress state variable $(\sigma_{ff} - u_{af})$

$(u_a - u_w)_f$ = matric suction at failure

ϕ^b = angle indicating the rate of increase in shear strength relative to matric suction $(u_a - u_w)_f$

The shear stress and the normal stress in Eq. 2 are given the subscripts "ff". The first subscript, f, refers to the failure plane and the second subscript, f, indicates the failure condition. One subscript "f" is given to the pore-water and pore-air pressures to indicate the failure condition. The pore-water and pore-air pressures act equally on all planes.

The shear strength equation for an unsaturated soil can be viewed as an extension of the shear strength equation for a saturated soil. For an unsaturated soil, two stress state variables are used to describe its shear strength while only one stress state variable (i.e., effective normal stress, $(\sigma_{ff} - u_{wf})$) is required for a saturated soil.

The shear strength equation for an unsaturated soil exhibits a smooth transition to the shear strength equation for a saturated soil. As the soil approaches saturation, u_w approaches u_a and the matric suction goes to zero. The matric suction component vanishes and Eq. 2 reverts to the equation for a saturated soil.

For an unsaturated soil, the Mohr circles corresponding to failure conditions can be plotted in three dimensions as illustrated in Fig. 1. The three-dimensional plot has shear stress, τ , as the ordinate and the two stress state variables, $(\sigma - u_a)$ and $(u_a - u_w)$ as abscissas. The frontal plane represents a saturated soil where the matric suction is zero. On the frontal plane, the $(\sigma - u_a)$ axis reverts to the $(\sigma - u_w)$ axis for a saturated soil since the pore-air pressure becomes equal to the pore-water pressure at saturation.

The Mohr circles for an unsaturated soil are plotted with respect to the $(\sigma - u_a)$ axis in the same manner as the Mohr circles are plotted for saturated soils with respect to $(\sigma - u_w)$ axis. However, the location of the Mohr circle plot in the third dimension is a function of the matric suction (Fig.2). The surface tangent to the Mohr circles at failure is referred to as the extended Mohr-Coulomb failure envelope for unsaturated soils. The extended Mohr-Coulomb failure envelope defines the shear strength of an unsaturated soil. The intersection line between the extended Mohr-Coulomb failure envelope and the frontal plane is the failure envelope for the saturated condition.

The direction of the theoretical failure plane is defined by joining the stress point on the Mohr circle that is tangent to the failure envelope to the pole point. The tangent point on the Mohr circle at failure represents the stress state on the failure plane at failure.

The extended Mohr-Coulomb failure envelope may be a planar surface or some what curved. A curved failure envelope can also be described by Eq.2 for finite changes in the stress state variables. Techniques for accommodating the nonlinearity of the failure envelope

are presented by Fredlund, Rahardjo and Gan (1987).

Figure 1 shows a planar failure envelope that intercepts the shear stress axis, giving a cohesion intercept, c' . The envelope has slope angles of ϕ' and ϕ^b with respect to the $(\sigma - u_a)$ and $(u_a - u_w)$ axes, respectively. Both angles are assumed to be constants. The cohesion intercept, c' , and the slope angles, ϕ' and ϕ^b , are the strength parameters used to relate the shear strength to the stress state variables. The parameters should not be considered as fundamental properties of the soil. The shear strength parameters represent many factors which have been simulated in the test. Some of these factors are density, void ratio, degree of saturation, mineral composition, stress history, strain rate, and many others. In other words, these factors have been combined and expressed mathematically in the strength parameters. The mechanical behaviour of an unsaturated soil is affected differently by changes in net normal stress than by changes in matric suction (Jennings and Burland, 1962). The increase in shear strength due to an increase in net normal stress is characterized by the friction angle, ϕ' . On the other hand, the increase in shear strength caused by the increase in matric suction is described by the angle, ϕ^b . The value of ϕ^b is consistently equal to or less than ϕ' as indicated in Table 2 for soils from various geographic locations.

The failure envelope intersects the shear stress versus matric suction plane along a line of intercepts as illustrated in Fig. 1. The line of intercepts indicates an increase in strength as matric suction increases. In other words, the increase in shear strength with increasing matric suctions is defined by the angle, ϕ^b . The equation for the line of intercept is as follows:

$$c = c' + (u_a - u_w)_f \tan \phi^b \quad [3]$$

where: c = intercept of the extended Mohr-Coulomb failure envelope with the shear stress axis at a specific matric suction, $(u_a - u_w)_f$, and zero net normal stress. It can be referred to as the "cohesion intercept".

The extended Mohr-Coulomb failure envelope can be presented as a horizontal projection onto the τ versus $(\sigma - u_a)$ plane. The horizontal projection can be made for various matric suction values, $(u_a - u_w)_f$. The horizontal projection of the failure envelope onto the τ versus $(\sigma - u_a)$ plane results in a series of contours shown in Fig.2. The lines have different cohesion intercepts depending upon their corresponding matric suctions. The cohesion intercept becomes the effective cohesion, c' , when the matric suction goes to zero. All lines have the same slope angle, ϕ' . The equation for these contour lines can be written as,

$$\tau_{ff} = c + (\sigma_{ff} - u_{af}) \tan \phi' \quad [4]$$

Substituting Eq. 3 into Eq. 4 yields the equation for the extended Mohr-Coulomb failure envelope (i.e., Eq. 2). Equation 4 is similar in form to Eq. 3 and Fig. 2 is a two dimensional representation of the extended Mohr-Coulomb failure envelope. The failure envelope projection illustrates the increase in shear strength as matric suction is increased while maintaining a specific net normal stress. The projected failure envelope is a simple, descriptive representation of the three-dimensional failure envelope. Equation 4 is also

convenient to use when performing numerical analyses of unsaturated soils.

The inclusion of matric suction in the definition of the cohesion intercept does not suggest that matric suction is a cohesion component of shear strength. Rather, the matric suction component (i.e., $(u_a - u_w) \tan \phi^b$) is lumped with effective cohesion, c' , for the purpose of translating the three-dimensional failure envelope to a two-dimensional plot. The suction component of shear strength has also been called the apparent cohesion (Taylor, 1948). A smooth transition from the unsaturated to the saturated conditions can be demonstrated using the extended Mohr-Coulomb failure envelope shown in Fig. 1. As the soil becomes saturated, the matric suction goes to zero and the pore-water pressure approaches the pore-air pressure. As a result, the three-dimensional failure envelope is reduced to the two-dimensional envelope on the τ versus $(\sigma - u_w)$ plane. The smooth transition can also be observed in Fig. 2. As the matric suction decreases, the failure envelope projection gradually lowers, approaching the failure envelope for the saturated condition. In this case, the cohesion intercept, c , approaches the effective cohesion, c' .

The extended Mohr-Coulomb failure envelope can also be projected horizontally onto the τ versus $(u_a - u_w)$ plane. The horizontal projection is made at various net normal stresses at failure, $(\sigma_{ff} - u_{af})$. The resulting contour lines have an ordinate intercept of $(c' + (\sigma_{ff} - u_{af}) \tan \phi)$ and a slope angle of ϕ^b . The horizontal projection shows an increase in shear strength as the net normal stress is increased at a specific matric suction.

2.2 HISTORY OF SHEAR STRENGTH TESTING OF UNSATURATED SOILS

The shear strength test results discussed in this review are selected from the many references on this subject. The selection of research papers to reference is based primarily upon whether or not the researcher ensured adequate control or measurement of the pore-pressures during the shearing process. The two commonly performed shear strength tests are the triaxial test and the direct shear test.

"Identical" soil specimens are required for the determination of the shear strength parameters in the laboratory. If the strength parameters of an undisturbed soil are measured, the test should be performed on specimens with the same geological and stress history. On the other hand, if the strength parameters for compacted soil are being measured, the specimen should be compacted at the same initial water content to produce the same density. The soil can then be allowed to equalize under a wide range of applied stress conditions. It is most important to realize that soils compacted at different water contents, to different densities, are different soils. In saprolitic soils, obtaining identical soil specimens is difficult due to the extreme variabilities of the material and of its microfabric.

The shear strength of a saturated soil is commonly described using the Mohr-Coulomb failure criterion and the effective stress concept (Terzaghi, 1936).

$$\tau_{ff} = c' + (\sigma_{ff} - u_{wf}) \tan \phi' \quad \dots \dots \dots [5]$$

where: τ_{ff} = shear stress on the failure plane at failure

c' = shear strength intercept on the shear stress axis when the effective normal stress is equal to zero. It is also called "effective cohesion"

$(\sigma_{ff} - u_{wf})$ = effective normal stress on the failure plane at failure

σ_{ff} = total normal stress on the failure plane at failure

u_{wf} = pore-water pressure at failure

ϕ' = effective angle of internal friction

Equation 5 defines a line which is commonly referred to as a failure envelope. The envelope represents possible combinations of shear stress and effective normal stress on the failure plane at failure.

The shear stress described by the failure envelope indicates the shear strength of the soil for each effective normal stress. The failure envelope is obtained by plotting a line tangent to a series of Mohr circles representing failure conditions. The slope of the line give the effective angle of internal friction, ϕ' , and its intercept on the ordinate is called the effective cohesion, c' . The direction of the failure plane in the soil is obtained by joining the pole point to the point of tangency between the Mohr circle and the failure envelope. The tangent point on the Mohr circle at failure represents the stress state on the failure plane at failure.

The use of effective stress in the Mohr-Coulomb failure criterion has been proved to be satisfactory in engineering practice associated with saturated soils. Similar attempts have been made to find a single-valued effective stress variable for unsaturated soils. If this were possible, a shear strength equation for unsaturated soils could be proposed. However, evidence increasingly supports the use of two independent stress state variables to define the stress state for an unsaturated soil (Matyas and Radhakrisna, 1968 and Fredlund and Morgenstern, 1977). See previous Section 2.1.

Numerous shear strength tests and other related studies for unsaturated soils have been conducted during the past thirty years. This section presents a review of studies related to the shear strength of unsaturated soils.

Similar to saturated soils, the shear strength testing of unsaturated soils can be viewed in two stages. The first stage is prior to shearing where the soils may be consolidated to a specific set of stresses or left unconsolidated. The second stage involves the control of drainage during the shearing process. The pore-air and pore-water phases can be independently maintained as undrained or drained during shear.

In the drained condition, the pore fluid is allowed to completely drain from the specimen. The desire is that there be no built up of excess pore pressures during shear. In other words, the pore pressures is controlled at a constant value during shear. In the undrained condition, no drainage of pore fluid is allowed and changing pore pressures during shear may or may not be measured. It is important, however, to measure or control the pore-air and pore-water pressures in order to determine the net normal stress and matric

suction at failure. The stress state variables at failure condition are necessary to properly assess the shear strength of the soil.

Many shear strength tests on unsaturated soils have been performed without either controlling or measuring pore-air and pore-water pressures during shear. In some cases, the matric suction of the soil was measured only at the beginning of the test. These results serve as a qualitative indicator of the soil shear strength since the actual stress state variables at failure are unknown.

A high air entry disc with an appropriate air entry value should be used when measuring pore-water pressures in an unsaturated soil. The absence of a high air entry disc can readily cause cavitation in the measuring system and result in erroneous pore-water pressure measurements. The interpretation of the results from shear strength tests on unsaturated soils become ambiguous when the stress state variables at failure are not known.

The first category is a review of shear strength tests where there has been adequate control or measurement of the pore-air and pore-water pressures. The second category is a review of shear strength tests of unsaturated soils where there has been inadequate control or measurement of pore pressures during shear.

A series of direct shear tests on unsaturated fine sand and coarse silt was conducted by Donald (1956). The tests were performed on a modified direct shear box as shown in Fig.3a. The top of the direct shear box was exposed to the atmosphere in order to maintain the pore-air pressure, u_a , at atmospheric pressure (i.e., zero gauge pressure). The pore-water pressure, u_w , was controlled at a negative value by applying a constant negative head to the water phase. The specimen was placed in contact with the water in the base of the shear box through use of a collodian membrane. The water in the base of the shear box was then connected to a constant head overflow tube at a desired negative gauge pressure (Fig.3b). The pore-water gauge pressure could be reduced to approximately negative one atmosphere before cavitation occurred in the measuring system. The soil specimens were consolidated under a total stress of approximately 48 kPa, to give uniform initial density. The desired negative pore-water pressure was applied for several hours in order for the specimens to reach equilibrium. The specimens were then sheared at a rate of 0.071 mm/sec.

The results are presented in Fig. 4. The shear strength at zero matric suction is the strength due to the applied total stress. As the matric suction is increased, the shear strength increased to a peak value and then decreases to a fairly constant shear strength. The drop in shear strength was correlated with the point of rapid desaturation from 100 % for the soil.

The United States Bureau of Reclamation has performed a number of studies on the shear strength of unsaturated, compacted soils in conjunction with the construction of earth fill dams and embankments (Gibbs, Hilf, Holtz and Walker, 1960; Knodel and Coffey, 1966; and Gibbs and Coffey, 1969). Undrained triaxial tests with pore-air and pore-water pressure measurements have been performed. The pore-air pressure, u_a , was measured through the use of a coarse ceramic disc at one end of the specimen. The pore-water pressure, u_w , was measured at the other end of the specimen. The pore-air and pore-water pressures were measured during the application of an isotropic pressure, σ_3 , and subsequently during the application of the deviator stress, $(\sigma_1 - \sigma_3)$. The pore-air pressure measurements agreed

closely with the pore-air pressure predictions using Hilf's analysis. No attempt was made to relate the measured shear strength to the matric suction, $(u_a - u_w)$. Rather, two sets of shear strength properties (i.e., c' and ϕ') were obtained by plotting two Mohr-Coulomb envelopes. The first envelope was tangent to Mohr circles plotted using the $(\sigma - u_w)$ stress variables (i.e., Eq. 5). The second envelope was tangent to Mohr circles plotted using the $(\sigma - u_a)$ stress variables. Fig. 5 presents typical plots of two envelopes for an unsaturated soil. The two failure envelopes indicate a more significant difference in their cohesion intercepts than in their friction angles.

An extensive research program on unsaturated soils was performed at Imperial College, London in the early 1960's. At the research conference in Boulder, Colorado, on the Shear Strength of Cohesive Soils, Bishop, Alpan, Blight and Donald (1960) proposed testing techniques and presented the results of five types of shear strength tests on unsaturated soils. The types of tests were i) consolidated drained, ii) consolidated undrained, iii) constant water content, iv) undrained, and v) unconfined compression tests. The tests were performed using a modified triaxial cell. The pore-air and pore-water pressures were either measured or controlled during the test. Bishop (1961) gave a discussion on the measurement of pore pressures in triaxial tests at the conference on Pore Pressure and Suction in Soils in London. Tests confirmed that pore-water pressures could be measured directly through a saturated coarse porous ceramic disc placed at the base of the soil specimen. The pore-water pressure measurements were made by balancing the pressure in the measuring system with the pore-water pressure measured using a null indicator to ensure no flow condition. This direct measurement, however, was limited to a gauge pressure range above negative 90 kPa. Bishop and Eldin (1950) have successfully measured pore-water pressures down to negative 90 kPa in a saturated soil specimen during a consolidated undrained test with a carefully deaired measuring system.

An indirect measurement of pore-water pressure using the axis translation technique (Hilf, 1956) was suggested when higher matric suction values were involved. The axis-translation technique translates the highly negative pore-water pressure to a pressure that can be measured without cavitation of the water in the measuring system. In addition, a high air entry disc with an air entry value greater than the matric suction must be used in order to prevent the passage of pore-air into the measuring system. A single layer of glass fibre cloth with a low attraction for water was placed on the top of the specimen for pore-air pressure measurement or control. The test results were presented in terms of stress points and plotted with respect to the $[(\sigma_1 + \sigma_3)/2 - u_w]_f$ and $[(\sigma_1 + \sigma_3) - u_a]_f$ stress variables at failure. Figure 6 shows a typical plot of results of a constant water content test. The condition when the $[(\sigma_1 - \sigma_3)/(\sigma_3 - u_w)]_f$ ratio reached a maximum was considered to be the failure condition.

In 1961, Bishop and Donald introduced a device called a "bubble pump" to remove and to measure the volume of air that diffused through the high air entry disc into the triaxial cell base. Pore-air diffusion through the rubber membrane into the water in the triaxial cell was prevented by completely surrounding the membrane (i.e., specimen) with mercury rather than with water. The results of a consolidated drained test on an unsaturated loose silt was used to verify the significance of the $(\sigma - u_a)$ and $(u_a - u_w)$ stress variables.

Laboratory testing techniques and details of various types of triaxial tests were explained and summarized by Bishop and Henkel in 1962.

The use of the axis translation technique in the shear strength testing of unsaturated soils was examined by Bishop and Blight (1963). A compression test with the net confinement kept at zero, was conducted on a compacted Selsset clay specimen using a stepwise series of axis-translations. The results show monotonic shear stress versus strain relations as long as the matric suction remains constant during the test. A comparison between the shear strengths obtained from similar tests with and without axis-translation was also performed on Talybont clay. The shear stress versus strain curves from the two types of tests agree closely. This experimentally confirms the applicability of the axis-translation technique for the laboratory testing of unsaturated soils. In addition, the ability of the pore-water to withstand absolute tensions greater than one atmosphere is confirmed since the test results without axis-translation yielded essentially the same shear strength as those with axis-translation.

The development of pore-air and pore-water pressures during undrained tests was also studied. Typical results of constant water content test were presented and discussed.

Donald (1963) presented further results of undrained tests on compacted Talybont clays with pore-air and pore-water pressure measurements. Pore-air and pore-water pressure changes during the compression were found to be a reflection of the volume change curve. The strain rate of testing affected the pore-air pressure response more than the pore-water response. The matric suction of the soil specimen increased markedly with axial strain.

In 1963, a research program on the engineering behaviour of unsaturated soils was undertaken by the Soil Engineering Division at the Massachusetts Institute of Technology (i.e., M.I.T.) in Boston. The triaxial apparatus was the same as that used by Bishop and Donald (1961) with the following exceptions (M.I.T., 1963). The null indicator for measuring pore-water pressure was replaced with an electrical pressure transducer. The glass fibre cloth at the top of the soil specimen, for measuring pore-air pressure, was substituted with a coarse porous disc. A series of consolidated undrained tests with pore pressure measurements and undrained tests with pore-air pressure control and pore-water pressure measurements was performed on compacted specimens. The specimens were a mixture of 80 percents ground quartz and 20 percents kaolin. Some difficulties was experienced in analyzing the test data using a single-valued stress variable.

Blight (1967) reported the results of several consolidated drained tests performed on unsaturated soil specimens. All specimens were compacted at a water content of 16.5 percent using a standard AASHTO compactive effort. The specimens were then brought to equilibrium at three matric suction values in a triaxial cell. Two specimens, subjected to a constant matric suction, were tested using two net confining pressures ($\sigma_3 - u_a$), (i.e., 13.8 kPa and 27.6 kPa). The deviator stress versus strain curves obtained from these tests are shown in Figure 7a. The results indicate an increase in shear strength with increasing matric suction and also with increasing net confining pressures. The water volume changes and overall specimen volume changes during compression are presented in Figures 7b and 7c respectively, for the specimens sheared under a constant matric suction of 137.9 kPa. Although pore-water was expelled from the specimen during shear, the overall volume of the specimen increased. In other words, the specimens dilated during compression.

The shear strength of two unsaturated, compacted soils from India; namely, Delhi silt

and Dhanauri clay, were tested by Gulhati (1975). Consolidated drained tests with pore pressure being maintained were performed in a modified triaxial cell. Constant water content test with pore-air pressure control and pore-water pressure measurement were also performed.

Research on the behaviour of unsaturated soils has been undertaken at the University of Saskatchewan, Canada. In 1977, Fredlund and Morgenstern proposed the use of $(\sigma - u_w)$ and $(u_a - u_w)$ as independent stress state variables. In 1978, a shear strength equation for an unsaturated soil was proposed using these independent stress state variables (Fredlund, Morgenstern and Widger, 1978). The shear strength of an unsaturated soil was considered to consist of an effective cohesion, c' and the independent contributions from net normal stress, $(\sigma - u_a)$, and matric $(u_a - u_w)$. The effective angle of internal friction, ϕ' , was associated with the shear strength contribution from the net normal stress state variable. Another angle; namely, ϕ^b , was introduced. It is related to the shear strength contribution from the matric suction stress state variable. Two sets of shear strength test results from Imperial College and one set of data from M.I.T. were used in the examination of the proposed shear strength equation. The test data indicated essentially a planar failure surface. The failure envelope was viewed as a three-dimensional surface. The three-dimensional plot with $(\sigma - u_a)$ and $(u_a - u_w)$ as abscissas can be visualised as an extension of the conventional Mohr-Coulomb failure envelope (Fredlund, 1979).

Satija (1978) conducted an experimental study on the shear strength behaviour of unsaturated Dhanauri clay. Constant water content and consolidated drained tests were conducted on compacted specimens for various values of $(\sigma - u_a)$ and $(u_a - u_w)$. The triaxial apparatus was similar to that used in the M.I.T. research program (M.I.T., 1963). Pore pressures were either controlled or measured throughout the shear test. The appropriate strain rate was found to decrease with a decreasing degree of saturation of the soil (Satija and Gulhati, 1979). The results were presented as a three-dimensional surface where half of the deviator stress at failure, $[(\sigma_1 - \sigma_3)/2]_f$, was plotted with respect to the net minor principal stress at failure, $(\sigma_3 - u_a)_f$, and the matric suction at failure $(u_a - u_w)_f$ (Gulhati and Satija, 1981).

A series of consolidated drained direct shear tests and a series of drained triaxial tests on unsaturated Madrid gray clay were reported by Escario in 1980. The tests were performed under controlled matric suction conditions using the axis-translation technique. A modified shear box device, enclosed in a pressure chamber was used to apply a controlled air pressure to the soil specimen. The specimen was placed on a high air entry disc in contact with water at atmospheric pressure. This arrangement is similar to the pressure plate technique where the matric suction is controlled by varying the pressure while the pore-water pressure is maintained constant. Prior to testing, the soil specimens were statically compacted and brought to the desired matric suction under an applied vertical normal stress. The results obtained from the direct shear test are presented in Fig. 8. The failure envelopes exhibit almost a parallel upward translation indicating an increase in the shear strength as the soil matric suction is increased.

The results of triaxial tests are shown in Fig. 9. The pore-water pressure was controlled at atmospheric pressure through a high air entry disc placed at the bottom of the soil specimen. An air pressure was applied to the soil specimen through a coarse porous disc

placed on top of the soil specimen. The specimen was enclosed in a rubber membrane and the confining pressure was applied through the water in the triaxial cell. The results further demonstrate the increase in shear strength due to matric suction.

In 1982, a series of multistage triaxial tests on unsaturated soils were performed by Ho and Fredlund. Undisturbed specimens of two residual soils from Hong Kong were used in the testing program. The soils were a decomposed rhyolite and a decomposed granite. The testing program consisted of consolidated drained tests with pore-air and pore-water pressure control during shear (Ho and Fredlund, 1982). The pore-air pressure was controlled from the top of the specimen through a coarse porous disc. The pore-water pressure was controlled from the bottom of the specimen using a high air entry disc sealed onto the base pedestal. The desired matric suction in the specimen was obtained by controlling the pore air and pore water pressures using the axis-translation technique. The strain rates required for shearing an unsaturated soil were discussed in details using a theoretical formulation described by Ho and Fredlund (1982).

The triaxial test results are shown as failure envelopes in the shear stress, τ , versus suction ($u_a - u_w$) plots in Fig. 10. The data points corresponding to these failure envelopes in the τ versus ($u_a - u_w$) plane were obtained by projecting the failure envelope defined by the Mohr circles in the τ versus ($\sigma - u_a$) plane to the τ versus ($u_a - u_w$) plane (i.e., $(\sigma - u_a) = 0$).

This technique is illustrated in Fig. 1 and is described in Section 2.1. Each envelope shown is obtained from the multistage shear conducted on a specimen. The ϕ^b angle, i.e., the slope angle of the τ versus ($u_a - u_w$) envelope, is fairly similar from one specimen to another. This shows that there is a unique shear stress versus matric relationship when results from 'identical' specimens are used. There is, however, a large spread in the envelopes obtained showing that there is a large variability in the material and/or structure from one specimen to another.

The ϕ^b angles have been measured for various soils and the results have been summarized by Fredlund (1985) in Table 2. The experimental results showed that the angle ϕ^b is always smaller than the internal friction angle, ϕ' .

Gan (1986) conducted a program of multistage direct shear tests on an unsaturated glacial till. A series of tests on saturated specimens was also performed to obtain the effective cohesion, c' , and the internal friction angle, ϕ' . All specimen were prepared by compaction according to the standard Proctor procedure. A modified direct shear box was developed for the tests on the unsaturated soil. The same equipment was used in this research program and a detailed description of the equipment will be presented in Section 3. A multistage shearing procedure was adopted for the tests on the unsaturated specimens. Each specimen had three to seven stages of shear. The net normal stress was maintained approximately constant at 72.6 kPa. The matric suction was varied from 0 to 500 kPa. Multistage shearing was preferred to reduce material variability. The multistage procedure proved ideal as the material does not strain-soften when failure is approached. Hence, it was possible to obtain unique envelope for each specimen. A typical set of test results is presented in Fig. 11. The corresponding failure envelope is shown in Fig. 12a where the shear stress, τ , is plotted with respect to the matric suction, ($u_a - u_w$), at a constant net

normal stress at failure of 72.6 kPa. The results show some nonlinearity of the failure envelope. The variation of ϕ^b with respect to matric suction is shown in Fig. 12b. The ϕ^b angle is equal to ϕ' (i.e., 25.5°) at low matric suctions. Beyond approximately 50 kPa of matric suction, the ϕ^b angle begins to decrease. The ϕ^b angle continues to decrease with matric suction until the matric suction is approximately 300 kPa. Beyond matric suctions of 300 kPa, the ϕ^b angle attains a constant value of 7° . The same trend was observed for all five specimens tested. The results of the tests on all five specimens are presented in Fig 13. The spread in the results presented in Fig. 13 is relatively minor. The spread is likely due to the variation in the initial void ratios of the specimens. In the linear section of the envelope where ϕ^b is equal to ϕ' , the soil behaves essentially as a saturated soil. With increasing suction (in this case, beyond approximately 50 kPa matric suction), the soil begins to desaturate and the ϕ^b angle decreases. The rate of desaturation is rapid initially. When the matric suction is high (beyond 300 kPa matric suction), the degree of saturation of the specimen is low and the rate of desaturation becomes insignificantly small. Thus, the ϕ^b angle becomes essentially a constant.

The nonlinearity in the shear strength versus matric suction relationship was also observed by Escario and Saez (1986), Drumright (1989) and Toll (1990).

Escario and Saez (1986) conducted direct shear tests on three soils; namely, Madrid grey clay, red clay of Guadalix de la Sierra, and Madrid clayey sand. The test were performed using a modified direct shear box and following the procedure described by Escario (1980). Nonlinear relationship between τ and $(u_a - u_w)$ were obtained in all three soils tested. The results are presented in Figure 14.

Consolidated drained and constant water content tests using multistage shearing procedure in the triaxial equipment were conducted by Drumright (1989). The material tested was a remolded, silty copper tailings sand. The specimens were prepared according to the Harvard kneading procedure. The 'undercompaction method' (Ladd, 1978) was used to achieve a more uniform density throughout the compacted specimens. Results from the consolidated drained (CD) tests and constant water content (CW) tests are presented in Figs. 15a, 15b, and 15c. The results show that the shear stress versus matric suction relationship is nonlinear. Also, there is no significant difference in the envelopes obtained from the CD and the CW tests, implying uniqueness of the failure envelope.

Recently, Toll (1990) also made use of the independent stress state variables, described earlier, to establish the critical state context for unsaturated soil behaviour. The tests were conducted on compacted Kiunyu gravel, a lateritic gravel from Kenya. The shear stress versus matric suction relationship, denoted by M_w , was found to vary with the degree of saturation, S_r (or with matric suction) as shown in Figure 16.

Peterson (1988) conducted constant water content triaxial compression tests on compacted Vicksburg buckshot clay. The suctions in the specimen were measured using psychrometers. The compacted specimens were subjected to different stress histories prior to shear to assess the influence of density on the shear strength of unsaturated soils.

Numerous shear strength tests on unsaturated soils have been conducted without a knowledge of the pore-air or pore-water pressures at failure. These shear tests cannot be

interpreted in terms of the strength parameters associated with the independent stress state variables. Most of these tests were unconfined compression tests where the initial matric suctions of the specimen were established or measured (Aitchison, 1959; Blight, 1966; Williams and Shaykewich, 1970; and Edil, Motan and Toha, 1981). Undrained triaxial tests with only pore-water pressure measurements during shear have also been performed (Kassif, 1957). Consolidated, undrained triaxial tests with only pore-water pressure measurements during shear have been conducted by Neves (1971). Neves (1971) used a high air entry disc in making the pore-water measurements. Komornik, Livneh and Smucha (1980) conducted consolidated undrained tests where the initial matric suction of the specimens was established using osmotic suction equilibrium. Lumb (1965) conducted drained triaxial tests on undisturbed unsaturated decomposed granite and decomposed rhyolite from Hong Kong. No suction measurements were attempted. However, the degree of saturation of the specimens were obtained. The results of these tests are presented in Fig. 17. The results show a large variability which is characteristic of undisturbed saprolitic soils.

The above tests where the pore pressures were not measured should be viewed as 'total stress' type tests. They are useful and can be justified for the simulation of specific drainage conditions. However, the interpretation of these tests becomes more meaningful in view of the theory presented earlier in Section 2.1. Research papers published by researchers from the University of Saskatchewan, Canada, on the shear strength and shear strength testing of unsaturated soils are included in the references and these are indicated with a *.

3. EQUIPMENT

Two direct shear machines were utilized in the present testing program. One machine was a conventional direct shear box apparatus. The other has a modified direct shear box contained within a pressure chamber. All test specimens were 50 mm x 50 mm. The machines are equipped with a data acquisition system. Each apparatus has a micro computer and a monitor to collect the data and to provide a visual display. The conventional direct shear box apparatus had three measurement devices. These were two displacement transducers (i.e., LVDT's) and one load cell. The LVDT's were used to monitor horizontal and vertical displacement.

The modified shear box apparatus has five measurement monitoring devices. There are two LVDT's for monitoring horizontal and vertical displacements, a pressure cell for monitoring water pressure, a load cell, and a burette for monitoring the water movement in the specimen. The air pressure in the chamber was controlled using a pressure regulator.

3.1 DESCRIPTION OF THE MODIFIED DIRECT SHEAR BOX OF THE GEOTECHNICAL ENGINEERING LABORATORY AT THE UNIVERSITY OF SASKATCHEWAN.

A conventional direct shear apparatus manufactured by Clockhouse Engineering Limited of England was selected for modification. The basic ideas presented by Escario (1980) for modifying the direct shear box were used in the development of the modified shear box at the University of Saskatchewan. The modified apparatus is shown in Fig. 18.

The main modification to the conventional direct shear apparatus was the design of an air pressure chamber. The air chamber completely enclosed the direct shear box and was used to elevate the ambient air pressure in which the test was run.

3.1.1 SHEAR BOX BASE DESIGN

A plan view of the shear box base is shown in Fig. 19. The high air entry ceramic disk is removed in order to show the details of the water chamber. The raised sections inside the water chamber serve both as a support for the high air entry disk and as a guide for water flow (Figs. 19, 20, and 21). Water can be circulated from the entry port to the exit port below the high air entry disk. This ensures a thorough flushing of the channels and compartment below the ceramic disk. The ceramic disk does not allow the passage of free air; however, dissolved air can diffuse through the water in the high air entry disk and appears as air bubbles below the disk.

The high air entry disk is placed on the raised channel guides. It is tightly sealed into position around its edges using epoxy cement to ensure that air will not enter the water chamber. The time for pressure equalization throughout the specimen affects the testing time, making a thin disk superior. On the other hand, a thin high air entry disk cracks more easily, particularly if care is not taken to ensure that the vertical load to the specimen and the air pressure are applied before pressurizing the water chamber beneath the high air entry

disk. On the basis of past experience, a 6.4 mm (i.e., 1/4 inch) thick ceramic disk has been found to be satisfactory.

In the original direct shear equipment and the present modified equipment, shearing is induced by longitudinally displacing the lower portion of the shear box. The base of the shear box is seated on rollers that run in grooved tracks on the chamber base. Steel tubing rolled into two flexible helical springs were used too connect the water chamber to its inlet and outlet in the chamber base (Figs. 19 and 20). The resistance to movement of the lower box resulting from these helical steel tubings, and the frictional resistance from the rollers do not introduce errors or inaccuracies to the shear resistance measured. The shear resistance is measured on the upper box.

Several features of the modified direct shear box are different from the design described by Escario (1980). The main differences relate to the lower portion of the shear box. In the design by Escario, the lower portion of the shear box was immovable and the shear force was applied through the upper portion of the box. This simplified the plumbing into the water chamber but resulted in problems related to eccentric normal loading of the specimen. The shear load in Escario's design was measured on the loading ram, thereby including the friction of the roller bearings. The present shear box also included the use of low friction, Teflon® seals, as well as a water volume change indicator and a diffused air volume indicator.

3.1.2 AIR PRESSURE CHAMBER DESIGN

A pressure chamber surrounds the entire shear box in order to maintain any selected air pressure in and around the specimen. The cylindrical chamber was built of stainless steel and was designed for pressures of up to 1000 kPa. Safety must be a high priority when working with compressed air, and this explains the robustness of the air pressure chamber.

The chamber consists of three components. These are i) the chamber cap, ii) the chamber body, and iii) the chamber base. All three components are built of stainless steel. The air-tightness of the entire chamber is ensured through the use of two rubber o-ring seals, one on the chamber cap and the other on the chamber base (Fig. 20). The cap is held to the body through the use of six cap screws. When testing soil specimens, only the chamber cap is removed. The chamber body is dismantled from the chamber base only in the event that the shear box base must be removed (i.e., for replacing the high air entry disk).

The chamber cap has an air valve and an axial loading ram (Fig. 20). The circular hole for the axial loading ram has a Teflon® ring seal to ensure air-tightness when the loading ram is in-place. Vacuum grease was used around the loading ram. An air supply is connected to the chamber via the air valve and is controlled by a pressure regulator.

The chamber body is made of a 26.5 mm thick stainless steel cylinder with a 220 mm internal diameter. Two holes, diametrically opposite each other, provide the necessary housing for the pistons that apply the shear force acting on the shear box assembly. These holes are lined on the inside with an airtight Teflon® seal. A plan view of the chamber base

along with the shear box base in position is shown in Fig. 22. Details of the chamber base are shown in Figs. 19, 20 and 21. The various components of the modified direct shear apparatus are shown in Fig. 23.

3.1.3 SUCTION CONTROL

The desired matric suction is applied to the soil specimen by maintaining a constant air pressure in the air pressure chamber and a constant water pressure in the water chamber below the high air entry disk. The pore-air and pore-water pressures in the soil are then allowed to come to equilibrium with these applied pressures. An applied air pressure causes water to flow out of the base of the specimen since the specimen is initially covered with water. The flow of water ceases when the desired suction value is attained. At equalization, the pore-water and pore-air pressures in the soil are equal to the applied pressures. The movement of water from the specimen is monitored using a water movement indicator.

3.2 TESTING PROCEDURE USING THE MODIFIED DIRECT SHEAR EQUIPMENT

Before the soil specimen is trimmed and mounted in the shear box, it is first necessary to saturate the high air entry disk with deaired water. This is done by flooding the base of the shear box with deaired water and subsequently pressurizing the air chamber to force the water through the ceramic disk. After each flooding, the water chamber is flushed to remove diffused air from below the high air entry disk. This procedure is repeated several times. When the process is complete, the air pressure chamber is opened and the shear box base is again flooded with deaired water. This time the air pressure chamber is covered with a plastic sheet to reduce evaporation and drying out of the high air entry disk until such time that the testing is to commence.

The two halves of the shear box are placed together and sealed with vacuum grease. This is to ensure that water will flow only in the direction of the high air entry disk. It is important not to smear vacuum grease onto the surface of the high air entry disk.

After the specimen is mounted in the shear box, the top coarse porous stone is put in place. The top level of the porous stone is noted by measuring its distance from the surface of the upper box. This measurement is used to determine the change in thickness of the sample upon saturation. An ample quantity of water is applied to the top of the specimen and the specimen is left to soak overnight. No vertical load was applied to the specimen during overnight soaking. The excess water above the porous stone is removed before placing the loading cap in place. The chamber cap is then fitted.

The predetermined axial load, the air pressure and the water pressure are applied in this sequence. If the water pressure is applied first, there is the possibility of cracking or dislodging the high air entry disk. It is important to check that there are no detectable leaks in the high air entry disk or the chamber.

Leakage through the high air entry disk is checked by flushing the water chamber. The presence of air bubbles shortly after the chamber pressure is applied means that there

is leakage in the ceramic disk. Leakage from the chamber is checked by means of applying a soap solution to all sealed areas. Air-tightness is most difficult to attain in the seals around moving parts. These seals for the moving parts are also the most difficult to correct when leakages does occur. Air-tightness is essential as leakage of air will render the equilibration of the applied suction difficult due to the continuous loss of moisture from the system.

Throughout the pressure equilibration process, readings are taken of 1) time, 2) vertical deflections, and 3) water movement from the specimen. Equalization is assured when the flow of water essentially ceases.

After suction equalization is achieved, the specimen is sheared at a constant displacement rate. In the Pilot and Preliminary Programs, shear reversal was used. The specimens were sheared to fairly large displacements in both the forward and the reverse directions. In the Main Testing Program, shearing was only performed in the forward direction. At each stage of loading, the specimen was sheared to its peak strength and the load was then released by reversing the direction of horizontal shear displacement. Only during the last stage of loading for each specimen was the shearing continued beyond the peak strength. This procedure entailed careful attention of the experiment.

4. SPECIMEN PREPARATION

The test specimen is obtained by careful trimming using a scalpel blade and a 50.8mm x 50.8mm x 21.4 mm mould. The mould was pressed into the soil with its bevelled cutting edge facing away from the specimen. The soil around the perimeter of the mould was trimmed carefully such that the mould could be advanced slowly by pressing down on the mould. The material was brittle and highly friable and the trimming process must be performed carefully. Large particles were often encountered, making the specimen preparation extremely difficult. The presence of numerous discontinuities, both visible and not visible, and the highly heterogeneous nature of the soil, presented great difficulty in obtaining good similar specimens for testing. The specimens were trimmed smooth on the top and bottom.

No photographs were taken of the individual specimens prior to testing. On completion of the shear test, each specimen was separated at the shear zone and the shear surfaces were photographed. Unfortunately these photographs did not turn out. The specimens used in the Main test program were kept till the end of the program and these specimens were rephotographed. These photographs are presented in the Appendices (i.e., Volume Two of this report). The specimens used in the Pilot test program and the Preliminary test program were not kept and it was not possible to rephotograph any of them.

It was difficult to determine if specimens were 'intact' (i.e., not containing any relict joints) during specimen preparation. It turns out that a large proportion of the specimens tested contain some sorts of joints.

5. TESTING PROGRAMS

The testing program was conducted in three parts as follows: 1) Pilot Test Program, 2) Preliminary Test Program, and 3) Main Test Program

5.1 PILOT TEST PROGRAM

The Pilot test program was conducted to assess the suitability of various test procedures. These procedures include the use of a single stage shear tests, a multi-stage shear tests and a combination of single stage shear tests and multi-stage shear tests. Multi-stage shear tests are preferred particularly when the soil is highly heterogeneous. The multi-stage procedure is advantageous in that it reduces the time required for trimming and preparing specimens and eliminates to a large extent, the variability in the data associated with heterogeneity. In addition, fewer specimens are required with this procedure.

The program in the contract requested that two pilot tests be conducted. One test was to be performed on a saturated specimen in a conventional shear box and the other test was to be performed on an unsaturated specimen under a small applied suction in a modified shear box. In the conventional shear box, the saturated specimen was to be subjected to a normal stress of 20 kPa. The unsaturated specimen was to be subjected to a normal stress of 10 kPa as well as a matric suction of 20 kPa. These specimens were to be subjected to a large displacement in order to obtain the complete shear stress versus displacement characteristics for the soil.

A shear rate of approximately 0.06 mm per min was used on the saturated specimen. In the modified shear apparatus, the shear rate used was approximately 0.04 mm per min. The different rates were due to the different gear combinations and motors that were available with each machine. The rates were selected to correspond to the 'medium' rate that was reported in GCO Special Project Report, SPR 5/87. Like the granitic soil in SPR 5/87, the present material is also considered to be highly permeable.

5.1.1 RESULTS AND DISCUSSION

The initial condition of the specimens are given in Table 3. The initial dimensions of all specimens are 50.8 mm x 50.8 mm x 21.4 mm.

The specific gravity of the solids, G_s , was measured at the University of Saskatchewan from two tests to be 2.71.

The results of the conventional direct shear apparatus are presented first, followed by the data from the modified direct shear apparatus.

5.1.1.1 RESULTS FROM CONVENTIONAL SHEAR BOX (FIRST TEST)

Specimen DS1B was subjected to a normal stress of 20 kPa in a conventional shear box. The sample was flooded and was left to consolidate for one day. There was no

detectable deflection during the consolidation process. The specimen was then subjected to thirteen cycles of shear. The shear stress versus horizontal shear displacement curves are shown in Figs. 24a to 27a, and in Figs. 28 and 30. The corresponding vertical displacement versus horizontal shear displacement curves are shown in Figs. 24b to 27b, and in Figs. 29 and 31. Fig. 24a shows that the shear stress peaked at approximately 39 kPa after a small displacement of 2 to 3 mm and then dropped rapidly to approximately 25 kPa after an additional 1 to 2 mm displacement. By the third cycle, the shear stress appeared to have reached a maximum value of approximately 17 kPa.

The shear stress versus horizontal shear displacement curves from the third cycle up to the thirteenth cycle fall approximately one on top of the other.

The vertical displacement versus horizontal shear displacement curves showed that the material continued to compress from one cycle to the next. This behaviour suggests that the soil structure may have a slight collapsing tendency. The collapse appears to initiate at the shear zone and propagate upwards and downwards away from the shear zone as shearing is continued. The pronounced peak during the first cycle also suggests that the material may still retain some of its original mineral to mineral bonding.

The jaggedness of the shear stress versus horizontal shear displacement plots was the result of 'electrical noise' due to poor shielding in the load cell circuit. A new load cell was used for all subsequent tests. The stepwise function in the vertical deflection versus horizontal shear displacement plots was due to low sensitivity setting for the deflection data acquisition system. This problem has since been rectified.

5.1.1.2 RESULTS FROM THE MODIFIED DIRECT SHEAR BOX

Specimen MDS1 was subjected to an air pressure of 140 kPa, a water pressure of 120 kPa and net normal stress ($\sigma_n - u_a$) of 10 kPa. The sample was flooded prior to the application of the above stresses. The vertical displacements of the specimen and the movement of water from the specimen was measured during the consolidation process. The volume of water expelled from the specimen versus the log of time in seconds is shown in Fig. 32. It took approximately 2 days for the water phase to come to equilibrium with the applied pressures. An ample amount of water was used to flood the sample to ensure proper equilibration. As in specimen DS1B, there was no detectable vertical deflection throughout the consolidation stage, suggesting that the soil has a fairly rigid structure.

The specimen was subjected to four cycles of shear. The shear stress versus horizontal shear displacement curves and the corresponding vertical displacement versus horizontal shear displacement curves are shown respectively in Figs. 33a and 33b. The shear stress reached a peak value of approximately 36 kPa after a horizontal shear displacement of about 2 mm. Unlike the saturated specimen DS1B, the peak stress did not drop substantially when shearing was continued in the same direction. The shear stress was approximately 32 kPa at a horizontal shear displacement of about 12 mm. During the second and the third cycles, the shear stress reached about 14 kPa, considerably less than the 32 kPa during the first cycle.

The vertical deflection versus horizontal shear displacement in Fig. 33b showed that during the first cycle, the specimen dilated throughout the shearing process in the forward direction. The specimen then compressed on displacement in the backward direction. The specimen compressed further on re-shearing in the forward direction and gradually dilated again. The same characteristics were repeated during subsequent cycles. There is a continual compression of the sample on shearing after the first cycle.

5.1.1.3 COMPARISON OF THE TWO PILOT TESTS

The two pilot tests resulted in two different types of shear stress versus horizontal shear displacement behaviour during the first cycle. Under a low normal stress of 20 kPa, the saturated specimen DS1B showed a distinct peak. Specimen MDS1, under a low normal stress of 10 kPa and a low suction of 20 kPa, showed a slow gradual reduction in shear stress with displacement prior to the reversal of the shearing direction. Due to the heterogeneous nature of the soil, it was decided that an additional test should be conducted to further examine the peaking phenomena of specimen DS1B.

5.1.1.4 RESULTS FROM THE CONVENTIONAL SHEAR BOX (SECOND TEST)

A second saturated specimen, DS1C, was subjected to a normal stress of 12.4 kPa and the resulting shear stress versus horizontal shear displacement curves and the corresponding vertical displacement versus horizontal shear displacement curves are shown in Figs. 34 and 35. The test results again showed a distinct peak of approximately 55 kPa at about 1 mm displacement. The shear stress dropped rapidly to about 20 kPa after an additional displacement of 1 mm. The results also showed that a maximum shear stress of approximately 16 kPa was reached after a shear displacement of 8 mm.

5.1.2 RECOMMENDATION

Results from the saturated specimens showed distinct peaks in the shear stress versus horizontal shear displacement curves. Results from the unsaturated specimen showed a gradual decrease from peak to ultimate value. In view of these results, it may not likely be possible to accurately obtain the peak strength envelope using the multi-stage approach. This is especially so under low normal stresses and/or suction. Under high normal stresses, the character of the shear strength envelope may not show the distinct peak.

In view of the present test results, single stage tests on individual specimens may appear to be the more reasonable approach for obtaining peak strength envelope. However, due to the heterogeneous nature of the material, it may be difficult to obtain unique strength envelope. In order to provide an optimum solution, it was suggested that individual specimens be used to provide peaks strength measurements and subsequent multi-stage shearing be done to obtain strength envelopes with respect to the ultimate strength.

The following recommendation was made for the next two stages of the program. For the saturated test series, multi-stage shearing will be conducted under various normal stresses. Under any normal stress, at least two cycles of shearing should be conducted. The

net normal stresses would be in keeping with the original proposal. These normal stresses will be 10 kPa, 30 kPa, 50 kPa, 100 kPa and 200 kPa. Each specimen should have one less stage of loading than the preceding specimen and should commence at the next higher normal stress level. Thus, the first specimen should commence at 10 kPa normal stress and should undergo five stages of shearing. The second specimen should commence at the next higher normal stress of 30 kPa and should undergo four stages of shearing, and so on. For each specimen, the first cycle of the first stage is intended to give both the peak strength and the residual strength of the specimen corresponding to the normal stress of the first stage. The subsequent stages and shear cycles should provide the ultimate strength values corresponding to the normal stresses at each stage. This should be possible since the pilot tests showed that the ultimate strengths were usually attained after one cycle of shearing.

The proposed procedure, was to yield the optimum quantity of data. First, the individual specimens should provide some information on the peak strength values. Second, the first two or three specimens should provide information on the ultimate strength of two (or three) individual specimens. Third, the ultimate strength data from all stages of all specimens should provide further information on the ultimate strength envelope of this material.

A shear rate of 0.03 mm/min was suggested for all subsequent tests. This rate of shear will allow the completion of two cycles of shear in about 24 hours (a travel of 10 mm in each direction giving a total displacement of 40 mm).

The revised programs for the preliminary program and the main program are presented in Table 4. The time schedule for the revised program is presented in Table 5.

In the original proposal for the Preliminary test program, there was to be one series of tests if the single stage option was selected or two series of tests if the multi-stage option was selected. Each series was to be conducted at five different net normal stresses of 10 kPa, 30 kPa, 50 kPa, 100 kPa and 200 kPa. This would give a total of five peak stress data points and five ultimate stress data points with the single stage option. If the multi-stage option was adopted, the two series would give ten peak stress data points. The single stage option would require tests to be conducted on five individual specimens. Only two specimens would be required with the multi-stage option, i.e., one for each series.

In the revised proposal for the Preliminary test program only one series of tests was proposed requiring five individual specimens. The first specimen will provide one peak stress data point corresponding to net normal stresses of 10 kPa and five ultimate stress data points corresponding to net normal stresses of 10 kPa, 30 kPa, 50 kPa 100 kPa and 200 kPa. The second specimen will provide one peak stress data point corresponding to a net normal stress of 30 kPa and four ultimate stress data points corresponding to normal stresses of 30 kPa, 50 kPa, 100 kPa and 200 kPa. The five specimens will, therefore, yield five peak stress data points and fifteen ultimate stress data points.

For the Main test program three series of tests were originally proposed for either the single stage option or the multi-stage option. Each series was to be conducted at different net normal stresses. These constant net normal stresses were 10 kPa, 50 kPa and 100 kPa. In each series, there were to be five stages. Each stage would correspond to suction values

of 20 kPa, 40 kPa, 80 kPa, 160 kPa and 320 kPa respectively. The single stage option would require tests to be conducted on fifteen individual specimens. This would give a total of fifteen peak stress data points and fifteen ultimate stress data points. If the multi-stage option was adopted only three specimens would be required. This would give a total of fifteen peak stress data points.

In the revised proposal, for the MAIN Test program, two series of tests were proposed. Each series were to be conducted at different normal stresses. The proposed normal stress values were 20 kPa and 100 kPa. Suction values of 20 kPa, 40 kPa, 80 kPa, 160 kPa and 320 kPa, respectively were suggested to correspond to the various stages. This procedure will require tests to be conducted on ten individual specimens. The first specimen in each series will give each one peak stress data point corresponding to a matric suction of 20 kPa and five ultimate stress data points corresponding to matric suction values of 20 kPa, 40 kPa, 80 kPa, 160 kPa, and 320 kPa. The second specimen in each series will each give one peak stress data point corresponding to a suction of 40 kPa and four ultimate stress data points corresponding to suction values of 40 kPa, 80 kPa, 160 kPa, and 320 kPa. The complete two series of tests will therefore give ten peak stress data points and thirty ultimate stress data points (see Table 4).

5.2 PRELIMINARY TEST PROGRAM

The objective of the preliminary test program was to determine the effective stress, shear strength parameters for the saturated soil. The procedure adopted was such that there will be sufficient data to obtain both the peak (undisturbed) strength and the residual strength Mohr envelopes. Five series of tests were proposed for this portion of the program. In all, six series were actually conducted. See Table 6. The test results are presented in Figs. 36 to 59. The initial conditions of the various specimens (i.e., natural water content, initial void ratios and degrees of saturation) are presented in Table 7. The actual shear rate used in the direct shear tests on the saturated specimens was 0.025 mm/min.

5.2.1 RESULTS AND DISCUSSION

The shear test results presented in Figs. 36 to 59 showed plateaus other than those corresponding to the constant shear stress at the critical state. In other words, the plateaus were partway up the shear stress versus horizontal displacement curves. This behaviour was observed on both the forward shear and the reverse shear directions. These plateaus appear to occur at approximately the same locations as shown in all cycles within the same stage of the shear test of a specimen. The shear stresses at which the plateaus occur increase linearly with the applied normal stresses on the specimens. This variation in the plateau stress with normal stress is shown in Fig. 60. The plateau stresses of Specimen P4 appear to deviate from the others and are consistently slightly lower.

The plateaus in the shear stress versus horizontal displacement curves appear to be due to slacks in the machine. A test run to check for slack was performed using a steel block for a dummy specimen. The results are presented in Fig. 61. The slack check was conducted at zero normal stress. Frictional effects appeared to be small and were in the order of 5 kPa. The total slack detected in the setup was approximately 2.35 mm. This

figure agrees fairly well with the slacks shown by the plateaus when testing the soil specimens. This agreement is portrayed by the plots of shear stress versus horizontal shear displacement shown in Figs. 62 and 63, the flat portions in the shear stress versus horizontal shear displacement curves are due to slacks originating from two sources. First, there is the slack due to the fitting of the specimen and the box. The slack due to seating of the specimen within the box is taken up by shear displacement at near zero shear stress levels, indicating that the frictional effect between the two halves of box is negligibly small. The second source of the slack comes from the connection between the upper box and the load cell. The upper box is connected to the load cell via a slip-on connector.

At the request of GCO, two additional specimens, i.e., P8 and P9, were tested. In these tests, the slacks were greatly reduced. The results of the tests on these specimens are presented in Figs. 64 to 70. The shear strength values from these tests are in agreement with the results of the other specimens where the slacks were not corrected .

The results show that this material reaches residual stress after approximately 3 to 4 mm of displacement.

The peak shear stress values and the residual shear stress values of specimens No. P2 to P9 are summarized in Table 8.

The Mohr envelopes corresponding to the peak values and the residual values are presented in Figs. 71 and 72. Values obtained from Specimen P4 are consistently lower than the others. The peak envelope (i.e., ignoring the values from Specimen P4) in Fig. 71 gave an effective friction angle of approximately 40° at high normal stresses. The residual envelope in Fig. 72 gave an effective friction angle of 33° and an effective cohesion of 10 kPa, respectively. Possible explanations for the cohesion not being equal to zero for residual value are: i) material variability ii) the shear strength at low normal stresses may be over-estimated due to insufficient shear displacement to reach residual value, iii) curvature of the envelope at low normal stresses and, iv) experimental error.

The consistently lower values for Specimen P4 may have been due to the loading yoke being caught in some way such that the total load was not fully transferred to the specimen. It might also be due to a variation in the material type and the presence of relict discontinuities. Depending on the orientation of the discontinuities in relation to the direction of shear, the material in the discontinuities can have a major effect on the measured shear strength. It is generally accepted that relict discontinuities in saprolites are often weaker than the weathered rock material (Massey and Pang, 1988). A third possible explanation could be related to the potential energy released as result of the vertical contraction of the specimen during shear. Part of the shearing (i.e., that due to the potential energy) is not accounted for in the measured shear strength.

The results presented so far suggest that this particular soil has a 'critical stress level' of about 100 kPa. The 'critical stress level' is defined as the normal stress above which the soil compresses upon shear. Consequently, below the 'critical stress level' the soil dilates with shear. Irfan (1988) and Massey et al (1989) reported similar type behaviour in granitic (saprolitic) soils from Hong Kong. Irfan (1988) attributed this change in behaviour in the higher applied stress range to the destruction of much of the primary (relict) and secondary

bonding, and the collapse of weak fabric elements during soaking and consolidation. In other words, significant damage to the fragile soil structure occurs at some 'critical stress level' as determined by the microfabric, which in turn is a function of degree and history of weathering and alteration.

5.2.2 SUGGESTED MODIFICATIONS TO THE MAIN TEST PROGRAM

After consideration, it was decided that the programs previously suggested should be slightly modified in order to obtain the most useful amount of data. It has been our experience that soils under suction usually exhibit a steeper shear stress versus shear displacement curve and as such peaks sooner than their saturated counterparts. Also, some preliminary tests carried out show that the specimens become separated at the shear zone if shearing persists too far beyond the peak. Once separation occurs, suction is no longer effective on the shear plane. It is, therefore, recommended that the procedure be modified so that shearing will be stopped once the peak stress is imminent. The shear load would then be removed before loads pertaining to the next stage were applied.

It is also suggested that the tests be confined to the lower suction values. The material is fairly coarse and it is anticipated that the air entry value of the material is not very high. It was recommended that the test suctions be revised to 10, 20, 40, 80, and 160 kPa in place of the previously suggested values of 20, 40, 80, 160 and 320 kPa. It is also recommended that reverse shearing be eliminated to prevent overshearing.

5.3 MAIN TEST PROGRAM

The objective of this part of the program is to determine the effect of applied matric suctions on the shear strength of the soil. The tests were conducted using the modified direct shear apparatus. Matric suctions were controlled using the axis-translation technique. Tests were conducted on 14 specimens. Leakage of air from the air pressure chamber occurred during the testing of three specimens and the results were abandoned. Replacement tests were then conducted.

5.3.1 TEST PROGRAM AND PRESENTATION OF RESULTS

Two series of tests were conducted. The first series of tests was conducted at a net normal stress of 20 kPa. In this series, six specimens were tested. The second series was conducted at a net normal stress of 100 kPa, and five specimens were tested. The pore-air pressures and the pore-water pressures at each stage of the tests are summarized in Table 9.

In the Pilot Test Program, a shear rate of 0.04 mm/min. was used on the modified direct shear box when testing the unsaturated soil specimen. The first test in this study was conducted at a slower rate of 0.028 mm/min. It was later decided to further lower the shearing rate to 0.006 mm/min. in view of the small shear displacement required to reach the peak stress for each stage. The motor for the modified direct shear box broke down after the test on specimen No. US-10. The shear box motor was then replaced. The replacement motor along with the same set of gears gave a shear rate of 0.01 mm/min. for specimen No. US-11. The gear ratio was subsequently changed such that a shear rate of approximately 0.006 mm/min was obtained for the remaining specimens No. US-12, US-13, and US-14. It is our opinion that these slight changes in the shear displacement rate will not affect the test results.

The results of the shear test are presented as plots of shear stress versus shear displacement and as vertical LVDT (linear variable differential transducer) reading versus shear displacement in Figs. 73 to 83. Tests on specimens No. US-2, US-7, and US-8 were abandoned due to air leakage from the chamber.

In Fig. 73 all data points are plotted. In the remaining figures, only every fourth data point is plotted. The plotted curves, however, go through every data points. This procedure is used to avoid cluttering of the plots. The vertical LVDT reading and the horizontal displacement are plotted as the actual readings and as a result are not initialized to start at zero.

The stresses are corrected for the chamber pressure according to the calibration presented in Fig. 84a. The chamber pressure exerts a load on the load-cell which does not induce a shear force to the soil. The data in Fig. 84a was obtained by shearing the shear box without a soil specimen. The usual coating of vacuum grease was applied between the box separation. Shear displacement was applied to the box at various chamber pressures. The shear rate used was 0.006 mm per min. The load-cell reading with respect to the horizontal shear displacement under various chamber pressures are plotted in Figure 84b.

Each specimen was subjected to anywhere from one to five stages of shear under different applied matric suctions. The matric suction values used in these tests were approximately 10 kPa, 20 kPa, 40 kPa, 80 kPa, and 160 kPa. For three specimens, matric suction values of approximately 320 kPa were also used.

During shearing, a continuous visual display of the shear stress development with horizontal displacement was shown on the monitor. Shearing was stopped and the shear load was removed when the visual display showed a levelling off in the developed shear stress. This procedure is admittedly qualitative and is subjective in that judgment is also affected by the scale used for the horizontal displacement. It is essential to limit the extent of shearing at each stage of a multistage shear test. The extent of oversharing or undershearing will affect the results of the subsequent stages.

Pressures equilibration at every stage was determined by monitoring the vertical deflection of the specimen and the water movement from the specimen. The vertical deflection for each stage is presented in Figs. 85 to 95. The volume of water expelled from the specimen with time is presented in Figs. 96 to 106. Generally, all specimens compressed immediately upon application of the net normal stress at the first stage. There was little compression after the first stage as the applied matric suctions were increased. This is an indication that the soil has a fairly rigid structure.

The water contents, degree of saturation, and void ratios of the specimens at natural condition and at equilibration condition of each stage are summarized in Table 10. The data from Table 10 are plotted in Figs. 107 and 108 as matric suction versus water content relationship and as matric suction versus degree of saturation relationship respectively. The initial (or natural) water content and the initial degree of saturation of the fine ash tuff range approximately between 25 % and 30 %, and between 70 % and 80 % respectively. The corresponding initial matric suction from Figs. 107 and 108 is between 15 kPa and 35 kPa.

Three Tempe-cell tests were also conducted on this material. The results are shown as volume of water expelled with time plots in Figs. 109, 110, and 111. The soil water characteristics of the material as established by these Tempe-cell tests are also shown in Figs. 107 and 108 for comparison. The data from Table 10 show good agreement with the results of the Tempe-cell tests. The maximum matric suction applicable in the Tempe-cell is 1 bar pressure. However, Tempe-cell No. 1 and Tempe-cell No. 2 began to leak at suctions of 50 kPa.

Upon attaining pressures equilibration, the net normal stress, the air pressure and the water pressure were applied in this sequence. The external loads were corrected to account for uplift on the loading piston due to the air pressure. With each stage, a corresponding load was added to the loading yoke as the chamber air pressure was increased.

Prior to the commencement of testing, the specimen was flooded with water for at least 8 hours. The height of the specimen before and after soaking was monitored. There was no detectable change in the specimen height at the end of the soaking period. After soaking, the excess water was removed. The measurement of the initial expulsion of water at the first stage is not crucial to the determination of the equilibrium pressure conditions or to the determination of the volume-weight relationships of the specimens.

There was a slight time lapse between the application of the stresses and the first reading of the water movements. This time lapse was inevitable in view of the various adjustments and measurements required by the operator at the start of the test. The water expulsion readings were taken manually.

The water expulsion responses with respect to time during pressures equilibration are shown previously in Figs. 96 to 106. The results indicate that the material is fairly permeable. Suction equilibration is generally well established in most cases, within a day. The first stage generally requires a longer time due to the amount of excess water in the specimen. Even so, suction equilibration is achieved by the second day. The delay is likely more controlled by the permeability of the high air entry disk than the permeability of the soil.

5.3.2 INTERPRETATION OF THE RESULTS

The shear stress versus shear displacement plots were shown in Figs. 73 to 83. The results indicate that generally the shear strength of the soil increases with suction. During the later stages of shear, some specimens (Specimens No. US-3, US-4, and US-6 of Figs. 74, 75, and 77) show a decrease in shear strength with higher suctions. This is likely associated with overshearing which leads to strain softening and/or a separation along the shear faces.

The soil being tested is weakly bonded and the shear stress peaks at relatively small displacements. The approximate shear displacements to peak stress for each stage of each specimens are presented in Table 11. The shear displacements to attain peak strength vary from 0.4 mm to 1.5 mm. Most are between 0.4 mm and 1.0 mm.

The phenomenon of "peaking" is expected to be more pronounced for higher matric suctions. This presents some difficulties in using the multistage shearing procedure for this material. This brittleness may lead to a separation of the shear faces. Once separation occurs, the applied matric suction is less effective across the shear zone. Due to these reasons, the accuracy of the results may decrease during the latter stages. It is speculated that the cohesion portion of the strength will be low or close to zero as shearing progresses from stage to stage. This has a major effect on the results as the matric suction may be considered to be mainly a contribution to the cohesion of the soil.

The difficulties associated with the brittleness of the material and the separation of the shear faces due to excessive shearing are more severe at low net normal stresses. All three specimens which show a decrease in shear strength with matric suction at the latter stages of shearing were subjected to the low net normal stress of 20 kPa. See Figs. 74, 75, and 77.

The specimens that were subjected to a net normal stress of 100 kPa did not show a decrease in shear strength with matric suction. In one specimen (Specimen No. US-5) which was tested at a net normal stress of 100 kPa, the shear strength levelled off after the third stage of shearing. See Fig. 76. The applied matric suction is probably less effective or not at all effective, after the third stage of shearing in this instance due to a separation of the shear faces. However, the shear resistance due to the net normal stress is still effective, resulting in a constant shear strength being obtained in the third and subsequent stages.

The peak shear stresses are plotted against the matric suction values at constant net normal stresses of 20 kPa and 100 kPa respectively in Figs. 112 and 113. The peak shear stress values are also shown tabulated in Table 11. The results show significant scatter. The saturated peak and residual shear strengths at the corresponding net normal stresses of 20 kPa and 100 kPa respectively, are also shown in Figs. 112 and 113. These saturated shear strength values were obtained from the Mohr envelopes for the saturated material which are shown in Figs. 71 and 72. The peak and residual friction angles of the saturated material are also shown in Figs. 112 and 113.

By comparing the saturated shear strength results with the unsaturated shear strength results, there is a definite increase in shear strength with matric suctions. Generally, the results in Figs. 112 and 113 show that the failure envelopes for the shear stress versus matric suction planes at constant net normal stresses have an angle of ϕ^b of approximately equal to ϕ' of 42° at low matric suction values of between 0 and 30 to 40 kPa. This is quite evident from the results of specimens No. US-4 and US-9 in Fig. 112, and the results of specimens No. US-1 and US-5 in Fig. 113. The ϕ^b angle becomes small and approaches zero beyond matric suction values of 70 kPa. In specimens No. US-3, US-4, and US-6, (Fig. 112), the strength envelopes that are likely, if excessive shearing did not occur, are shown by the broken lines.

The initial (or natural) matric suction of the fine ash tuff was estimated from the initial water contents together with the soil water characteristics of the fine ash tuff (Figs. 107 and 108) to be between 15 kPa and 35 kPa. The increase in shear strength due to the initial matric suction value of between 15 kPa and 35 kPa is equivalent to an increase in the cohesion of the fine ash tuff of $\{[15 \text{ kPa to } 35 \text{ kPa}] \times \tan 40^\circ = \underline{12.6 \text{ kPa to } 29.4 \text{ kPa}}\}$ since the ϕ^b angle is approximately equals to the ϕ' angle.

Results of the saturated specimens (see Figs. 71 and 72) show relatively little scatter when compared to the unsaturated test results. The saturated Mohr envelope appears fairly unique. Similar observations were made by Lumb (1965) from tests on undisturbed decomposed granite and decomposed rhyolite. These results were presented previously in Fig. 17. It was reported by Lumb (1965) that the cohesion of the material was strongly affected by the degree of saturation of the specimens. Lumb (loc. cit.) stated that when the soil was saturated, the cohesion dropped to zero and the soil behaved as purely frictional material. However, when the specimens were unsaturated, the cohesion could be as high as 215 kPa (4500 psf). In other words, he was suggesting that there could be a large variation in the cohesion for the unsaturated specimens. No suction measurements were attempted in the tests performed by Lumb (loc. cit.).

A series of triaxial tests on undisturbed decomposed granite and decomposed rhyolite at various applied matric suctions were conducted by Ho and Fredlund (1982) using the multistage shearing procedure. Results from these tests are presented in Fig. 10. The results illustrate the large variability which can occur between specimens. Within each specimen, however, the shear stress to matric suction relationship appears to be quite consistent. There is, however, some nonlinearity in the envelope produced by the smaller increase in strength at higher stages of applied matric suction.

The extreme variability in the shear strength is likely due to the importance of the

initial soil structure of the unsaturated specimens. In saprolitic soils, the structure of the soil is, amongst other factors, also strongly affected by the microfabric of the soils. The microfabric is a function of the nature and intensity of the weathering process (Massey, et al, 1989). Soils from the same block sample could vary considerably in microfabric from point to point.

Material variations within the shear zone were observed from one specimen to another. These variations are difficult to classify by way of particle size distribution or plasticity indices. Grain size distribution analyses conducted on some specimens early in the program are shown in Figs. 114 to 116. Index tests showed that the material passing the No. 10 sieve is nonplastic. A description of the material observed on the shear planes are given in the Appendices (i.e., Volume Two of this report). The description is mainly with regard to color and the appearance of joints. The description is not in terms of mineralogy, petrology or geological properties.

The vertical deflection of the specimen with shear displacement would indicate that the initial fabric of the soil may be maintained from one stage to another. In Figures 73b to 83b, it is observed that the specimens dilate with shear displacement and the specimen is not compressed from one stage to another with increase in matric suction. This can be explained as being the result of particles riding over each other when shearing occurs in a rigid structured soil. This observation is quite different from that observed in Figs. 36 to 59 for the tests on the saturated specimens. In addition the matric suction may be keeping the soil fabric intact in the vicinity of the shear plane by preventing collapse of fragile elements during the shearing process, resulting in a rough surface. Also, the large dilatation occurring at larger shear displacements is probably related to separation of the rough shear surfaces, particularly at low net normal stresses.

In the shear tests on the saturated specimens it was observed that the specimen height generally dilates a little with shear within each cycle of shearing, especially under low normal stresses. However, the specimen height generally decreases from one cycle to another and from one stage to another. This suggests that the structure of the material within the shear zone is continuously breaking down. This may explain the fairly unique Mohr envelopes shown in Figs. 71 and 72 for the saturated specimens. Also, the small vertical deflections with respect to time during pressures equilibration at each stage of the tests further attests to the rigid structure particularly when the soil is subjected to an applied matric suction. (See Figs. 85 to 95).

The tendency for the soil structure to be preserved in soils under applied matric suctions, makes it difficult to establish the failure envelope from single stage tests. In this situation, uniqueness in the relationships between shear stress and shear displacement can be obtained only if the specimens are initially "identical". The problem of "non-identical specimen" can be partly circumvented through the use of the multistage shearing procedure. On the other hand, the brittleness of this material and its pronounced "peaking" phenomenon makes the multistage shearing procedure difficult. However, a combination of both procedures (ie., single stage and multistage shear), can hopefully be used to produce meaningful results.

For single specimens undergoing multistage shear at various applied matric suctions

(e.g., specimen No. US-1), it was generally found that the shear strength increased with matric suction. This was particularly evident in the first to possibly the third stage of the test. Beyond the third stage, the shear strength generally drops due to excessive shearing. Some loss in shear strength is expected due to the shear displacement at each stage. It would appear that the shear strength observed for each stage beyond the first stage is slightly below the actual shear strength which would be observed, if the effects of the shear displacements of the earlier stages were not experienced. Taking this into account, it would appear that the shear strength is, in general, increasing with matric suction.

6. CONCLUSIONS

Following are specific conclusions arrived at as a result of the testing program conducted on the fine ash tuff samples from Hong Kong.

- (i) The effective shear strength parameters as determined from direct shear strength tests on the saturated fine ash tuff from Hong Kong are

$$\begin{aligned}\phi'_{\text{peak}} &= 40^\circ, \\ \phi'_{\text{residual}} &= 33^\circ, \\ c'_{\text{residual}} &= 10 \text{ kPa}\end{aligned}$$

There appears to be some curvature or nonlinearity in the peak strength envelope at low stress levels. This nonlinearity at low stress levels is of significance particularly in slope stability involving shallow slip surfaces.

- (ii) The saturated peak stress and residual stress Mohr envelopes appears to be fairly unique, despite the variability of the specimens and its microfabric. The residual shear strengths appear to have a larger spread at normal stresses of about 200 kPa.
- (iii) The peak strength envelope suggests that the fine ash tuff has a 'critical stress level' of about 100 kPa. The 'critical stress' is the stress at which the soil changes from one with dilatant behaviour with shear to one with compressional behaviour with shear.
- (iv) The soil water characteristics of the fine ash tuff as expressed by its suction versus water content relationship and its suction versus degree of saturation relationship bear the classic "S" shape. The saturated water content ranges between 30 % and 45 %. The soil has an air entry value close to zero matric suction. The soil water drains rapidly at low matric suction values. Increasing the matric suction from zero to 50 kPa results in a reduction in the water content of the fine ash tuff from 44 % - 31 % to 28 % - 22 %. The residual water content appears to be at approximately 12 %. The corresponding residual degree of saturation is approximately 30 %. A specimen at the residual water content undergoes very small changes in water content with further increase in the matric suction.
- (v) The initial (natural) water content of the fine ash tuff is between 25 % and 30 %. The initial degree of saturation is between 70 % and 80 %. The estimated initial (natural) matric suction of the fine ash tuff is between 15 kPa and 35 kPa.
- (vi) The fine ash tuff is quite permeable. Matric suction equilibration time for specimen of size 50 mm x 50 mm x 21.4 mm is about 1 day at matric suctions of 0 to 300 kPa. The time to equilibration may be partly controlled by the permeability of the high air entry disk at the base of the specimen.

- (vii) The shear strength of the fine ash tuff increases with matric suction. The increase in shear strength with matric suction as described by the parameter ϕ^b is approximately equal to ϕ' (i.e. 40°) at low matric suctions ranging from 0 to about 30 kPa to 40 kPa. With higher matric suctions, the ϕ^b angle begins to decrease. The ϕ^b angle approaches an angle of zero degrees at matric suctions above 70 kPa.
- (viii) The effect of matric suction on the fine ash tuff at the estimated natural (insitu) matric suctions of 15 kPa to 35 kPa is significant since the ϕ^b angle is approximately equal to ϕ' for matric suctions below about 30 kPa to 40 kPa. The increase in shear strength due to the insitu suction is equivalent to an increase in cohesion of 12.6 kPa to 29.4 kPa. This increase in shear strength is substantial especially in slope stability involving shallow slip surfaces.
- (ix) The unsaturated fine ash tuff has a rigid structure. The soil shows negligible volume change with change in matric suction. The initial fabric appears to have a major influence on the shear strength of the soil. As a result, the shear strength versus matric suction relationship of the fine ash tuff at a constant net normal stress, is highly variable. This variability in the shear strength appears to be due to the variability in the material and its microfabric from one specimen to another. The large variability in the unsaturated shear strengths makes it difficult to use exclusively single stage shear tests. The random scatter of the shear strength results makes interpretation difficult.
- (x) Direct shear tests conducted on saturated specimens of the fine ash tuff show that the shear strength peaks after a small shear displacement of 3 mm to 4 mm. Direct shear tests conducted on the fine ash tuff under applied matric suctions show that the soil reaches peak shear strength after a smaller displacement of 1 mm and less. The fine ash tuff thus becomes more brittle with matric suctions.
- (xi) The brittleness of the fine ash tuff makes it difficult to use exclusively the multistage shearing procedure for this soil. Excessive shearing could lead to a total loss in cohesion and may also cause a separation of shear planes. Once separation occurs, the matric suction is less effective across the shear zone.

7. RECOMMENDATION FOR FURTHER RESEARCH

7.1 LABORATORY STUDIES

Considerable scatter in the data was observed in the present study when attempting to define the shear stress versus applied matric suction relationship. The scatter is believed to be primarily due to the heterogeneity of the material and possibly the large variability in the microfabric of the specimens. As a result, it is difficult to accurately define the shear strength.

The test results from the present study show that the shear strengths do indeed increase with matric suction. However, it was found difficult to define the failure envelope using either the single stage shear procedure or the multistage shear procedure.

Using the single stage shear procedure, scatter in the results is inevitable due to the heterogenous nature of the material. This is particularly accentuated through the use of small test specimens. When using the multistage shear procedure, excessive shearing of the specimens results in strain softening. This reduces the shear strength and becomes particularly significant beyond the second stage.

The scatter in the test data could possibly be reduced using one of several ways. Several alternatives which could be considered for phase two of the research program are listed as follows.

7.1.1 ALTERNATIVE NO. 1

Conduct a series of two stage direct shear tests using the modified shear box equipment. All specimens should be subjected in the first stage to the same normal stress and matric suction. In the second stage, the matric suctions could be varied for each specimen.

The data obtained from the first stage could be used for comparison or for normalization such that specimens with similar properties can be selected for comparison. The shear strength at a selected shear displacement (prior to peak stress) in the first stage would likely be used in the analysis. This would also reduce the possibility of excessive shearing during the first stage. The peak strengths from the second stage could be separated into groups according to data from the first stage. In this way one envelope could be obtained for each group of soils.

7.1.2 ALTERNATIVE NO. 2

Conduct two stage direct shear tests using the modified direct shear box. In both stages, the specimens could be sheared to obtained peak strengths. In the first stage, the specimens could be unloaded when the peak strength is approached. Shearing in the second stage could proceed beyond the peak strength.

Different combinations of matric suctions could be investigated keeping the normal stress constant. For example, in the first stage, specimens could be subjected to matric suctions of 10 kPa, 20 kPa, 40 kPa, 80 kPa, etc., and in the second stage the corresponding specimens could be subjected to matric suctions of 60 kPa, 70 kPa, 90 kPa, 130 kPa, etc., keeping a constant increment of 50 kPa between the first and second stage. Other variations could also be investigated. For example, a different matric suction increment (e.g., 80 kPa) could be used. Or else, different matric suction increments could be used for each specimen. In this way, various two point envelopes could be established.

Two stage shear tests are preferable as the effects of matric suction are more easily observed by comparing the results of each pair (i.e., 'identical' specimens for the first and second stages). In one stage shear tests, the random scatter of the data makes interpretation difficult and the effects of matric suction are then difficult to quantify.

7.1.3 ALTERNATIVE NO. 3

The procedure as described in alternative No. 1 and alternative No. 2 could be conducted on larger specimens. With larger specimens, the effects of material heterogeneity and the variability of microfabric would be suppressed. The existing modified shear box is made for a specimen size of 50 mm by 50 mm. To handle larger specimens (e.g., 100 mm by 100 mm), a new direct shear box (and possibly a new chamber) would have to be fabricated.

Our estimate is that the costs to build a new shear box (without the chamber) would be in the order of \$6000 (Canadian). The chamber and accessories would cost another approximately \$7000 (Canadian). These costs are only a rough estimate and a firm quotation would have to be obtained from the fabricators.

7.1.4 OTHER SUGGESTIONS

Another avenue for further research involves the use of triaxial tests under applied matric suctions. Early in our proposal on the direct shear testing of soils under applied suctions, GCO expressed an interest in also conducting a parallel program of triaxial tests. In view of the relatively high permeability of the soil being tested, it is our opinion that triaxial testing equipment would work satisfactorily. 2 1/2 - inch diameter specimens would be preferable to 4 - inch diameter specimens in order to ensure a reasonable testing time.

The multistage shearing procedure appeared to be quite successful in a previous test program on decomposed granite and decomposed rhyolite from Hong Kong (Ho and Fredlund, 1982). It is suggested that the multistage shearing procedure be attempted for the fine ash tuff.

7.2 ANALYTICAL STUDIES

The goal of the shear strength studies is presumably their application in the area of

slope stability analysis. In a thorough stability analysis, the strength characterization of the soils is only one component. Equally important is the characterization of the permeability properties of the soil. The climate being another factor of importance.

7.2.1 INTEGRATED SLOPE STABILITY-SEEPAGE MODELLING

In the characterization of the shear strength of the soil, It is necessary to determine the changes of the shear strength with respect to changes in negative pore-water pressures, assuming that the total stresses do not change. Changes in the negative pore-water pressures are, however, affected by the climatic conditions, the geometry of the slope, and the permeability of the material.

As a separate phase of research, we would suggest that an analytical study could be conducted. This phase would be divided into two parts. The first part of the study would be used to characterize the permeability properties of the soil. This would be done through the use of Tempe-cell tests and/or pressure plate tests and saturated permeability tests.

The second part of the study would be to model some typical slopes taking into consideration the climatic factors and engineering properties of the soil. Various surface flux boundary conditions could be obtained from hydrological modelling based on the regional climatic conditions. Saturated-unsaturated flow modelling could then be combined with limit equilibrium slope stability analysis to study the response of the slope to various microclimatic conditions.

It may also be worthwhile to consider performing three-dimensional slope stability analysis for shallow slip surfaces. The three-dimensional analysis would more accurately model insitu conditions. We believe that with this type of analysis, the contribution of matric suction to slope stability will prove to be quite significant.

In addition, a review of cases presented in literature shows that failures in saprolites and residual soils are usually of the three-dimensional type (Massey and Pang, 1988). Slope stability in weathered rocks are strongly affected by the weaker relict discontinuities. Often the orientation of these relict discontinuities will result in narrow zones of unstable slopes and end effects are highly significant, making a three-dimensional analysis mandatory.

7.2.2 STRESS PATH DEPENDENCY

There may be some concern that the stress paths being followed in the laboratory studies are not the same as the stress paths followed in the field. The significance of this difference could be investigated through a laboratory study and a theoretical or analytical study.

The laboratory study would investigate the significance of differing stress paths on the shear strength of the soil as it is defined in terms of the stress state variables.

8. REFERENCES

- Aitchison, G. D., 1959. "The Strength of Quasi-Saturated and Unsaturated Soils in Relation to the Pressure Deficiency in the Pore Water", Proceedings of the Fourth International Conference on Soil Mechanics and Foundation Engineering, London, pp. 135-139.
- Bishop, A. W. and Eldin, E. K. G., 1950. "Undrained Triaxial Tests on Saturated Soils and their Significance in the General Theory of Shear Strength", *Geotechnique*, Vol. 2, pp. 13-32.
- Bishop, A. W., 1959. "The Principle of Effective Stress", Lecture delivered in Oslo, Norway in 1955, printed in *Teknisk Ukeblad*, Vol. 106, No.39, pp. 859-863.
- Bishop, A. W., Alpan, I., Blight, G. E. and Donald I. B., 1960. "Factors Controlling the Shear Strength of Partly Saturated Cohesive Soils", ASCE Research Conference on Shear Strength of Cohesive Soils, Boulder, Colorado, pp. 505-532.
- Bishop, A. W., 1961. "The Measurement of Pore Pressure in the Triaxial Test", Proceedings of the Conference on Pore Pressure and Suction in Soils, Butterworths, London, pp. 38-46.
- Bishop, A. W. and Donald, I. B., 1961. "The Experimental Study of Partly Saturated Soil in the Triaxial Apparatus", Proceedings of the Fifth International Conference on Soil Mechanics and Foundation Engineering, Paris, pp. 13-21.
- Bishop, A. W. and Henkel, D. J., 1962. *The Measurement of Soil Properties in the Triaxial Test*, Second Edition, Edward Arnold (Publisher) Ltd., London, pp.180-211.
- Bishop, A. W. and Blight, G. E., 1963. "Some Aspects of Effective Stress in Saturated and Unsaturated Soils", *Geotechnique*, Vol. 13, No. 3, pp. 177-197.
- Blight, G. E., 1966. "Strength of Desiccated Clays", *Journal of the Soil Mechanics and Foundation Division, ASCE*, Vol. 92, SM6, pp. 19-37.
- Blight, G. E., 1967. "Effective Stress Evaluation for Unsaturated Soils", *Journal of the Soil Mechanics and Foundation Division, ASCE*, Vol. 93, SM2, pp. 125-148.
- Chantawarangul, K., 1983. "Comparative Study of Different Procedures to Evaluate Effective Stress Strength Parameters for Partially Saturated Soils." M.Eng. Thesis, Asian Institute of Technology, Bangkok, Thailand.
- Donald, I. B., 1956. "Shear Strength Measurements in Unsaturated, Non-Cohesive Soils with Negative Pore Pressures", Proceedings of the Second Australia and New Zealand Conference on Soil Mechanics and Foundation Engineering, pp. 200-205.
- Donald, I. B., 1963. "Effective Stress Parameters in Unsaturated Soils", Proceedings of the Fourth Australia and New Zealand Conference on Soil Mechanics and Foundation Engineering, Adelaide, pp. 41-46.

- Drumright, E. E., 1989. "The Contribution of Matric Suction to the Shear Strength of Unsaturated Soils", Ph.D Thesis, University of Colorado, Fort Collins, USA.
- Edil, T. S., Motan, S. E. and Toha, F. X., 1981. "Mechanical Behaviour and Testing Methods of Unsaturated Soils", Laboratory Shear Strength of Soil, ASTM Special Technical Publication No. 740, edited by Yong R. N. and Townsend F. C., pp. 114-129.
- Escario, V., 1980. "Suction Controlled Penetration and Shear Tests", Proceedings of the Fourth International Conference on Expansive Soils, Denver, ASCE, Vol. 2, pp. 781-797.
- Escario, V., and Saez J., 1986. "The Shear Strength of Partly Saturated Soils", *Geotechnique*, Vol.36, No. 3, pp. 453-456.
- *Fredlund, D. G., 1979. "Second Canadian Colloquium : Appropriate Concepts and Technology for Unsaturated Soils", *Canadian Geotechnical Journal.*, Vol. 16, No. 1, pp. 121-139.
- *Fredlund, D. G., 1989. "The Character of the Shear Strength Envelope for Unsaturated Soils", *De Mello Volume*, edited by Penna J. C., Editura Edgard Blucher Ltd., Sao Paulo, pp. 142-149.
- *Fredlund, D. G., and Morgenstern, N. R., 1977. "Stress State Variables for Unsaturated Soils", *Journal of the Geotechnical Engineering Division, ASCE* Vol. 103, GT5, pp.447-466.
- *Fredlund, D. G., Morgenstern, N. R., and Widger, R. A., 1978, "The Shear Strength of Unsaturated Soils", *Canadian Geotechnical Journal*, Vol. 15, No. 3, pp.313-321.
- *Fredlund, D. G., Rahardjo, H. and Gan, J. K., 1987. "Nonlinearity of the Strength Envelope for Unsaturated Soils", *Proceedings of the Sixth International Conference on Expansive Soils*, New Delhi, pp 49-54.
- *Gan, J. K., 1986. "Direct Shear Strength Testing of Unsaturated Soils", M.Sc Thesis, Department of Civil Engineering, University of Saskatchewan, Saskatoon, Canada.
- *Gan, J. K., and Fredlund, D. G., 1988. "Multistage Direct Shear Testing of Unsaturated Soils", *ASTM Geotechnical Testing Journal*, Vol. 11, No. 2, pp. 132-138.
- *Gan, J. K., Fredlund, D. G. and Rahardjo, H., 1988. "Determination of the Shear Strength Parameters of an Unsaturated Soil using the Direct Shear Test", *Canadian Geotechnical Journal*, Vol. 25, No. 8, pp. 500-510.
- Gibbs, H. J., Hilf, J. W., Holtz, W. G. and Walker, F. C., 1960. "Shear Strength of Cohesive Soils", *ASCE Research Conference on Shear Strength of Cohesive Soils*, Boulder, Colorado, pp. 33-162.

- Gibbs, H. J. and Coffey, C. T., 1969. "Application of Pore Pressure Measurements to Shear Strength of Cohesive Soils", Report No. EM-761, Soils Engineering Branch, U. S. Department of the Interior, Bureau of Reclamation, Denver, Colorado.
- Gulhati, S. K. and Satija, B. S., 1981. " Shear Strength of Partially Saturated Soils", Proceedings of the Tenth International Conference on Soil Mechanics and Foundation Engineering, Stockholm, Sweden, Vol. 1, pp 609-612.
- Hilf, J. W., 1956. "An Investigation of Pore Pressures in Compacted Cohesive Soils", Technical Memo, 654, U. S. Department of Interior, Bureau of Reclamation, Denver, Colorado.
- *Ho, D. Y. F. and Fredlund, D. G., 1982a. "Multi-Stage Triaxial Tests for Unsaturated Soils", ASTM Geotechnical Testing Journal, Vol. 5, pp. 18-25.
- *Ho, D. Y. F. and Fredlund, D. G., 1982b. "Strain Rates for Unsaturated Soil Shear Strength Testing", Proceedings of the Seventh Southeast Asian Geotechnical Conference, Hong Kong, pp 787-803.
- Irfan, T. Y., 1988. "Fabric Variability and Index Testing of a Granitic Saprolite." Proceedings of the Second International Conference on Geomechanics in Tropical Soils, Singapore, Vol. 1, pp. 25-35.
- Jennings, J. E. and Burland, J. B., 1962. "Limitations of the Use of Effective Stresses in Partly Saturated Soils", Geotechnique, Vol. 12, No. 2, pp.125-144.
- Kassif, G., 1957. "Compaction and Shear Characteristics of Remoulded Negev Loess", Proceedings of the Fourth International Conference on Soil Mechanics and Foundation Engineering, London, pp. 56-61.
- Knodel, P. C. and Coffey, C. T., 1966. "Measurement of Negative Pore Pressure of Unsaturated Soils - Shear and Pore Pressure Research - Earth Research Program", Laboratory Report No. EM-738, Soil Engineering Branch, U.S. Department of the Interior, Bureau of Reclamation, Denver, Colorado, 20 p.
- Komornik, A., Livneh, M. and Smucha, S., 1980. "Shear Strength and Swelling of Clays Under Suction", Proceedings of the Fourth International Conference on Expansive Soils, Colorado, Vol. 1, pp. 206-226.
- Ladd, R. S., 1978. "Preparing Test Specimens using Undercompaction." ASTM Geotechnical Testing Journal, Vol. 1, No. 1, pp. 16-23.
- Lumb, P., 1965. "The Residual Soils of Hong Kong", Geotechnique, Vol. 15, pp. 180-194.
- Massachusetts Institute of Technology, 1963. "Engineering Behaviour of Partially Saturated Soils", Phase Report No. 1 to U. S. Army Engineers, Waterways Experimental Station, Vicksburg, Mississippi, Soil Engineering Department, Department of Civil Engineering, M. I. T., Contract No. DA-22-079-ENG-288.

- Massey, J. B. and Pang, P. L. R., 1988. "General Report : Stability of Slopes and Excavations in Tropical Soils," Second International Conference on Geomechanics in Tropical Soils, Singapore, Vol. 2, pp. 551-570.
- Massey, J. B., Irfan, T. Y. and Cipullo, A., 1989. "The Characterization of Granitic Saprolitic Soils", International Conference on Soil Mechanics and Foundation Engineering, Rio de Janeiro, Vol. 1, pp. 533-542.
- Matyas, E. L. and Radhakrishna, H. S., 1968. "Volume Change Characteristics of Partially Saturated Soils", Geotechnique, Vol. 18, No. 4, pp. 432-448.
- Neves, E. M. D., 1971. "Influência das Tensões Neutras Negativas nas Características Estruturais dos Solos Compactados", Ministério das Obras Públicas, Laboratório Nacional de Engenharia Civil, Memoria No. 386.
- Peterson, R. W., 1988. "Interpretation of Triaxial Compression Test Results on Partially Saturated Soils", Advanced Triaxial Testing of Soil and Rock, ASTM Special Technical Publication No. 977, pp. 512- 538.
- Satija, B. S., 1978. "Shear Behaviour of Partly Saturated Soils", Unpublished Ph.D. Thesis, Indian Institute of Technology, Delhi, India.
- Satija, B. S., and Gulhati S. K., 1979. "Strain Rate for Shear Testing of Unsaturated Soils", Proceedings of the Sixth Asian Reg. Conference on Soil Mechanics and Foundation Engineering, Singapore, pp. 83-86.
- Taylor, D. W., 1948. Fundamentals of Soil Mechanics, John Wiley and Sons, New York.
- Terzaghi, K., 1936. "The Shearing Resistance of Saturated Soils." Proceedings of the First International Conference on Soil Mechanics and Foundation Engineering, Cambridge, Massachusetts, Vol. 1, pp 54-56.
- Toll, D. G., 1990. " A Framework for Unsaturated Soils Behaviour", Geotechnique, Vol. 40, No. 1, pp. 31-44.
- Williams, J. and Shaykewich, C. F., 1970. "The Influence of Soil Water Matric Potential on the Strength Properties of Unsaturated Soil", Proceedings of the Soil Science Society of America, Vol. 34, No. 6, Div. S-1, pp. 835-840.

LIST OF TABLES

Table No.		Page No.
1	Summary of Effective Stress Equations for Unsaturated Soils (From Chantawarangul, 1983)	49
2	Experimental Value of ϕ^b	50
3	Initial Conditions of Direct Shear Specimens in the Pilot Test Programs	51
4	Revised Preliminary and Main Test Programs	51
5	Time Schedule for Revised Program	52
6	Normal Stresses Applied at Various Stages in the Preliminary Test Program	53
7	Initial Conditions of Direct Shear Specimens in Preliminary Test Program	53
8	Peak Shear Strengths and Residual Shear Strengths of Specimens in the Preliminary Test Program and the Pilot Test Program	54
9	Pore-air Pressures, Pore-water Pressures and Net Normal Stresses used in Main Test Program	55
10	Water Content, Degree of Saturation and Void Ratios of Specimens in Main Test Program	56
11a	Applied Matric Suction Values, Peak Strength Values and Approximate Shear Displacement to Attain Peak Strength. Specimens Subjected to Net Normal Stresses of 100 kPa	57
11b	Applied Matric Suction Values, Peak Strength Values and Approximate Shear Displacement to Attain Peak Strength. Specimens Subjected to Net Normal Stresses of 20 kPa	57

Table 1 - Summary of Effective Stress Equations for Unsaturated Soils
(from Chantawarangul, 1983)

Authority	Equation	Description of Variables
BISHOP (1959)	$\sigma' = \sigma - u_a + x (u_a - u_w)$	x = parameter related to the degree of saturation u _a = pressure in gas and vapor phase
CRONEY et al (1958)	$\sigma' = \sigma - \beta' u_w$ (atmospheric pressure)	u _w = pressure in liquid phase β' = holding or bonding factor which is a measure of number of bonds under tension effective in contributing to soil strength
LAMBE (1960)	$\sigma' = \bar{\sigma} a_m + u_a a_a + u_w a_w + R - A$	σ = combined total stress between adjacent particles
LAMBE & WHITMAN (1969)	$\sigma' = \sigma - u_a + a_w (u_a + u_w)$	$\bar{\sigma}$ = contact stress where the particles are in mineral-mineral contact a _m = ratio mineral-mineral contact to total area a _a = fraction of total area that is air-mineral cont. a _w = "-", water-mineral cont. R-A = Repulsive minus attractive pressures between particles
AITCHISON (1960)	$\sigma' = \sigma + \psi p''$ (atmospheric pressure)	ψ = parameter with values ranging from zero to one p'' = pore water pressure deficiency
JENNINGS (1960)	$\sigma' = \sigma + \beta p''$ (atmospheric pressure)	β = statical factor of same type as contact area should be measured experimentally in each case
RICHARDS (1966)	$\sigma' = \sigma - u_a + X_m (h_m + u_a) + x_s (h_s + u_a)$	X _m = effective stress parameter for capillary / matrix suction h _m = capillary / matrix suction X _s = effective parameter for solute suction h _s = solute suction (osmotic effect)

Table 2 - Experimental Value of ϕ^b

Soil Type	c' (kPa)	ϕ' (degrees)	ϕ^b (degrees)	Test Procedure	Reference
Compacted shale; $v = 18.6\%$	15.8	24.6	18.1	Constant water content triaxial	Bishop, Alpan, Blight and Donald (1960)
Boulder clay; $v = 11.6\%$	9.6	27.3	21.7	Constant water content triaxial	Bishop, Alpan, Blight and Donald (1960)
Dhanauri clay; $v = 22.2\%$, $\rho_d = 1580 \text{ kg/m}^3$	37.3	28.5	16.2	Consolidated drained triaxial	Satiya, (1978)
Dhanauri clay; $v = 22.2\%$, $\rho_d = 1478 \text{ kg/m}^3$	20.3	29.0	12.6	Consolidated drained triaxial	Satiya, (1978)
Dhanauri clay; $v = 22.2\%$, $\rho_d = 1580 \text{ kg/m}^3$	15.5	28.5	22.6	Constant water content triaxial	Satiya, (1978)
Dhanauri clay; $v = 22.2\%$, $\rho_d = 1478 \text{ kg/m}^3$	11.3	29.0	16.5	Constant water content triaxial	Satiya, (1978)
Madrid gray clay; $v = 29\%$ $\rho_d = 131 \text{ kg/m}^3$	23.7	22.5 ^a	16.1	Consolidated drained direct shear	Escario, (1980)
Undisturbed decomposed granite; Hong Kong	28.9	33.4	15.3	Consolidated drained multi-stage triaxial	Ho and Fredlund (1982)
Undisturbed decomposed rhyolite; Hong Kong	7.4	35.3	13.8	Consolidated drained multi-stage triaxial	Ho and Fredlund (1982)
Tappen-Notch Hill silt; $v = 21.5\%$, $\rho_d = 1590 \text{ kg/m}^3$	0	35.0	16.0	Consolidated drained multi-stage triaxial	Krahn, Fredlund and Klassen (1987)

^a Average value.

Table 3 - Initial Conditions of Direct Shear Specimens in the Pilot Test Programs

Specimen No.	Natural Water Content %	Void Ratio	Degree of Saturation %
DS1B	27.7	0.940	80.0
DS1C	24.5	0.880	71.0
MDS1	25.2	1.000	68.0

Table 4 - Revised Preliminary and Main Test Programs

Preliminary tests to establish c' and ϕ' (saturated specimens).							
Specimen No.	Normal stress, kPa						
	10	30	50	100	200		
1	1*	2	3	4	5		
2		1	2	3	4		
3			1	2	3		
4				1	2		
5					1		
Main test program (unsaturated specimens)							
Series No.	Normal stress, kPa	Specimen No.	Suction, kPa				
			20	40	80	160	320
1	20	6	1*	2	3	4	5
		7		1	2	3	4
		8			1	2	3
		9				1	2
		10					1
2	100	11	1*	2	3	4	5
		12		1	2	3	4
		13			1	2	3
		14				1	2
		15					1
* denotes stage no.							

Table 5 - Time Schedule for Revised Program

Preliminary Test (Saturated Specimens)		
Specimen No. 1 (5 stages)		
- Preparation of Specimen		
Trimming and saturation		1 day
Stage 1	Consolidation	1 day
	Shear test (2 cycles)	
Stage 2		2 days
Stage 3		2 days
Stage 4		2 days
Stage 5		2 days
Taking down specimens and preparation for next test		3 days
		<u>14 days</u>
Specimen No. 2 (4 stages)		12 days
Specimen No. 3 (3 stages)		10 days
Specimen No. 4 (2 stages)		8 days
Specimen No. 5 (1 stage)		6 days
		<u>50 days</u> 50 days
Main Program (unsaturated specimens)		
- Testing equipment to ensure proper functioning		7 days/series 14 days
Specimen No. 1 (5 stages)		
- Preparation of specimen		
Trimming and saturation		1 days
Stage 1	Equalization of pressure	2 days
	Shear test (2 cycles)	1 day
Stage 2		3 days
Stage 3		3 days
Stage 4		3 days
Stage 5		3 days
Taking down specimens and preparation for next test		3 days
		<u>19 days</u>
Specimen No. 2 (4 stages)		16 days
Specimen No. 3 (3 stages)		13 days
Specimen No. 4 (2 stages)		10 days
Specimen No. 5 (1 stage)		7 days
		<u>65 days</u>
2 Series @ 65 days/series		130 days
One month to analyze data and prepare the final report. Have it reviewed by GCO and finalized		30 days
		<u>224 days</u>

Table 6 - Normal Stresses Applied at Various Stages in the Preliminary Test Program

Series No.	Specimen No.	Stage No.				
		1	2	3	4	5
1	P2	49.8	100.1	201.2		
2	P3	9.4	29.7	50.2	100.5	201.7
3	P4	207.1	107.4	55.9	29.7	9.4
4	P5	101.5	202.7			
5	P6	30.0	50.3	100.9	202.0	
6	P7	201.0	99.8	54.2	30.5	16.2
7	P8	50.4	101.1	202.1		
8	P9	28.8	54.1	104.6	211.7	

units of kPa

Table 7 - Initial Conditions of Direct Shear Specimens in Preliminary Test Program

Specimen No.	Natural Water Content %	Void Ratio	Degree of Saturation %
P2	28.4	0.987	78.1
P3	27.3	0.936	79.1
P4	27.9	1.095	69.2
P5	29.0	1.121	70.2
P6	28.2	1.013	75.6
P7	31.0	1.056	79.5
P8	27.3	1.000	74.0
P9	24.8	0.961	70.0

Table 8 - Peak Shear Strengths and Residual Shear Strengths of Specimens in the Preliminary Test Program and the Pilot Test Program

SPECIMEN NO.	STAGE NO.	NORMAL STRESS kPa	PEAK STRESS kPa	RESIDUAL STRESS kPa
P2	S1	49.8	76	40
	S2	101.1		75
	S3	201.2		145
P3	S1	9.4	28	17
	S2	29.7		36
	S3	50.2		50
	S4	100.5		80
	S5	201.7		140
P4	S1	207.1	120	120
	S2	107.4		70
	S3	55.9		37
	S4	29.7		23
	S5	9.4		7
P5	S1	101.5	85	74
	S2	202.1		135
P6	S1	30.1	66	32
	S2	50.3		44
	S3	100.9		81
	S4	200.1		150
P7	S1	201.1	180	160
	S2	99.8		80
	S3	54.2		47
	S4	30.5		27
	S5	16.2		17
P8	S1	50.4	85	50
	S2	101.1		75
	S3	202.1		135
P9	S1	28.8	60	32
	S2	54.1		50
	S3	104.6		80
	S4	211.7		170
DS1B		20.0	39	20
DS1C		12.4	53	18

Table 9 - Pore-air Pressures, Pore-water Pressures and Net Normal Stresses used in Main Test Program

Specimen no.	Stage No. 1			Stage No. 2			Stage No. 3			Stage No.4			Stage No.5			$\sigma - u_a$
	u_a	u_w	$u_a - u_w$	u_a	u_w	$u_a - u_w$	u_a	u_w	$u_a - u_w$	u_a	u_w	$u_a - u_w$	u_a	u_w	$u_a - u_w$	
US- 1	110.0	103.4	6.6	121.0	103.9	17.1	144.0	102.9	41.1	170.0	101.7	68.3	257.0	104.4	152.6	100
US- 3	83.0	39.8	43.2	128.0	40.8	87.2	223.0	40.9	182.1	372.0	40.7	331.3				20
US- 4	55.0	44.6	10.4	66.0	45.1	20.9	89.0	44.6	44.4	134.0	45.4	88.6	234.0	45.0	189.0	20
US- 5	69.0	51.7	17.3	90.0	50.1	39.9	135.0	52.5	82.5	235.0	52.2	182.8	359.0	53.0	306.0	100
US- 6	127.0	47.6	79.4	207.0	47.1	159.9	368.0	48.8	319.2							20
US- 9	50.0	31.7	18.3	90.0	31.8	58.2	195.0	30.0	165.0							20
US-10	108.0	29.3	78.7	192.0	30.4	161.6										100
US-11	70.0	31.3	38.7	115.0	33.5	81.5	214.0	33.1	180.9							100
US-12	200.0	41.1	158.9													20
US-13	214.0	55.3	158.7													100
US-14	200.0	39.0	161.0													20

units of kPa

Table 10 - Water Content, Degree of Saturation and Void Ratios of Specimens in Main Test Program

Specimen no.	Initial			Stage No. 1			Stage No. 2			Stage No. 3			Stage No. 4			Stage No.5		
	w %	S _r %	e	w %	S _r %	e	w %	S _r %	e	w %	S _r %	e	w %	S _r %	e	w %	S _r %	e
US- 1	31.1	73.5	1.15	35.9	89.8	1.11	34.7	86.6	1.10	29.7	73.8	1.09	21.3	52.7	1.09	15.7	38.4	1.08
US- 3	28.3	70.7	1.08	25.4	63.6	1.08	19.0	47.6	1.08	13.9	34.9	1.08	11.6	29.1	1.08			
US- 4	27.9	81.4	0.93	28.7	83.7	0.93	27.1	78.9	0.93	23.7	69.1	0.93	17.7	51.5	0.93	13.5	39.3	0.93
US- 5	27.6	77.9	0.96	31.4	90.5	0.94	27.0	77.8	0.94	20.2	58.2	0.94	14.7	42.4	0.94	11.8	34.0	0.94
US- 6	28.4	76.1	1.01	18.6	49.8	1.01	13.9	37.3	1.01	10.9	29.2	1.01						
US- 9	28.0	75.6	1.00	27.7	75.0	1.00	21.7	58.7	1.00	14.3	38.6	1.00						
US-10	27.0	75.6	0.97	17.9	50.9	0.95	11.3	32.1	0.95									
US-11	26.3	75.1	0.95	20.4	60.2	0.92	17.7	52.2	0.92	12.3	36.2	0.92						
US-12	25.7	68.5	1.09	16.8	43.0	1.06												
US-13	26.8	64.3	1.13	15.0	37.0	1.10												
US-14	21.6	65.7	0.89	13.2	40.2	0.89												

w - water content

S_r - degree of saturation

e - void ratio

S1 - Stage 1, S2 - Stage 2, S3 - Stage 3, S4 - Stage 4, S5 - Stage 5

These are values at suction equilibration condition.

Table 11a - Applied Matric Suction Values, Peak Strength Values and Approximate Shear Displacement to Attain Peak Strength. Specimens Subjected to Net Normal Stresses of 100 kPa

Specimen No.	Stage No.	Matric Suction kPa	Peak Stress kPa	Shear Displacement mm
US- 3	1	43.2	77.0	0.7
	2	87.2	82.6	0.45
	3	182.1	80.2	0.5
	4	331.3	68.8	0.5
US- 4	1	10.4	95.6	0.7
	2	20.9	99.2	0.45
	3	44.4	98.5	0.4
	4	88.6	82.0	0.4
	5	189.0	74.0	0.45
US- 6	1	79.4	87.3	0.065
	2	159.9	94.9	0.5
	3	319.2	81.3	0.4
US- 9	1	18.3	51.5	1.0
	2	58.2	67.2	0.65
	3	165.0	71.4	0.6
US-12	1	158.9	37.4	1.5
US-14	1	161.0	65.5	0.7

Table 11b - Applied Matric Suction Values, Peak Strength Values and Approximate Shear Displacement to Attain Peak Strength. Specimens Subjected to Net Normal Stresses of 20 kPa

Specimen No.	Stage No.	Matric Suction kPa	Peak Stress kPa	Shear Displacement mm
US- 1	1	6.6	80.2	0.9
	2	17.1	96.3	0.9
	3	41.1	110.1	0.8
	4	68.3	120.9	0.8
	5	152.6	129.7	0.8
US- 5	1	17.3	162.5	0.85
	2	39.9	177.5	0.65
	3	82.5	184.8	0.65
	4	182.8	184.5	0.6
	5	306.0	179.7	0.65
US-10	1	78.7	153.5	1.10
	2	161.6	166.5	0.60
US-11	1	38.7	153.2	0.55
	2	81.5	156.7	0.4
	3	180.9	161.2	0.4
US-13	1	158.7	156.8	1.3

LIST OF FIGURES

Figure No.		Page No.
1	Extended Mohr-Coulomb Failure Envelope	69
2	Two Dimensional Representation of Failure Envelopes Corresponding to Different ($U_a - U_w$)	69
3	Shear Box Apparatus for Testing Soils under Low Matric Suctions (from Donald, 1956)	70
4	Results of Direct Shear Tests on Sands under Low Matric Suctions (from Donald, 1956)	71
5	Two Failure Envelopes for an Unsaturated Soil (from Gibbs and Coffey, 1969)	72
6	Results of Constant Water Content Triaxial Tests on a Shale (Clay Fraction 22%) Compacted at a Water Content of 18.6% (from Bishop, Alpan, Blight and Donald, 1960)	73
7	Consolidated Drained Tests on an Unsaturated Silt: (a) Typical Stress-Strain Curves; (b) Pore-water Volume Change; (c) Soil Volume Change. (from Blight, 1967)	74
8	Increase in Shear Strength Due to Matric Suction as Indicated by Direct Shear Test Results (from Escario, 1980)	75
9	Increase in Shear Strength Due to Matric Suction as Indicated by Triaxial Test Results (from Escario, 1980)	76
10	Increase in Shear Strength Due to Matric Suction for Two Hong Kong Soils as Indicated by Triaxial Test Results: (a) Decomposed Rhyolite; (b) Decomposed Granite. (from Ho and Fredlund, 1982)	77
11	Multistage Direct Shear Test Results on an Unsaturated Glacial Till Specimen: (a) Shear Stress versus Horizontal Displacement; (b) Vertical Deflection versus Horizontal Displacement; (c) $\tau/(U_a - U_w)$ versus Horizontal Displacement. (from Gan, Fredlund and Rahardjo, 1988)	78

Figure No.		Page No.
12	Failure Envelope Obtained from an Unsaturated Glacial Till Specimen: (a) Failure Envelope on τ versus $(U_a - U_w)$ Plane; (b) Corresponding ϕ^b Values. (from Gan, Fredlund and Rahardjo, 1988)	79
13	Failure Envelopes Obtained from Unsaturated Glacial Till Specimens: (a) Failure Envelopes on τ versus $(U_a - U_w)$ Plane; (b) ϕ^b Values Corresponding to the Three Failure Envelopes. (from Gan, Fredlund and Rahardjo, 1988)	80
14	Results of Direct Shear Test with Applied Matric Suctions: (a) Madrid Grey Clay; (b) Red Clay of Guadalix de la Sierra; (c) Madrid Clayey Sand. (from Escario and Saez, 1986)	81
15a	CD and CW Triaxial Test on a Copper Tailings Sand with Applied Matric Suctions; Using Linear Regression for ϕ' (from Drumright, 1989)	82
15b	CD and CW Triaxial Test on a Copper Tailings Sand with Applied Matric Suctions; Using Bilinear Regression for ϕ' (from Drumright, 1989)	83
15c	Shear Strength versus Matric Suction Relationship for an Unsaturated Copper Tailings Sand from CD and CW Triaxial Tests with Applied Matric Suction (from Drumright, 1989)	84
16	Variation of Critical State Stress Ratios, M_a and M_w with Degree of Saturation (in Eqn. $q = M_a (p - u_a) + M_w (u_a - u_w)$) (from Toll, 1990)	85
17	Variation of Cohesion with Degree of Saturation from Triaxial Tests: (a) Decomposed Granite; (b) Decomposed Rhyolite. (from Lumb, 1965)	85
18	Layout of the Complete Modified Direct Shear Box Apparatus (from Gan and Fredlund, 1988)	86

Figure No.		Page No.
19	Plan View of Modified Shear Box in Pressure Chamber (with High Air Entry Disk Removed) (from Gan and Fredlund, 1988)	87
20	Cross-sectional View A-A of Modified Shear Box and Pressure Chamber (from Gan and Fredlund, 1988)	87
21	Cross-sectional View B-B of Modified Shear Box and Pressure Chamber (from Gan and Fredlund, 1988)	88
22	Details of Shear Box Base and Chamber Base (from Gan and Fredlund, 1988)	89
23	Dismantled Direct Shear Apparatus Showing the Various Components (from Gan and Fredlund, 1988)	89
24a	Shear Stress versus Horizontal Displacement - 1st and 2nd Cycle (Specimen No. DS1B)	90
24b	Vertical Deflection versus Horizontal Displacement - 1st and 2nd Cycle (Specimen No. DS1B)	91
25a	Shear Stress versus Horizontal Displacement - 3rd and 4th Cycle (Specimen No. DS1B)	92
25b	Vertical Deflection versus Horizontal Displacement - 3rd and 4th Cycle (Specimen No. DS1B)	93
26a	Shear Stress versus Horizontal Displacement - 5th and 6th Cycle (Specimen No. DS1B)	94
26b	Vertical Deflection versus Horizontal Displacement - 5th and 6th Cycle (Specimen No. DS1B)	95
27a	Shear Stress versus Horizontal Displacement - 7th and 8th Cycle (Specimen No. DS1B)	96
27b	Vertical Deflection versus Horizontal Displacement - 7th and 8th Cycle (Specimen No. DS1B)	97
28	Shear Stress versus Horizontal Displacement - 9th and 10th Cycle (Specimen No. DS1B)	98

Figure No.		Page No.
29	Vertical Deflection versus Horizontal Displacement - 9th and 10th Cycle (Specimen No. DS1B)	99
30	Shear Stress versus Horizontal Displacement - 11th to 13th Cycle (Specimen No. DS1B)	100
31	Vertical Deflection versus Horizontal Displacement - 11th and 13th Cycle (Specimen No. DS1B)	101
32	Volume of Water Expelled versus Log Time (Specimen No. MDS1)	102
33	Results of Modified Direct Shear Test in Pilot Test on Specimen No. MDS1 (a) Shear Stress versus Horizontal Displacements, (b) Vertical Deflection versus Horizontal Displacement	103
34	Shear Stress versus Horizontal Displacement - 1st to 4th Cycle (Specimen No. DS1C)	104
35	Vertical Deflection versus Horizontal Displacement - 1st to 4th Cycle (Specimen No. DS1C)	105
36	Multistage Direct Shear Test on Specimen No. P2 - Stage 1	106
37	Multistage Direct Shear Test on Specimen No. P2 - Stage 2	107
38	Multistage Direct Shear Test on Specimen No. P2 - Stage 3	108
39	Multistage Direct Shear Test on Specimen No. P3 - Stage 1	109
40	Multistage Direct Shear Test on Specimen No. P3 - Stage 2	110
41	Multistage Direct Shear Test on Specimen No. P3 - Stage 3	111
42	Multistage Direct Shear Test on Specimen No. P3 - Stage 4	112
43	Multistage Direct Shear Test on Specimen No. P3 - Stage 5	113
44	Multistage Direct Shear Test on Specimen No. P4 - Stage 1	114
45	Multistage Direct Shear Test on Specimen No. P4 - Stage 2	115
46	Multistage Direct Shear Test on Specimen No. P4 - Stage 3	116
47	Multistage Direct Shear Test on Specimen No. P4 - Stage 4	117

Figure No.		Page No.
48	Multistage Direct Shear Test on Specimen No. P4 - Stage 5	118
49	Multistage Direct Shear Test on Specimen No. P5 - Stage 1	119
50	Multistage Direct Shear Test on Specimen No. P5 - Stage 2	120
51	Multistage Direct Shear Test on Specimen No. P6 - Stage 1	121
52	Multistage Direct Shear Test on Specimen No. P6 - Stage 2	122
53	Multistage Direct Shear Test on Specimen No. P6 - Stage 3	123
54	Multistage Direct Shear Test on Specimen No. P6 - Stage 4	124
55	Multistage Direct Shear Test on Specimen No. P7 - Stage 1	125
56	Multistage Direct Shear Test on Specimen No. P7 - Stage 2	126
57	Multistage Direct Shear Test on Specimen No. P7 - Stage 3	127
58	Multistage Direct Shear Test on Specimen No. P7 - Stage 4	128
59	Multistage Direct Shear Test on Specimen No. P7 - Stage 5	129
60	Plateau Stress Reading versus Normal Stress	130
61	Check for Slack in Direct Shear Apparatus Using a Steel Block	131
62	Typical Shear Stress versus Horizontal Displacement Curve with Plateau Indicating Slacks in Apparatus (Specimen No. P7 - Stage 1 - Cycle 1 of Multistage Test)	132
63	Typical Shear Stress versus Horizontal Displacement Curve with Plateaus Indicating Slacks in Apparatus (Specimen No. P7 - Stage 2 - Cycle 1 of Multistage Test)	133
64	Multistage Direct Shear Test on Specimen No. P8 - Stage 1	134
65	Multistage Direct Shear Test on Specimen No. P8 - Stage 2	135
66	Multistage Direct Shear Test on Specimen No. P8 - Stage 3	136
67	Multistage Direct Shear Test on Specimen No. P9 - Stage 1	137
68	Multistage Direct Shear Test on Specimen No. P9 - Stage 2	138

Figure No.		Page No.
69	Multistage Direct Shear Test on Specimen No. P9 - Stage 3	139
70	Multistage Direct Shear Test on Specimen No. P9 - Stage 4	140
71	Peak Strength Mohr Envelope from Direct Shear Test	141
72	Residual Strength Mohr Envelope from Direct Shear Test	142
73a	Shear Stress versus Horizontal Displacement - Specimen No. US-1	143
73b	Vertical Deflection versus Horizontal Displacement - Specimen No. US-1	144
74a	Shear Stress versus Horizontal Displacement - Specimen No. US-3	145
74b	Vertical Deflection versus Horizontal Displacement - Specimen No. US-3	146
75a	Shear Stress versus Horizontal Displacement - Specimen No. US-4	147
75b	Vertical Deflection versus Horizontal Displacement - Specimen No. US-4	148
76a	Shear Stress versus Horizontal Displacement - Specimen No. US-5	149
76b	Vertical Deflection versus Horizontal Displacement - Specimen No. US-5	150
77a	Shear Stress versus Horizontal Displacement - Specimen No. US-6	151
77b	Vertical Deflection versus Horizontal Displacement - Specimen No. US-6	152
78a	Shear Stress versus Horizontal Displacement - Specimen No. US-9	153
78b	Vertical Deflection versus Horizontal Displacement - Specimen No. US-9	154

Figure No.		Page No.
79a	Shear Stress versus Horizontal Displacement - Specimen No. US-10	155
79b	Vertical Deflection versus Horizontal Displacement - Specimen No. US-10	156
80a	Shear Stress versus Horizontal Displacement - Specimen No. US-11	157
80b	Vertical Deflection versus Horizontal Displacement - Specimen No. US-11	158
81a	Shear Stress versus Horizontal Displacement - Specimen No. US-12	159
81b	Vertical Deflection versus Horizontal Displacement - Specimen No. US-12	160
82a	Shear Stress versus Horizontal Displacement - Specimen No. US-13	161
82b	Vertical Deflection versus Horizontal Displacement - Specimen No. US-13	162
83a	Shear Stress versus Horizontal Displacement - Specimen No. US-14	163
83b	Vertical Deflection versus Horizontal Displacement - Specimen No. US-14	164
84a	Correction for Chamber Pressures on Load-cell Reading	165
84b	Load-cell Readings with Respect to Shear Displacement at Various Chamber Pressures	166
85a	Vertical Deflection with Time during Pressures Equilibration for Specimen No. US-1, Stage 1	167
85b	Vertical Deflection with Time during Pressures Equilibration for Specimen No. US-1, Stage 2	168
85c	Vertical Deflection with Time during Pressures Equilibration for Specimen No. US-1, Stage 3	169

Figure No.		Page No.
85d	Vertical Deflection with Time during Pressures Equilibration for Specimen No. US-1, Stage 4	170
85e	Vertical Deflection with Time during Pressures Equilibration for Specimen No. US-1, Stage 5	171
86a	Vertical Deflection with Time during Pressures Equilibration for Specimen No. US-3, Stage 1	172
86b	Vertical Deflection with Time during Pressures Equilibration for Specimen No. US-3, Stage 2	173
86c	Vertical Deflection with Time during Pressures Equilibration for Specimen No. US-3, Stage 3	174
86d	Vertical Deflection with Time during Pressures Equilibration for Specimen No. US-3, Stage 4	175
87a	Vertical Deflection with Time during Pressures Equilibration for Specimen No. US-4, Stage 1	176
87b	Vertical Deflection with Time during Pressures Equilibration for Specimen No. US-4, Stage 2	177
87c	Vertical Deflection with Time during Pressures Equilibration for Specimen No. US-4, Stage 3	178
87d	Vertical Deflection with Time during Pressures Equilibration for Specimen No. US-4, Stage 4	179
87e	Vertical Deflection with Time during Pressures Equilibration for Specimen No. US-4, Stage 5	180
88a	Vertical Deflection with Time during Pressures Equilibration for Specimen No. US-5, Stage 1	181
88b	Vertical Deflection with Time during Pressures Equilibration for Specimen No. US-5, Stage 2	182
88c	Vertical Deflection with Time during Pressures Equilibration for Specimen No. US-5, Stage 3	183
88d	Vertical Deflection with Time during Pressures Equilibration for Specimen No. US-5, Stage 4	184

Figure No.		Page No.
88e	Vertical Deflection with Time during Pressures Equilibration for Specimen No. US-5, Stage 5	185
89a	Vertical Deflection with Time during Pressures Equilibration for Specimen No. US-6, Stage 1	186
89b	Vertical Deflection with Time during Pressures Equilibration for Specimen No. US-6, Stage 2	187
89c	Vertical Deflection with Time during Pressures Equilibration for Specimen No. US-6, Stage 3	188
90a	Vertical Deflection with Time during Pressures Equilibration for Specimen No. US-9, Stage 2	189
90b	Vertical Deflection with Time during Pressures Equilibration for Specimen No. US-9, Stage 3	190
91a	Vertical Deflection with Time during Pressures Equilibration for Specimen No. US-10, Stage 1	191
91b	Vertical Deflection with Time during Pressures Equilibration for Specimen No. US-10, Stage 2	192
92a	Vertical Deflection with Time during Pressures Equilibration for Specimen No. US-11, Stage 1	193
92b	Vertical Deflection with Time during Pressures Equilibration for Specimen No. US-11, Stage 2	194
92c	Vertical Deflection with Time during Pressures Equilibration for Specimen No. US-11, Stage 3	195
93	Vertical Deflection with Time during Pressures Equilibration for Specimen No. US-12, Stage 1	196
94	Vertical Deflection with Time during Pressures Equilibration for Specimen No. US-13, Stage 1	197
95	Vertical Deflection with Time during Pressures Equilibration for Specimen No. US-14, Stage 1	198
96	Movement of Water from Specimen during Suction Equilibration for Specimen No. US-1	199

Figure No.		Page No.
97	Movement of Water from Specimen during Suction Equilibration for Specimen No. US-3	200
98	Movement of Water from Specimen during Suction Equilibration for Specimen No. US-4	201
99	Movement of Water from Specimen during Suction Equilibration for Specimen No. US-5	202
100	Movement of Water from Specimen during Suction Equilibration for Specimen No. US-6	203
101	Movement of Water from Specimen during Suction Equilibration for Specimen No. US-9	204
102	Movement of Water from Specimen during Suction Equilibration for Specimen No. US-10	205
103	Movement of Water from Specimen during Suction Equilibration for Specimen No. US-11	206
104	Movement of Water from Specimen during Suction Equilibration for Specimen No. US-12	207
105	Movement of Water from Specimen during Suction Equilibration for Specimen No. US-13	208
106	Movement of Water from Specimen during Suction Equilibration for Specimen No. US-14	209
107	Suction versus Water Content Relationship of Direct Shear Test Specimens in Main Test Program and of Tempe-cell Specimens	210
108	Suction versus Degree of Saturation Relationship of Direct Shear Test Specimens in Main Test Program and of Tempe-cell Specimens	211
109	Results of Tempe-cell Test No. 1	212
110	Results of Tempe-cell Test No. 2	213
111	Results of Tempe-cell Test No. 3	214

Figure No.		Page No.
112	Shear Stress versus Matric Suction Relationship of Fine Ash Tuff as Obtained from Direct Shear Tests at Various Applied Matric Suctions and a Constant Net Normal Stress of 20 kPa	215
113	Shear Stress versus Matric Suction Relationship of Fine Ash Tuff as Obtained from Direct Shear Tests at Various Applied Matric Suctions and a Constant Net Normal Stress of 100 kPa	216
114	Grain Size Distribution of Specimen Trimmings	216
115	Grain Size Distribution of Specimen No. P2	218
116	Grain Size Distribution of Specimen No. P3	219

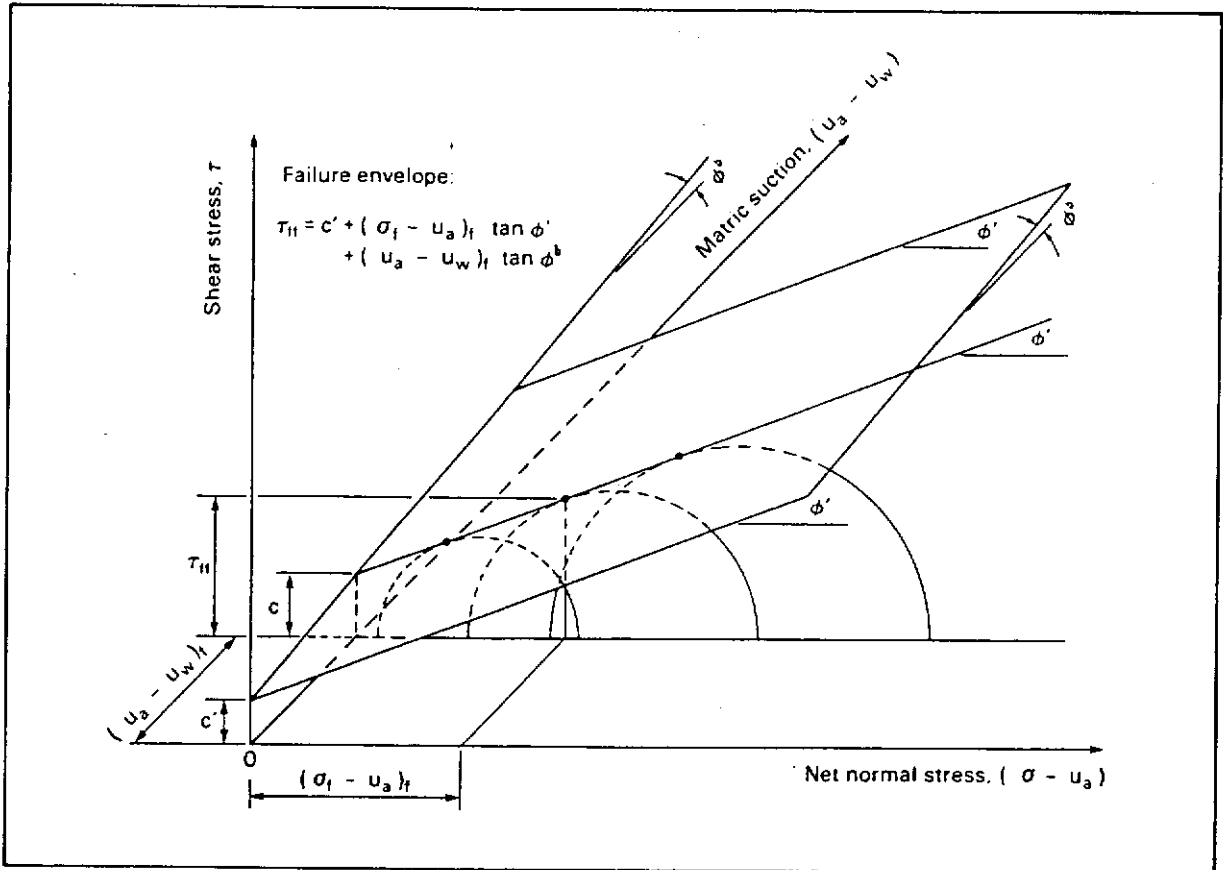


Figure 1 - Extended Mohr-Coulomb Failure Envelope

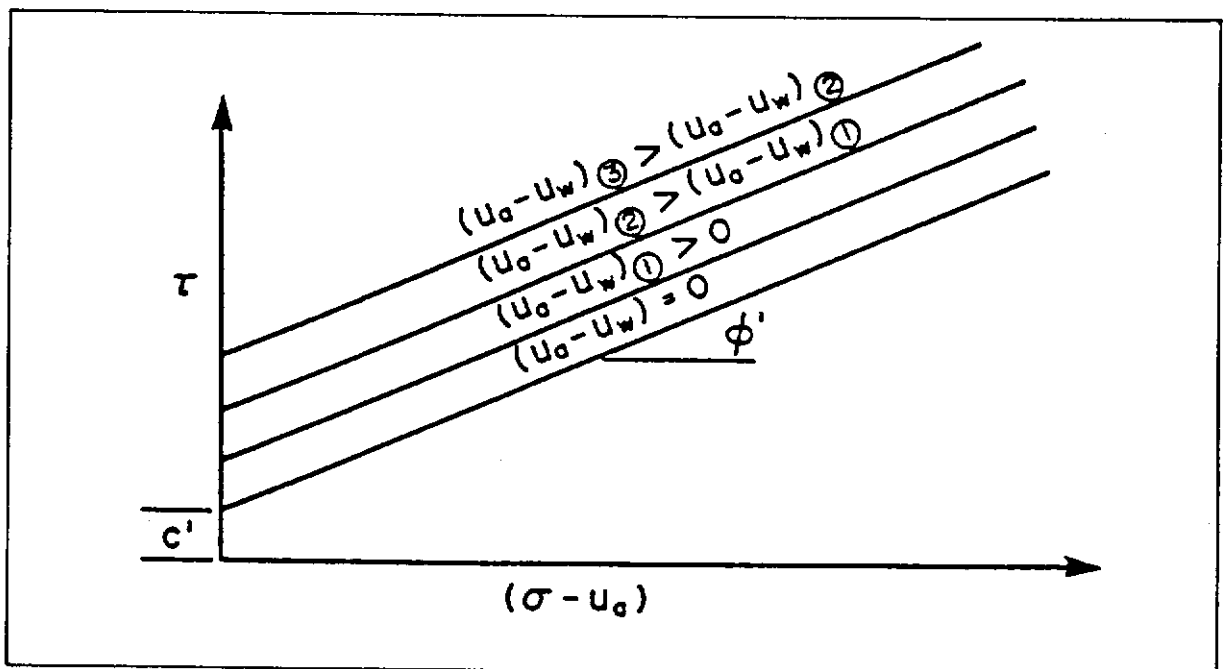


Figure 2 - Two Dimensional Representation of Failure Envelopes Corresponding to Different $(U_a - U_w)$

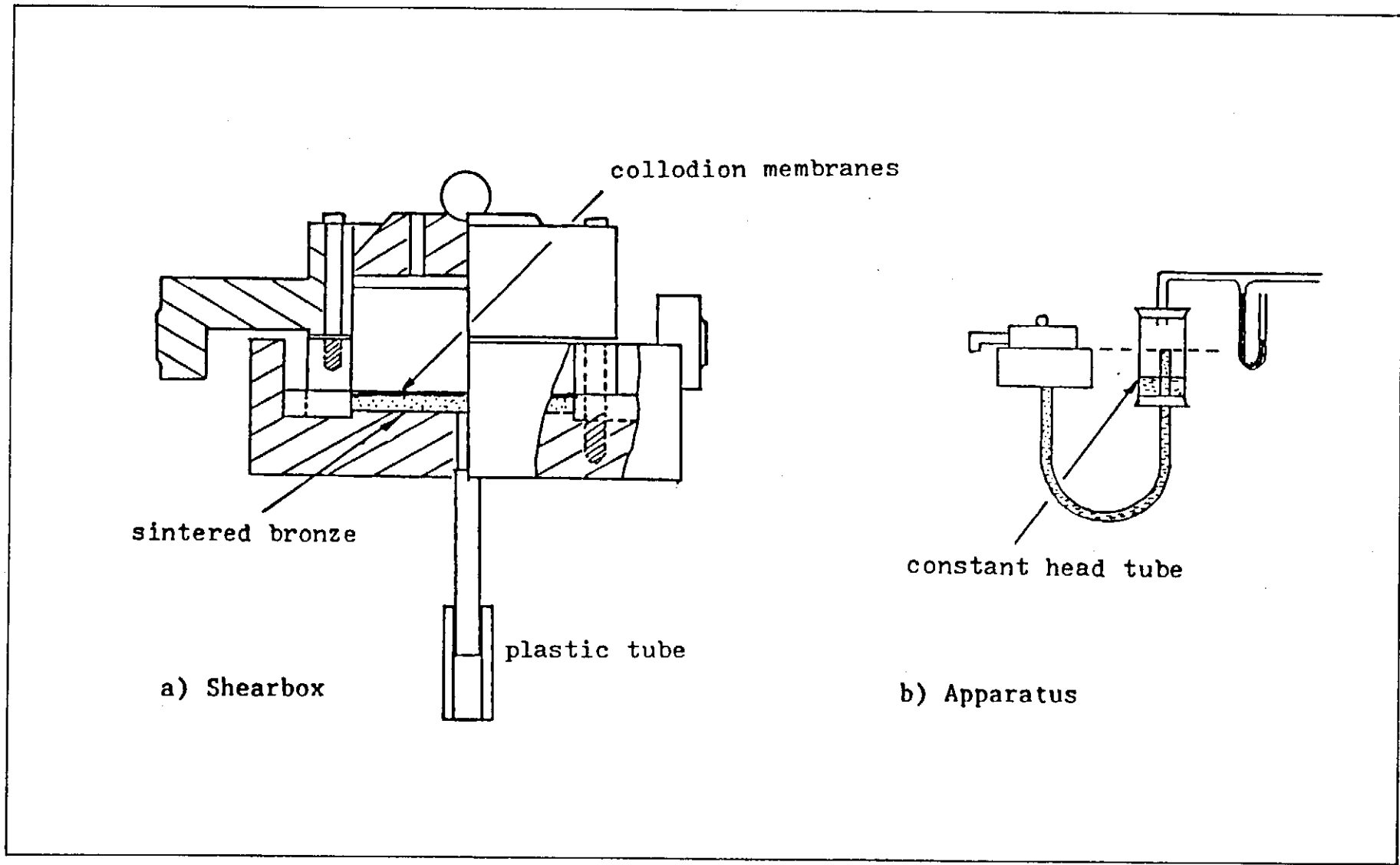


Figure 3 - Shear Box Apparatus for Testing Soils under Low Matric Suctions (from Donald, 1956)

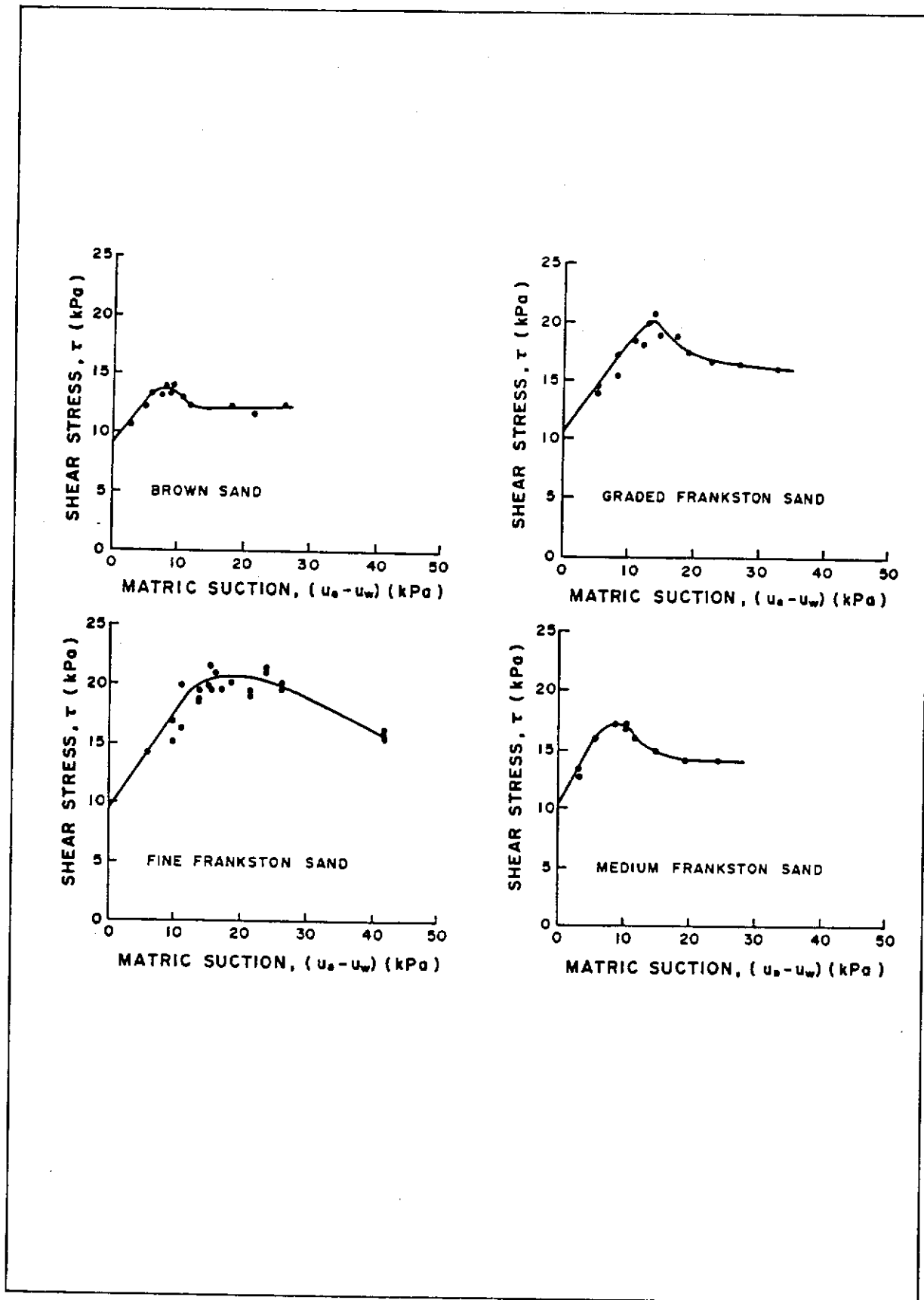


Figure 4 - Results of Direct Shear Tests on Sands under Low Matric Suctions (from Donald, 1956)

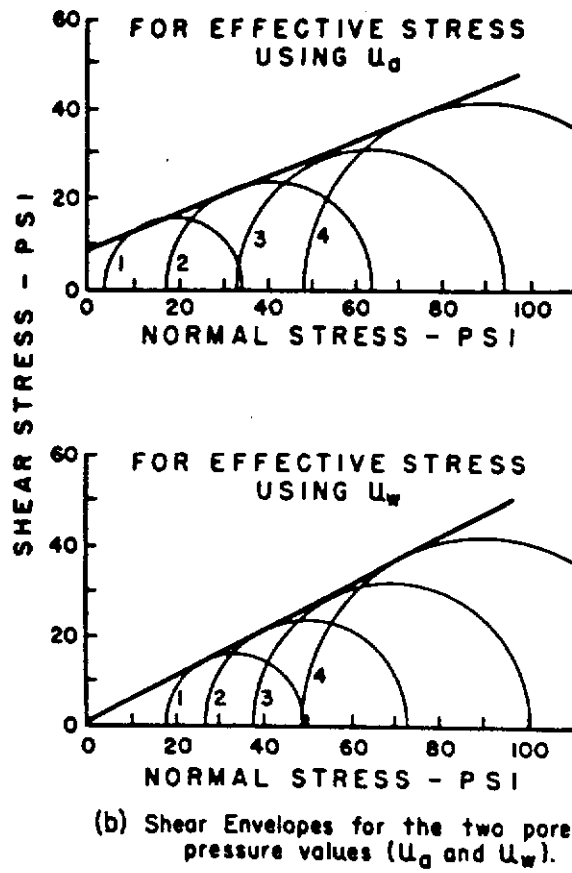


Figure 5 - Two Failure Envelopes for an Unsaturated Soil
(from Gibbs and Coffey, 1969)

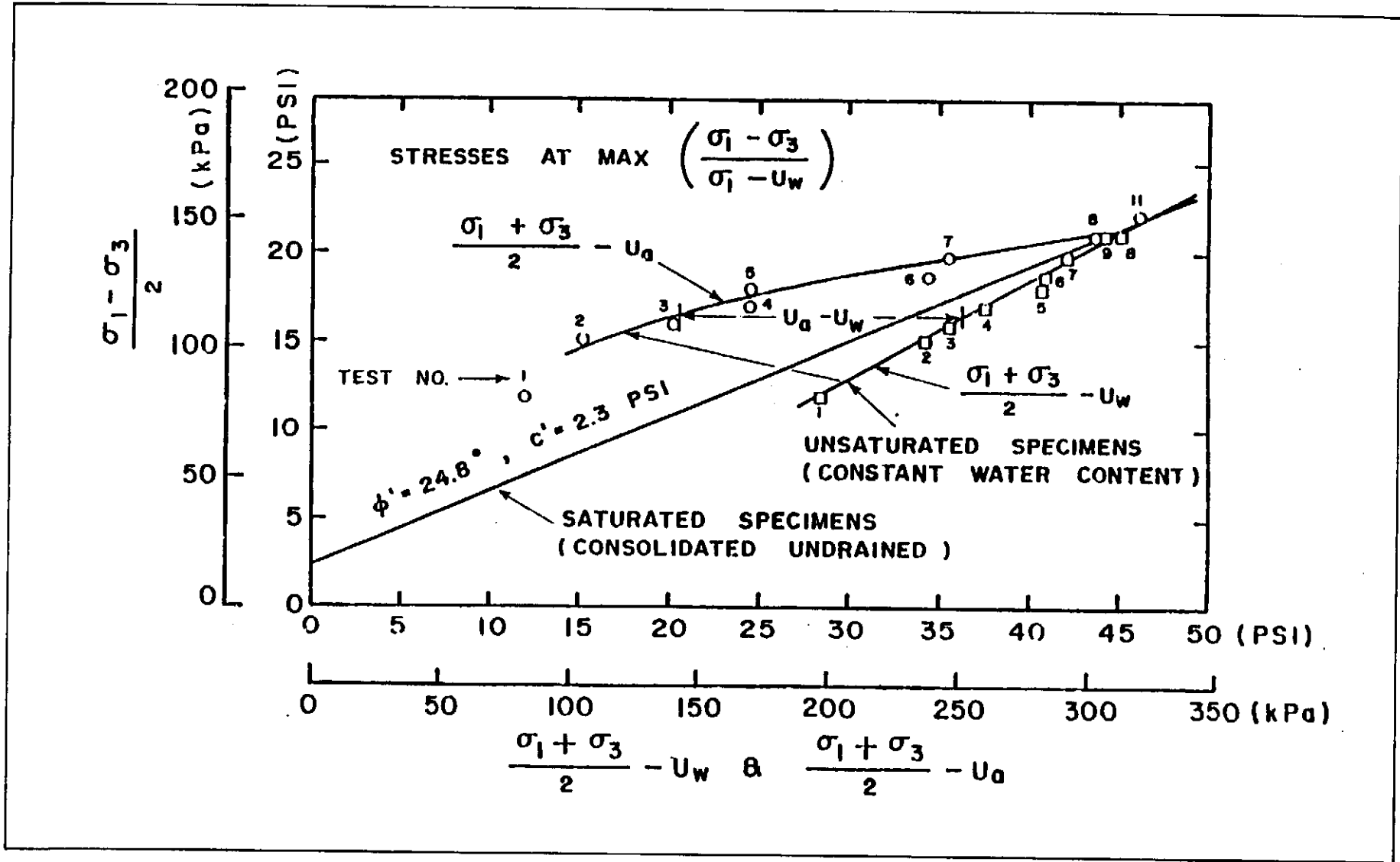
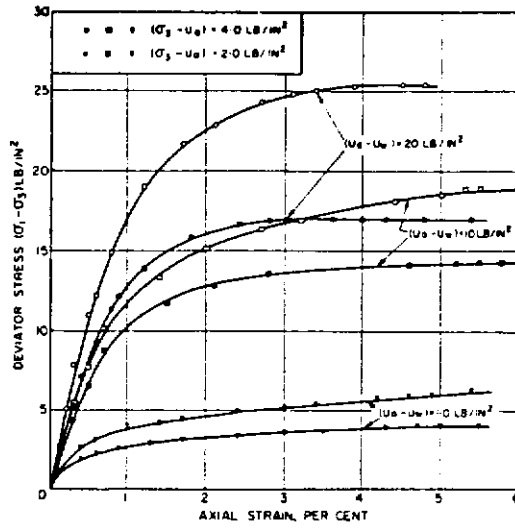
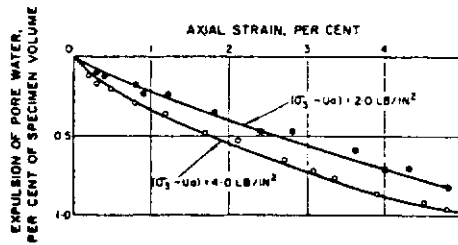


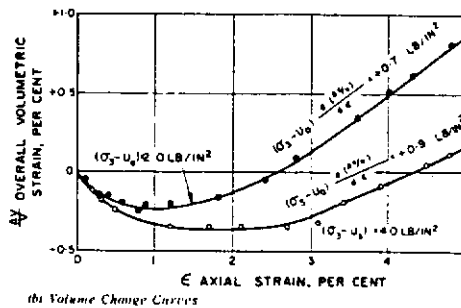
Figure 6 - Results of Constant Water Content Triaxial Tests on a Shale (Clay Fraction 22%) Compacted at a Water Content of 18.6% (from Bishop, Alpan, Blight and Donald, 1960)



(a)



(b)



(c)

Figure 7 - Consolidated Drained Tests on an Unsaturated Silt:
 (a) Typical Stress-Strain Curves;
 (b) Pore-water Volume Change;
 (c) Soil Volume Change.
 (from Blight, 1967)

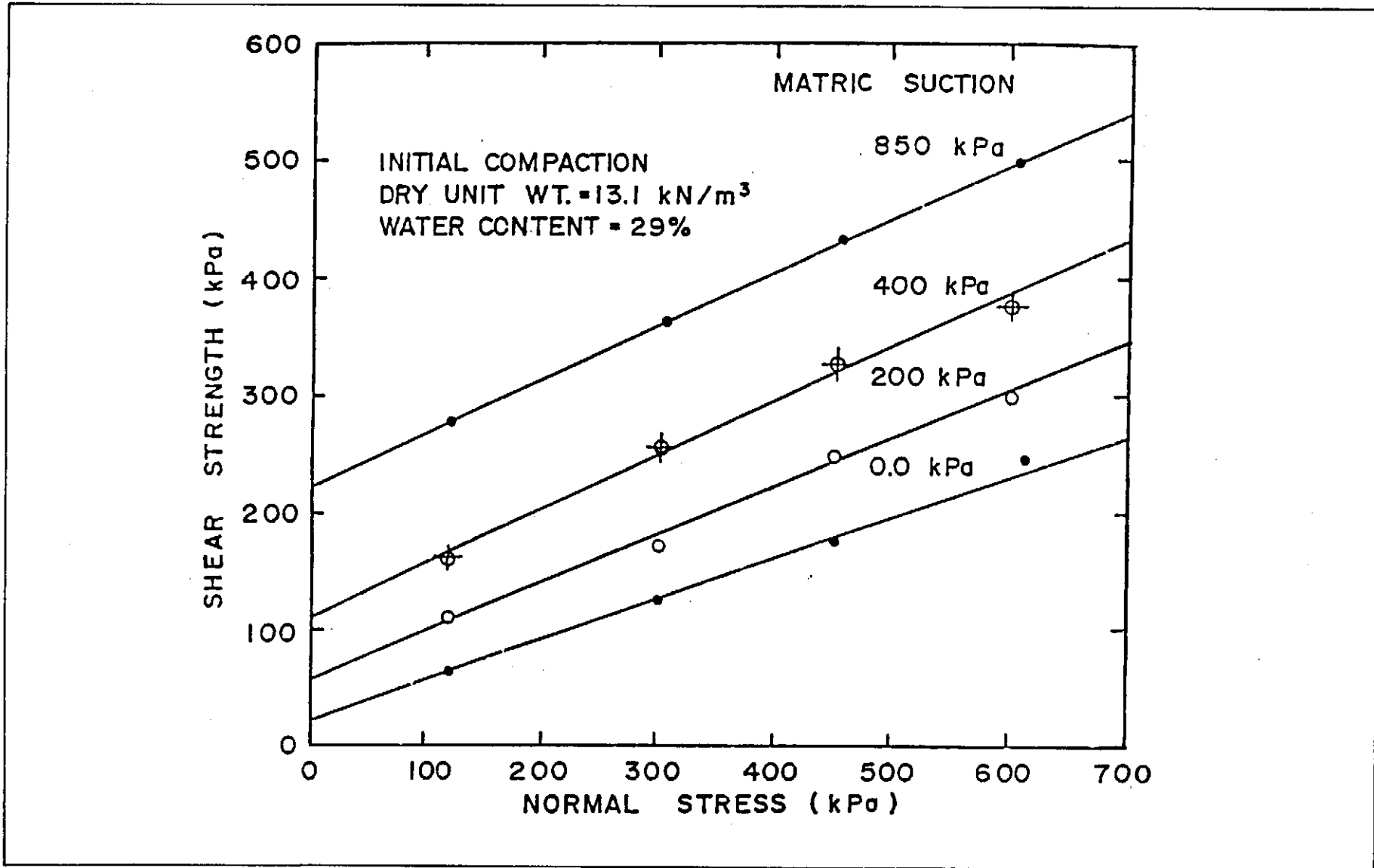


Figure 8 - Increase in Shear Strength Due to Matric Suction as Indicated by Direct Shear Test Results (from Escario, 1980)

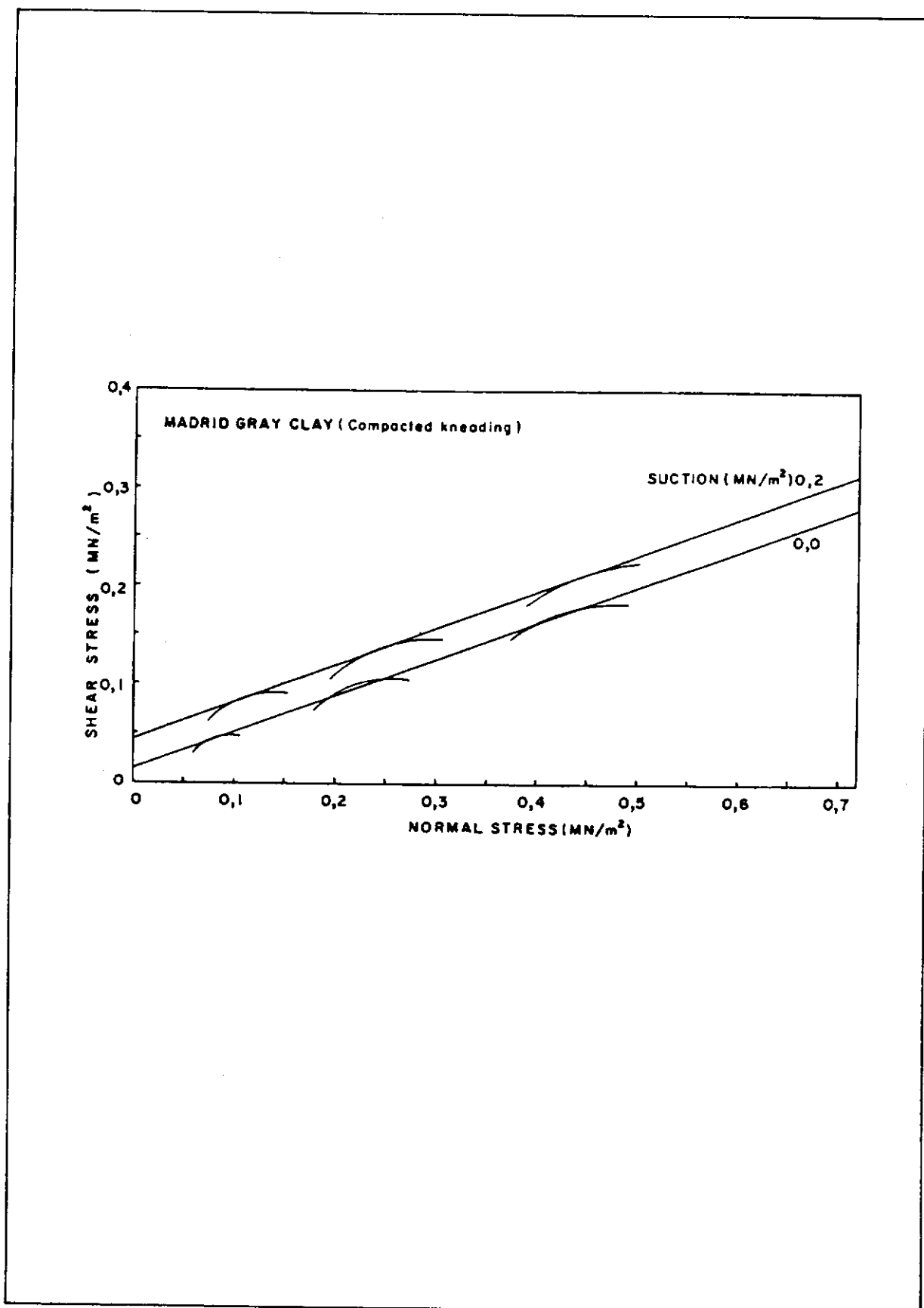


Figure 9 - Increase in Shear Strength Due to Matric Suction as Indicated by Triaxial Test Results (from Escario, 1980)

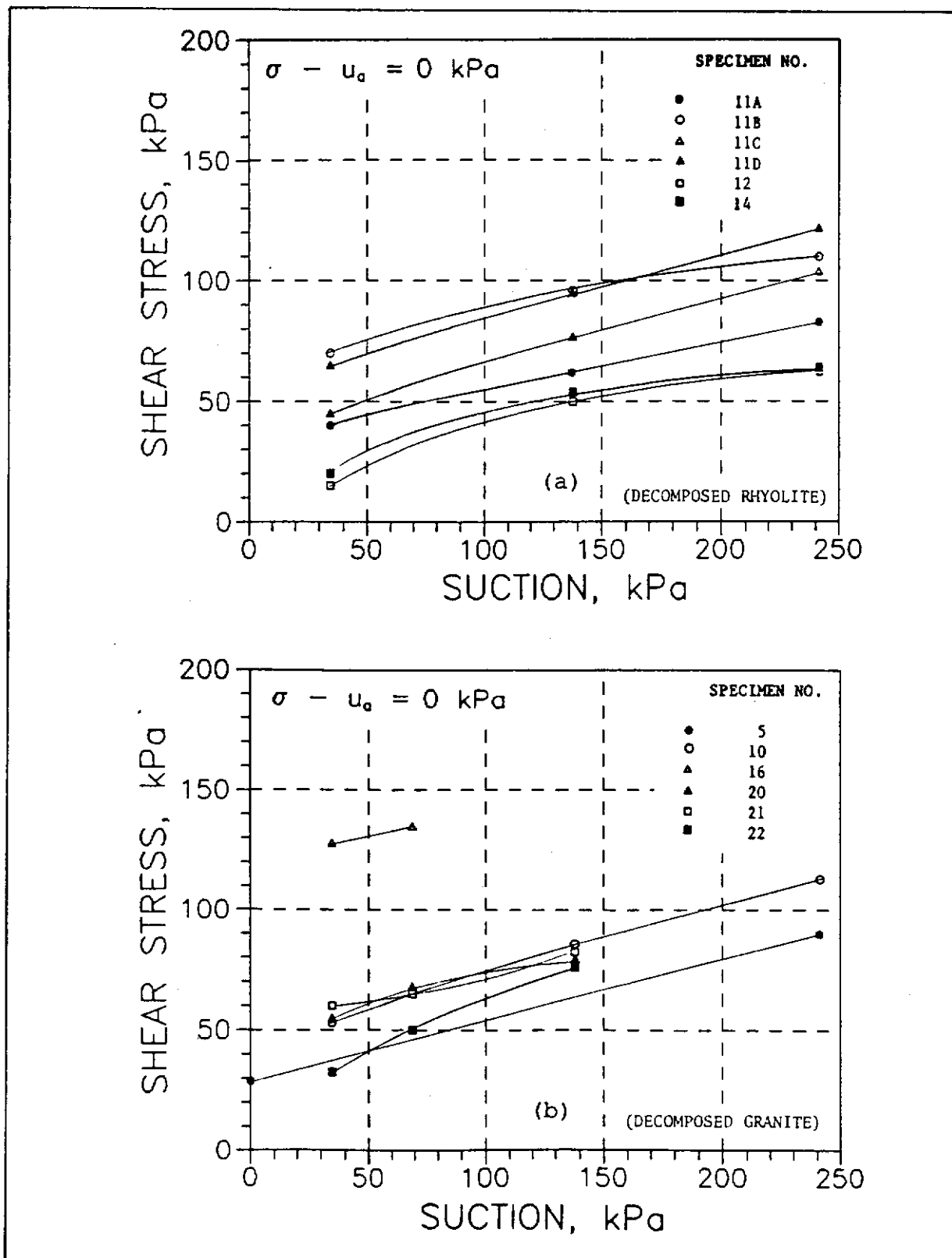


Figure 10 - Increase in Shear Strength Due to Matric Suction for Two Hong Kong Soils as Indicated by Triaxial Test Results:
(a) Decomposed Rhyolite;
(b) Decomposed Granite.
(from Ho and Fredlund, 1982)

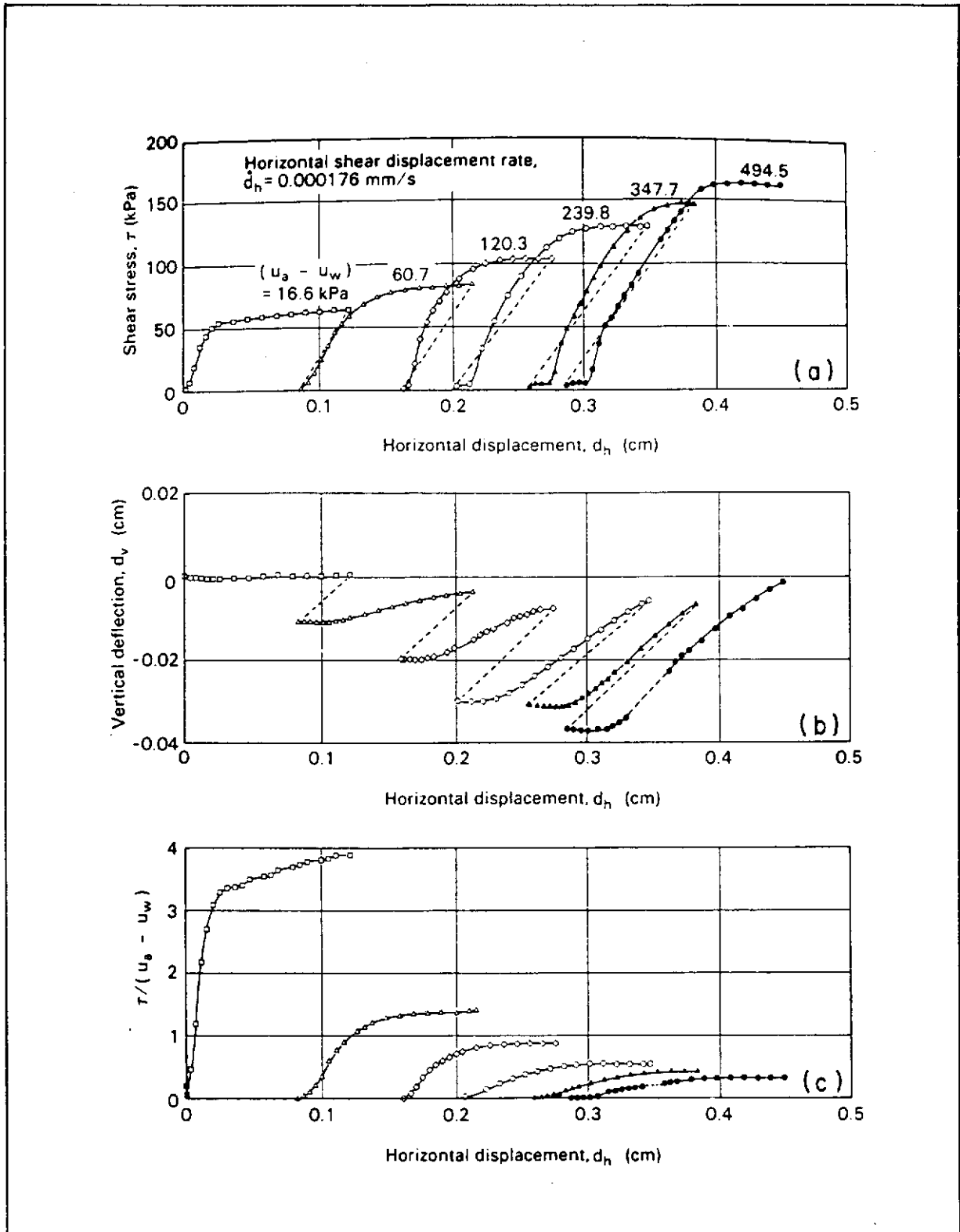


Figure 11 - Multistage Direct Shear Test Results on an Unsaturated Glacial Till Specimen:
(a) Shear Stress versus Horizontal Displacement;
(b) Vertical Deflection versus Horizontal Displacement;
(c) $\tau / (u_a - u_w)$ versus Horizontal Displacement.
(from Gan, Fredlund and Rahardjo, 1988)

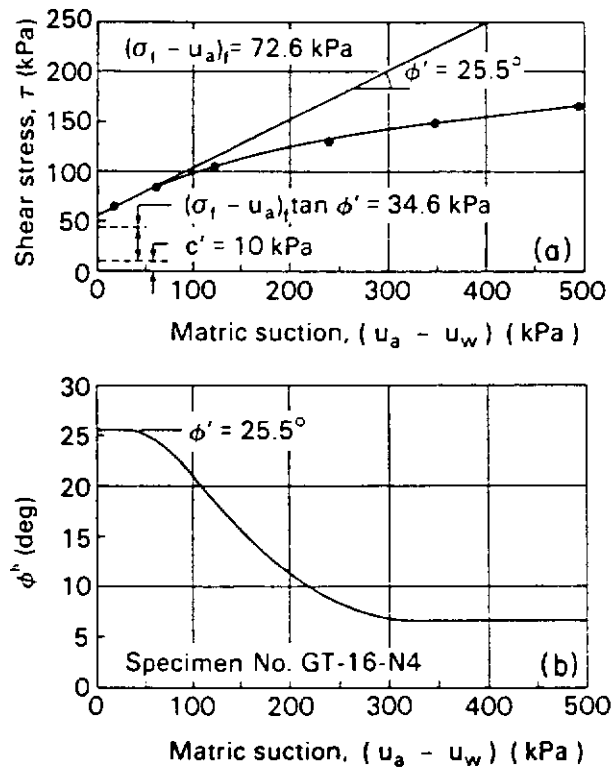


Figure 12 - Failure envelope Obtained from an Unsaturated Glacial Till Specimen:
(a) Failure Envelope on τ versus $(U_a - U_w)$ Plane;
(b) Corresponding ρ^b Values.
(from Gan, Fredlund and Rahardjo, 1988)

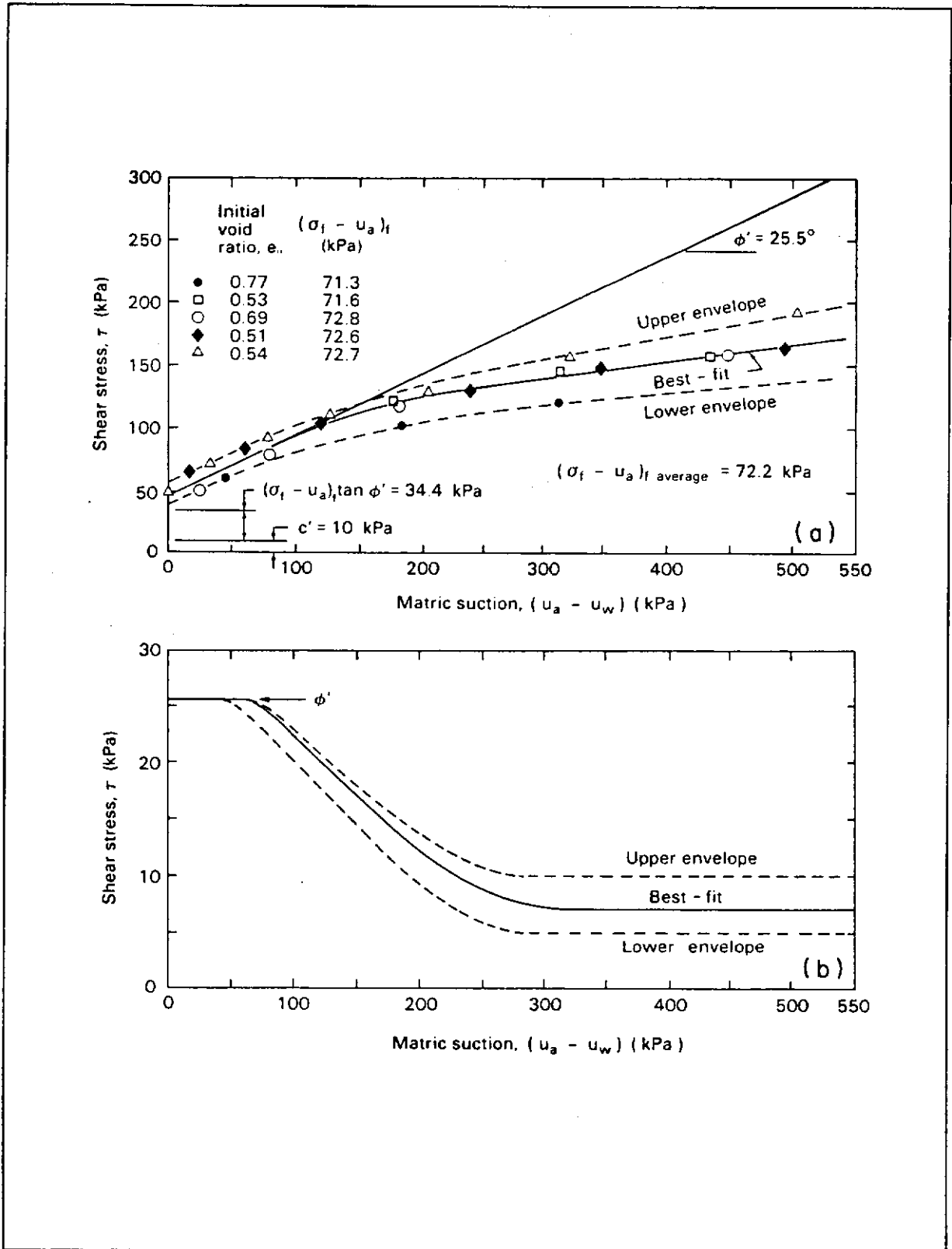


Figure 13 - Failure Envelopes Obtained from Unsaturated Glacial Till Specimens:
 (a) Failure Envelopes on τ versus $(U_a - U_w)$ Plane;
 (b) ρ^b Values Corresponding to the Three Failure Envelopes.
 (from Gan, Fredlund and Rahardjo, 1988)

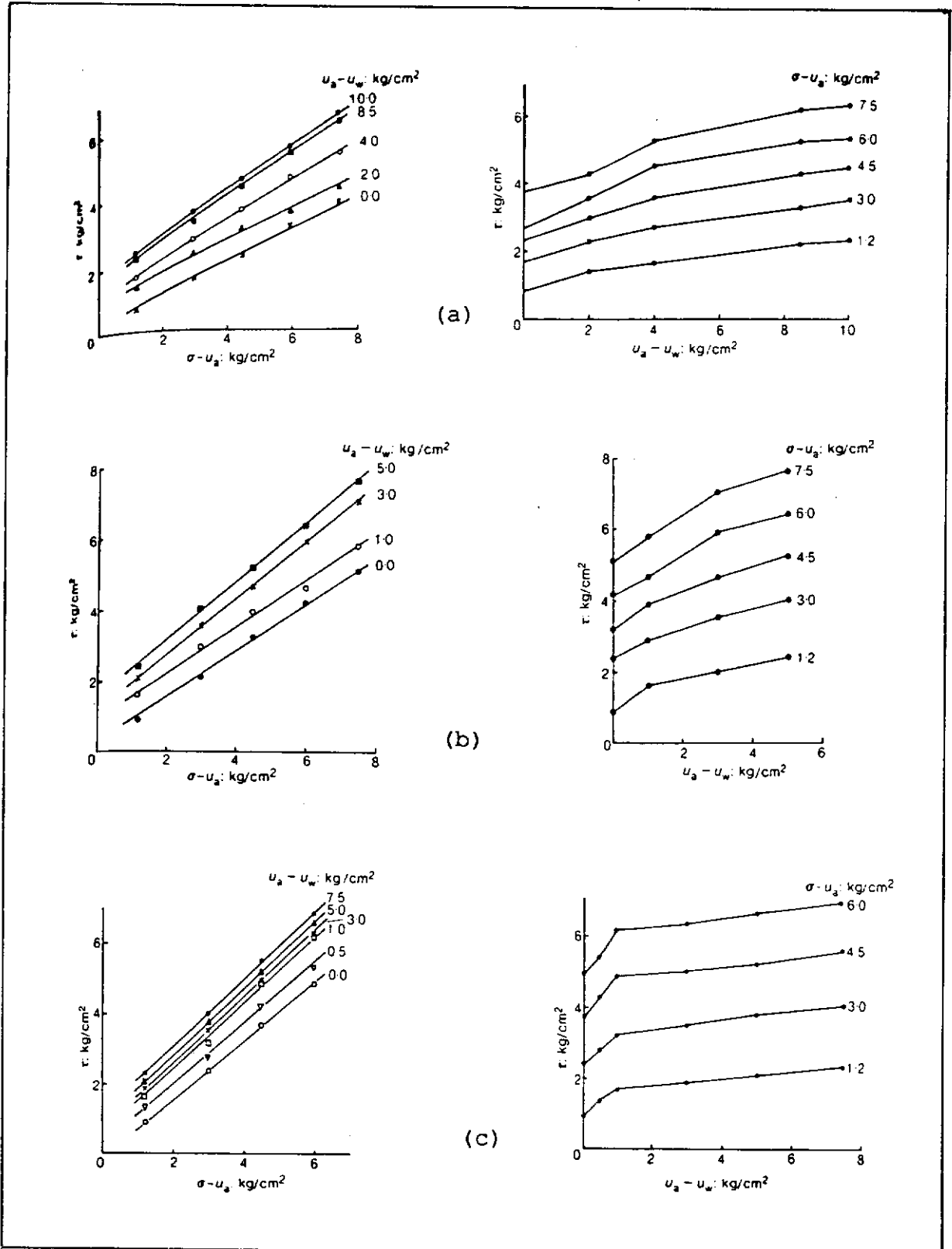


Figure 14 - Results of Direct Shear Test with Applied Matric Suctions:
(a) Madrid Grey Clay;
(b) Red Clay of Guadalix de la Sierra;
(c) Madrid Clayey Sand.
(from Escario and Saez, 1986)

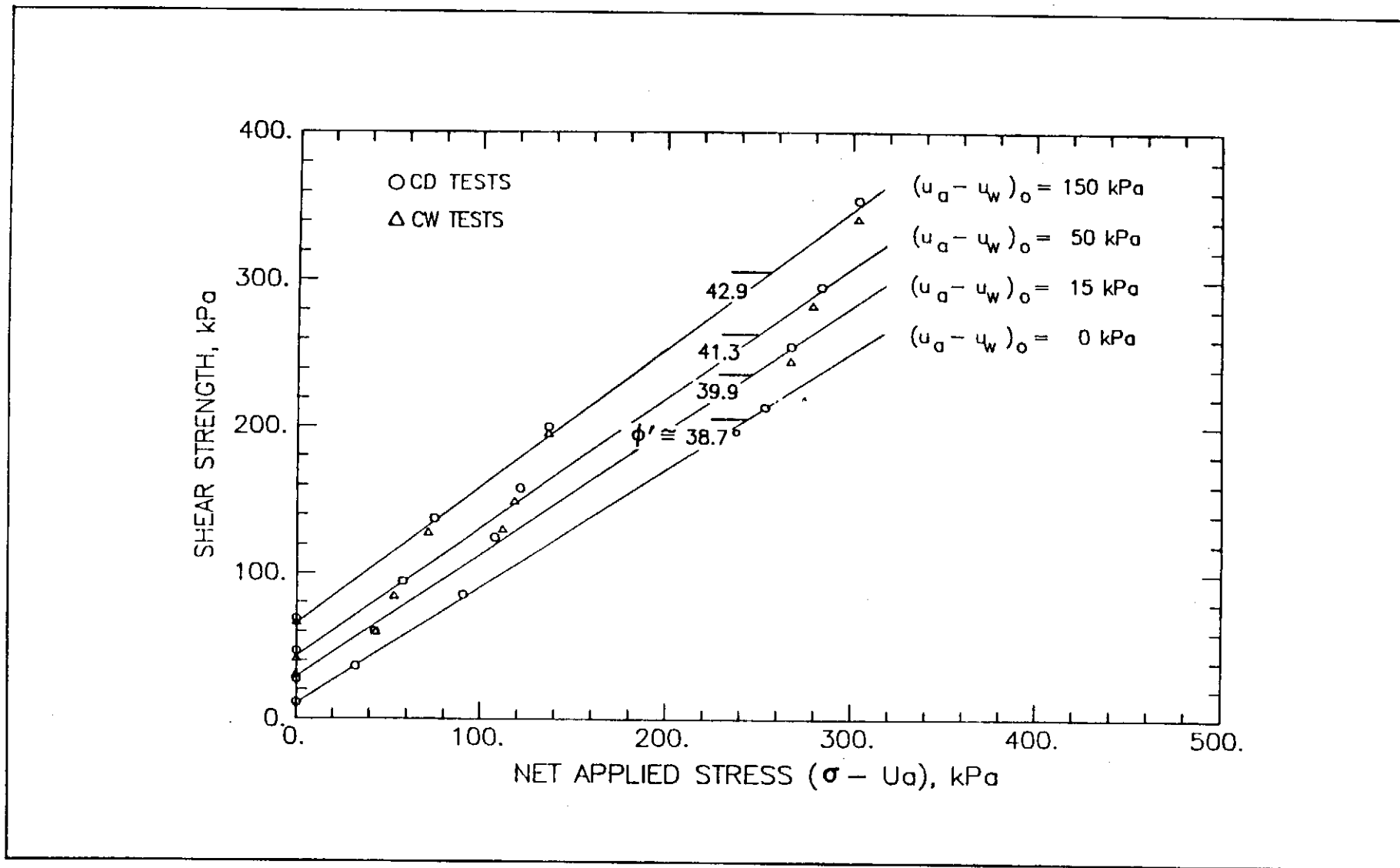


Figure 15a - CD and CW Triaxial Test on a Copper Tailings Sand with Applied Matric Suctions; Using Linear Regression for ϕ' (from Drumright, 1989)

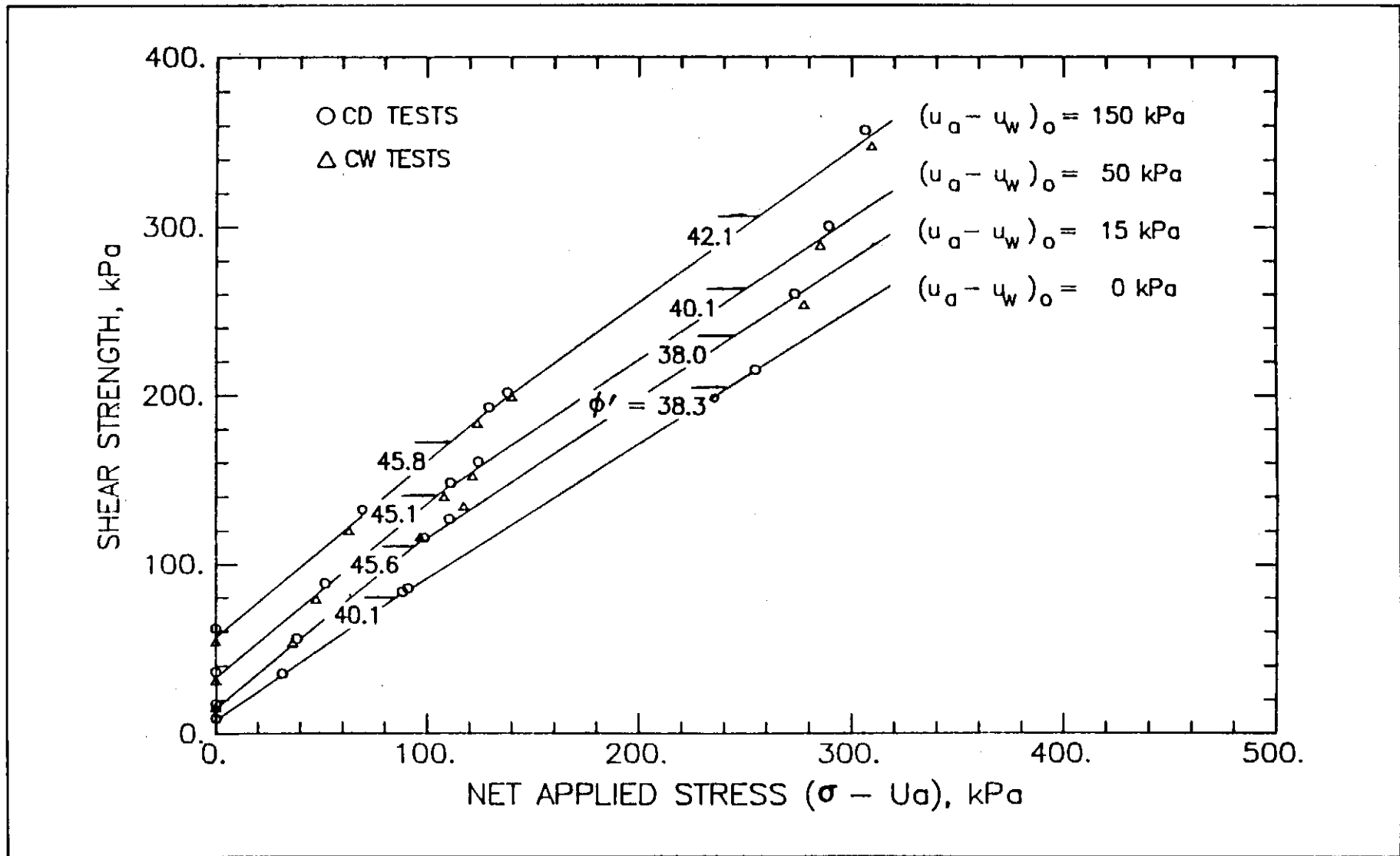


Figure 15b - CD and CW Triaxial Test on a Copper Tailings Sand with Applied Matric Suctions; Using Bilinear Regression for ϕ' (from Drumright, 1989)

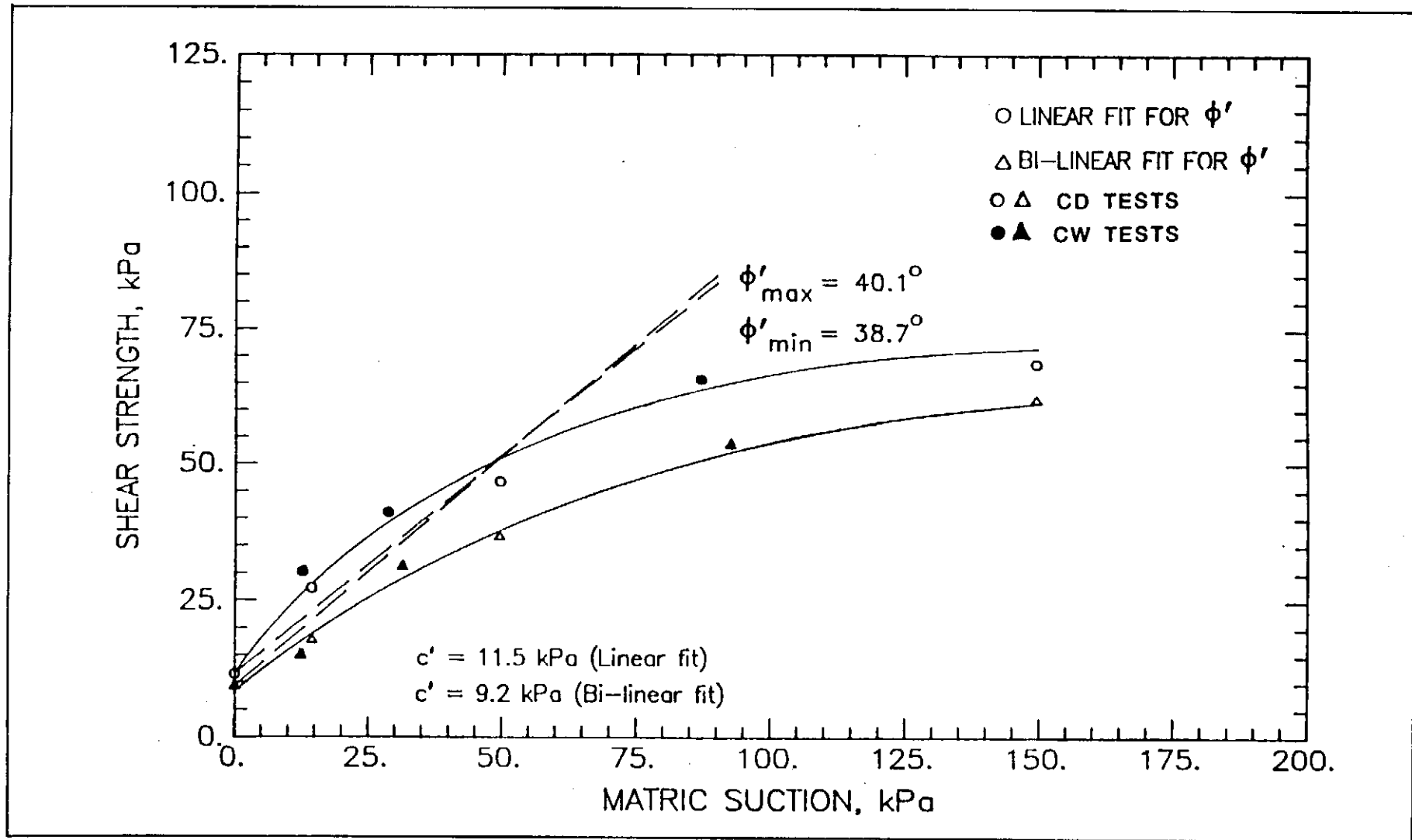


Figure 15c - Shear Strength versus Matric Suction Relationship for an Unsaturated Copper Tailings Sand from CD and CW Triaxial Tests with Applied Matric Suction (from Drumright, 1989)

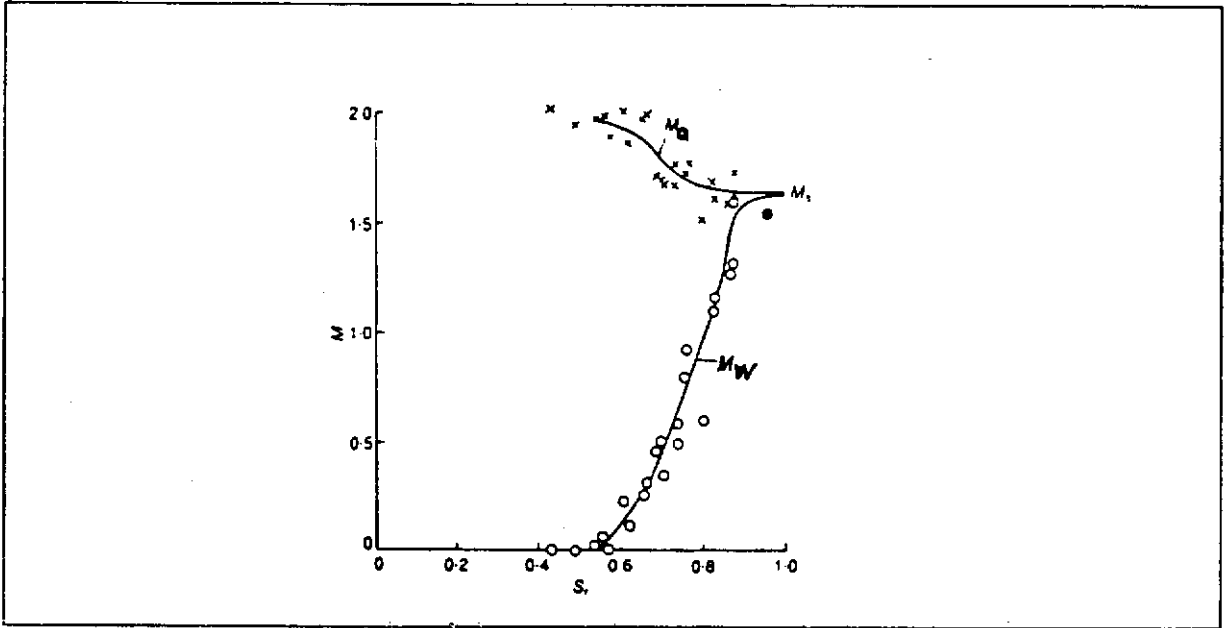


Figure 16 - Variation of Critical State Stress Ratios, M_a and M_w with Degree of Saturation (in Eqn. $q = M_a (p - u_a) + M_w (u_a - u_w)$) (from Toll, 1990)

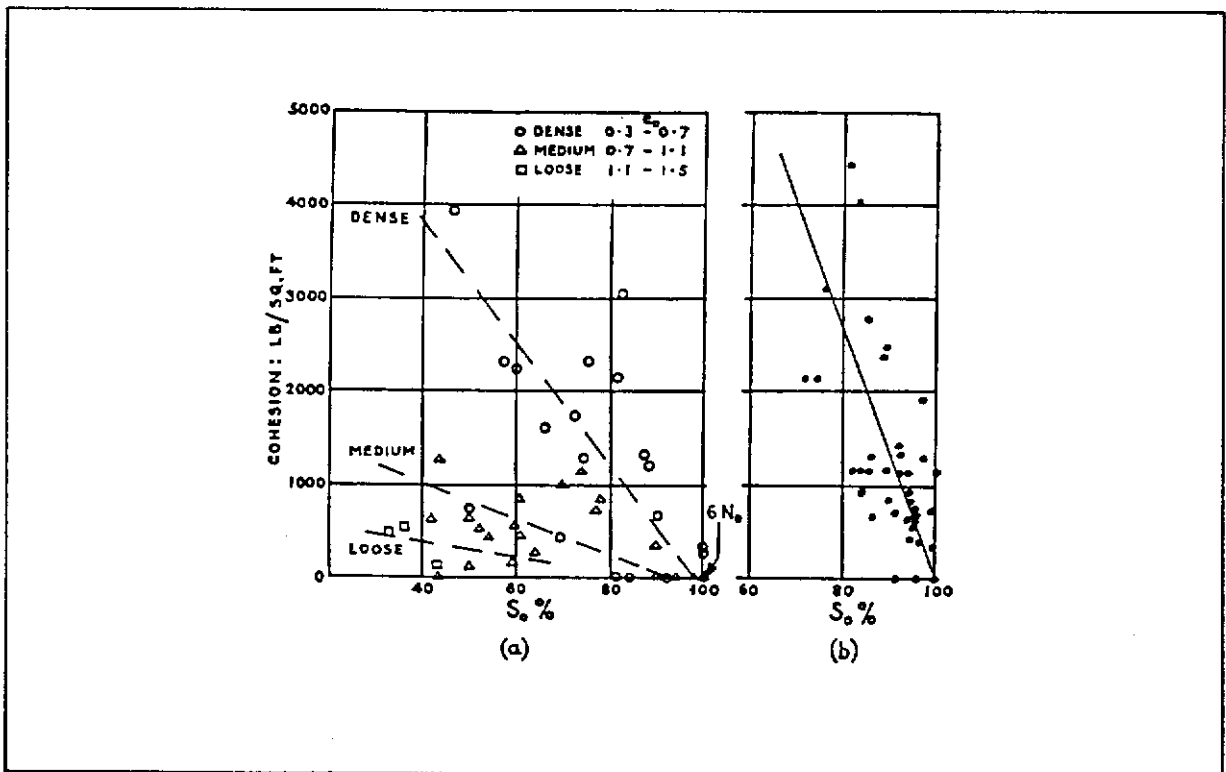


Figure 17 - Variation of Cohesion with Degree of Saturation from Triaxial Tests:
 (a) Decomposed Granite;
 (b) Decomposed Rhyolite.
 (from Lumb, 1965).

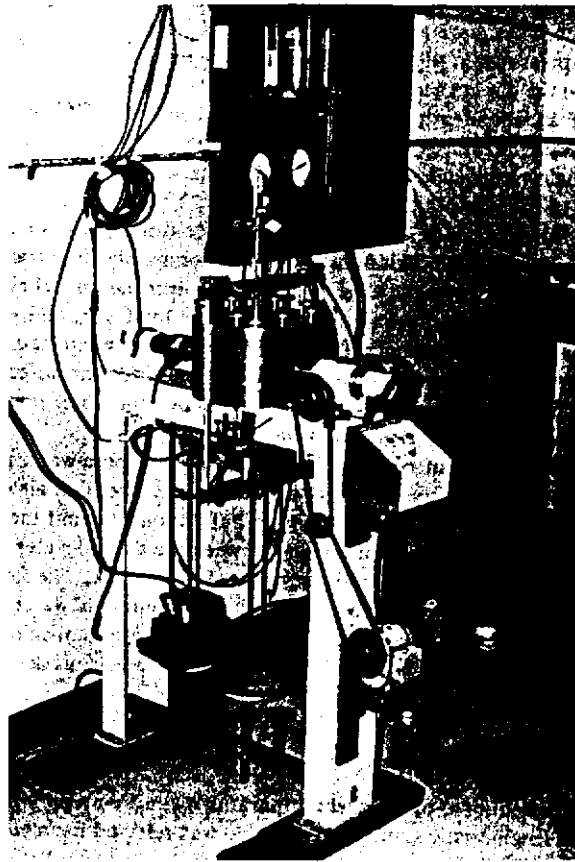


Figure 18 - Layout of the Complete Modified Direct Shear Box Apparatus
(from Gan and Fredlund, 1988)

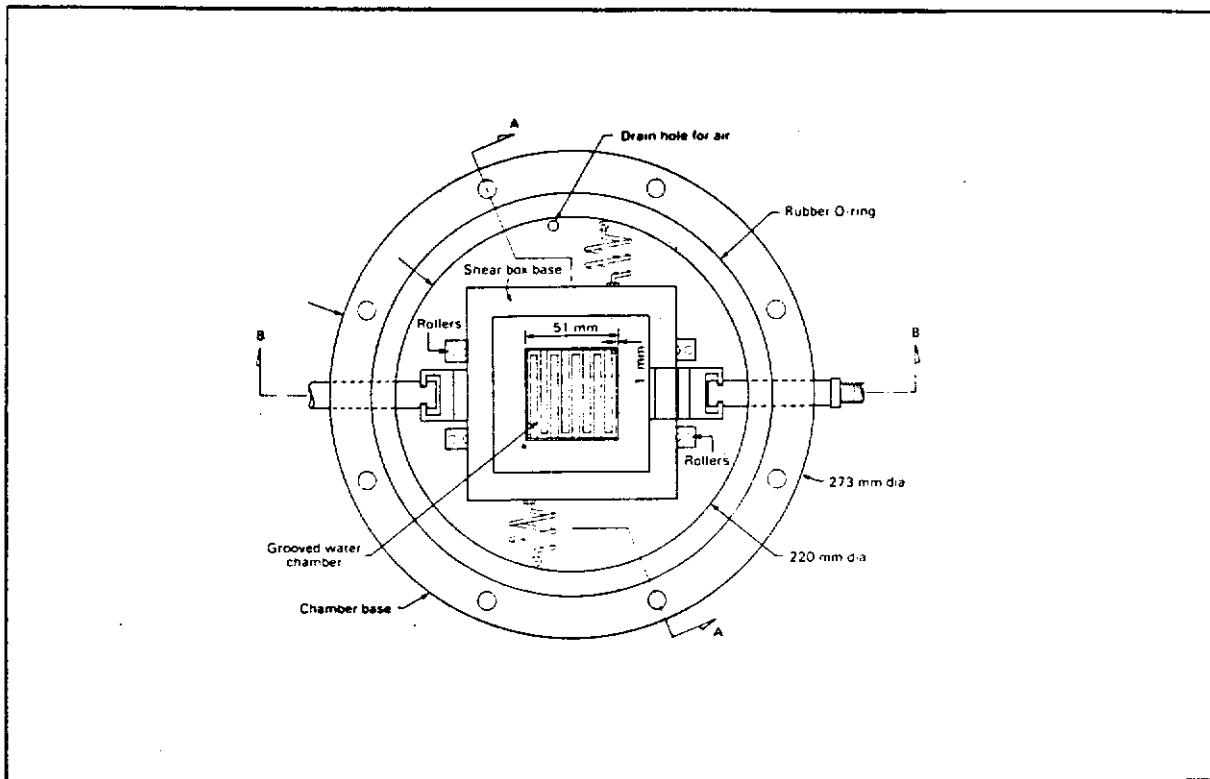


Figure 19 - Plan View of Modified Shear Box in Pressure Chamber
(with High Air Entry Disk Removed)
(from Gan and Fredlund, 1988)

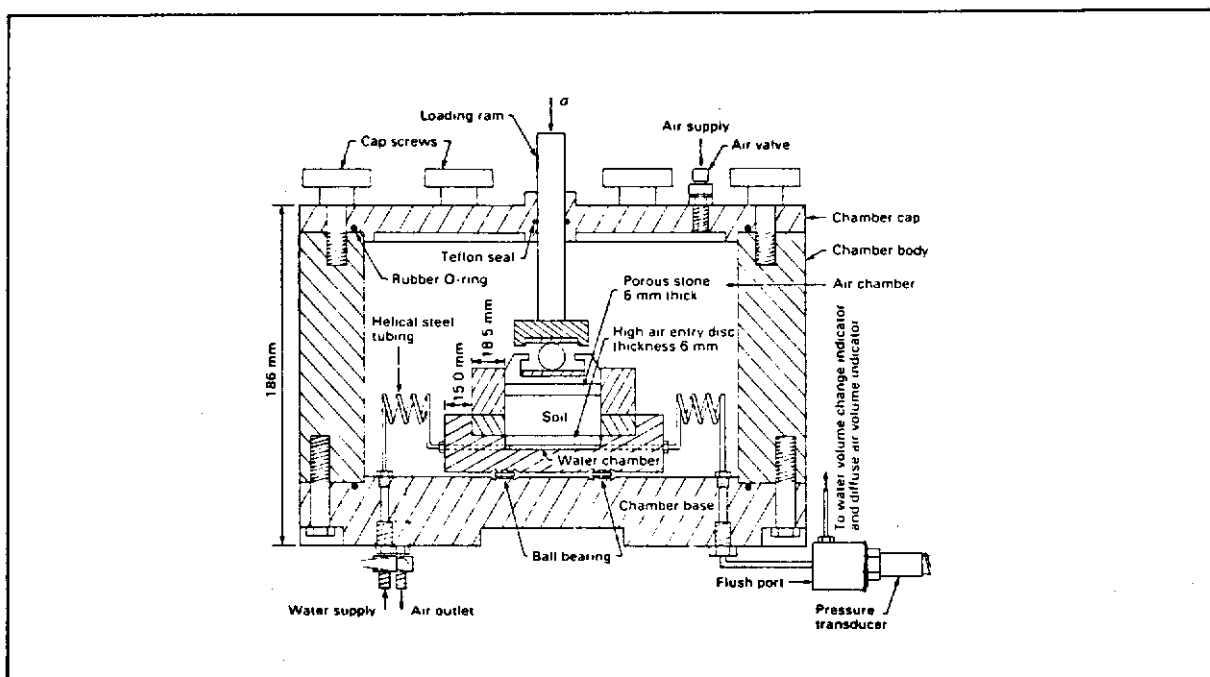


Figure 20 - Cross-sectional View A-A of Modified Shear Box and Pressure Chamber
(from Gan and Fredlund, 1988)

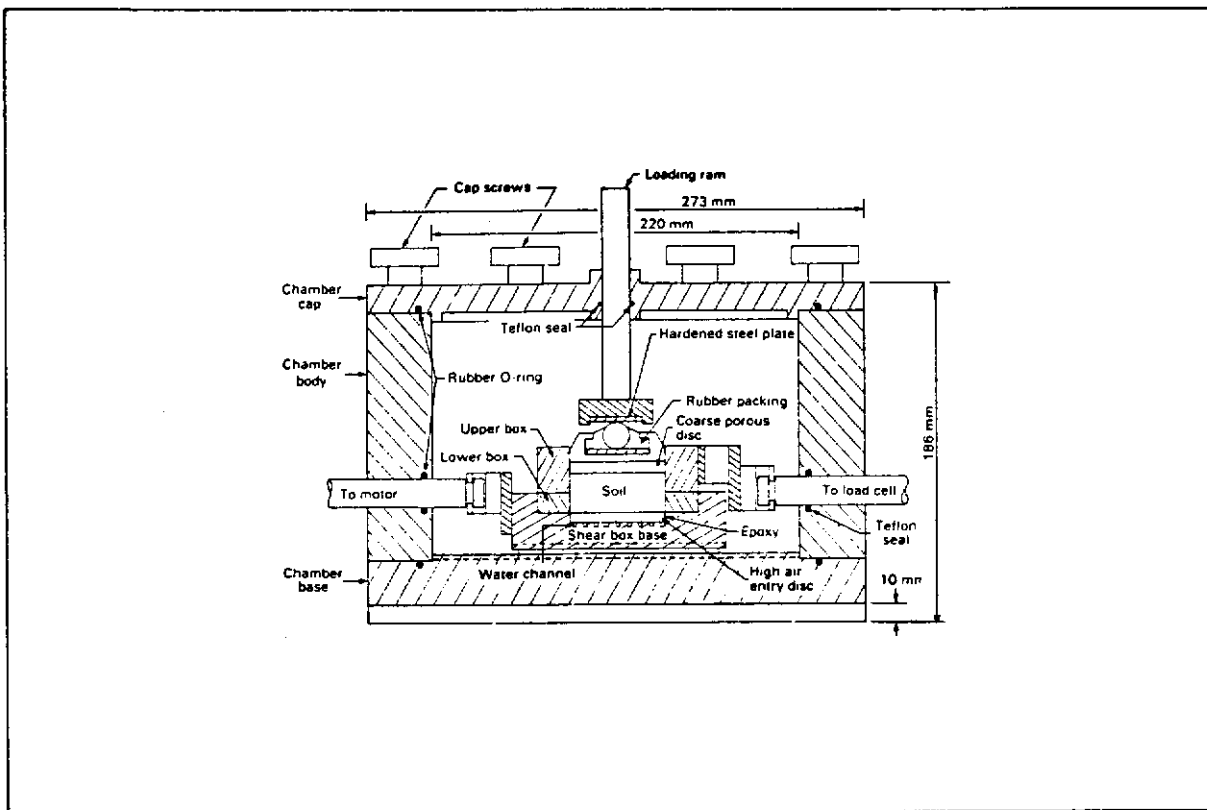


Figure 21 - Cross-sectional View B-B of Modified Shear Box and Pressure Chamber (from Gan and Fredlund, 1988)

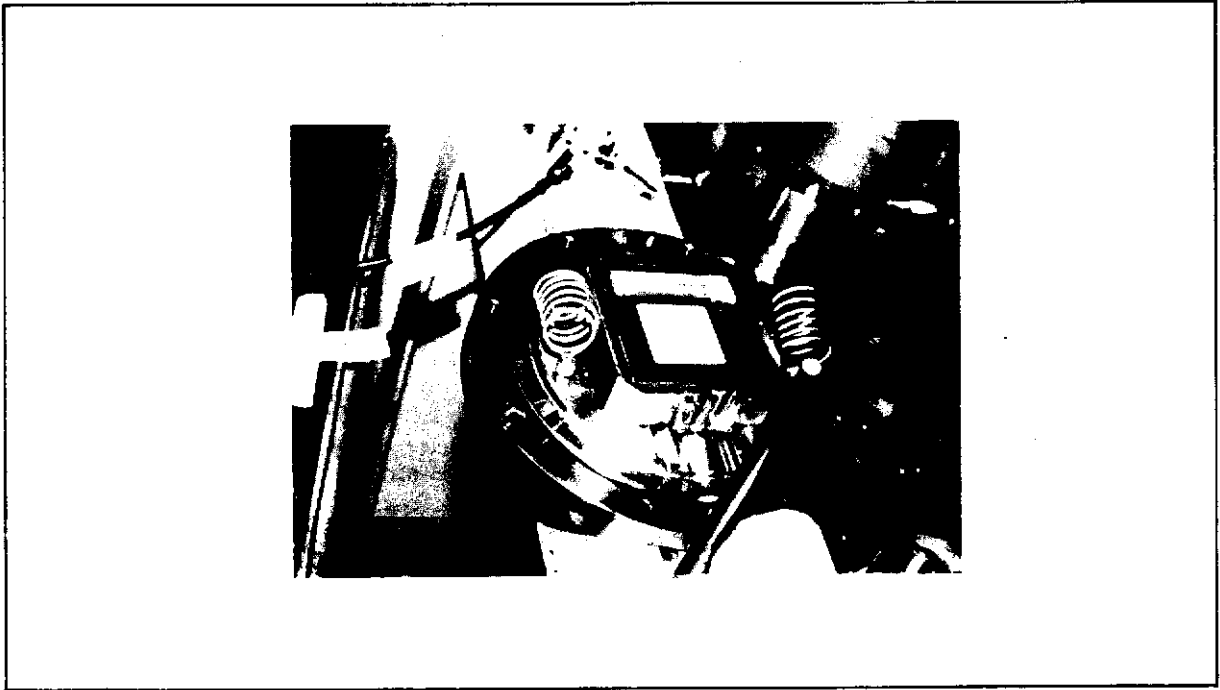


Figure 22 - Details of Shear Box Base and Chamber Base
(from Gan and Fredlund, 1988)

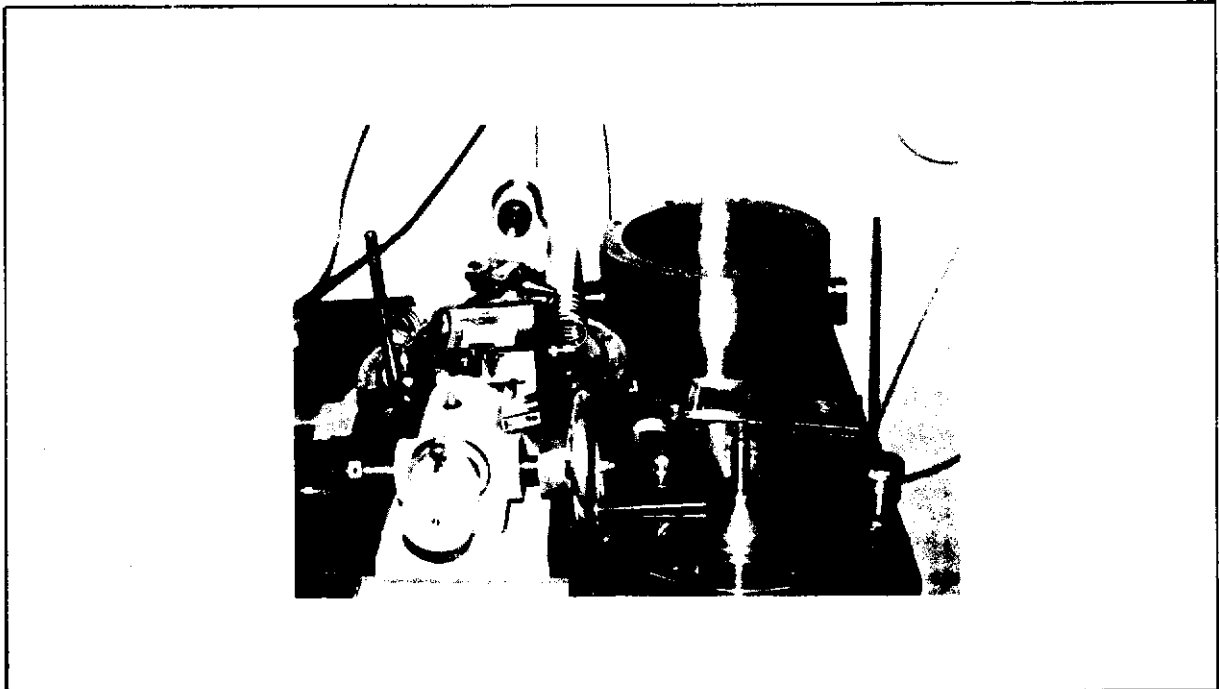


Figure 23 - Dismantled Direct Shear Apparatus Showing the Various Components
(from Gan and Fredlund, 1988)

SATURATED DIRECT SHEAR TEST

SPECIMEN NO. DS1B, SIGMA = 20 kPa

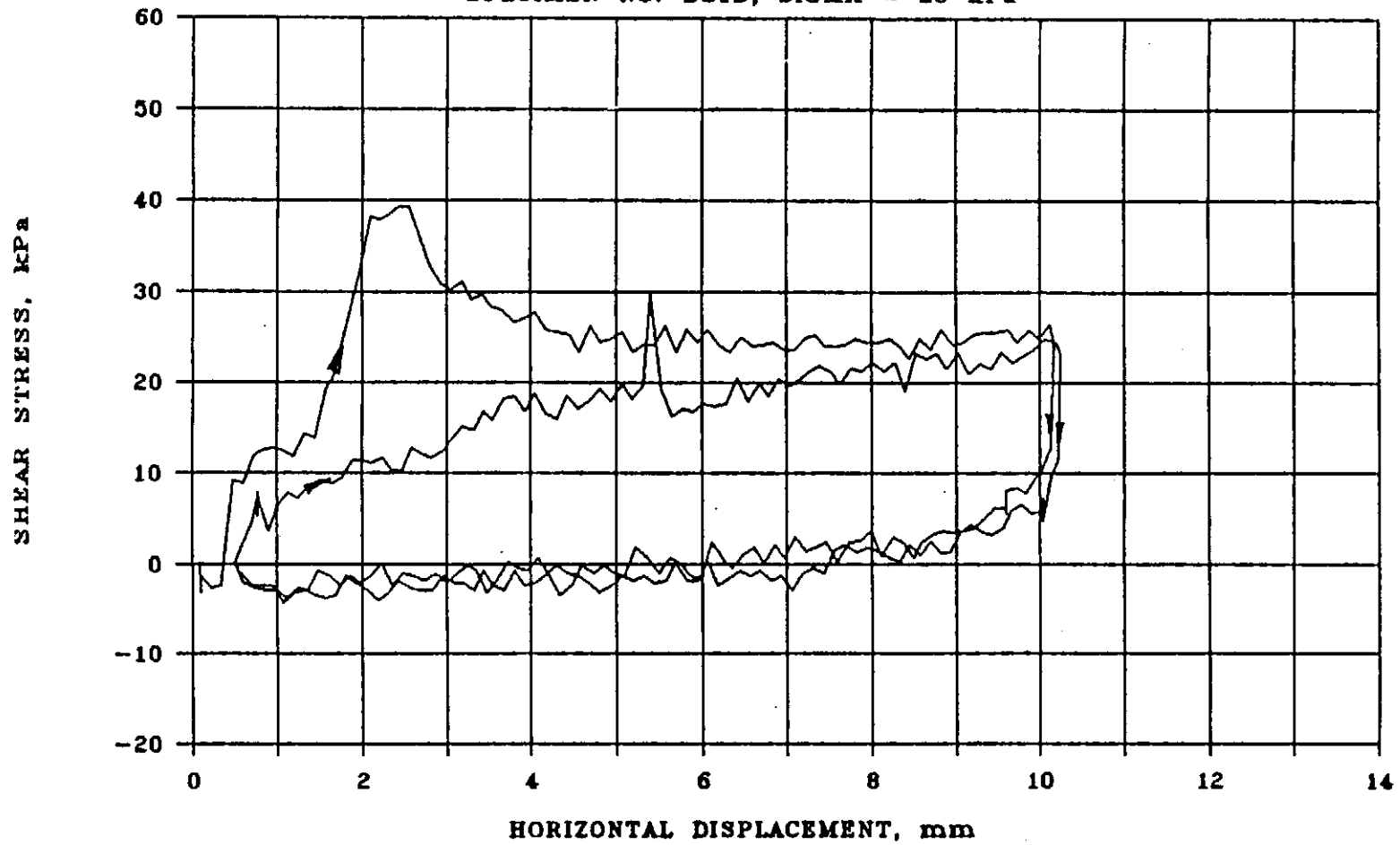


Figure 24a - Shear Stress versus Horizontal Displacement - 1st and 2nd Cycle (Specimen No. DS1B)

SATURATED DIRECT SHEAR TEST

SPECIMEN NO. DS1B, SIGMA = 20 kPa

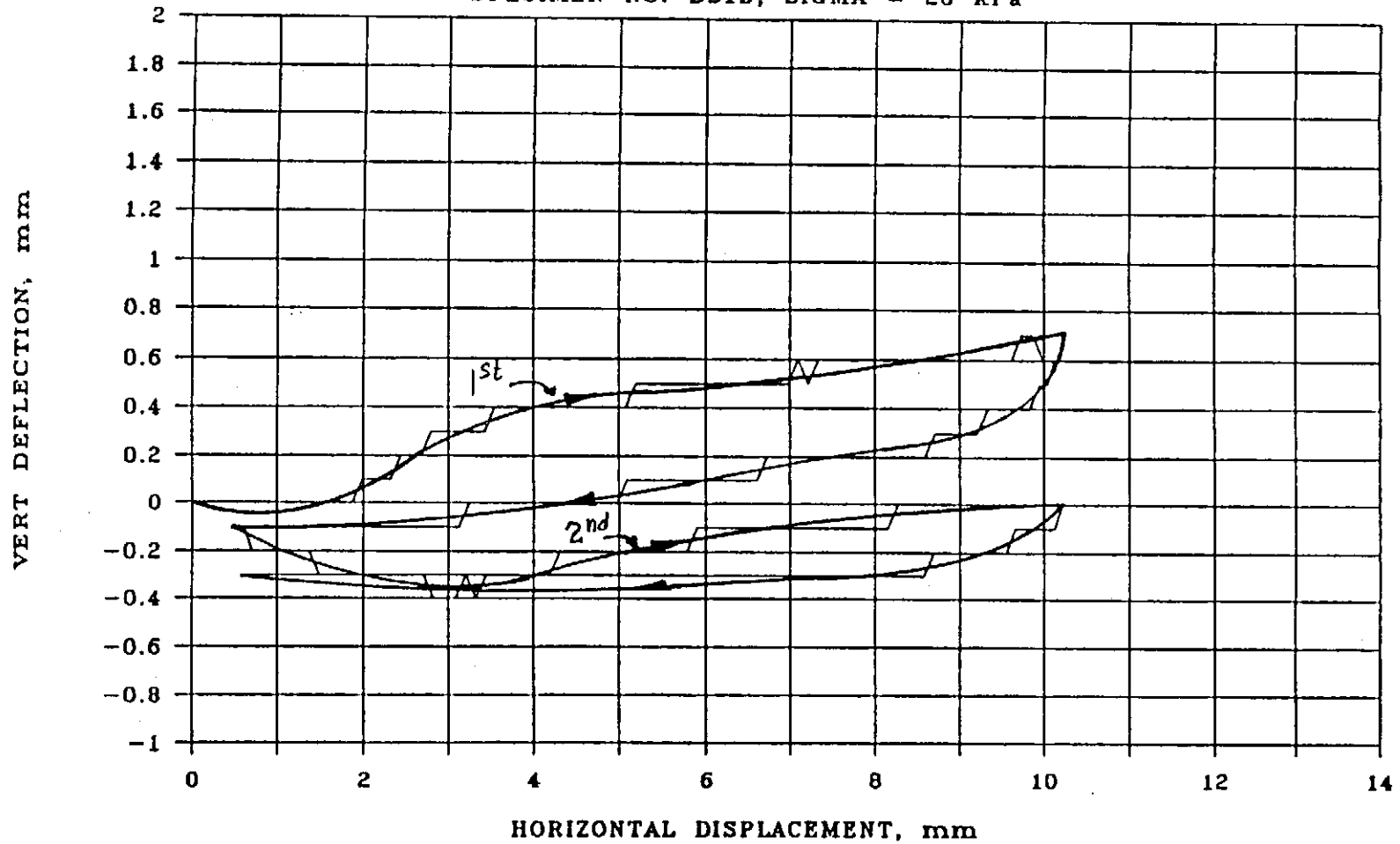


Figure 24b - Vertical Deflection versus Horizontal Displacement - 1st and 2nd Cycle (Specimen No. DS1B)

SATURATED DIRECT SHEAR TEST

SPECIMEN NO. DS1B, SIGMA = 20 kPa

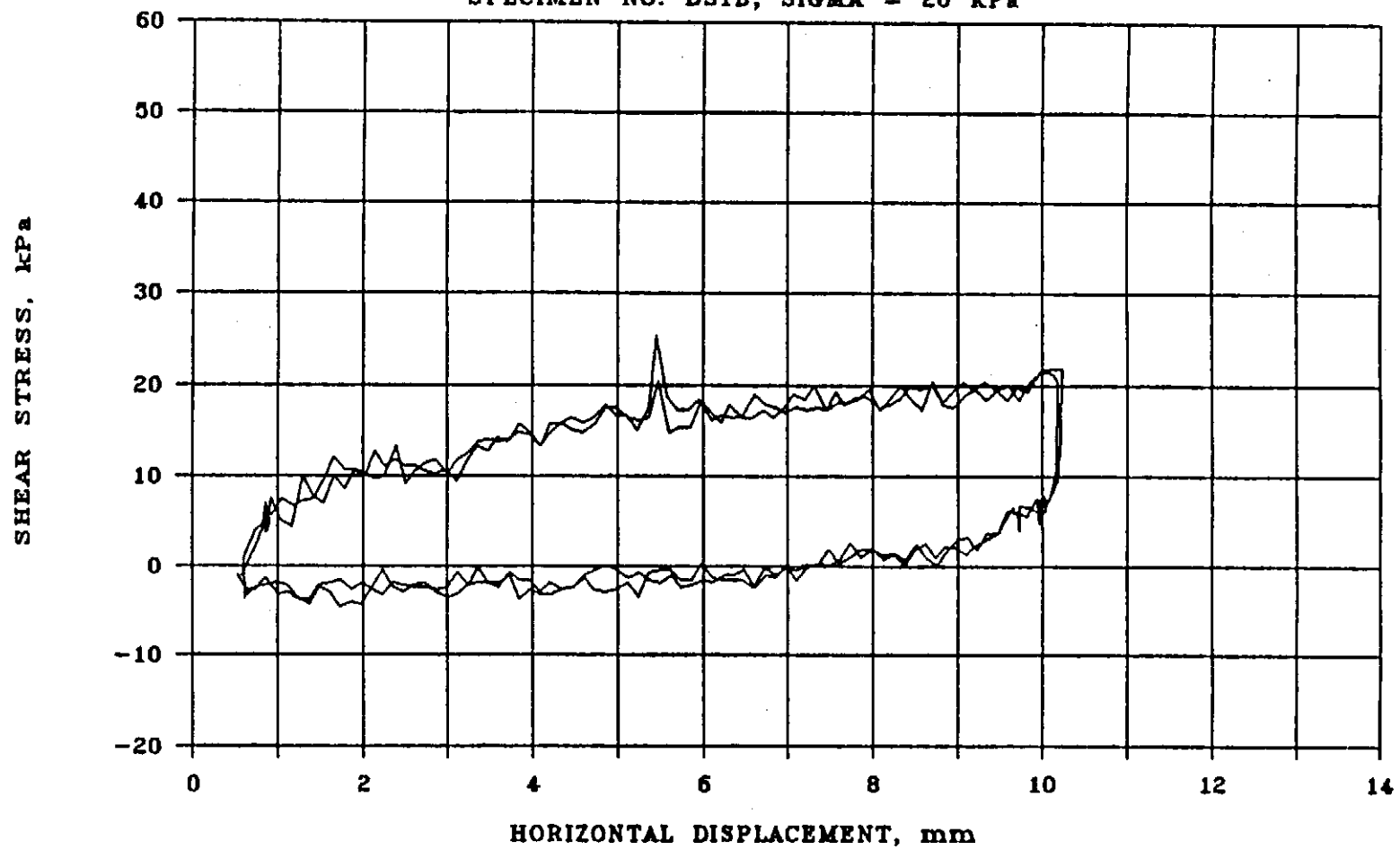


Figure 25a - Shear Stress versus Horizontal Displacement - 3rd and 4th Cycle (Specimen No. DS1B)

SATURATED DIRECT SHEAR TEST

SPECIMEN NO. DS1B, SIGMA = 20 kPa

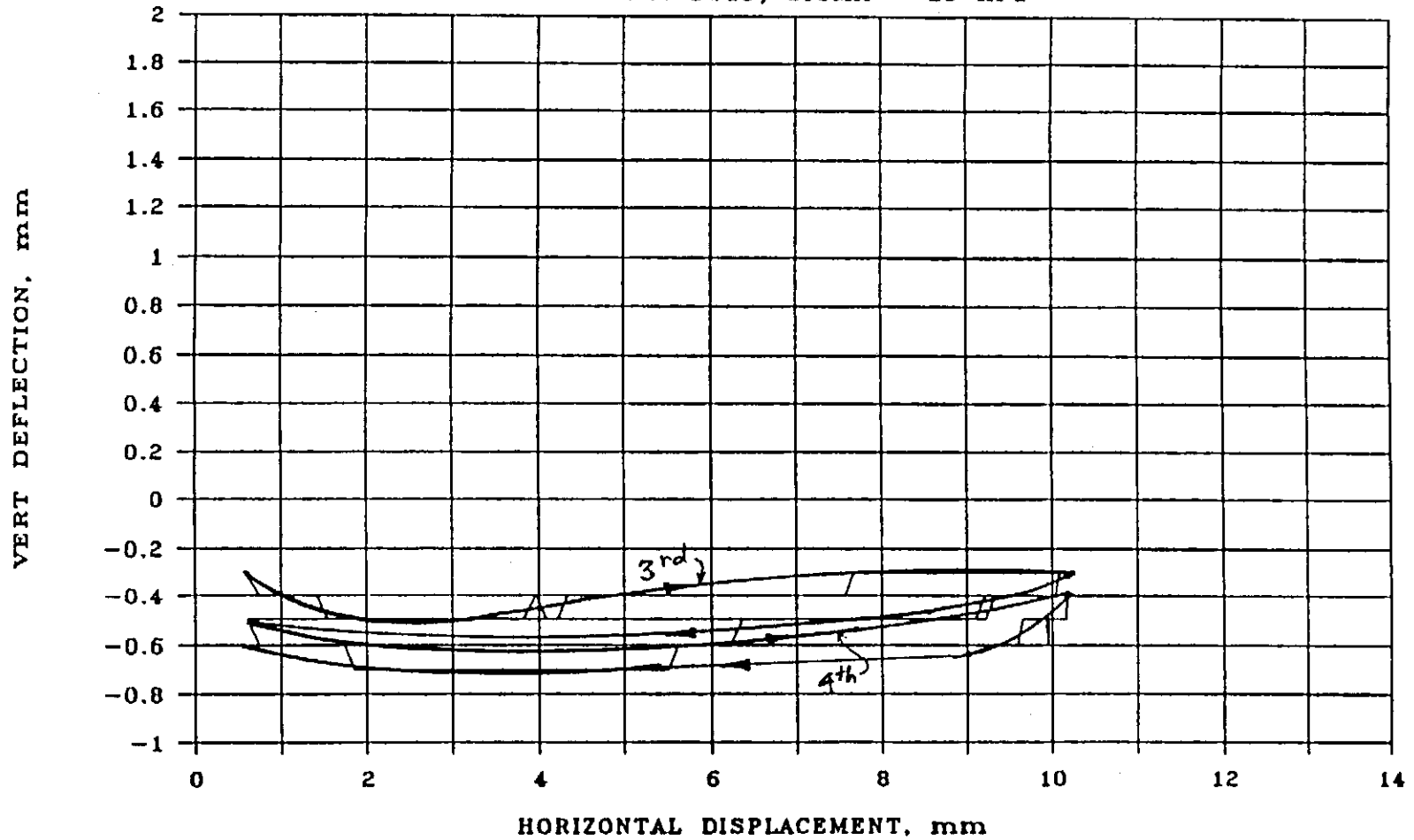


Figure 25b - Vertical Deflection versus Horizontal Displacement - 3rd and 4th Cycle (Specimen No. DS1B)

SATURATED DIRECT SHEAR TEST

SPECIMEN NO. DS1B, SIGMA = 20 kPa

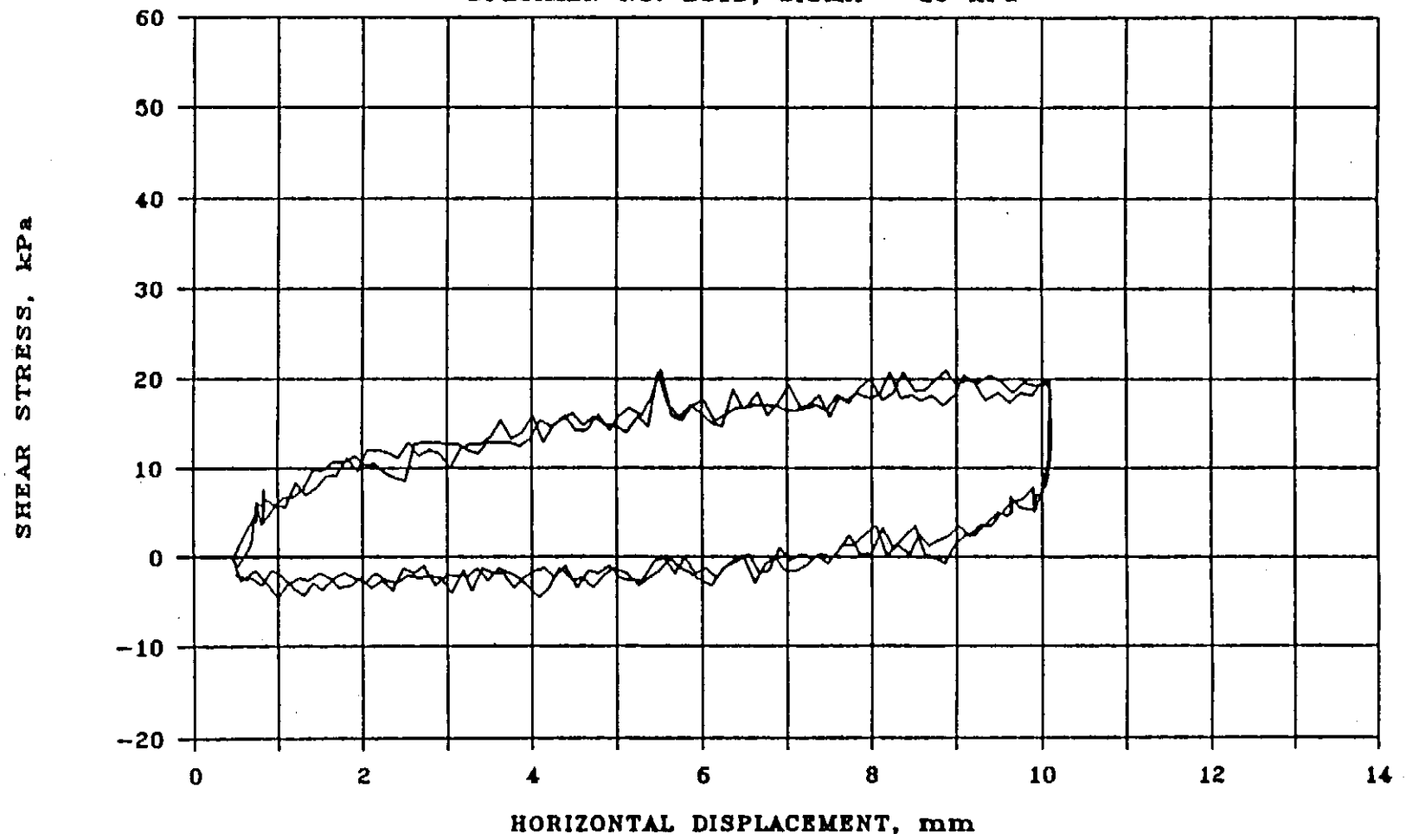


Figure 26a - Shear Stress versus Horizontal Displacement - 5th and 6th Cycle (Specimen No. DS1B)

SATURATED DIRECT SHEAR TEST

SPECIMEN NO. DS1B, SIGMA = 20 kPa

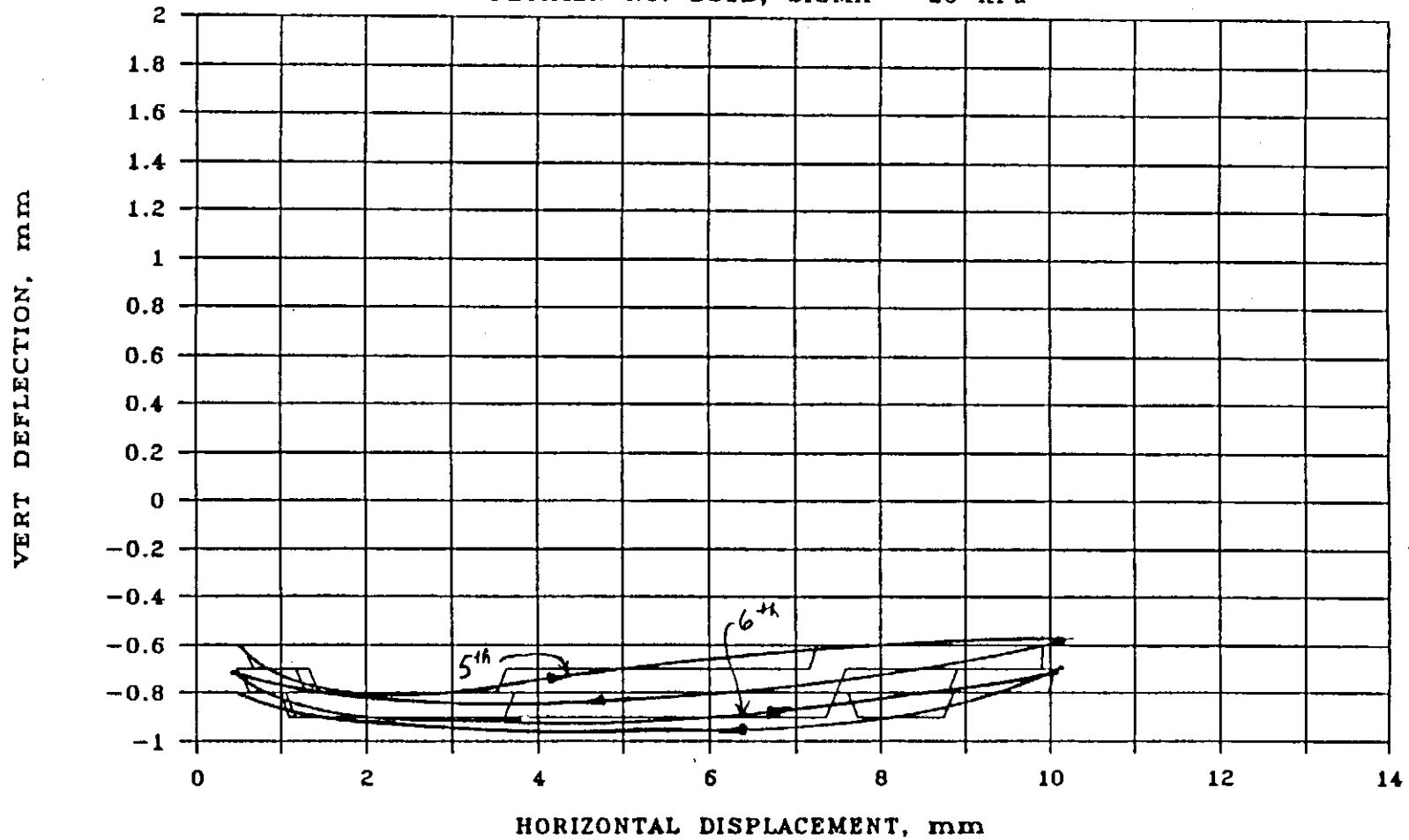


Figure 26b - Vertical Deflection versus Horizontal Displacement - 5th and 6th Cycle (Specimen No. DS1B)

SATURATED DIRECT SHEAR TEST

SPECIMEN NO. DS1B, SIGMA = 20 kPa

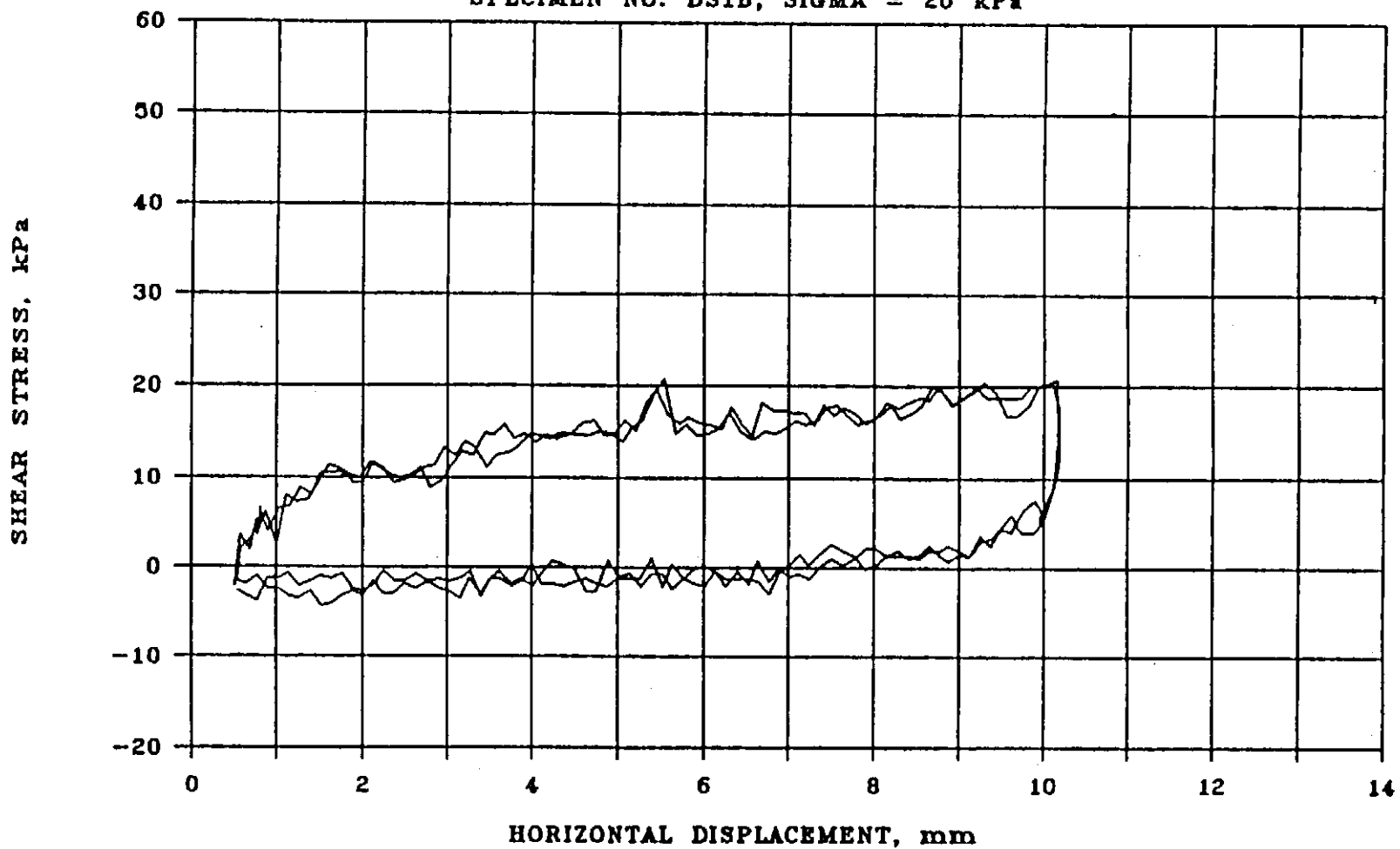


Figure 27a - Shear Stress versus Horizontal Displacement - 7th and 8th Cycle (Specimen No. DS1B)

SATURATED DIRECT SHEAR TEST

SPECIMEN NO. DS1B, SIGMA = 20 kPa

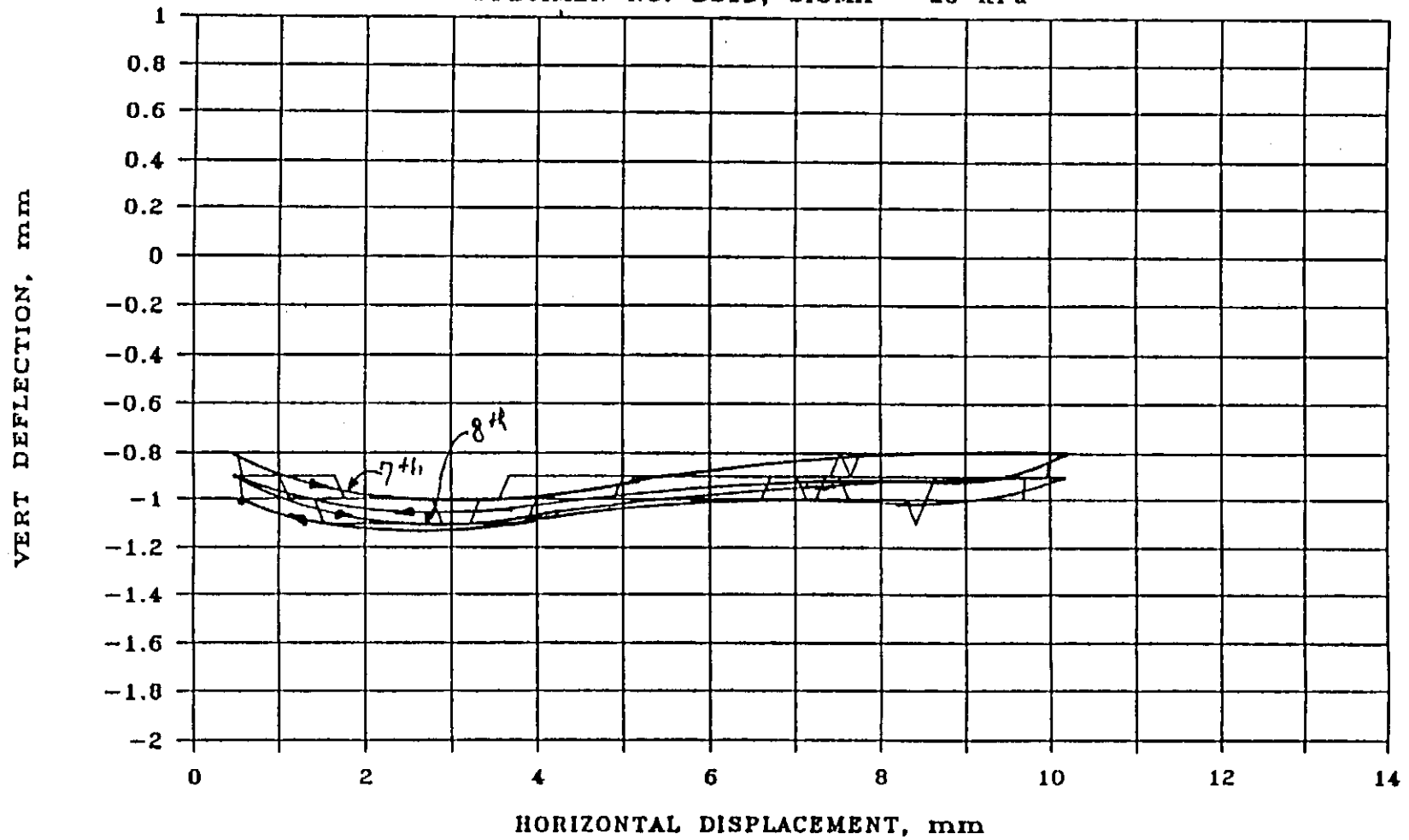


Figure 27b - Vertical Deflection versus Horizontal Displacement - 7th and 8th Cycle (Specimen No. DS1B)

SATURATED DIRECT SHEAR TEST

SPECIMEN NO. DS1B, SIGMA = 20 kPa

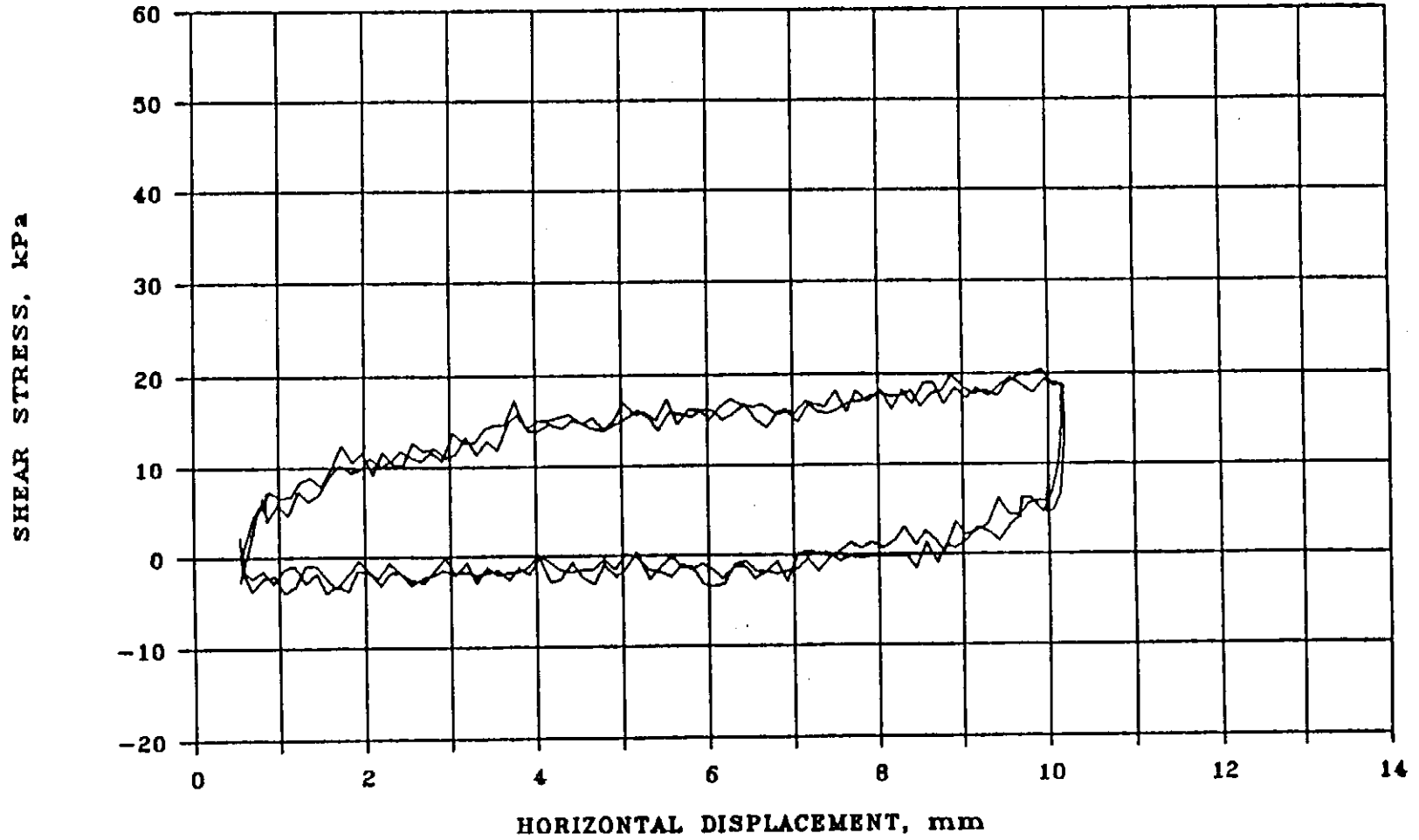


Figure 28 - Shear Stress versus Horizontal Displacement - 9th and 10th Cycle (Specimen No. DS1B)

SATURATED DIRECT SHEAR TEST

SPECIMEN NO. DS1B, SIGMA = 20 kPa

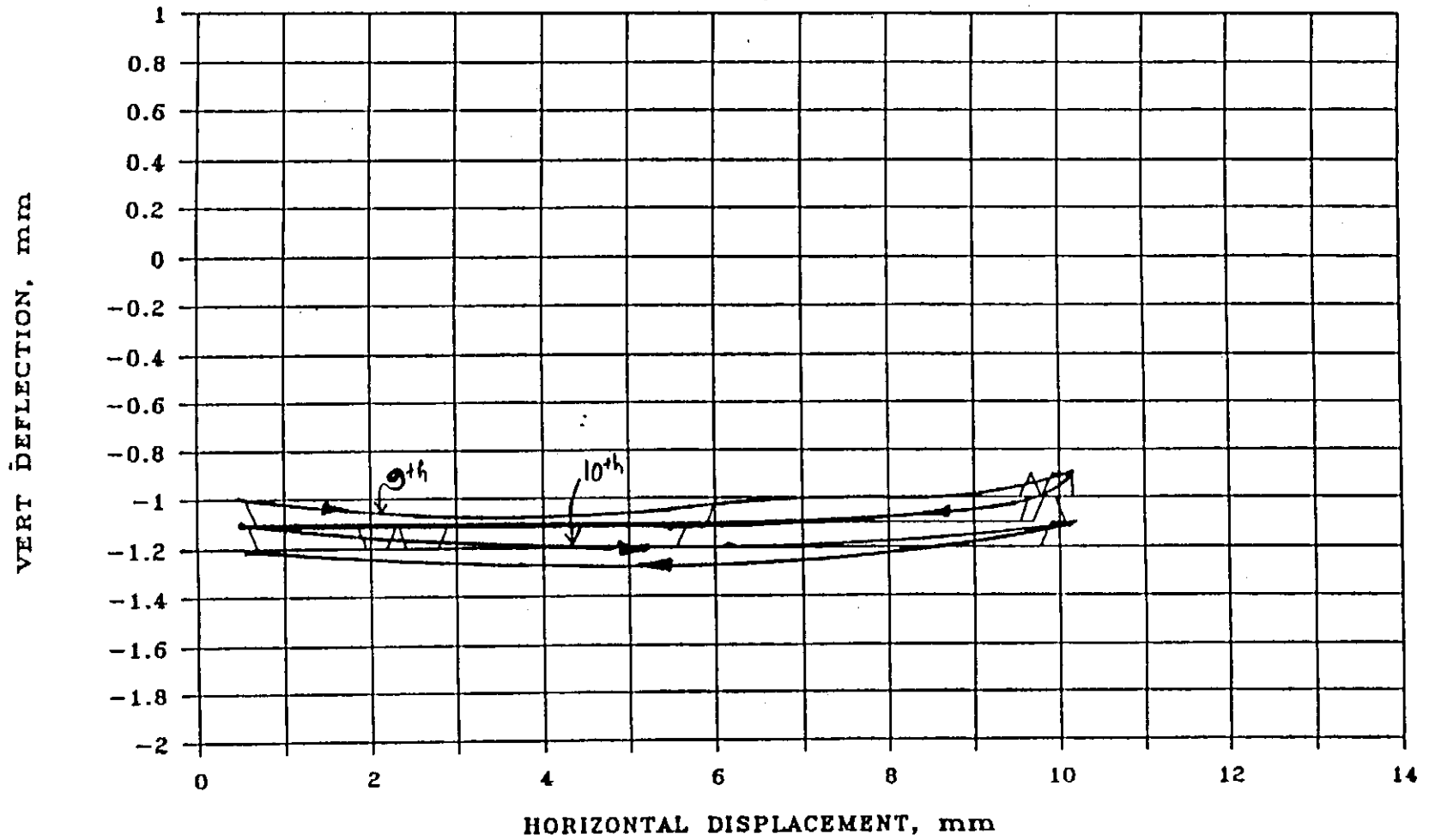


Figure 29 - Vertical Deflection versus Horizontal Displacement - 9th and 10th Cycle (Specimen No. DS1B)

SATURATED DIRECT SHEAR TEST

SPECIMEN NO. DS1B, SIGMA = 20 kPa

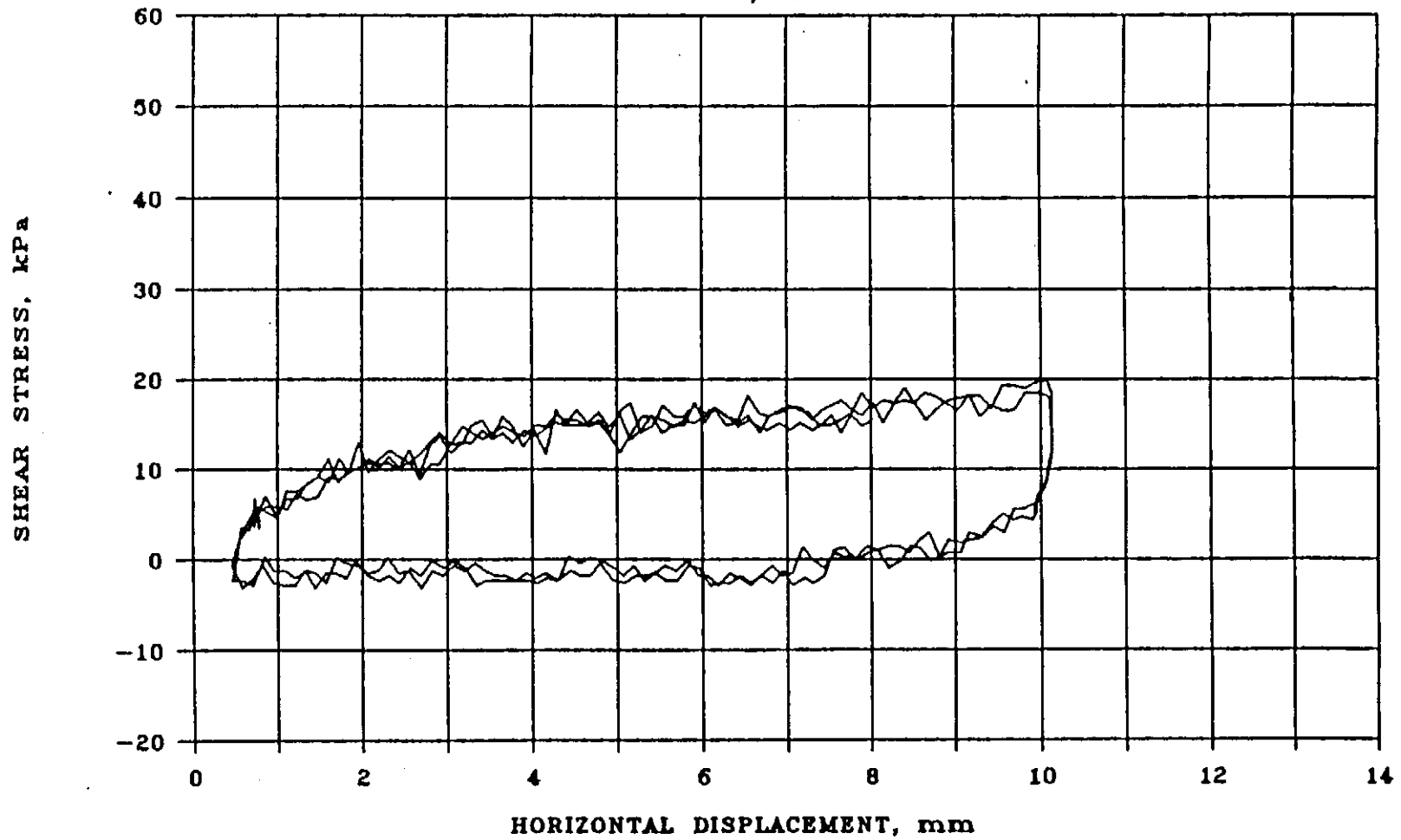


Figure 30 - Shear Stress versus Horizontal Displacement - 11th to 13th Cycle (Specimen No. DS1B)

SATURATED DIRECT SHEAR TEST

SPECIMEN NO. DS1B, SIGMA = 20 kPa

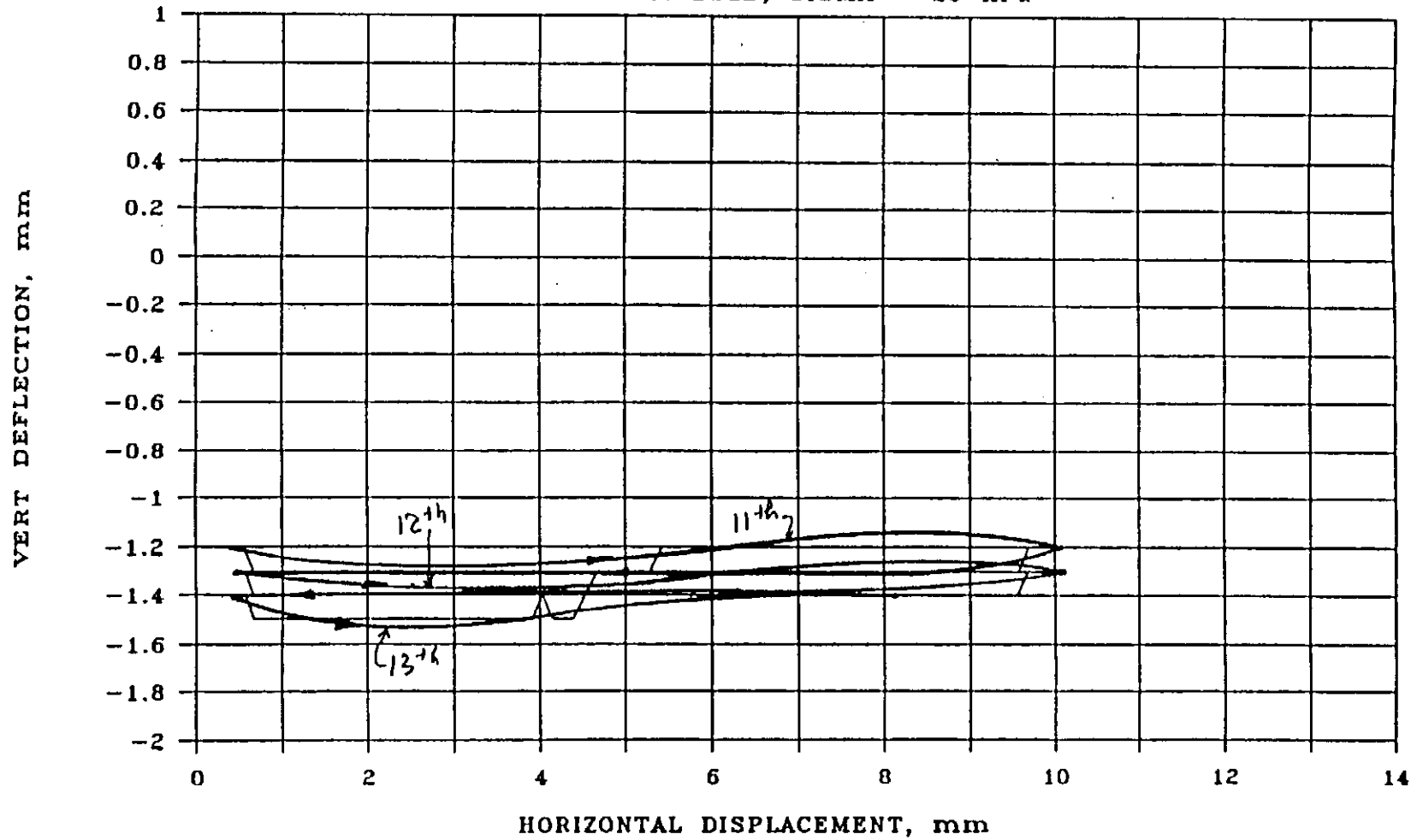


Figure 31 - Vertical Deflection versus Horizontal Displacement - 11th and 13th Cycle (Specimen No. DS1B)

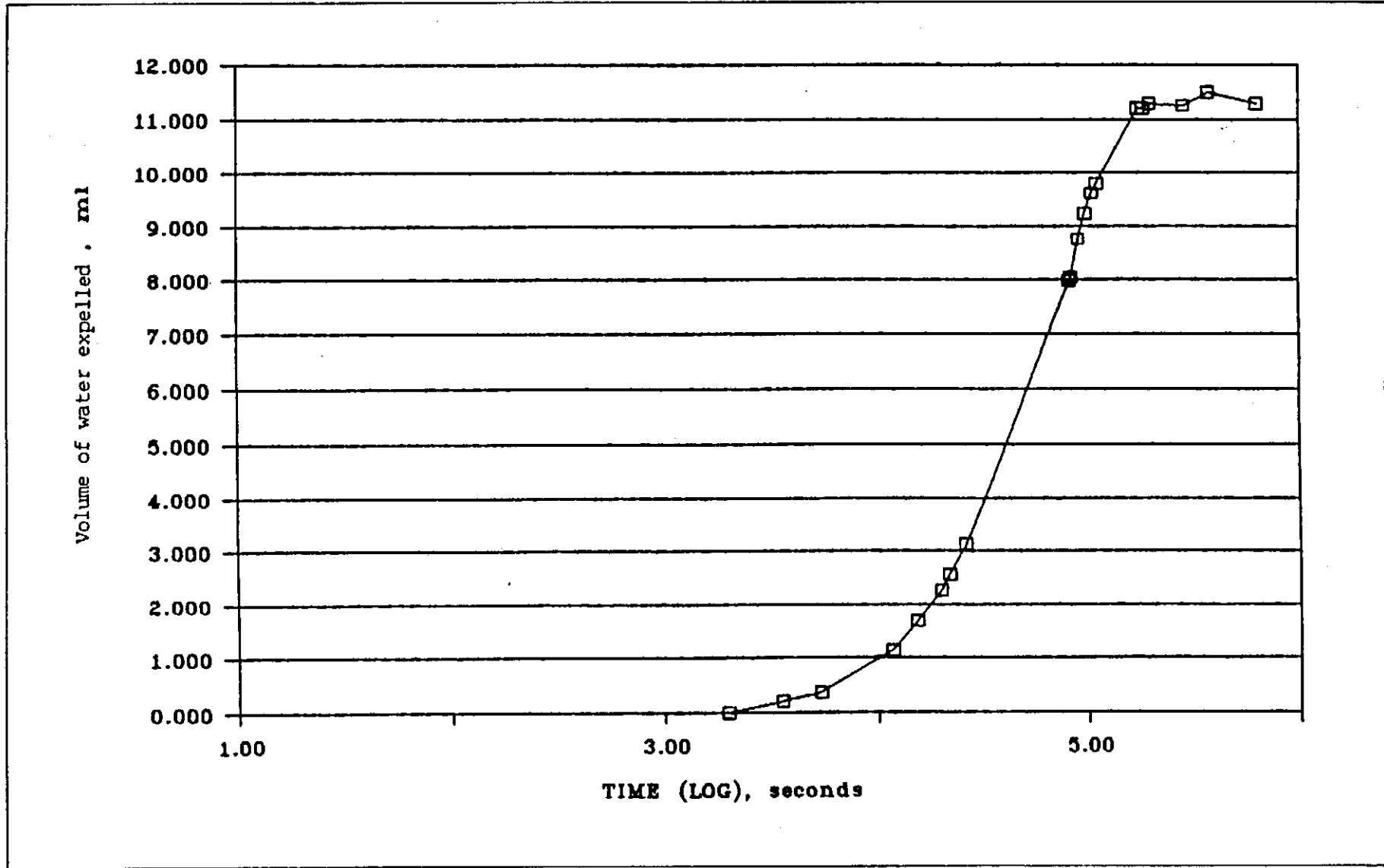


Figure 32 - Volume of Water Expelled versus Log Time (Specimen No. MDS1)

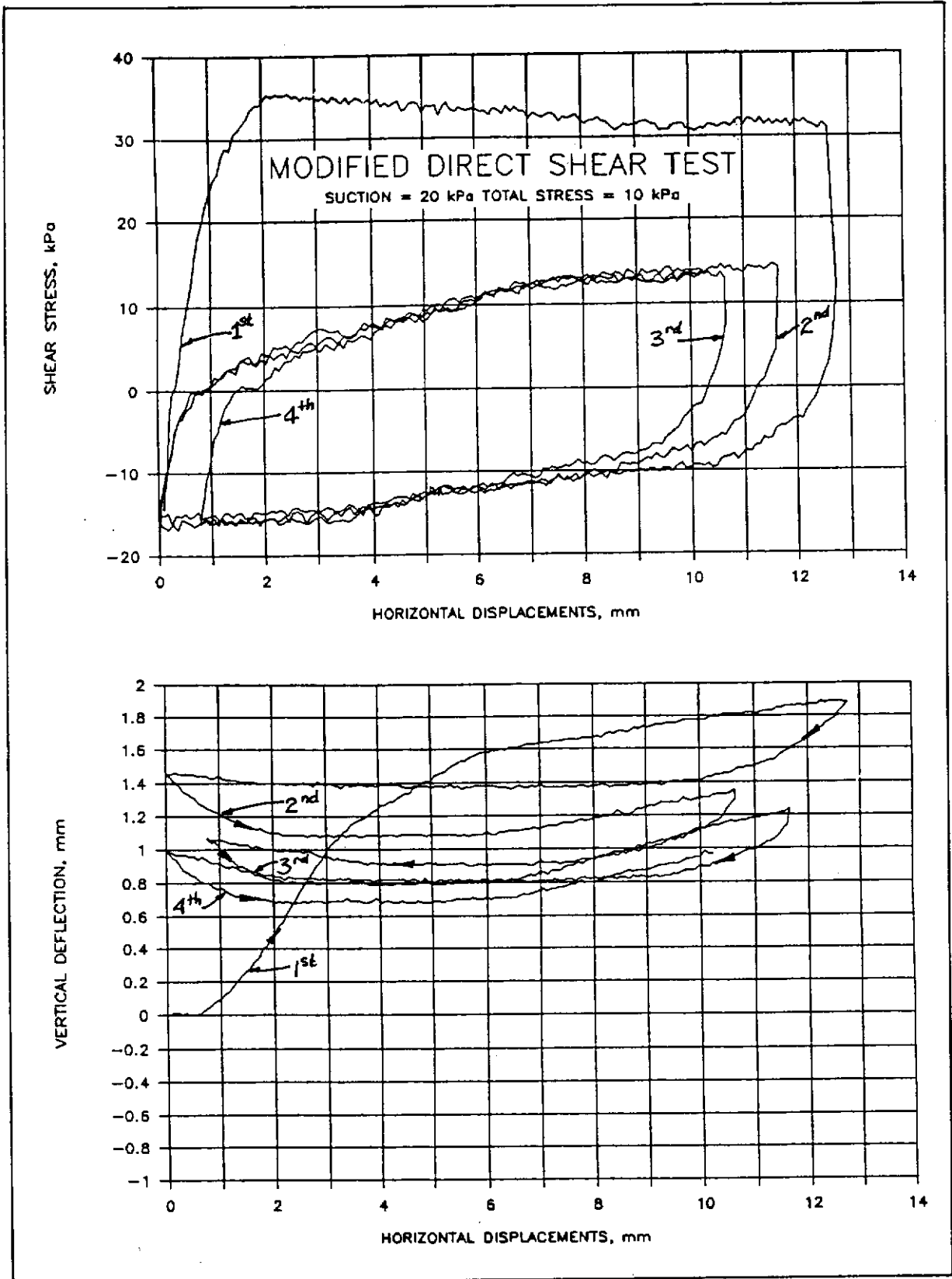


Figure 33 - Results of Modified Direct Shear Test in Pilot Test on Specimen No. MDS1
(a) Shear Stress versus Horizontal Displacements,
(b) Vertical Deflection versus Horizontal Displacement

SATURATED DIRECT SHEAR TEST

SPECIMEN NO. DS1C, SIGMA = 12.4 kPa

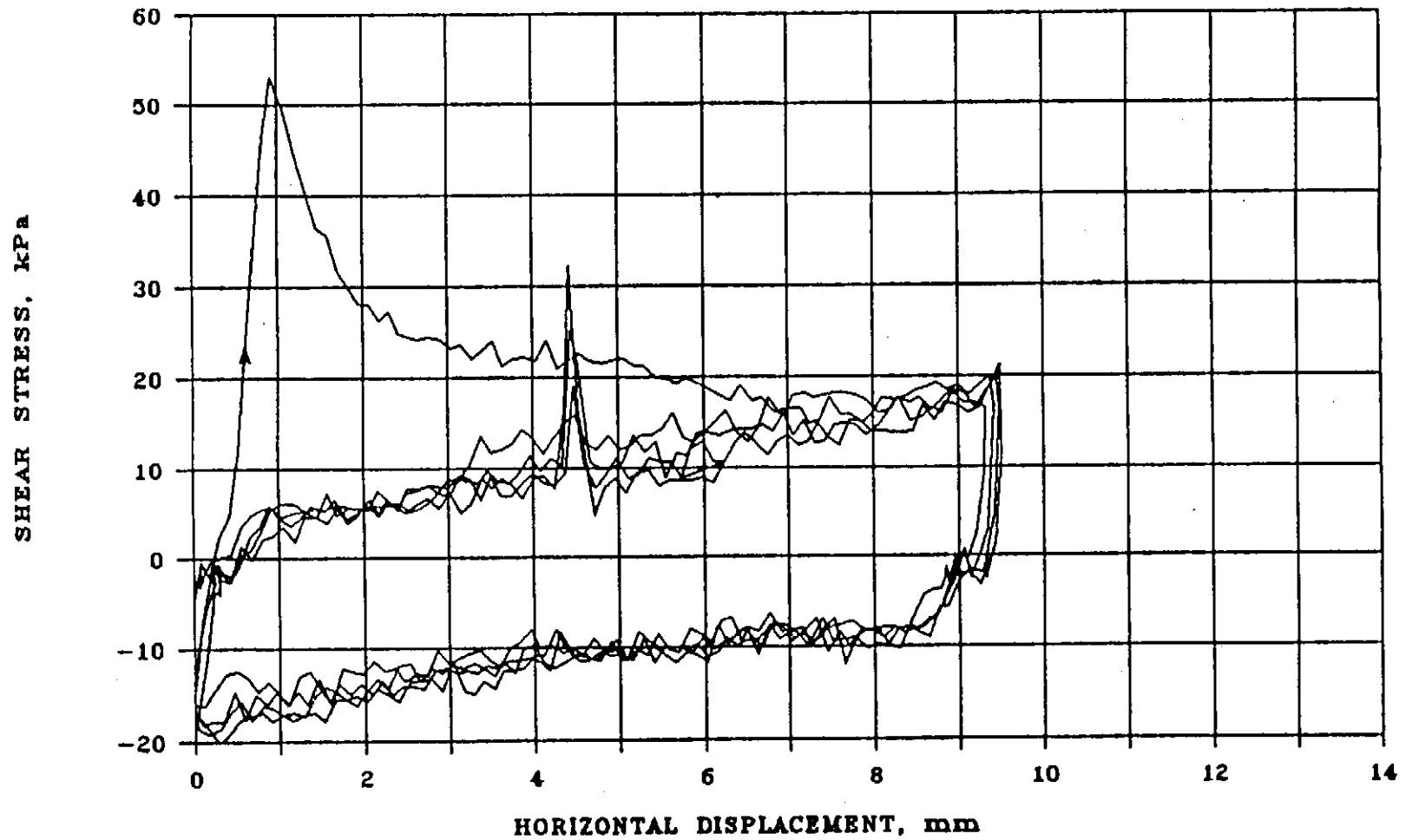


Figure 34 - Shear Stress versus Horizontal Displacement - 1st to 4th Cycle (Specimen No. DS1C)

SATURATED DIRECT SHEAR TEST

SPECIMEN NO. DS1C, SIGMA = 12.4 kPa

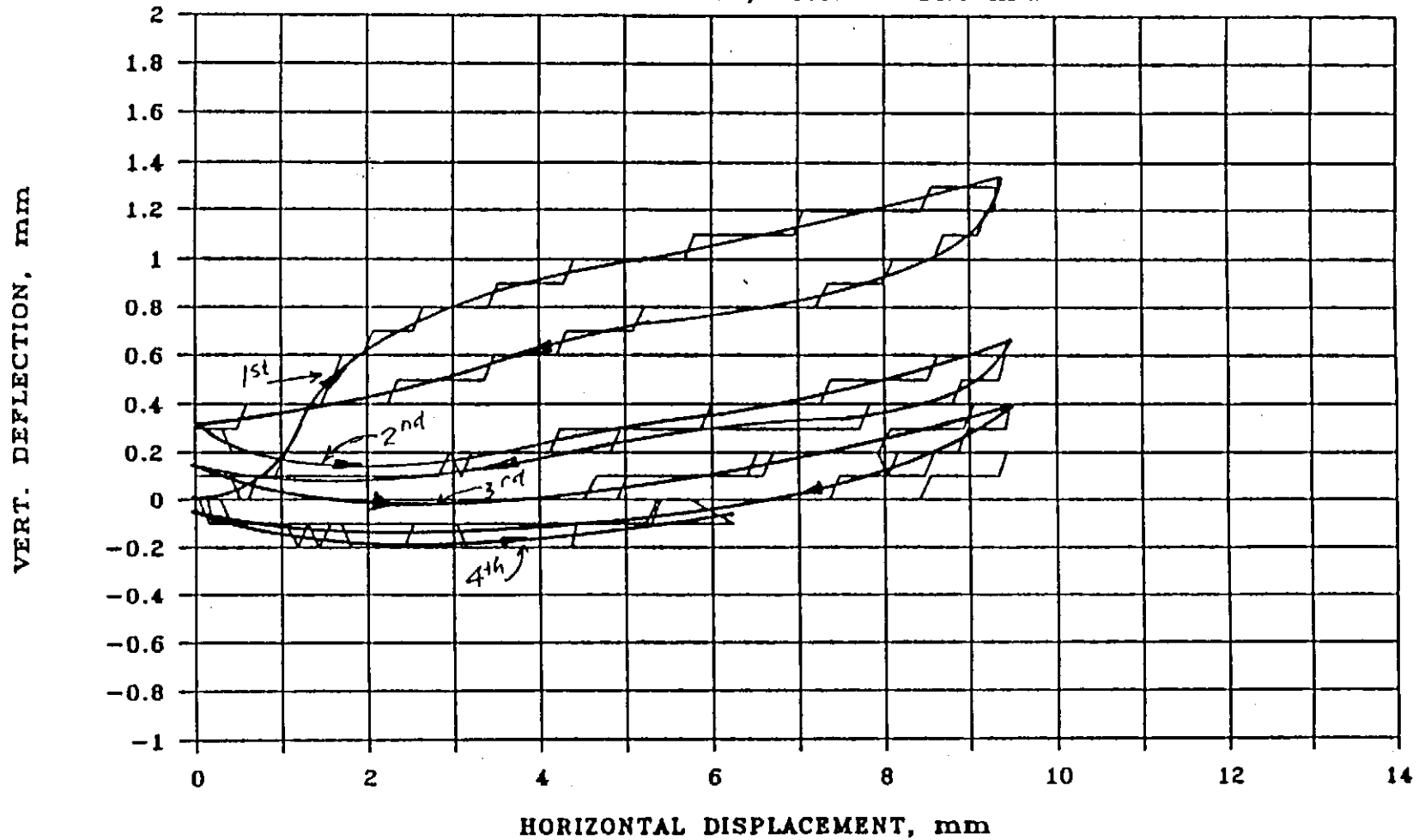


Figure 35 - Vertical Deflection versus Horizontal Displacement - 1st to 4th Cycle (Specimen No. DS1C)

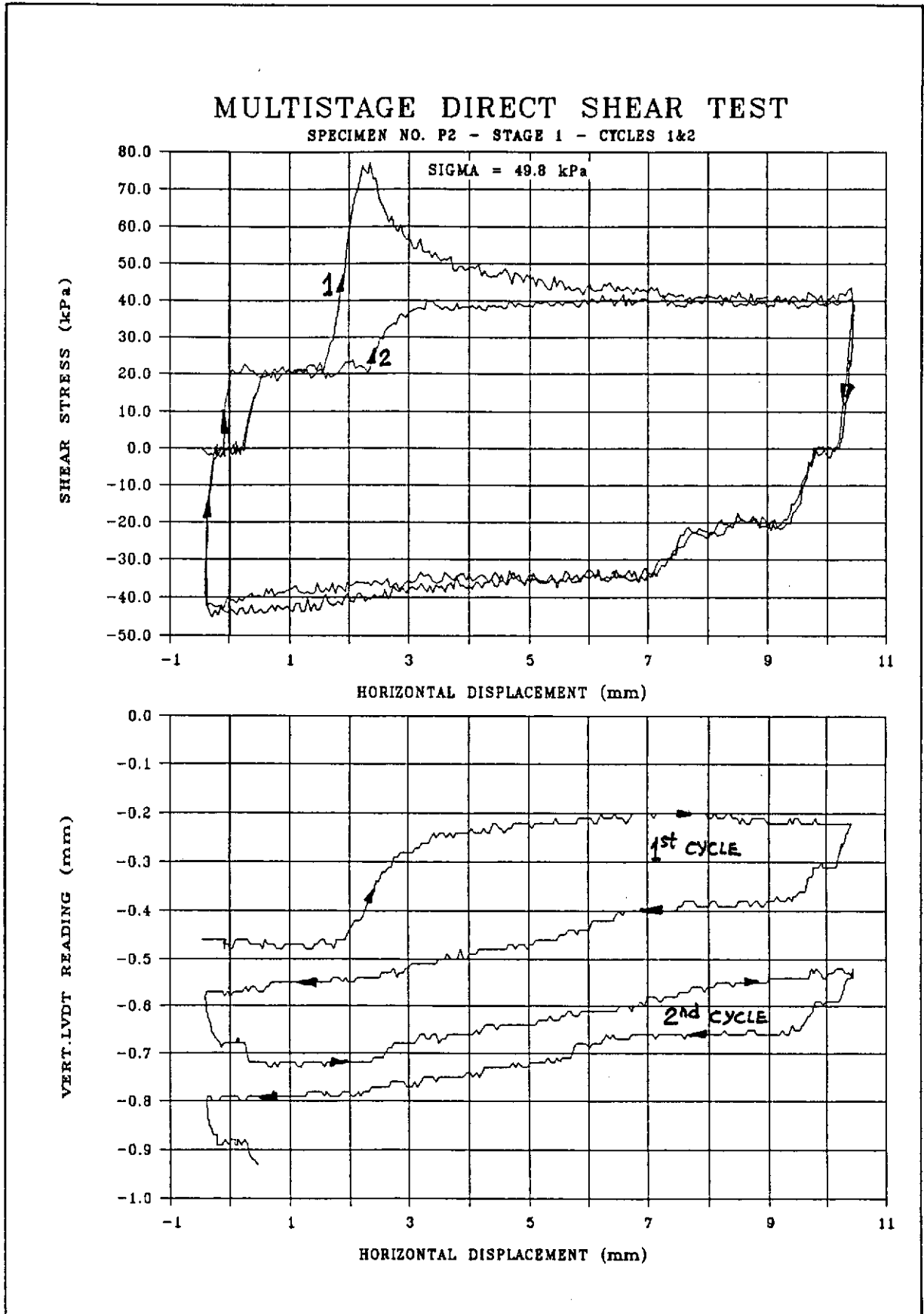


Figure 36 - Multistage Direct Shear Test on Specimen No. P2 - Stage 1

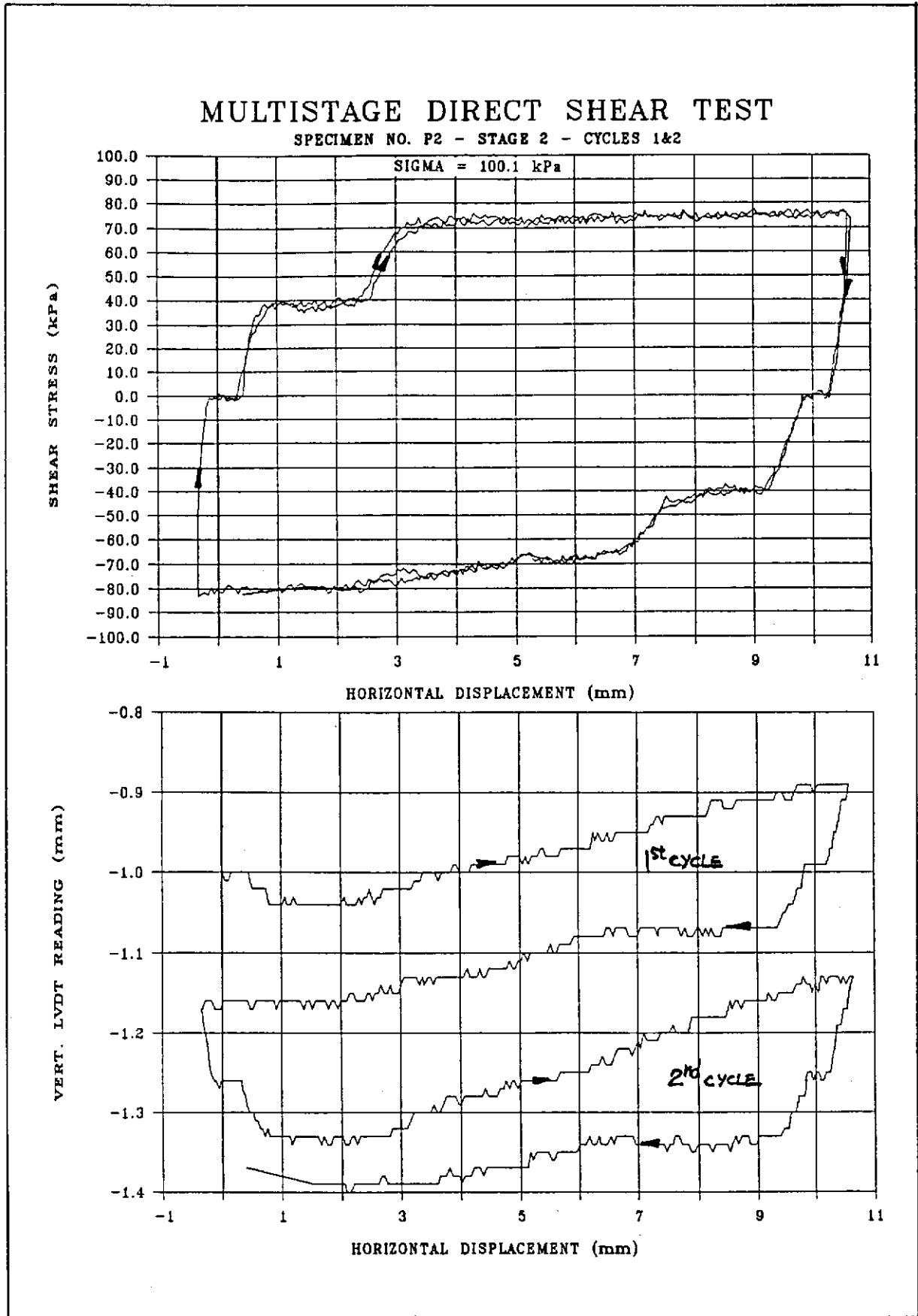


Figure 37 - Multistage Direct Shear Test on Specimen No. P2 - Stage 2

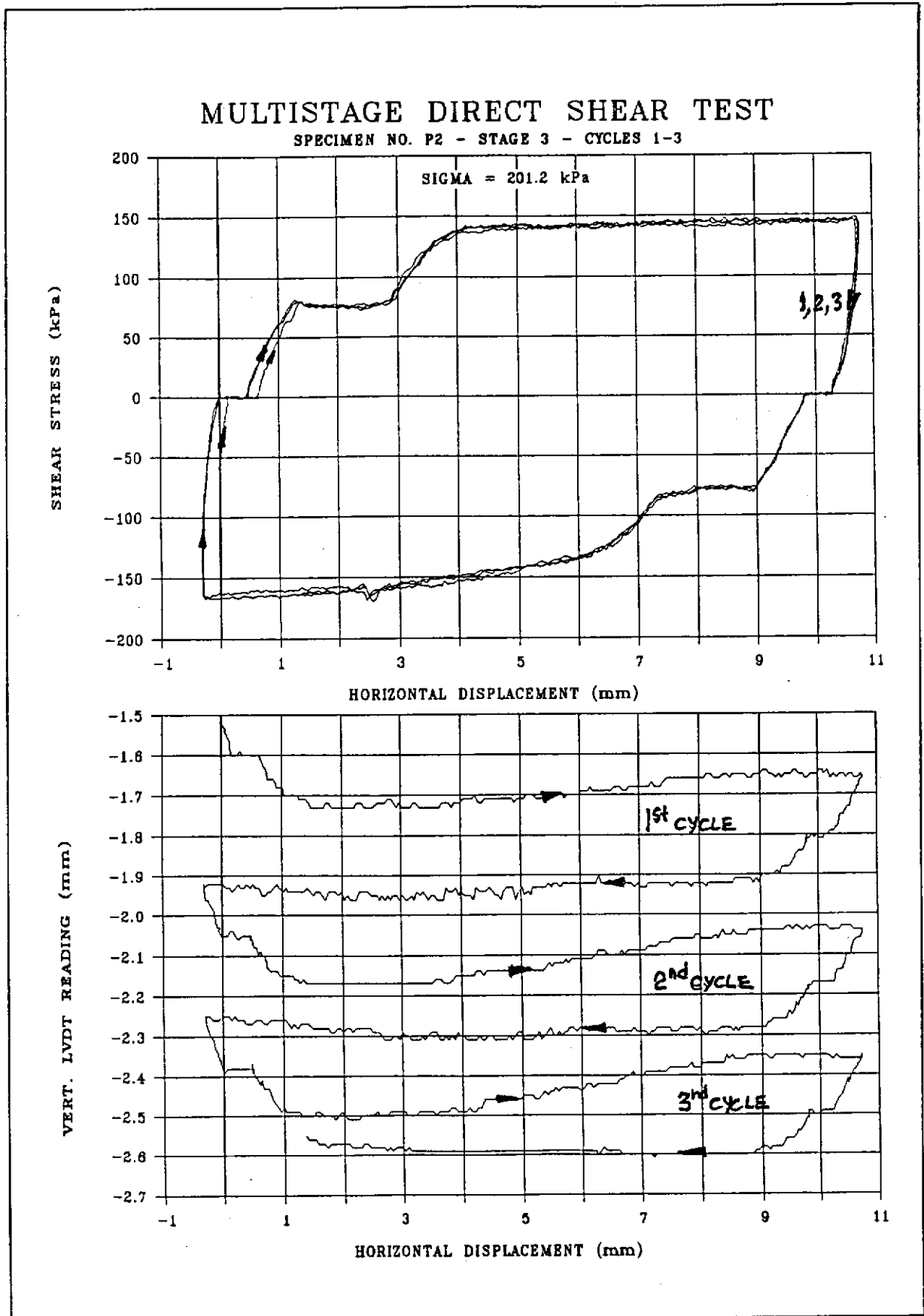


Figure 38 - Multistage Direct Shear Test on Specimen No. P2 - Stage 3

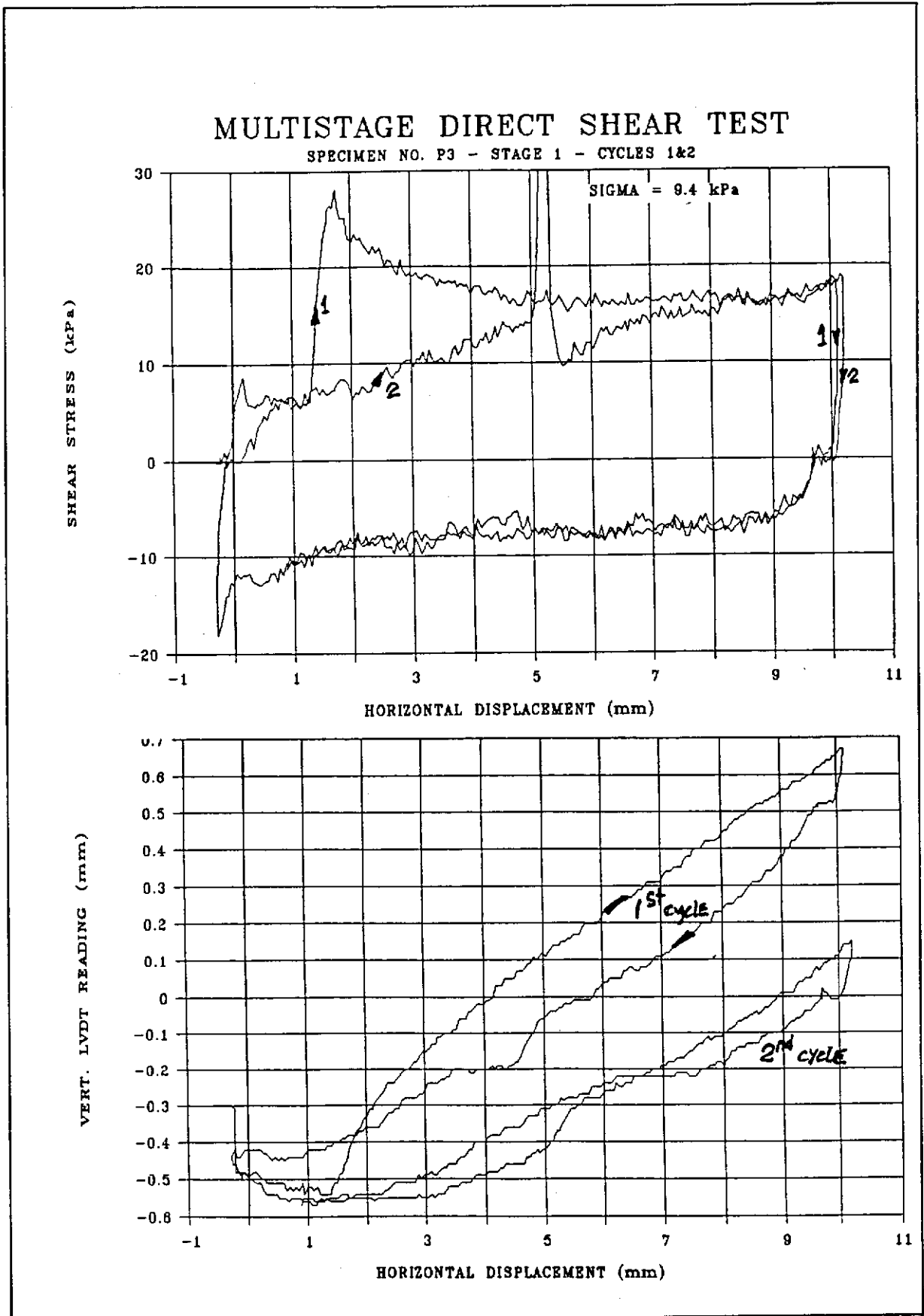


Figure 39 - Multistage Direct Shear Test on Specimen No. P3 - Stage 1

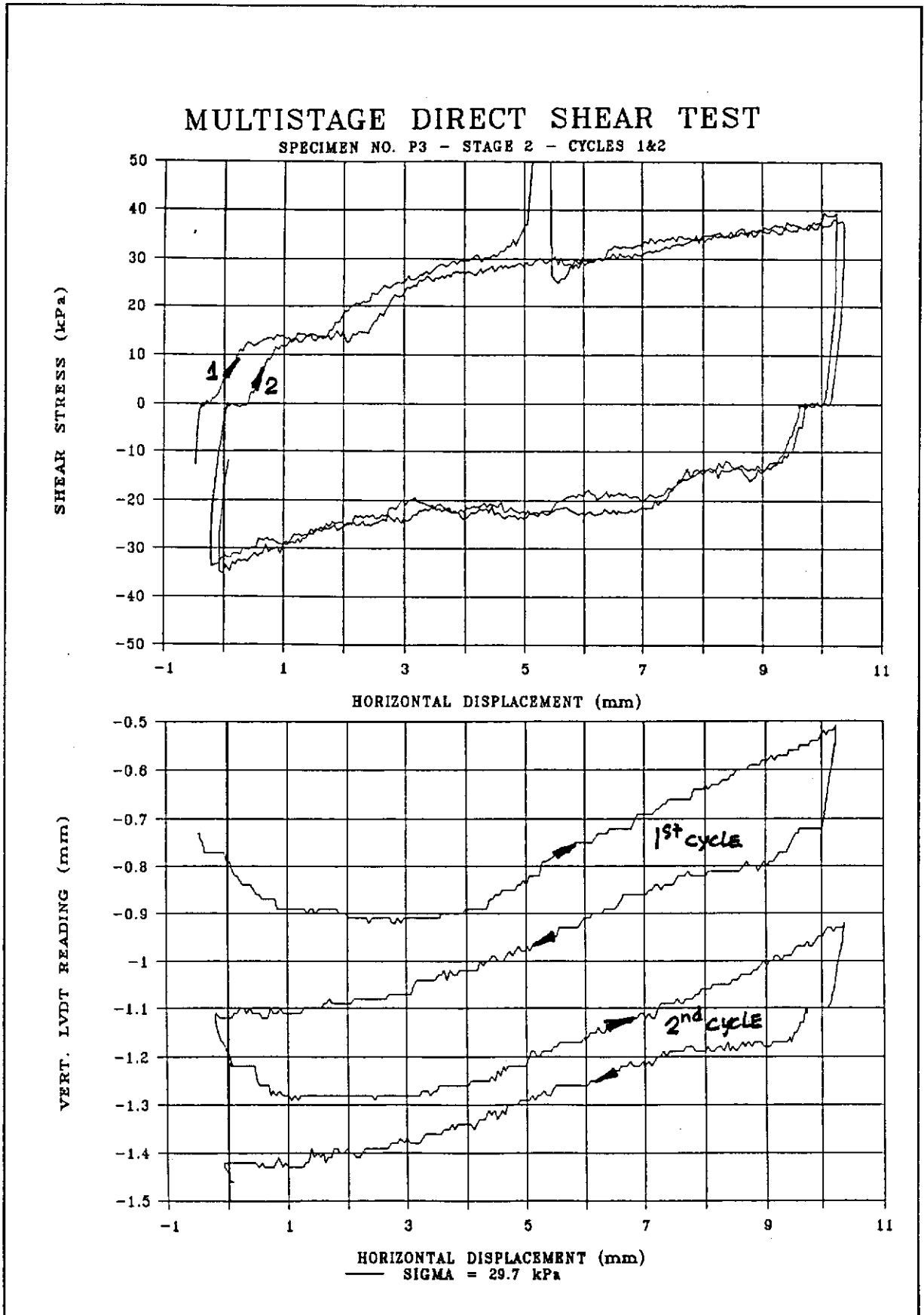


Figure 40 - Multistage Direct Shear Test on Specimen No. P3 - Stage 2

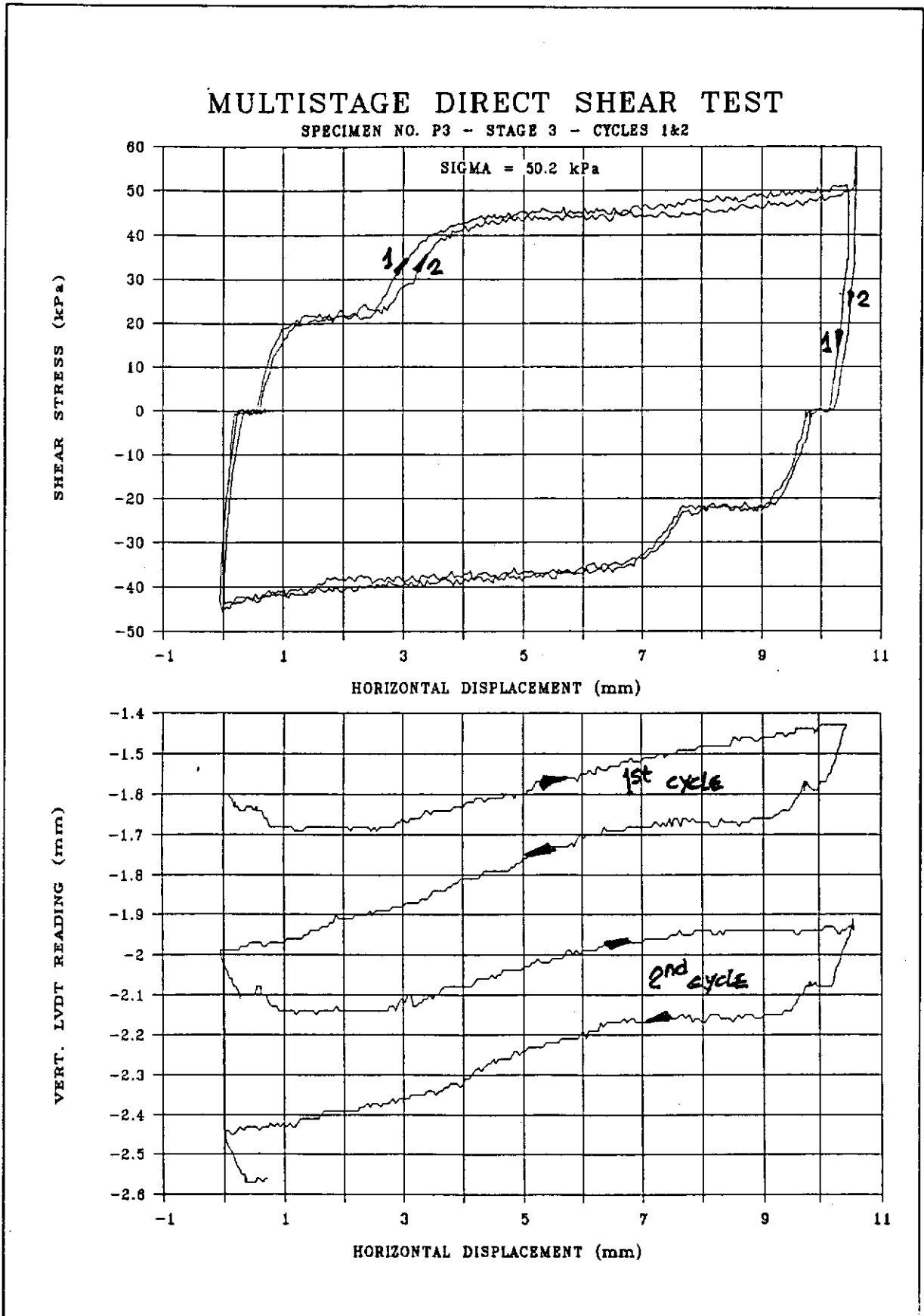


Figure 41 - Multistage Direct Shear Test on Specimen No. P3 - Stage 3

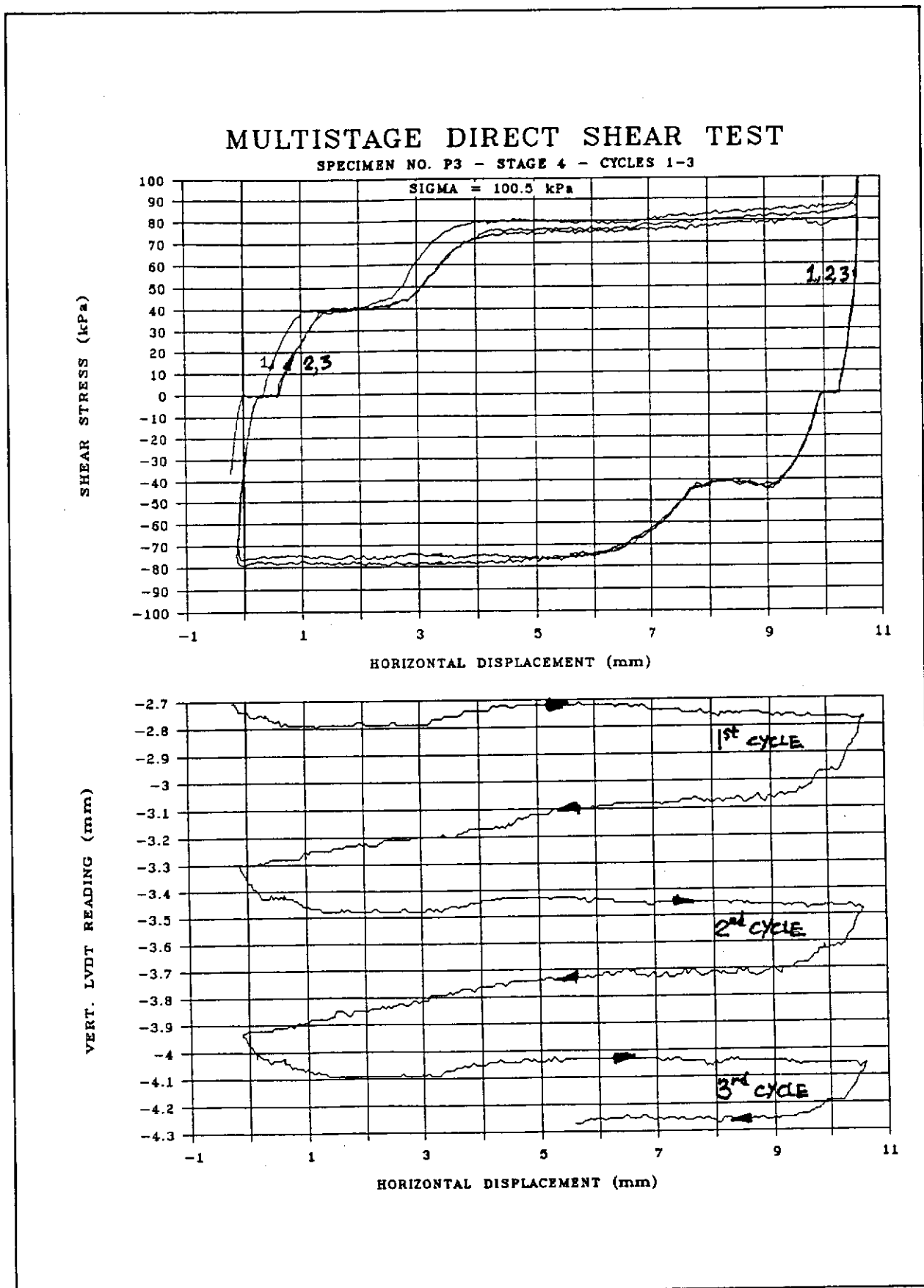


Figure 42 - Multistage Direct Shear Test on Specimen No. P3 - Stage 4

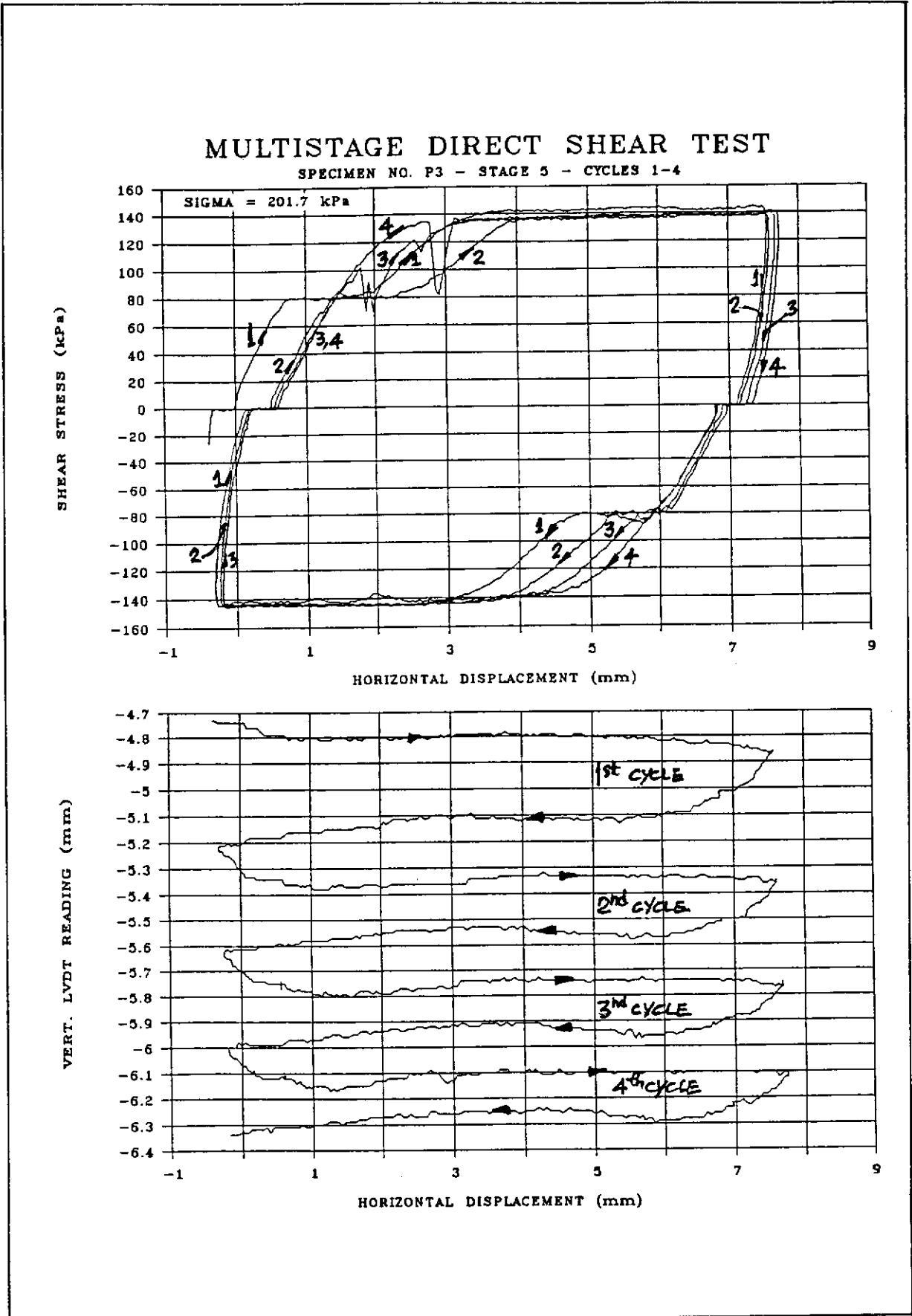


Figure 43 - Multistage Direct Shear Test on Specimen No. P3 - Stage 5

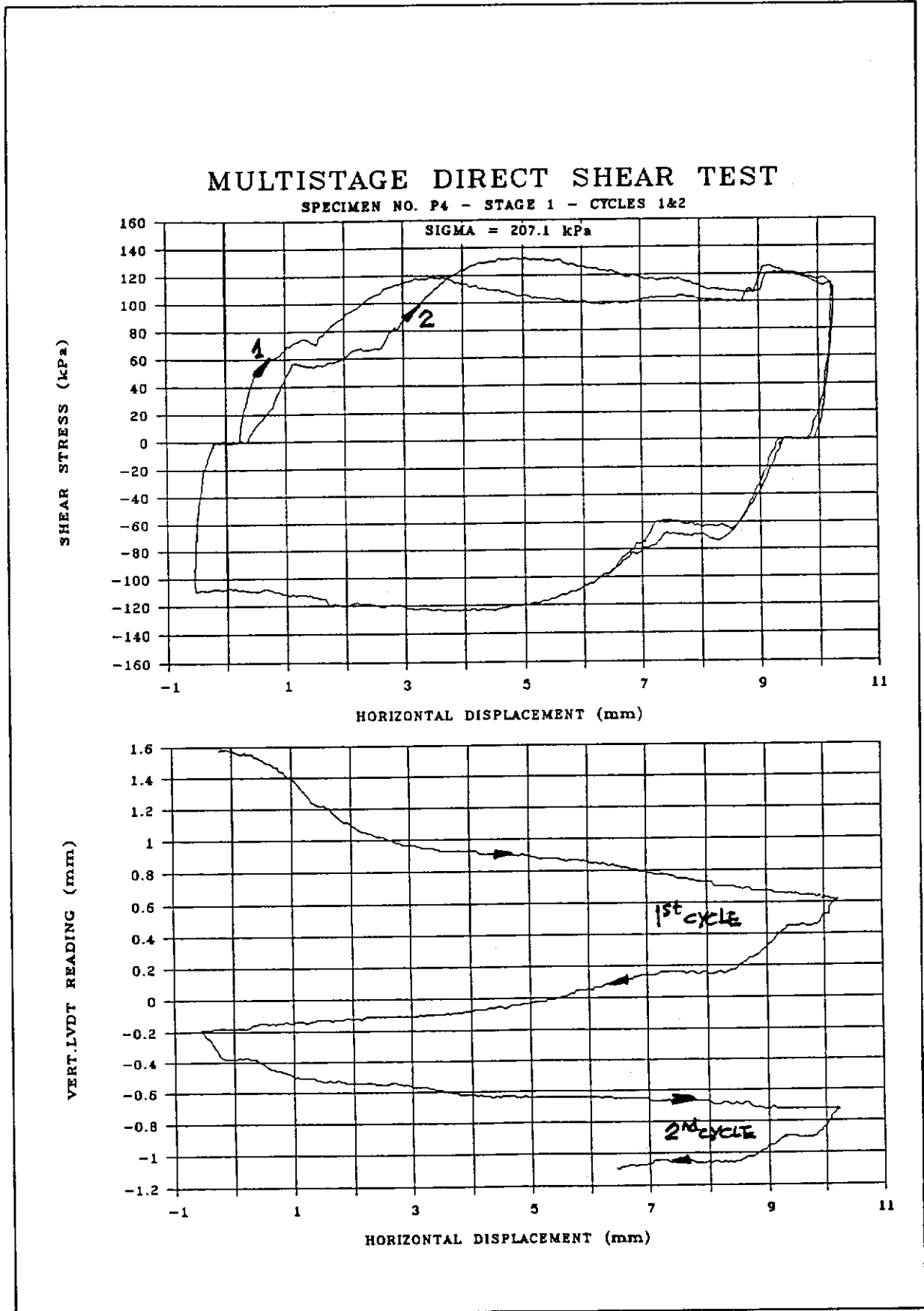


Figure 44 - Multistage Direct Shear Test on Specimen No. P4 - Stage 1

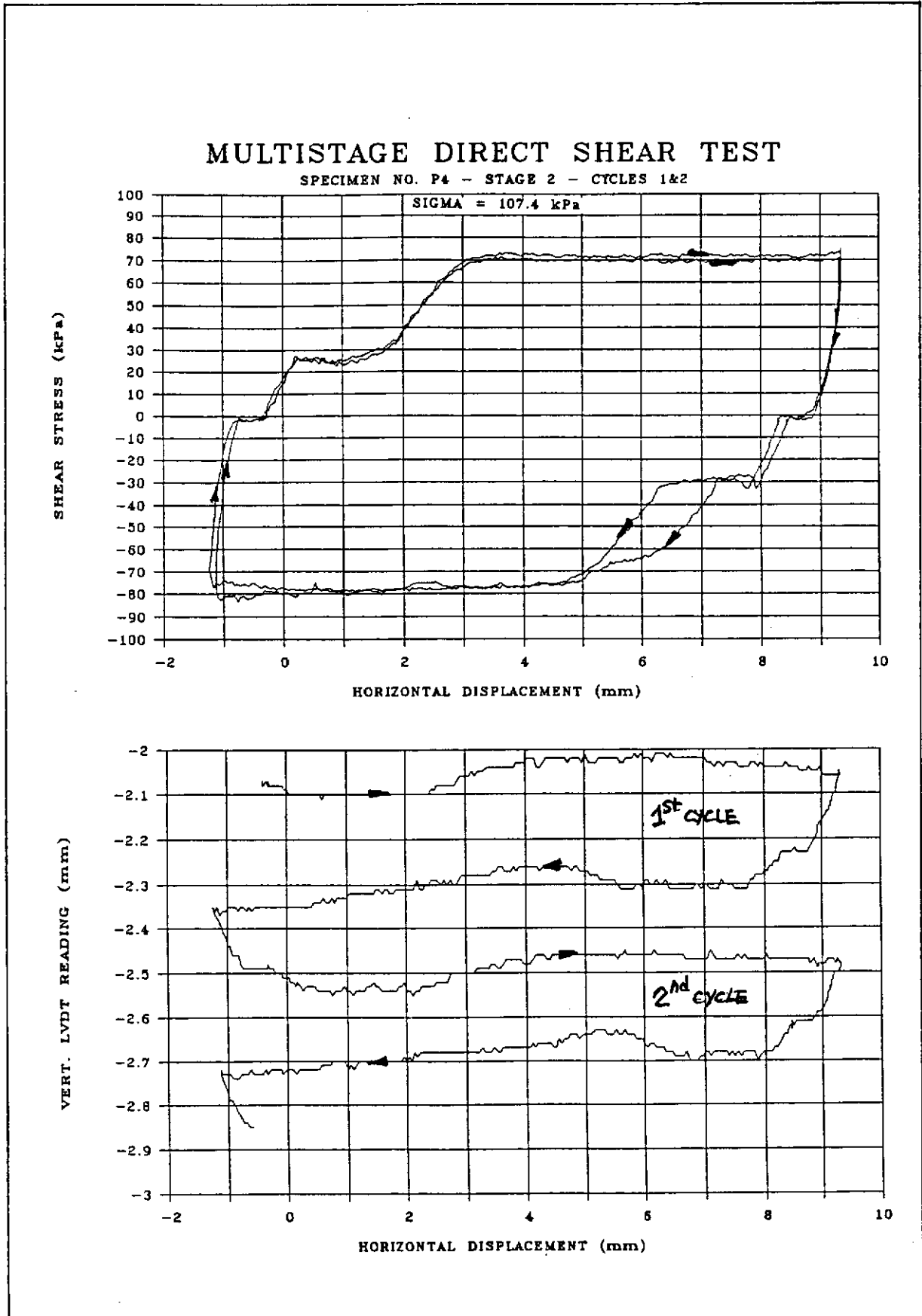


Figure 45 - Multistage Direct Shear Test on Specimen No. P4 - Stage 2

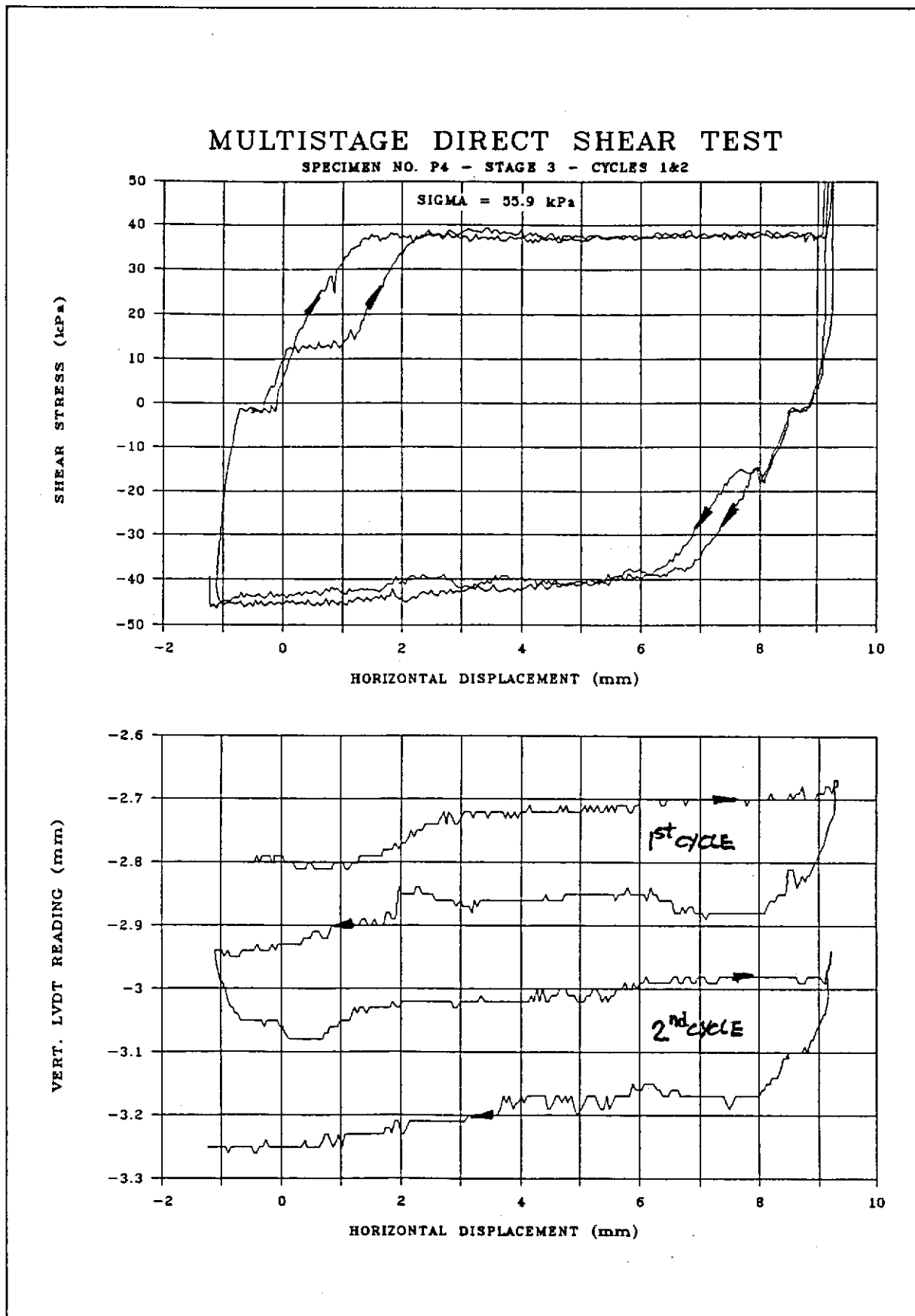


Figure 46 - Multistage Direct Shear Test on Specimen No. P4 - Stage 3

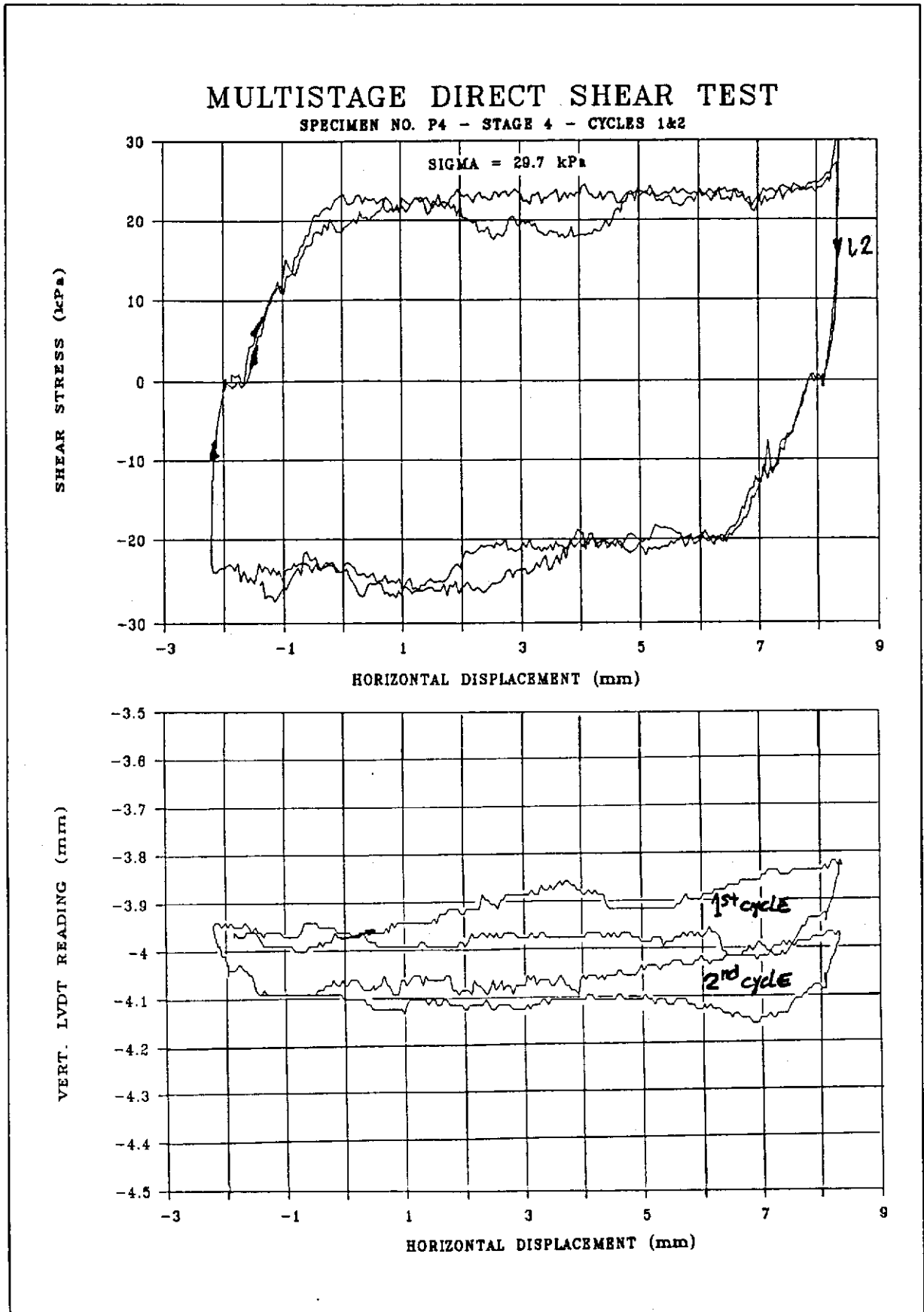


Figure 47 - Multistage Direct Shear Test on Specimen No. P4 - Stage 4

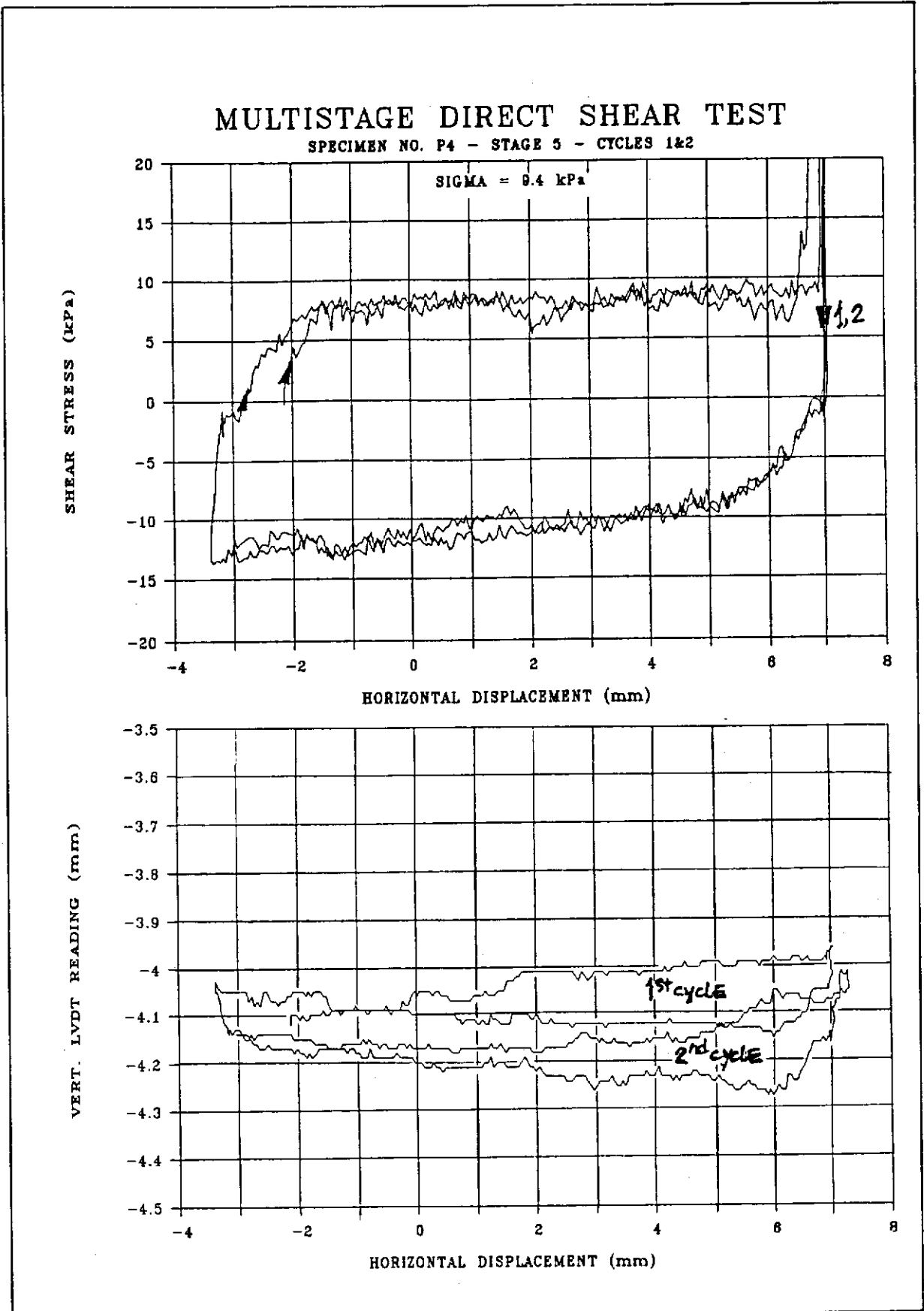


Figure 48 - Multistage Direct Shear Test on Specimen No. P4 - Stage 5

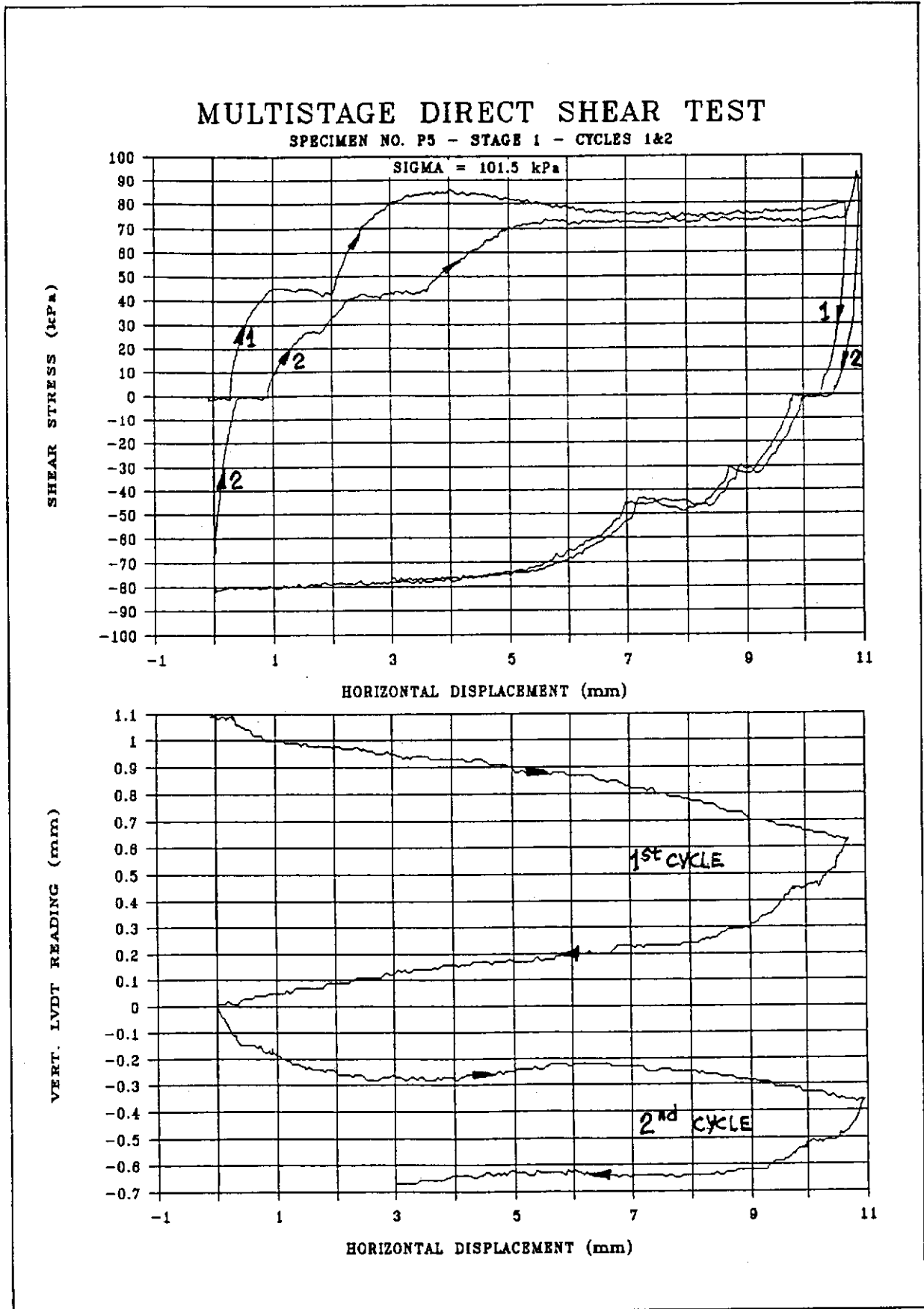


Figure 49 - Multistage Direct Shear Test on Specimen No. P5 - Stage 1

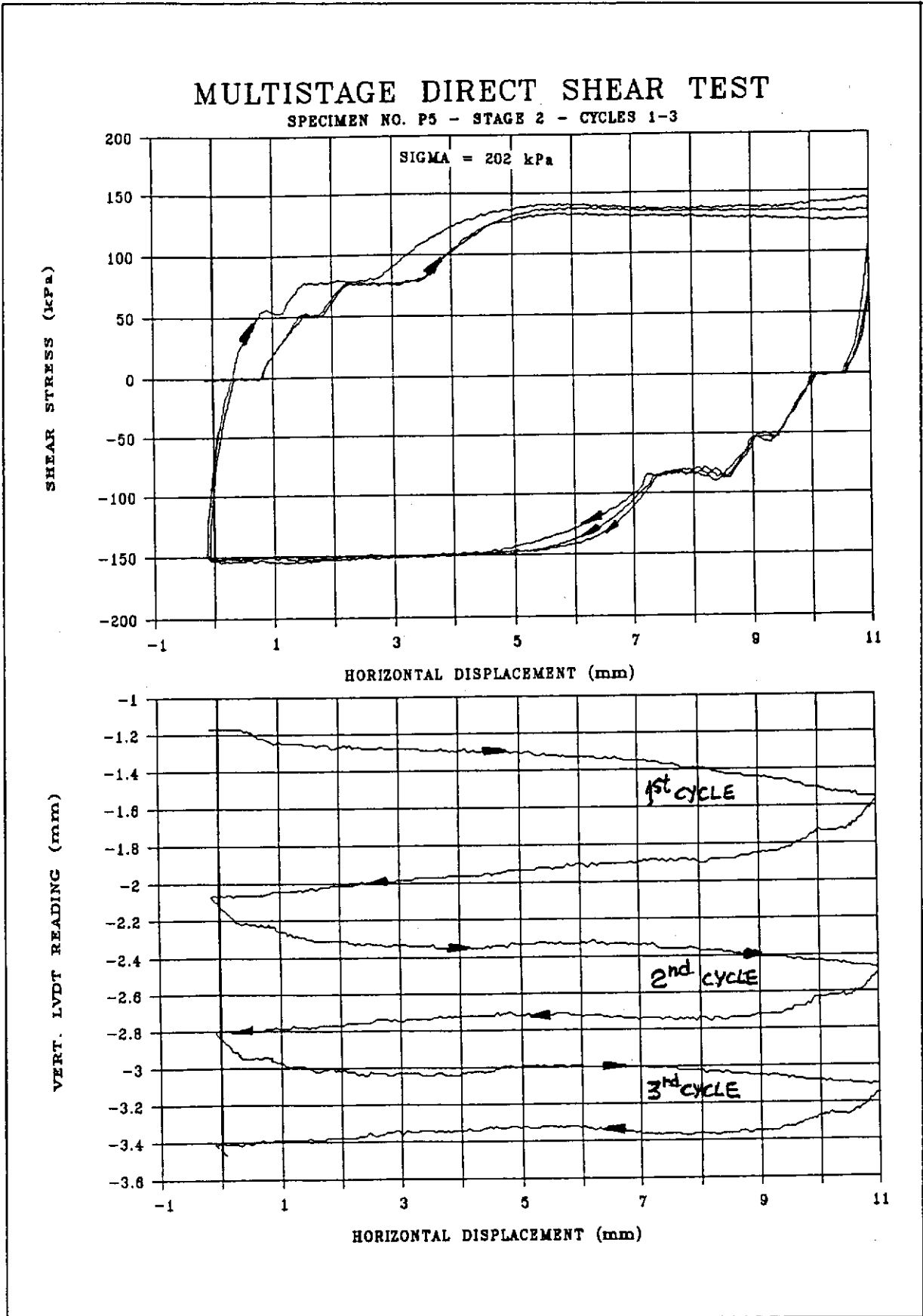


Figure 50 - Multistage Direct Shear Test on Specimen No. P5 - Stage 2

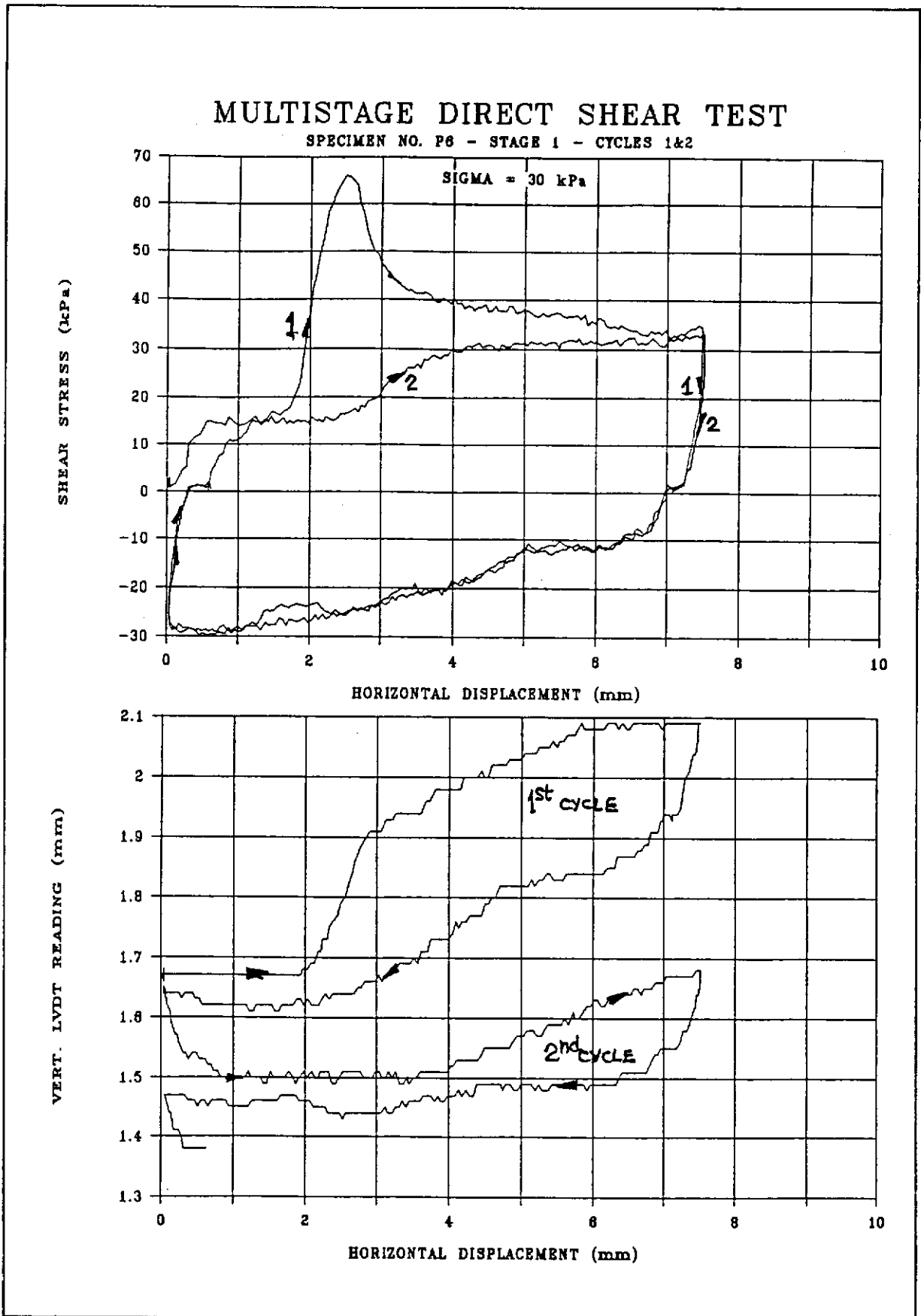


Figure 51 - Multistage Direct Shear Test on Specimen No. P6 - Stage 1

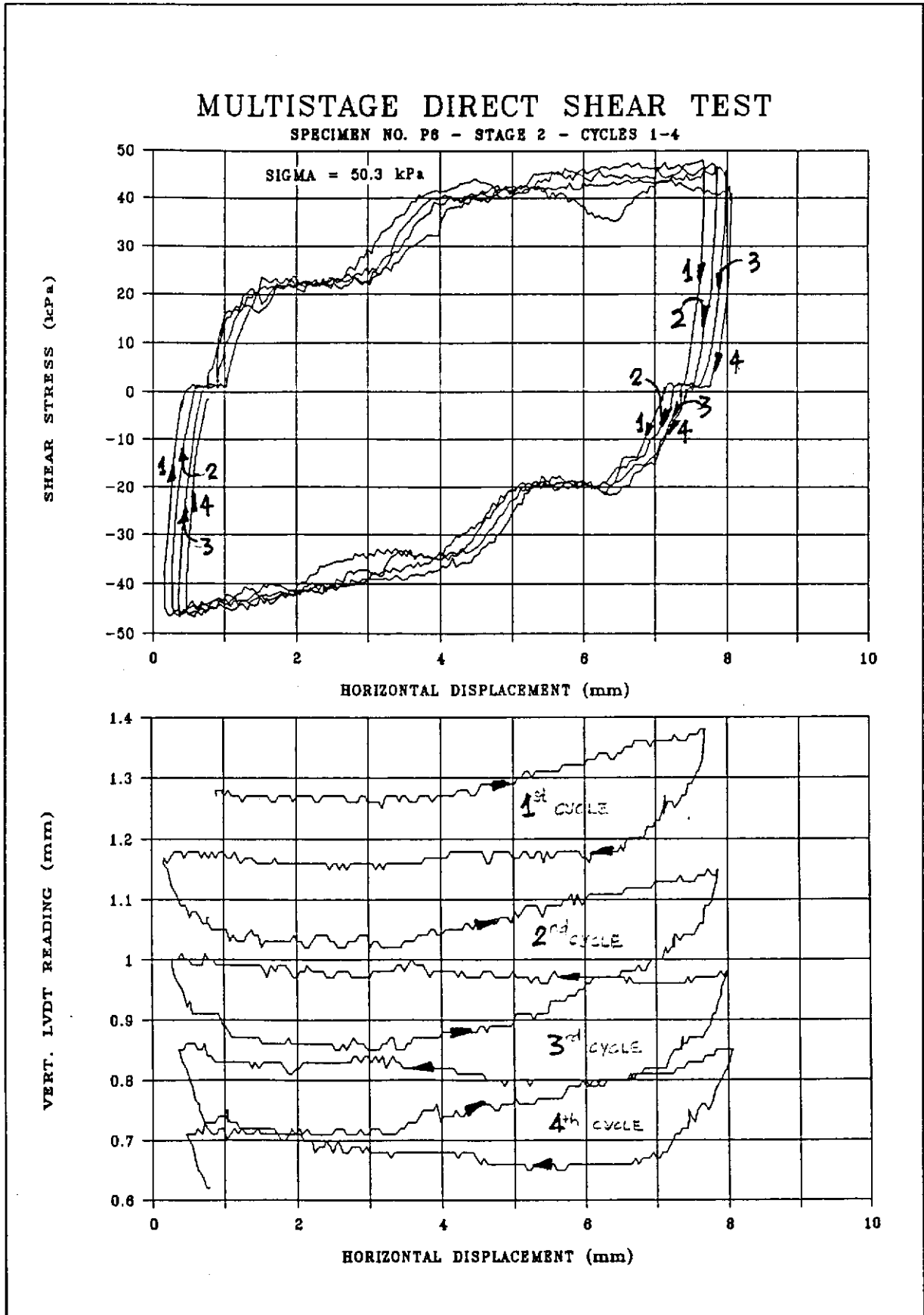


Figure 52 - Multistage Direct Shear Test on Specimen No. P6 - Stage 2

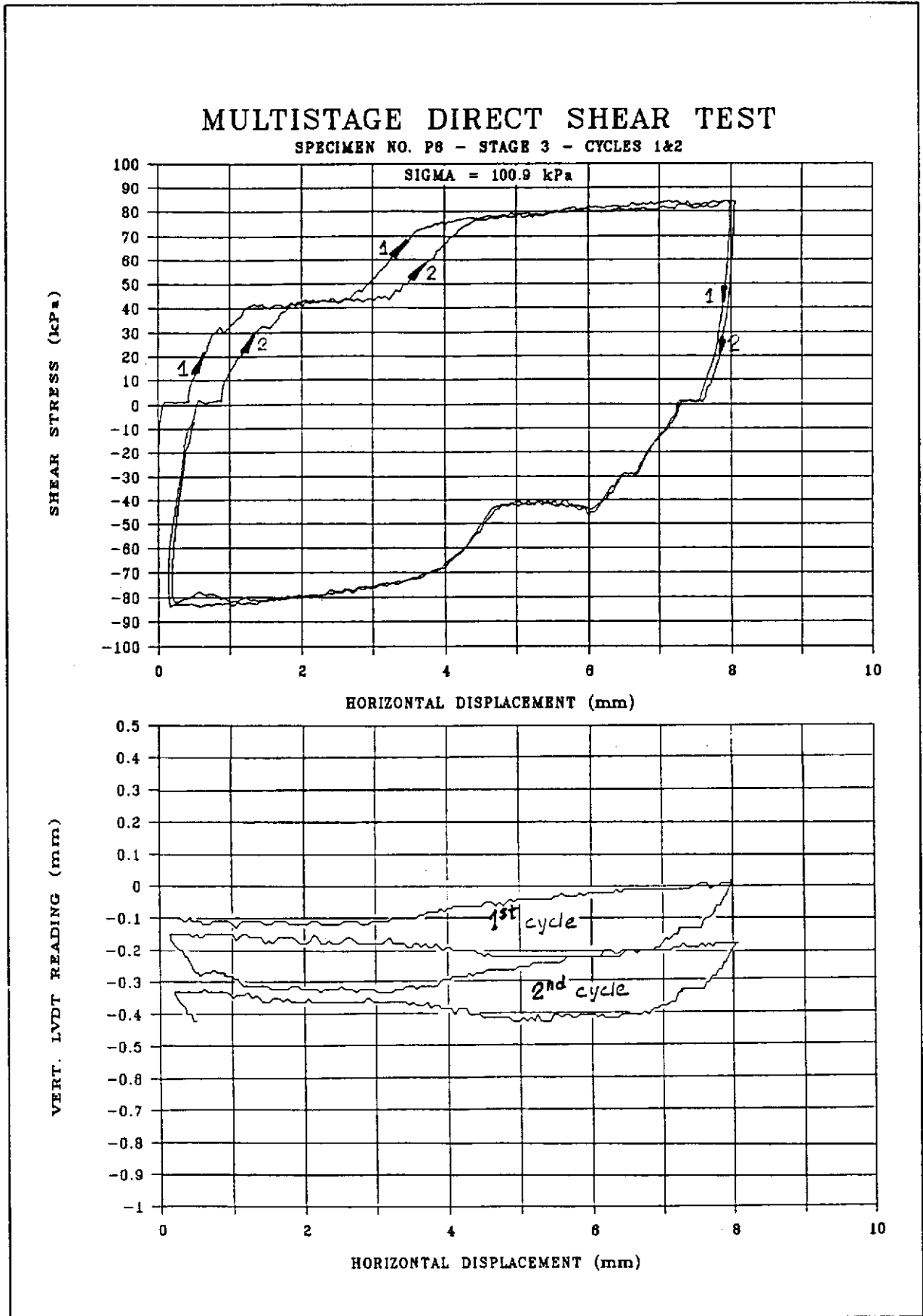


Figure 53 - Multistage Direct Shear Test on Specimen No. P6 - Stage 3

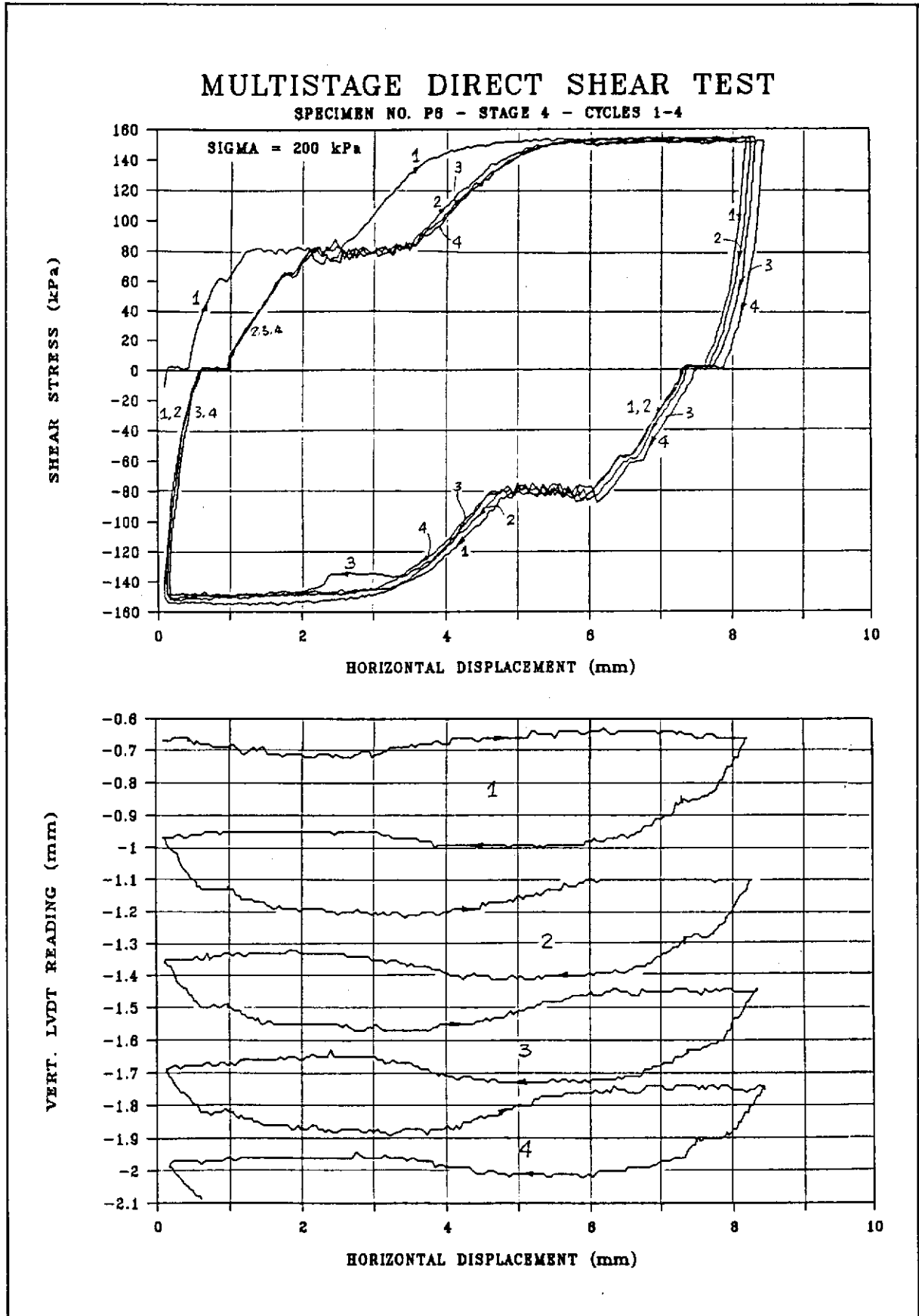


Figure 54 - Multistage Direct Shear Test on Specimen No. P6 - Stage 4

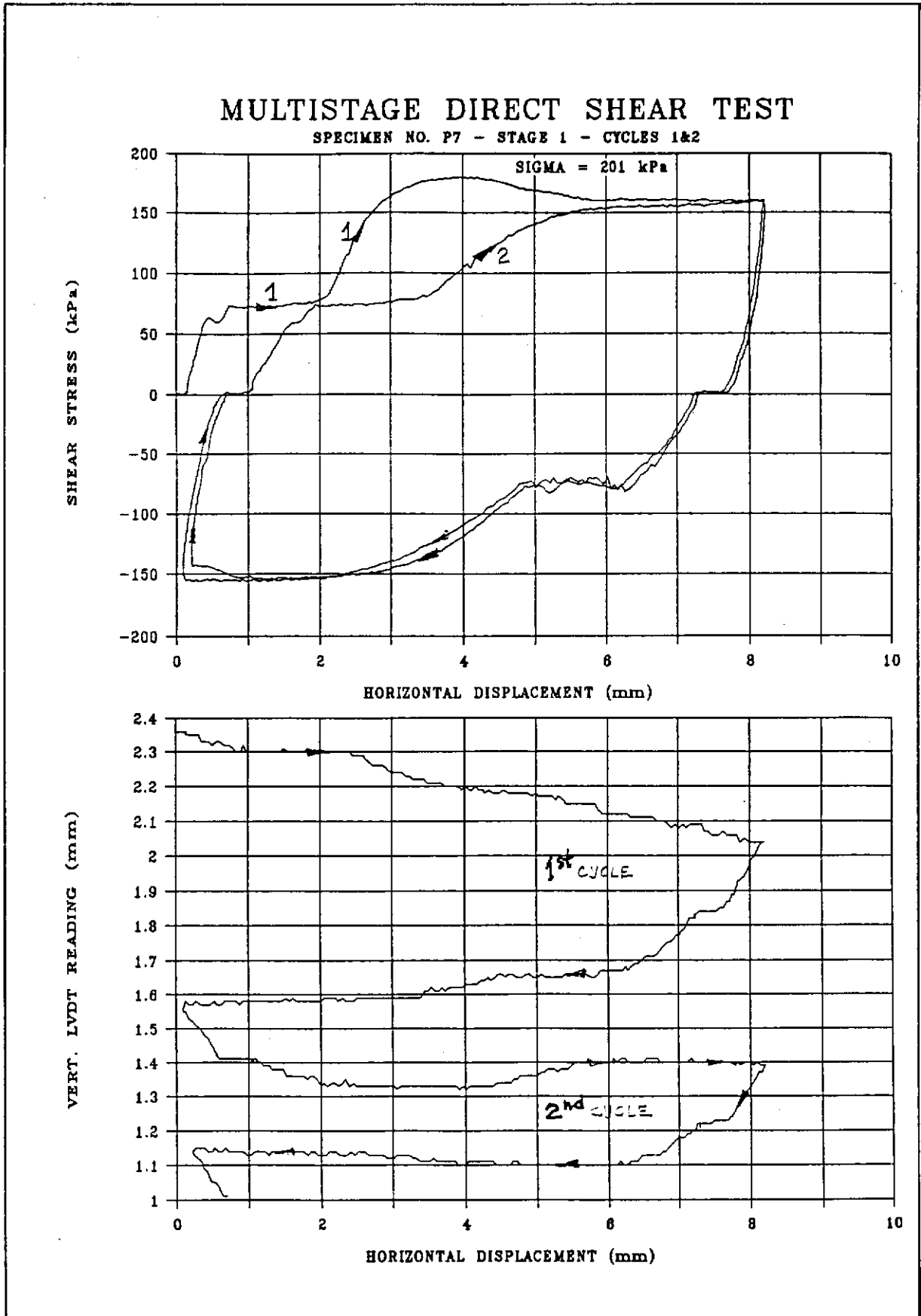


Figure 55 - Multistage Direct Shear Test on Specimen No. P7 - Stage 1

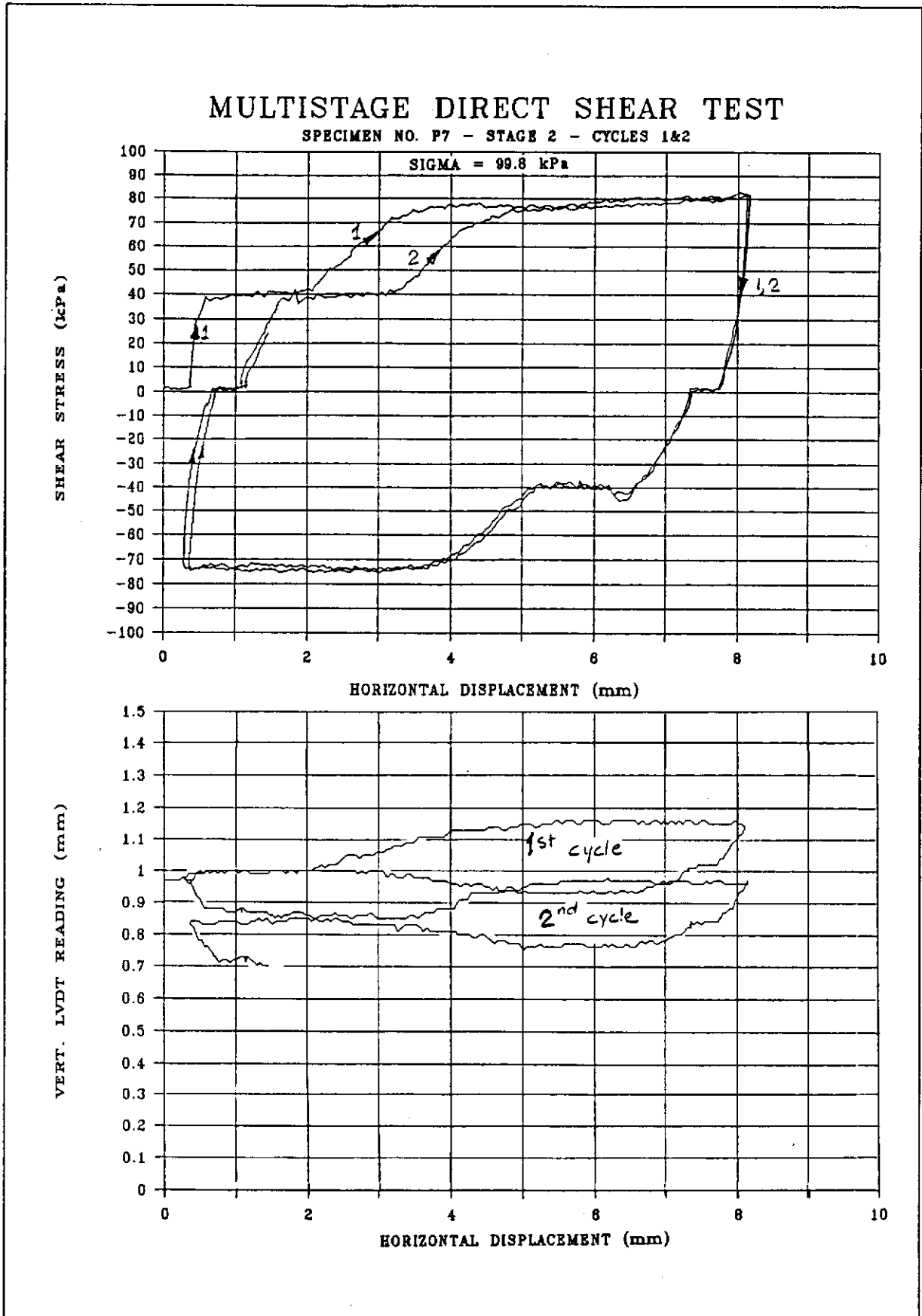


Figure 56 - Multistage Direct Shear Test on Specimen No. P7 - Stage 2

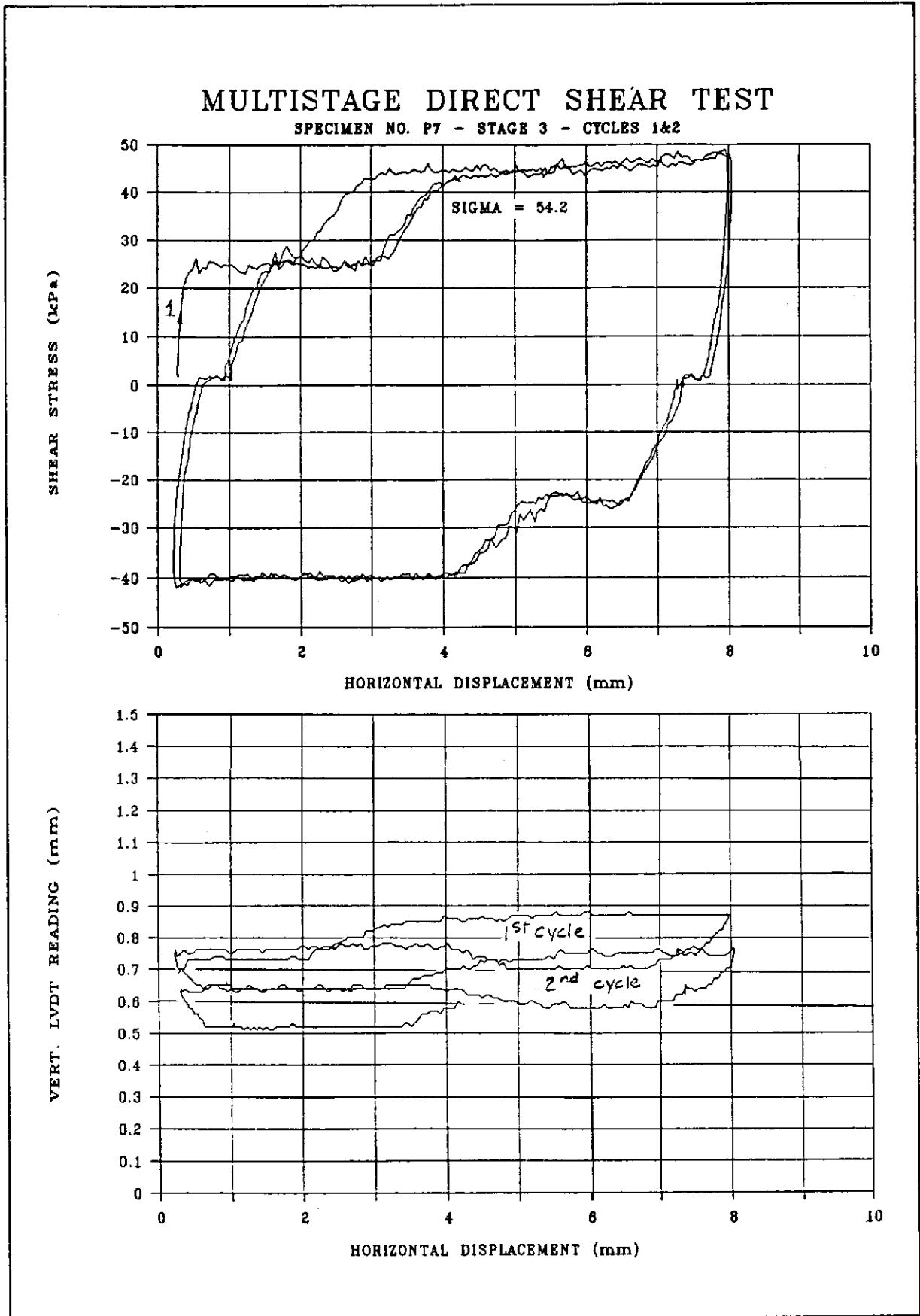


Figure 57 - Multistage Direct Shear Test on Specimen No. P7 - Stage 3

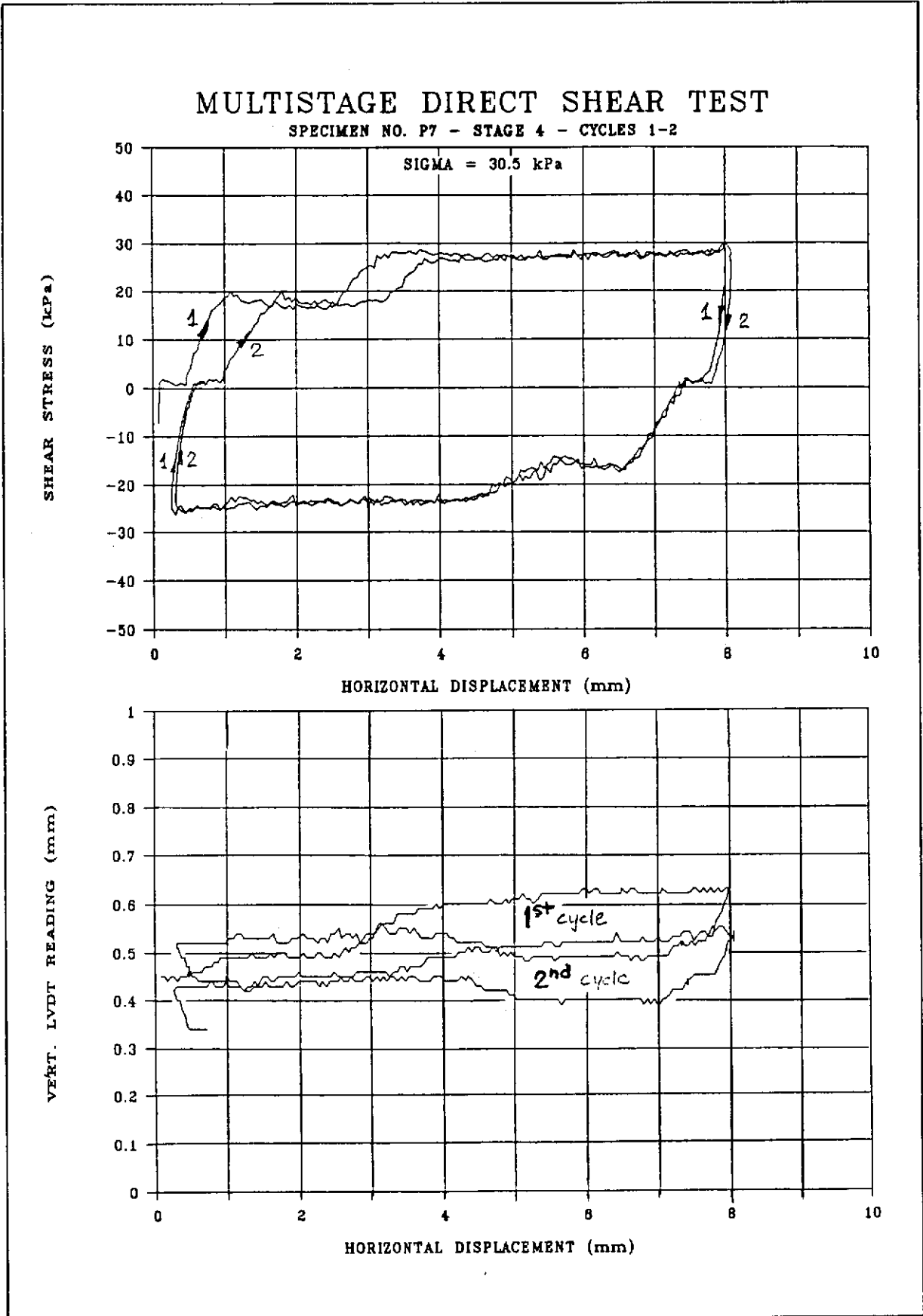


Figure 58 - Multistage Direct Shear Test on Specimen No. P7 - Stage 4

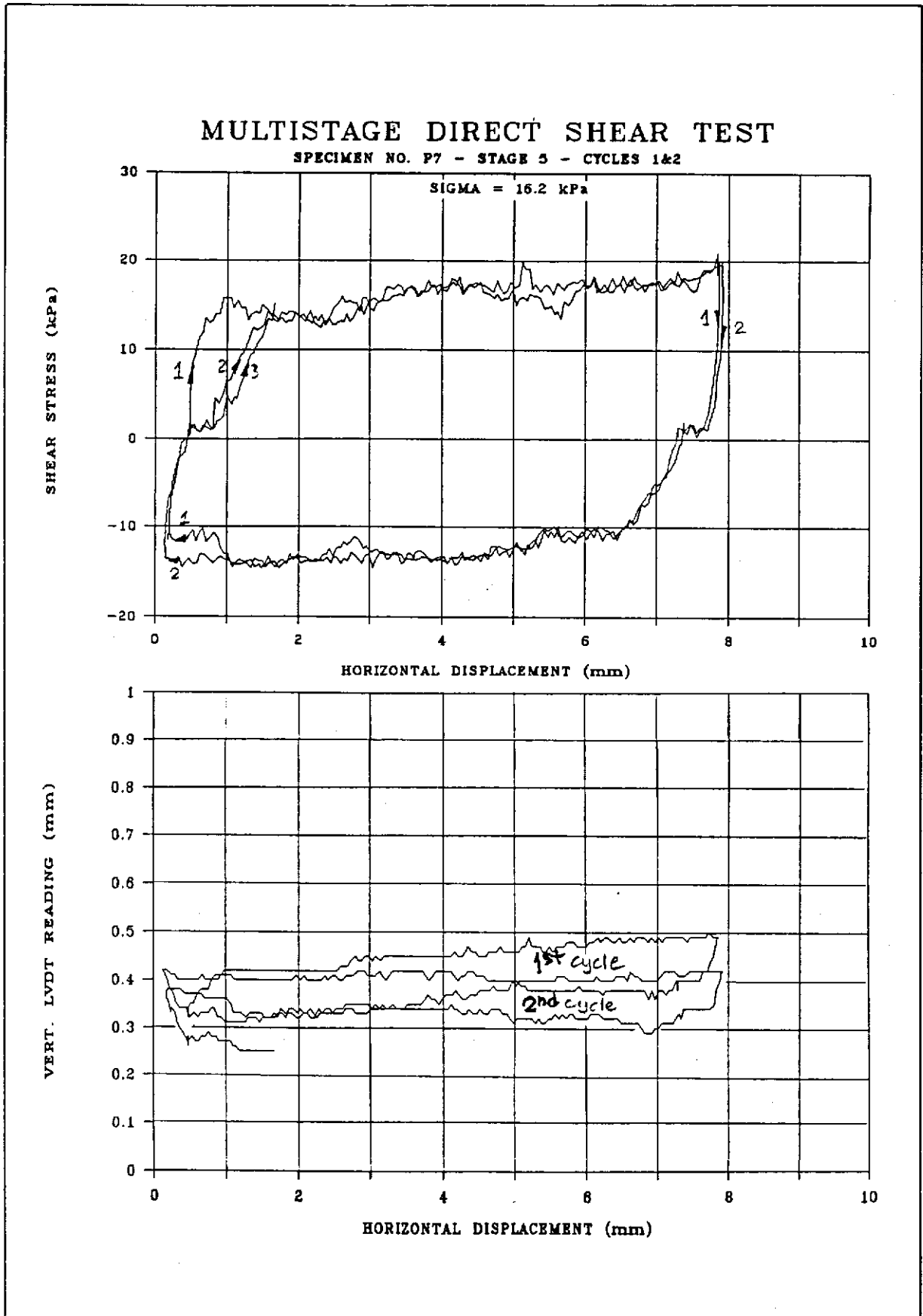


Figure 59 - Multistage Direct Shear Test on Specimen No. P7 - Stage 5

PLATEAU STRESS VERSUS NORMAL STRESS

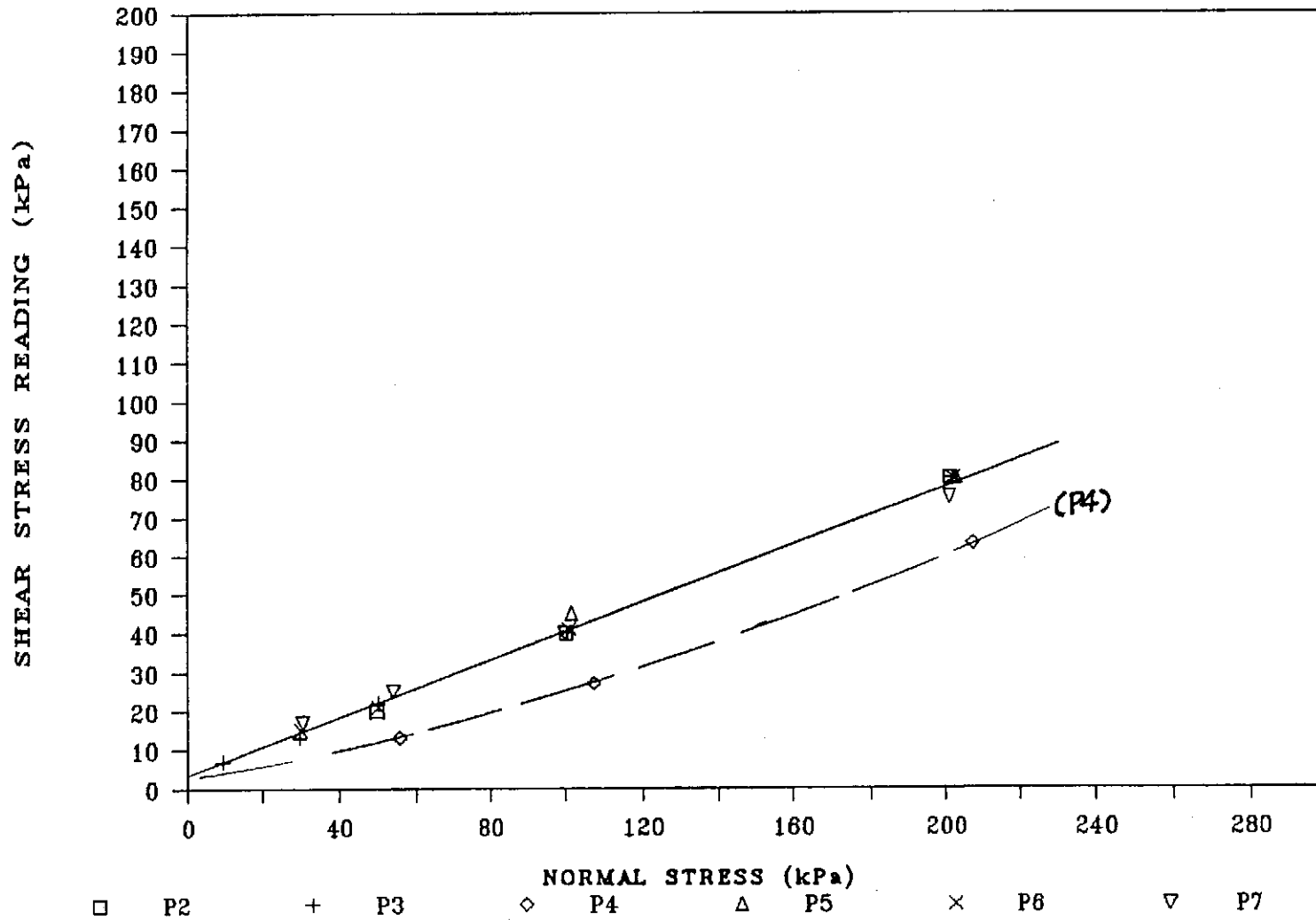


Figure 60 - Plateau Stress Reading versus Normal Stress

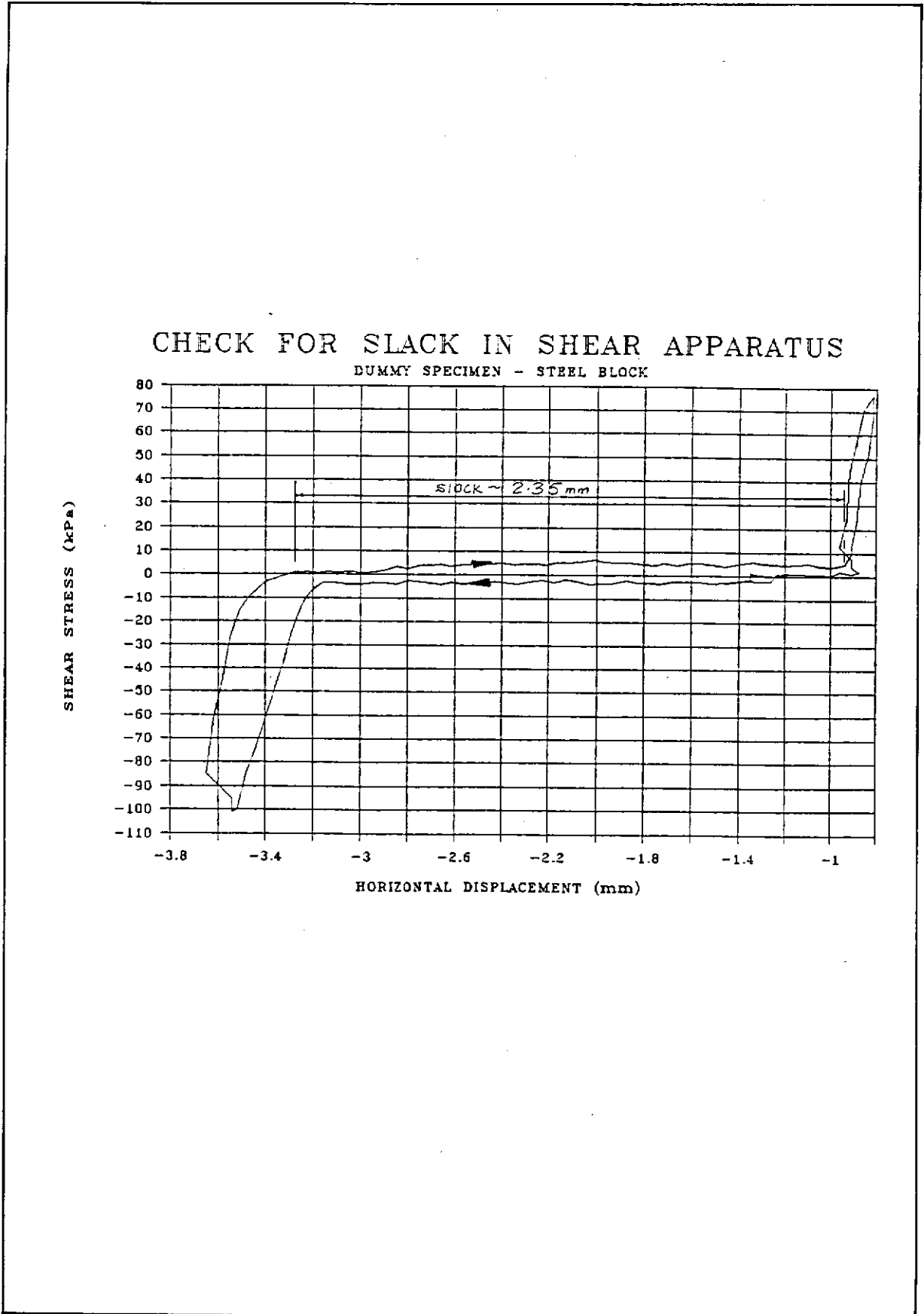


Figure 61 - Check for Slack in Direct Shear Apparatus Using a Steel Block

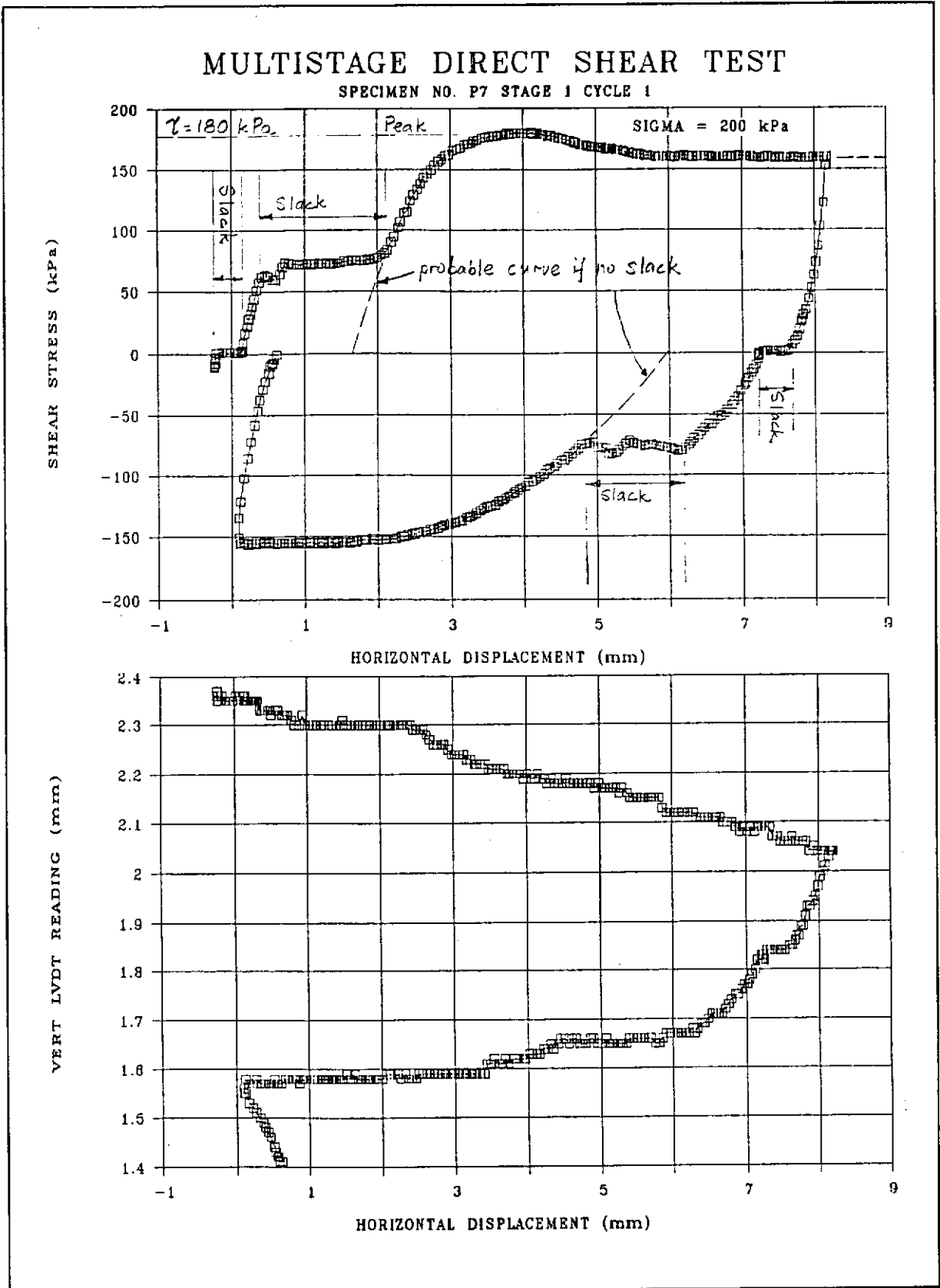


Figure 62 - Typical Shear Stress versus Horizontal Displacement Curve with Plateau Indicating Slacks in Apparatus (Specimen No. P7 - Stage 1 - Cycle 1 of Multistage Test)

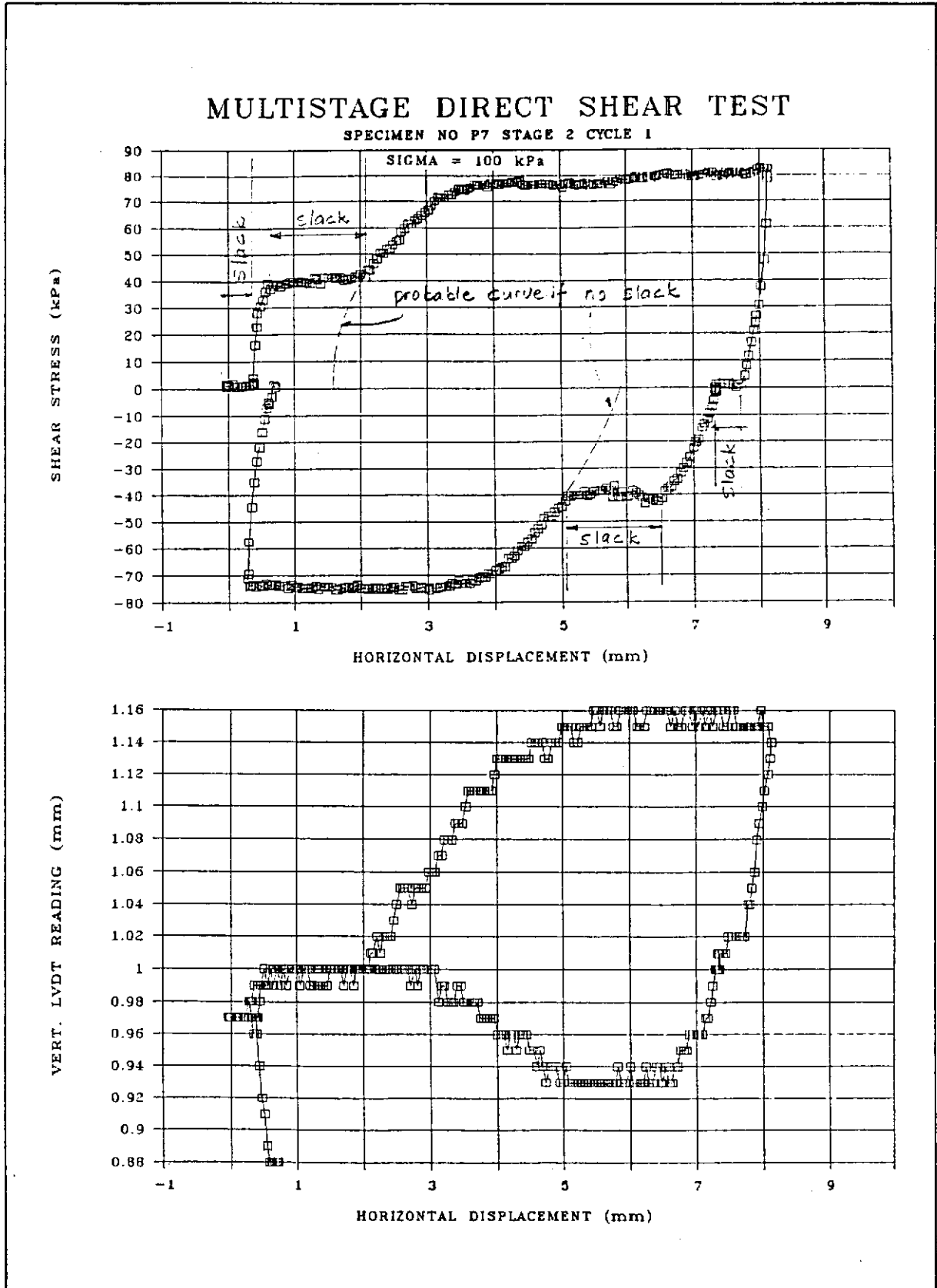


Figure 63 - Typical Shear Stress versus Horizontal Displacement Curve with Plateaus Indicating Slacks in Apparatus (Specimen No. P7 - Stage 2 - Cycle 1 of Multistage Test)

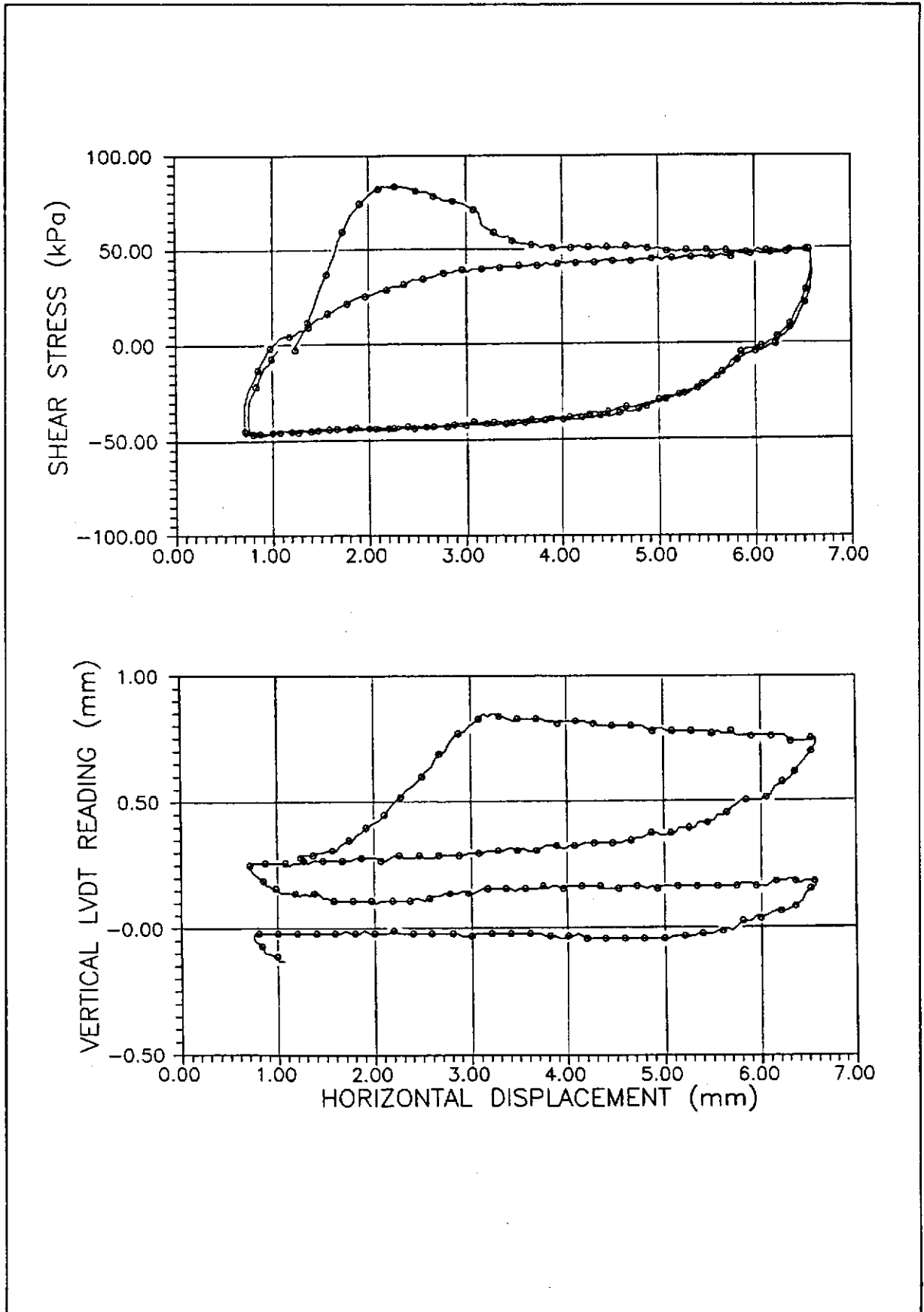


Figure 64 - Multistage Direct Shear Test on Specimen No. P8 - Stage 1

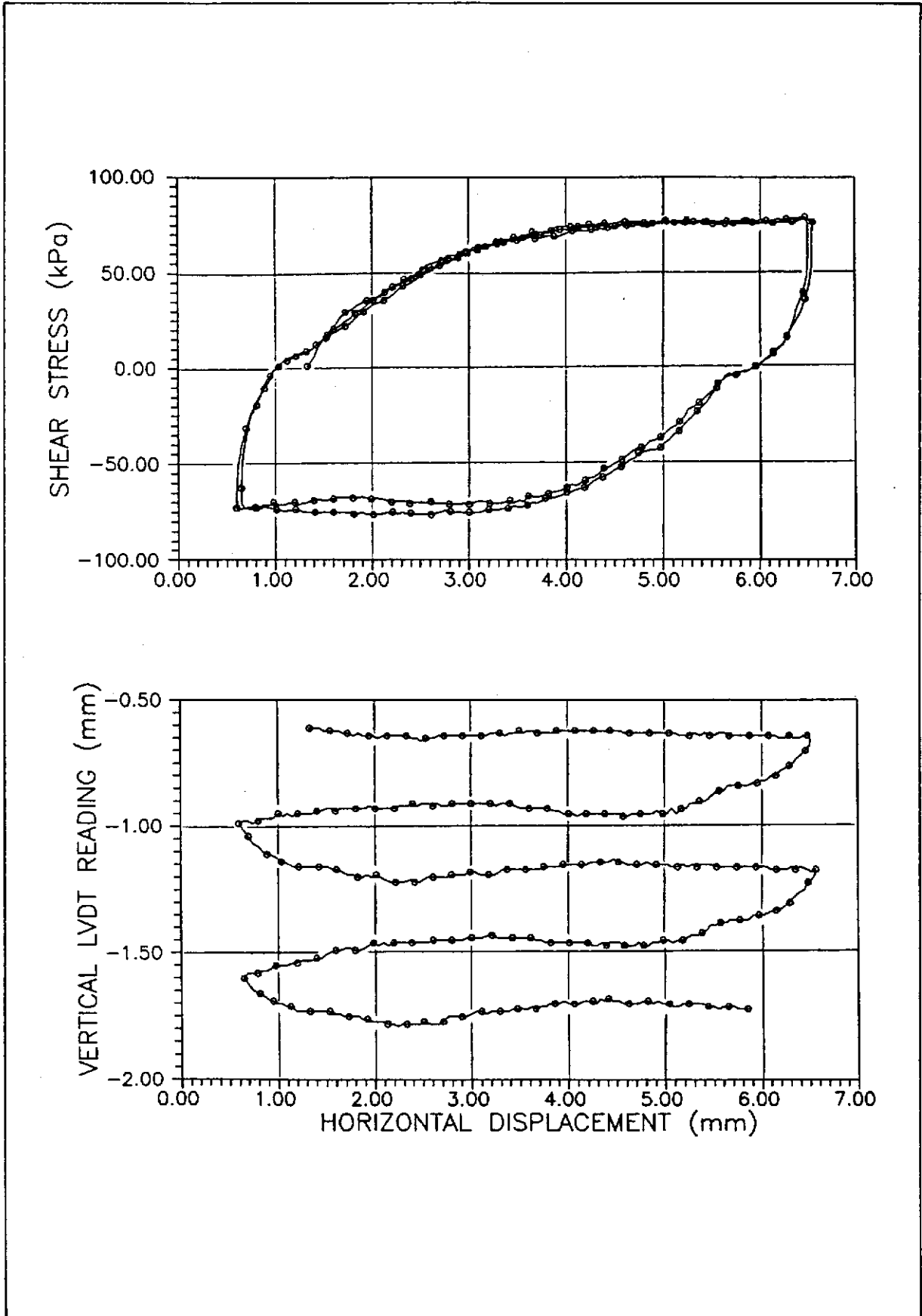


Figure 65 - Multistage Direct Shear Test on Specimen No. P8 - Stage 2

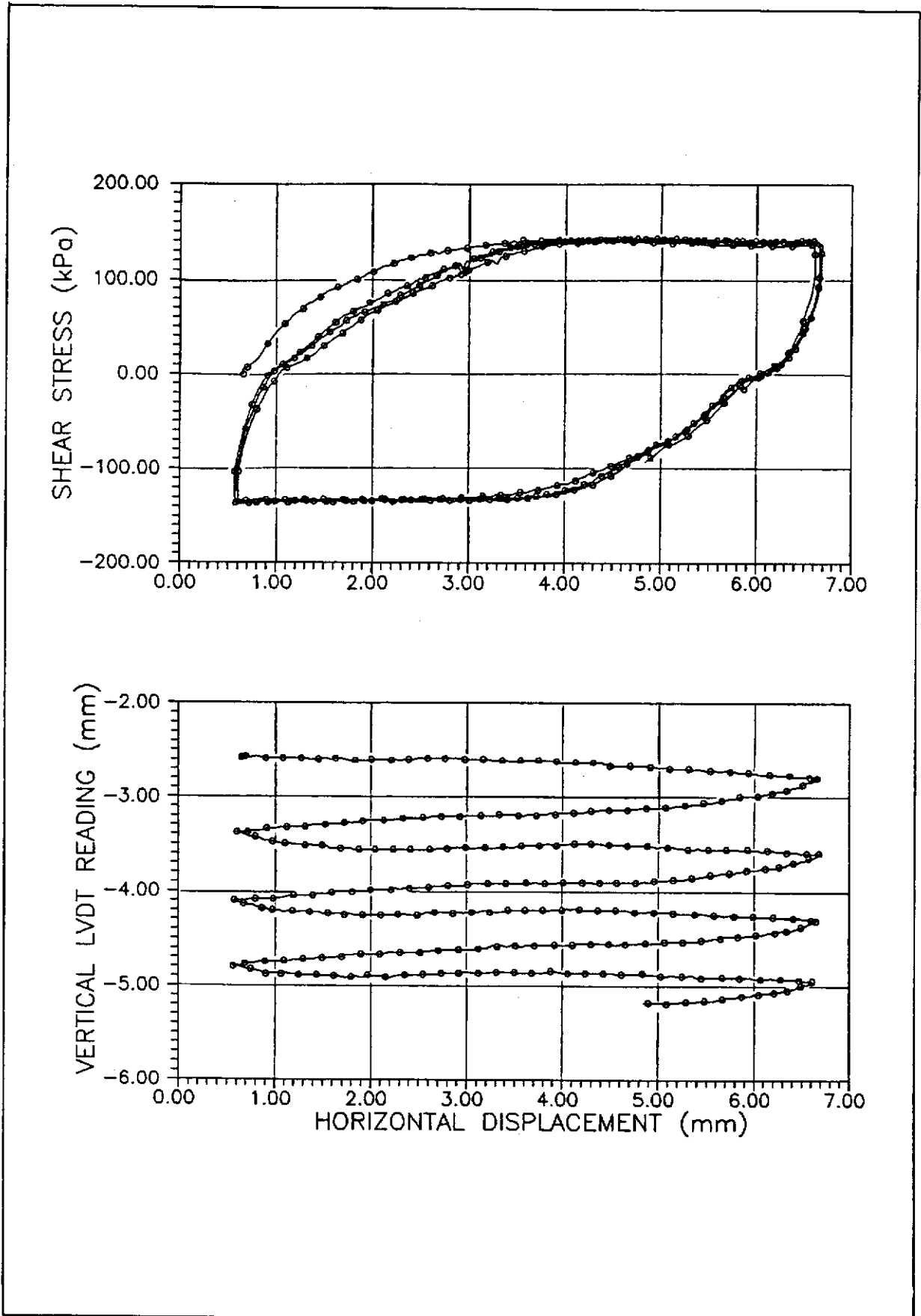


Figure 66 - Multistage Direct Shear Test on Specimen No. P8 - Stage 3

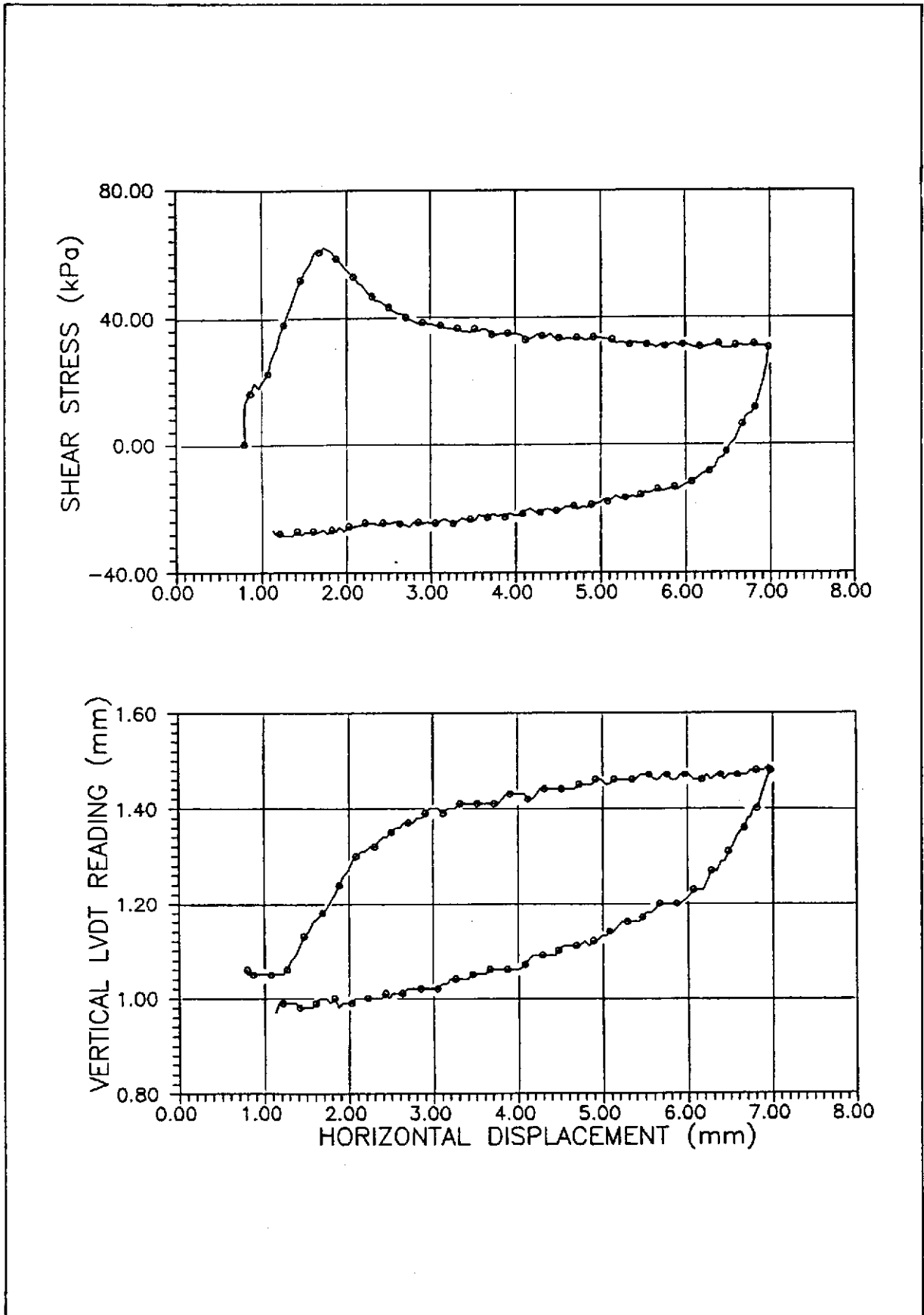


Figure 67 - Multistage Direct Shear Test on Specimen No. P9 - Stage 1

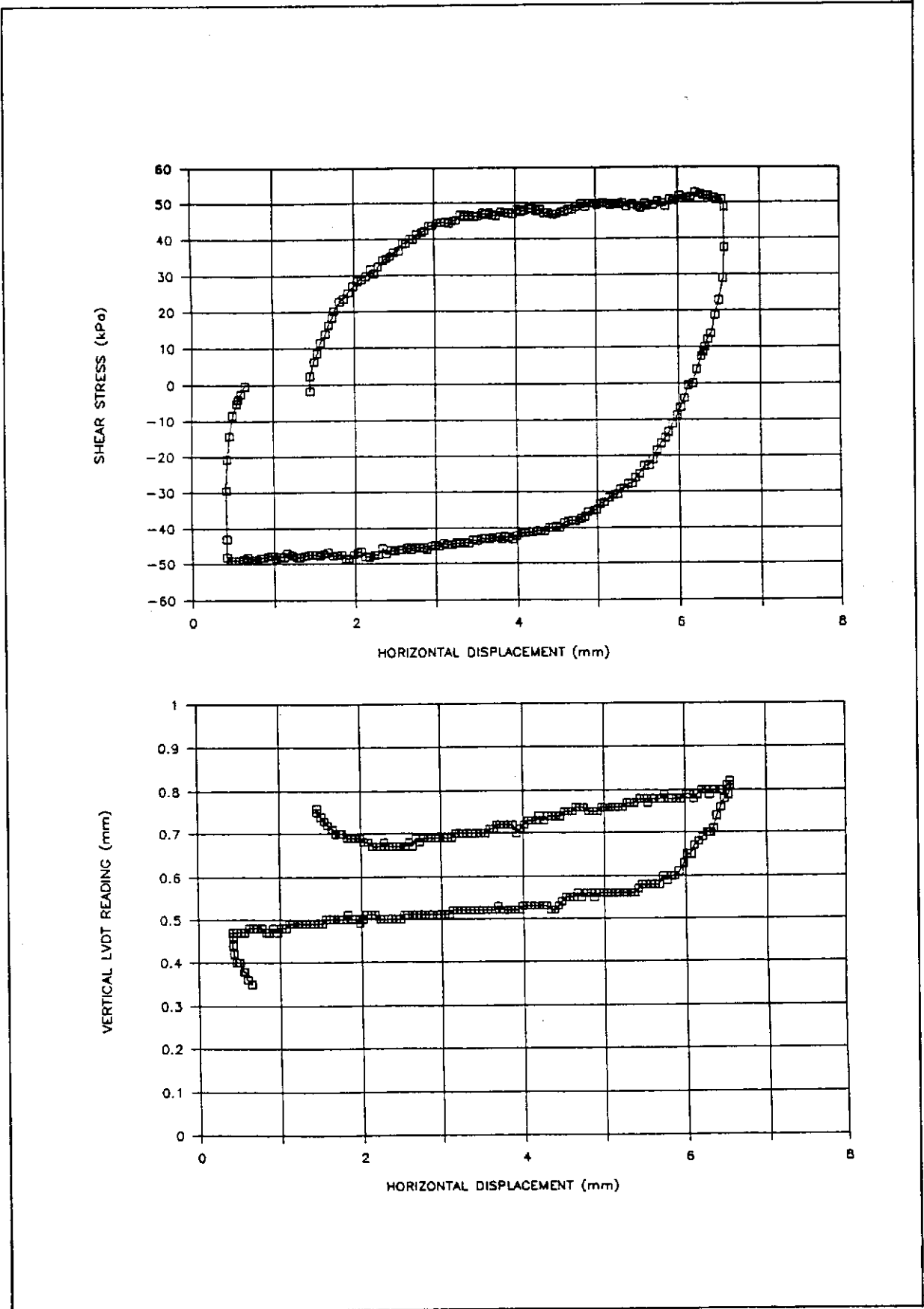


Figure 68 - Multistage Direct Shear Test on Specimen No. P9 - Stage 2

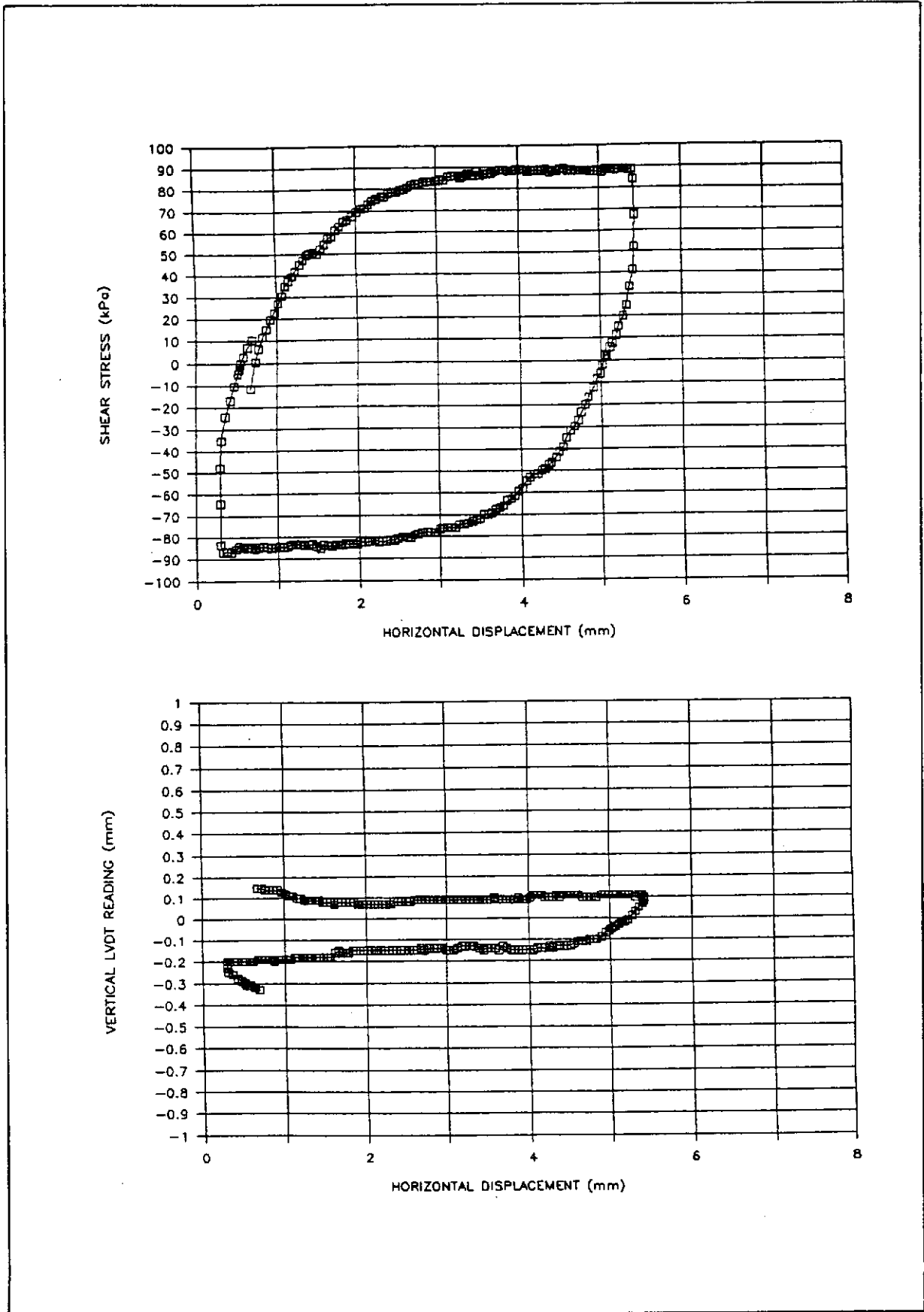


Figure 69 - Multistage Direct Shear Test on Specimen No. P9 - Stage 3

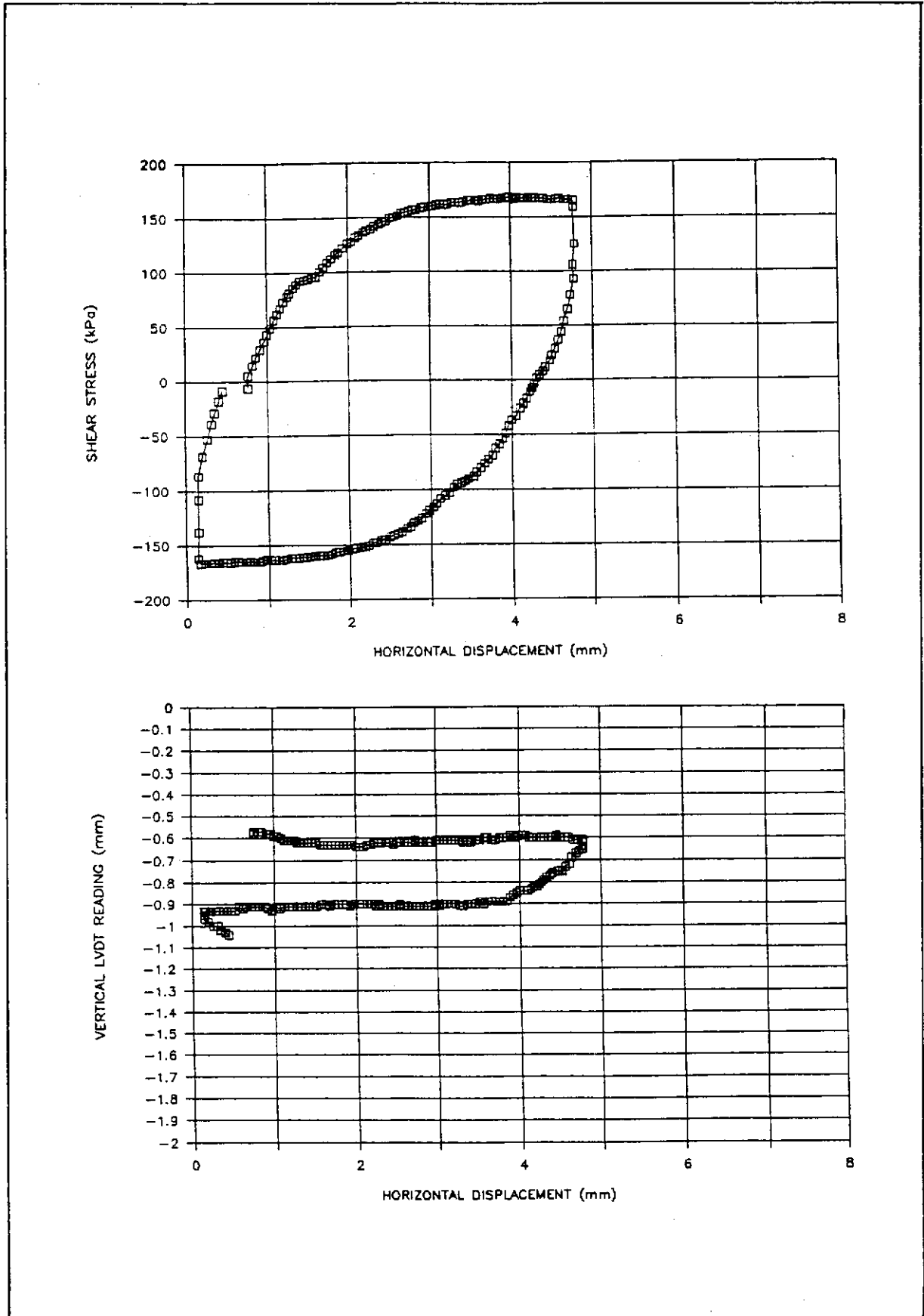


Figure 70 - Multistage Direct Shear Test on Specimen No. P9 - Stage 4

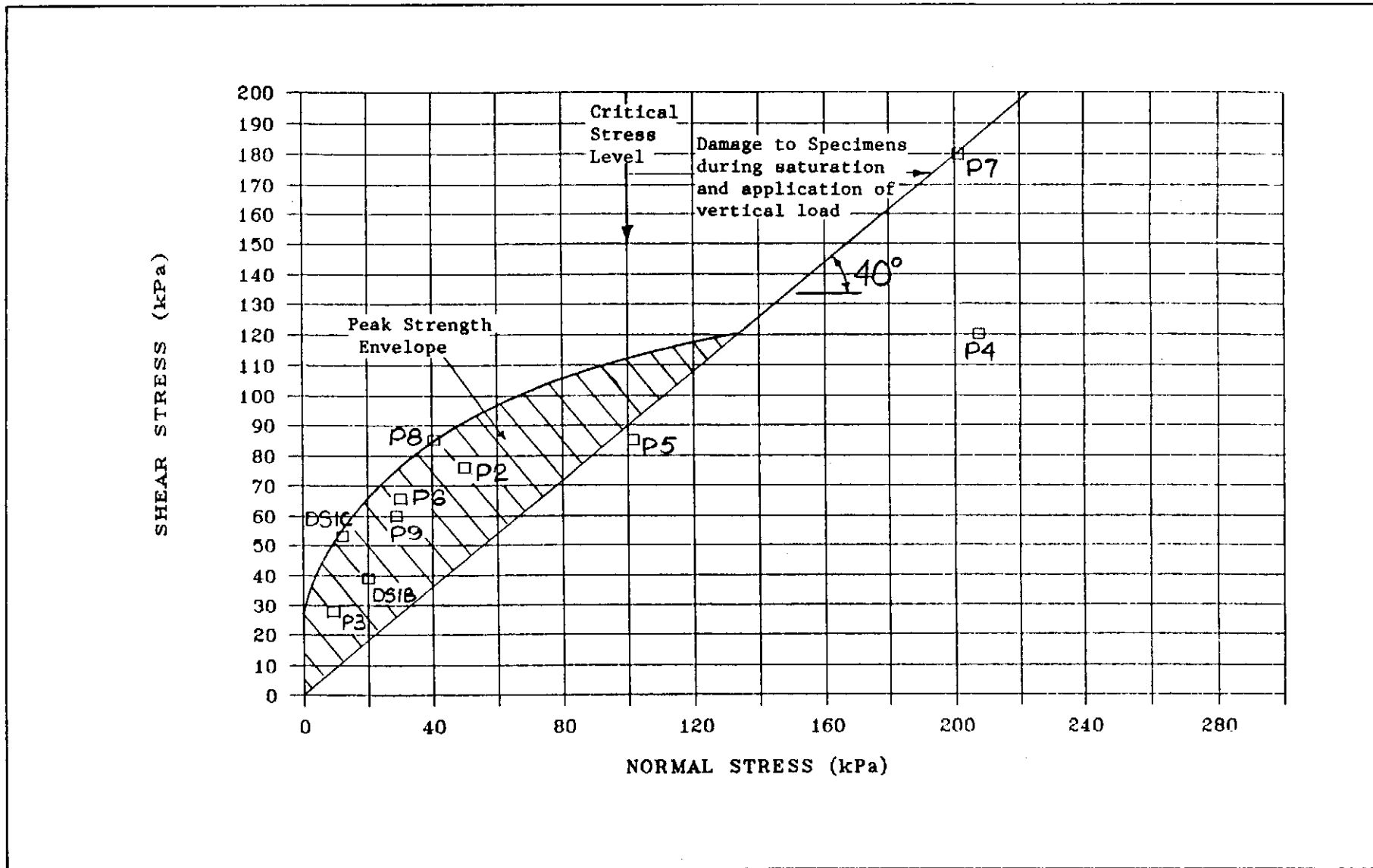


Figure 71 - Peak Strength Mohr Envelope from Direct Shear Test

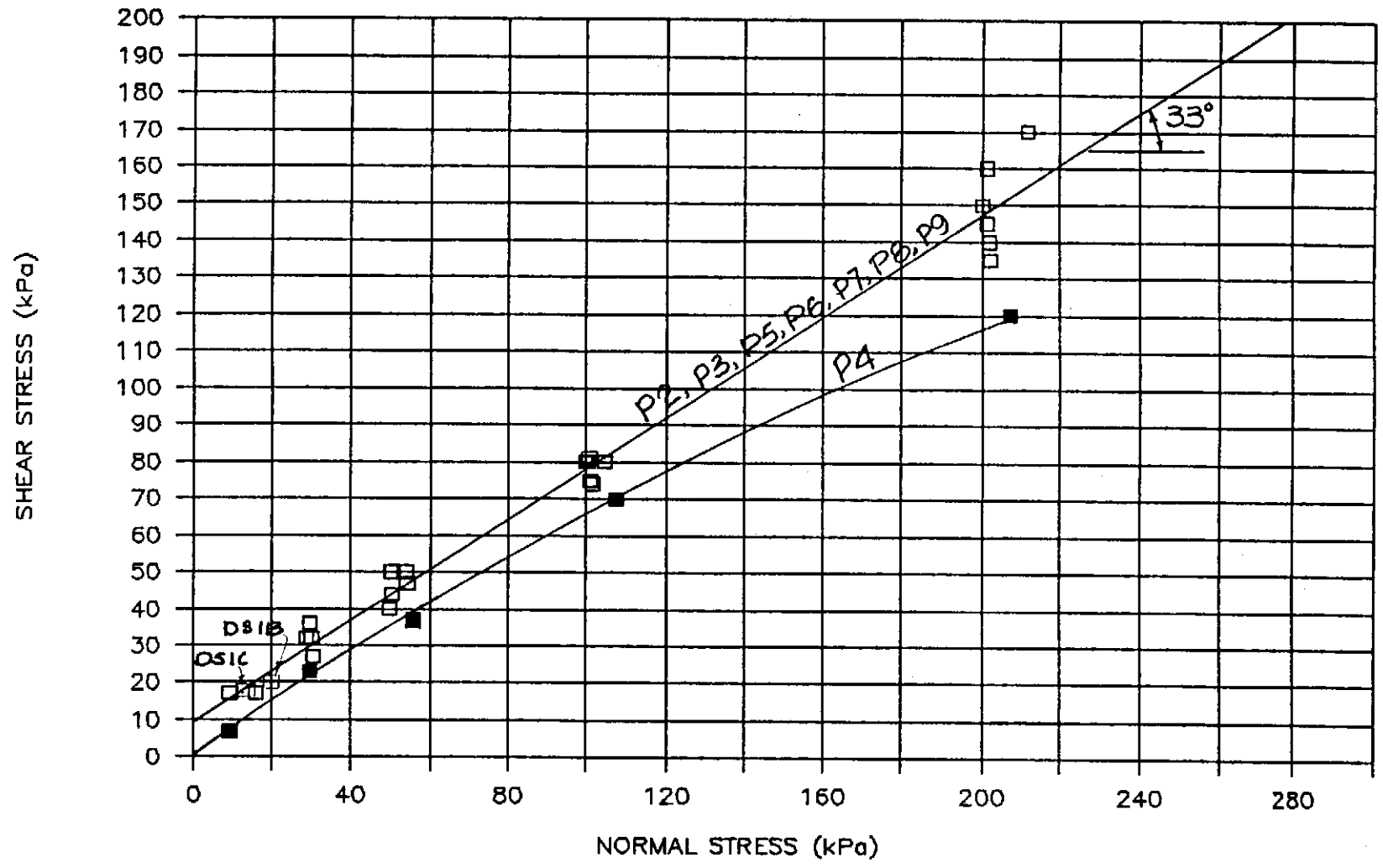


Figure 72 - Residual Strength Mohr Envelope from Direct Shear Test

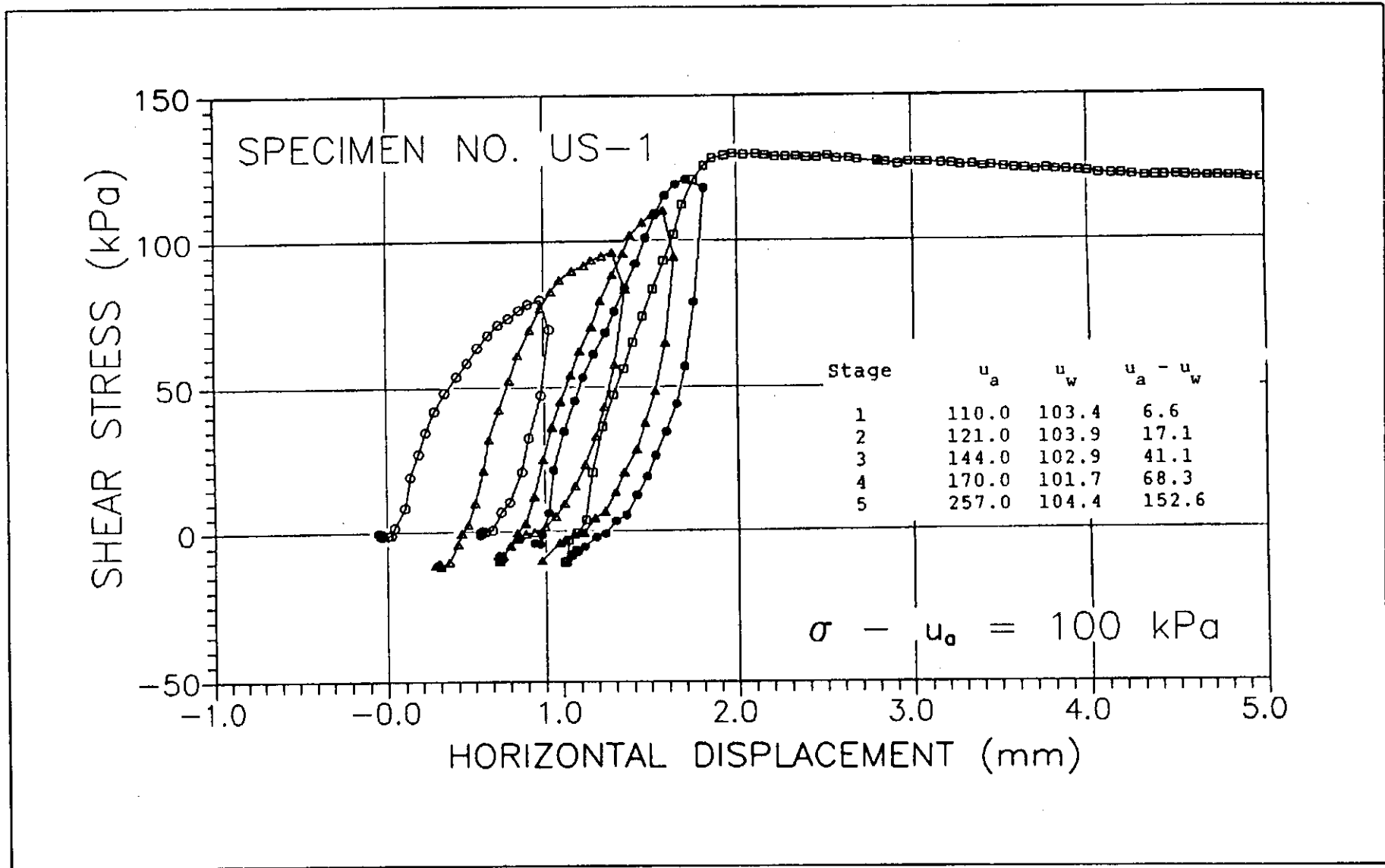


Figure 73a - Shear Stress versus Horizontal Displacement - Specimen No. US-1

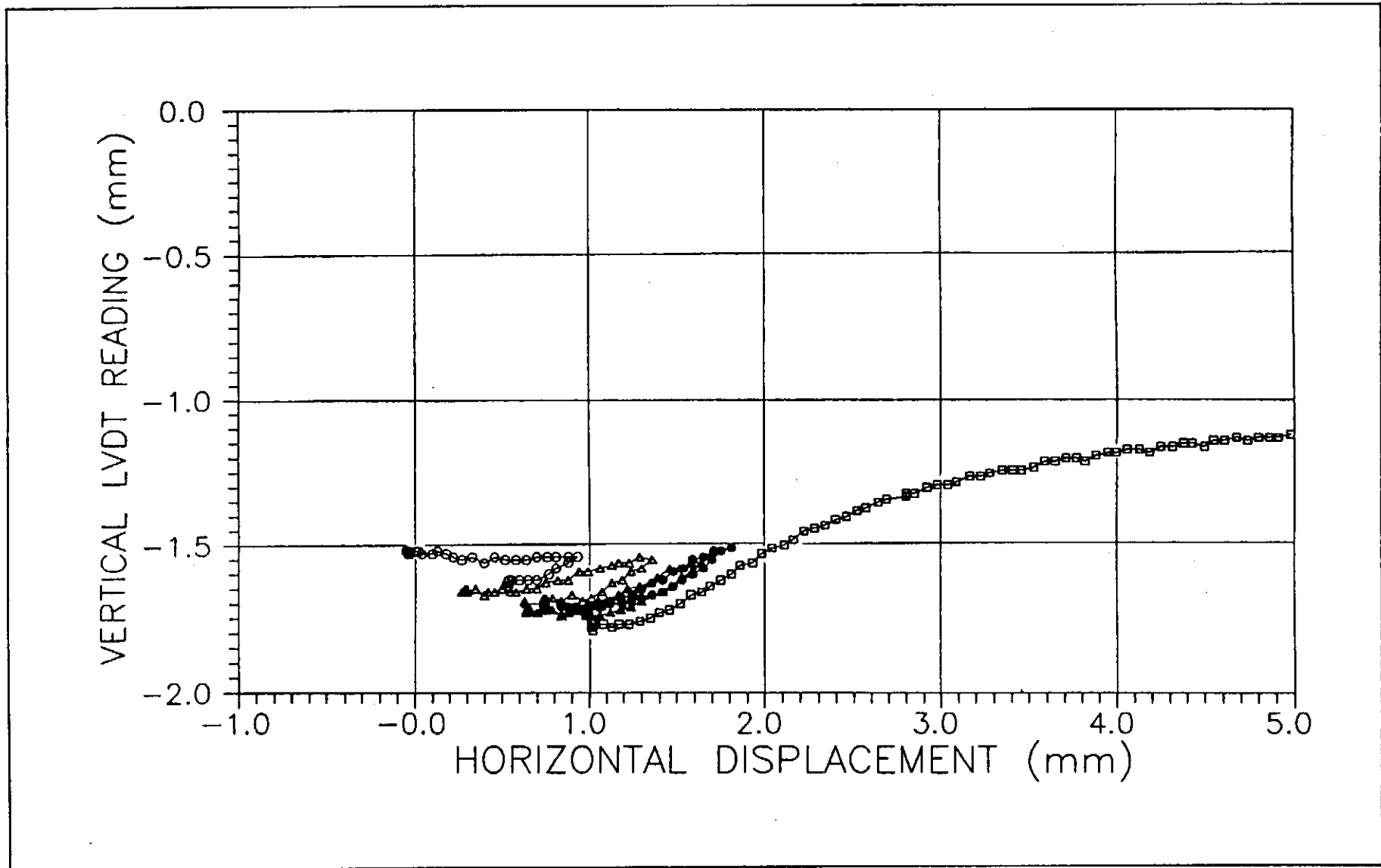


Figure 73b - Vertical Deflection versus Horizontal Displacement - Specimen No. US-1

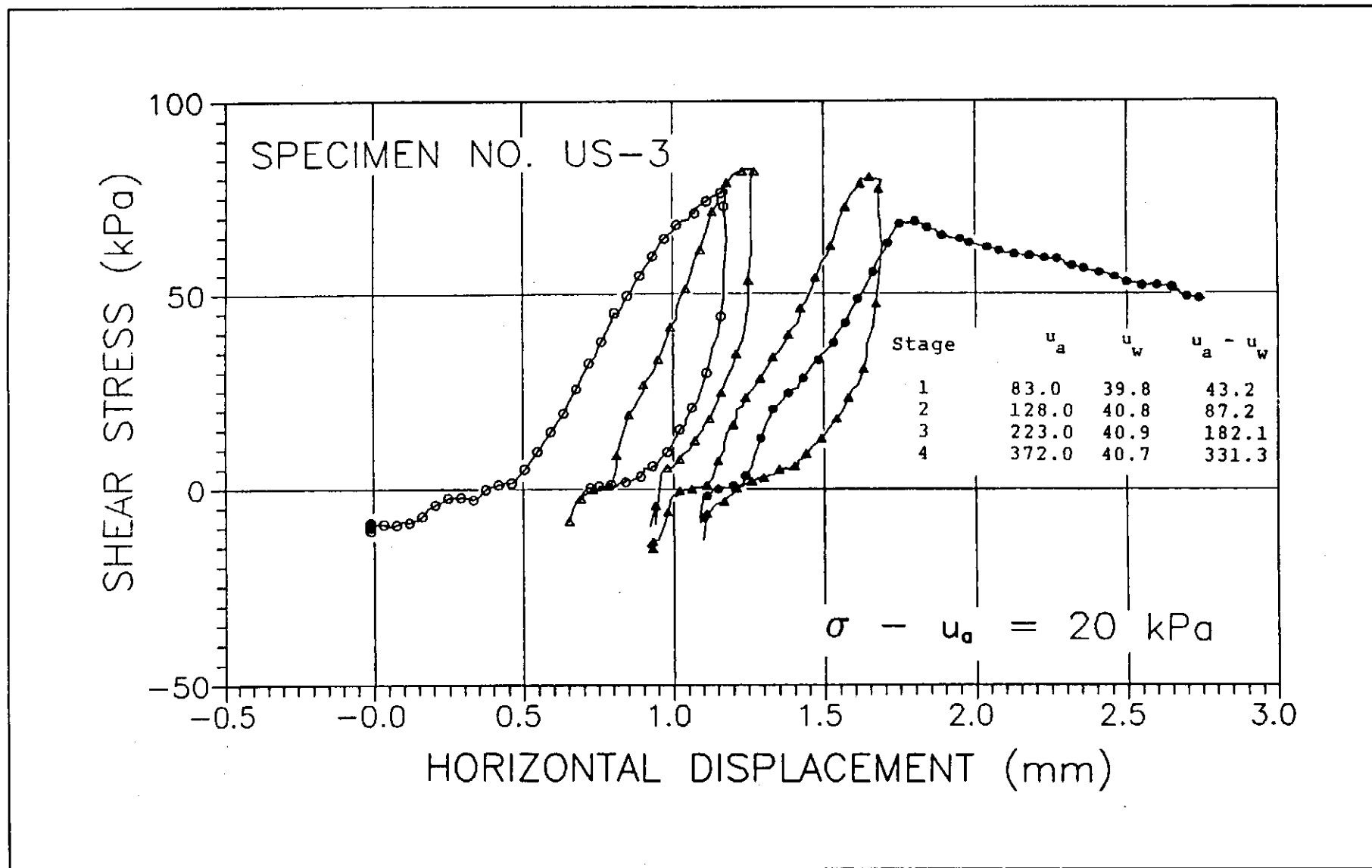


Figure 74a - Shear Stress versus Horizontal Displacement - Specimen No. US-3

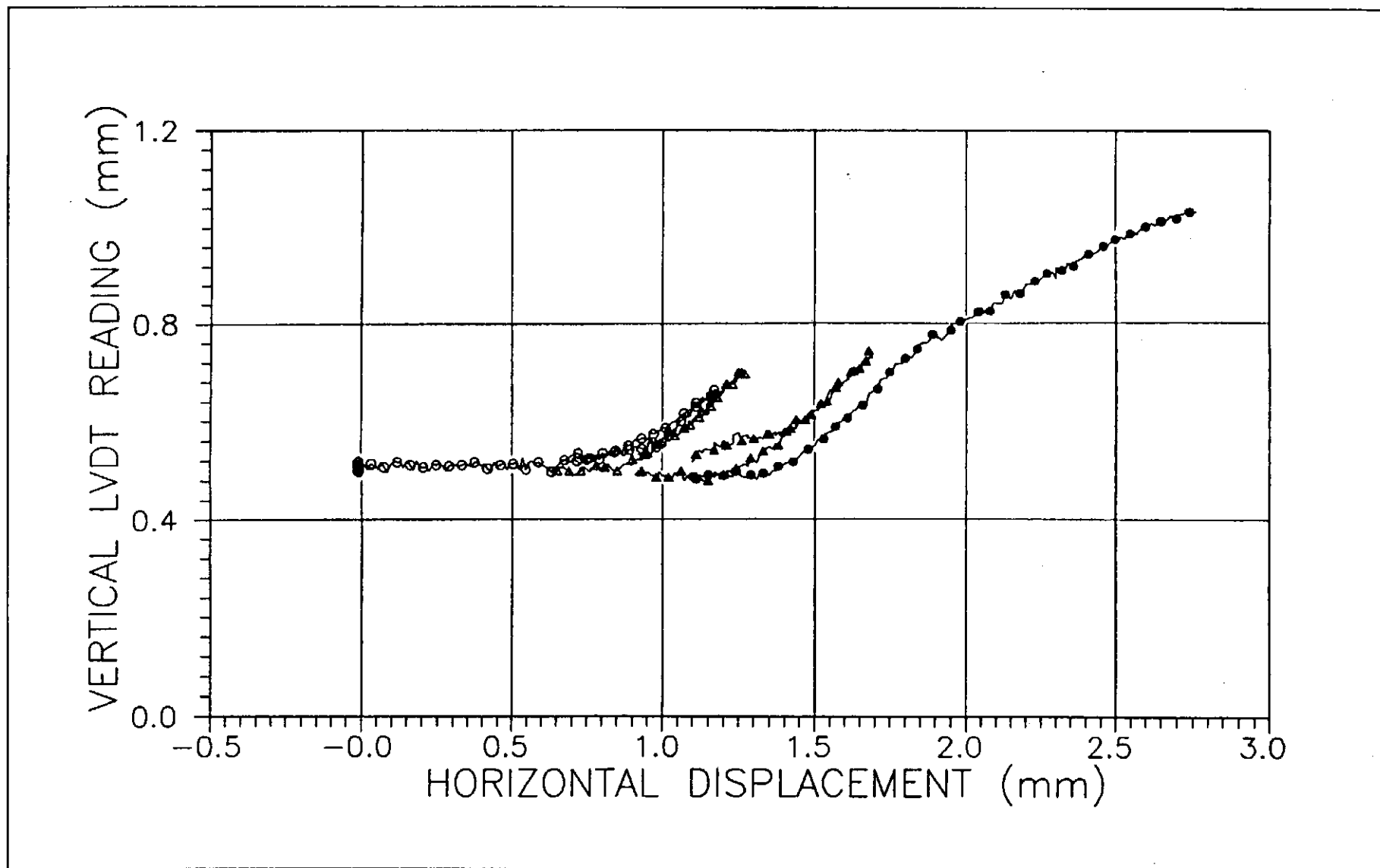


Figure 74b - Vertical Deflection versus Horizontal Displacement - Specimen No. US-3

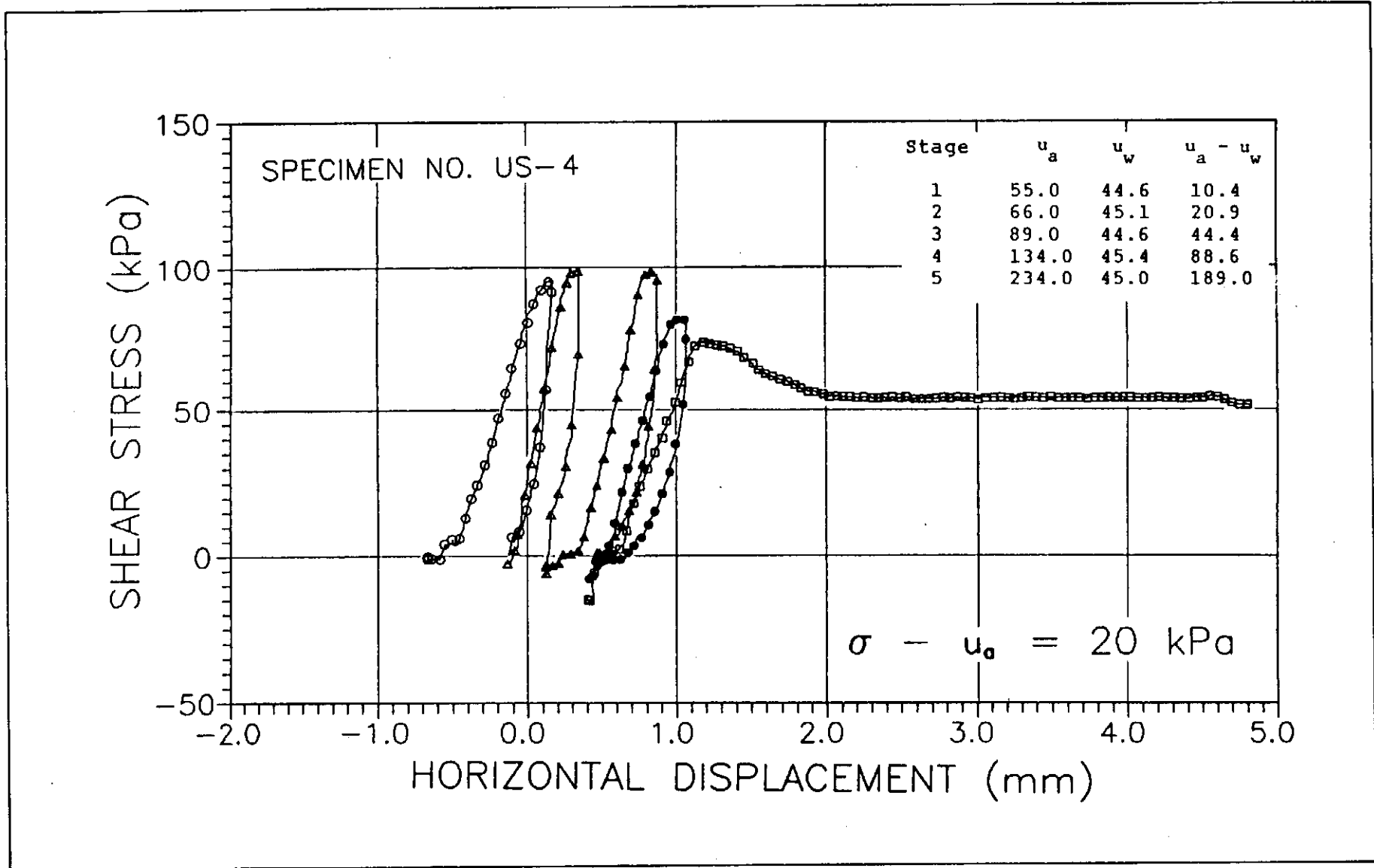


Figure 75a - Shear Stress versus Horizontal Displacement - Specimen No. US-4

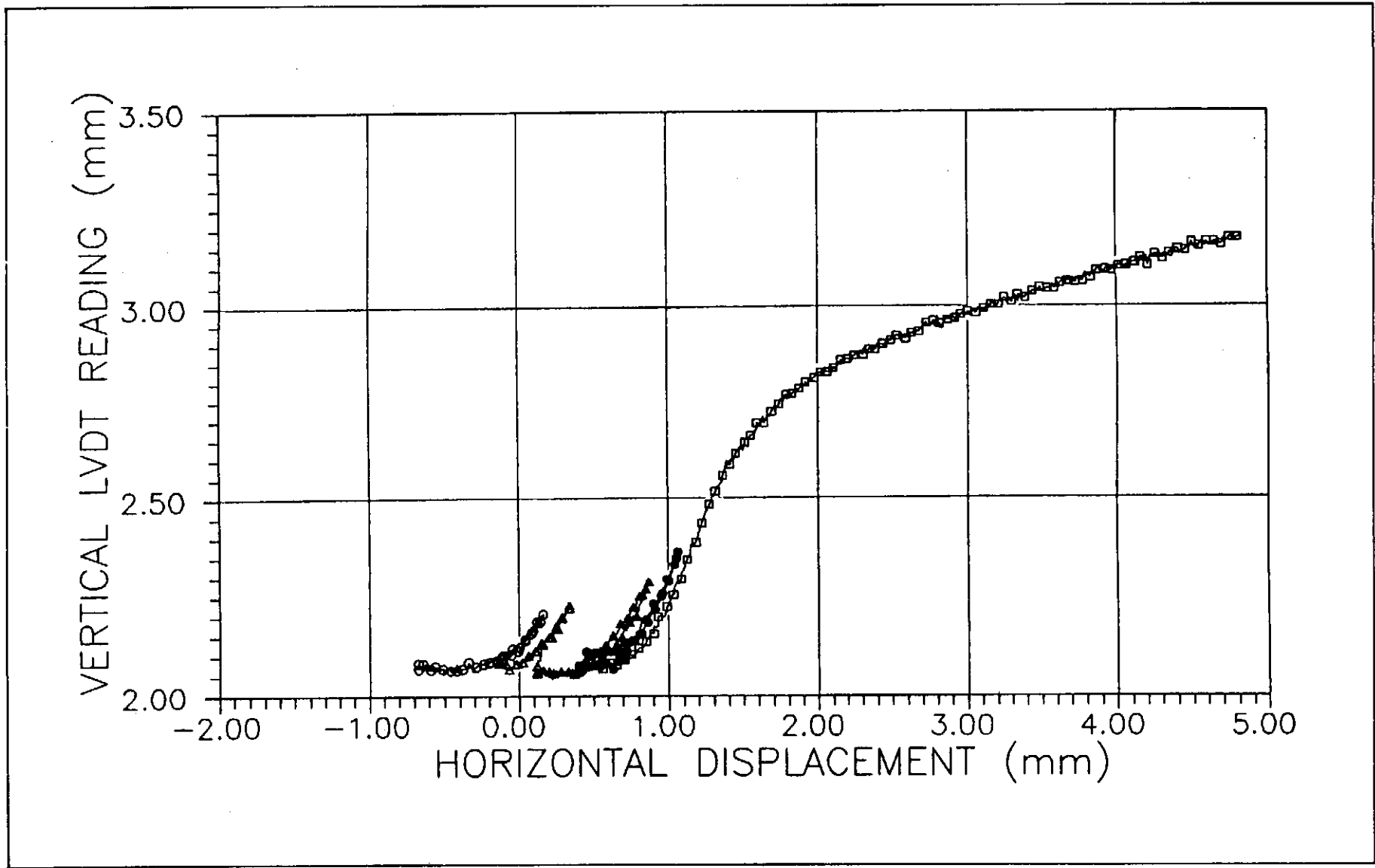


Figure 75b - Vertical Deflection versus Horizontal Displacement - Specimen No. US-4

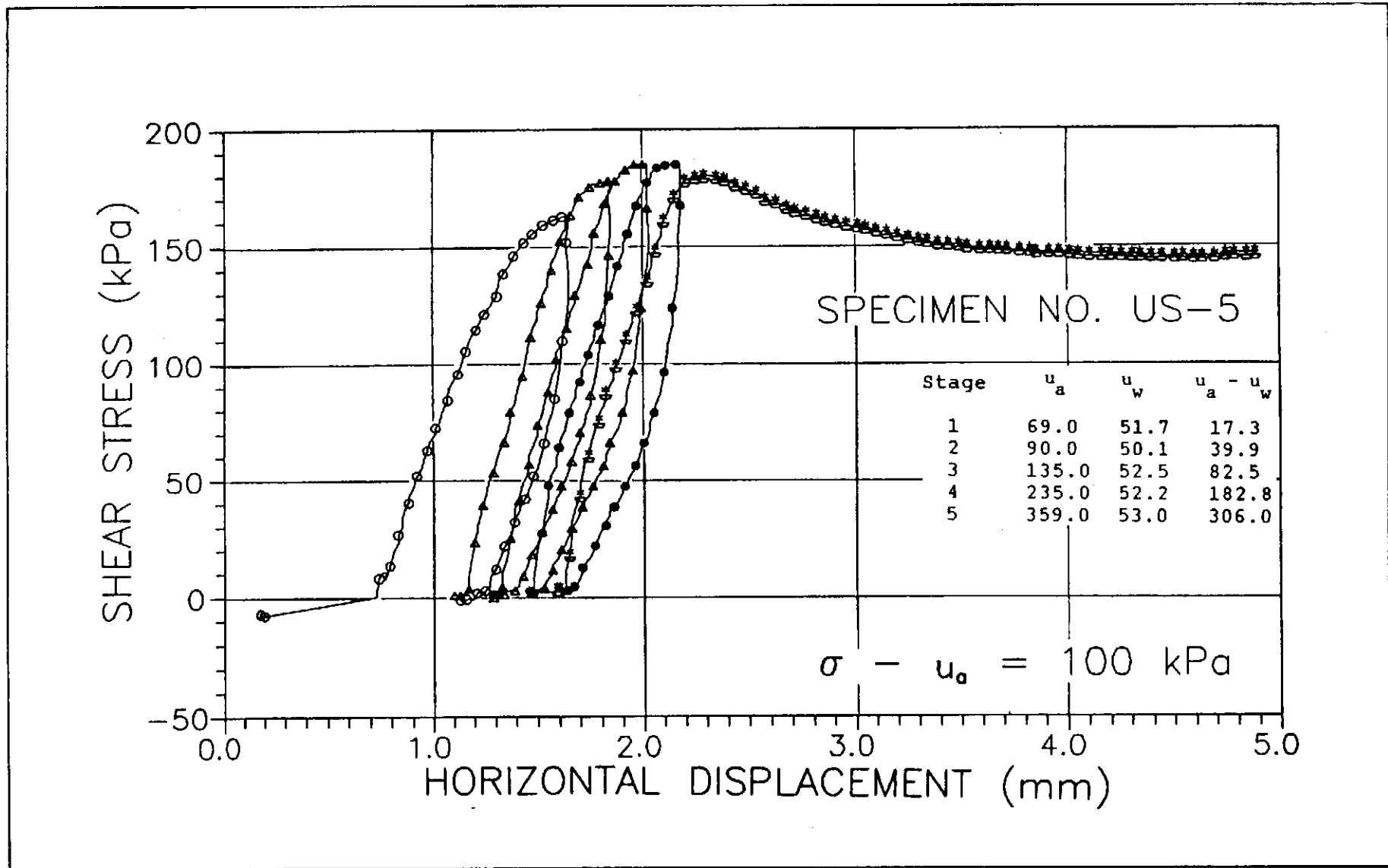


Figure 76a - Shear Stress versus Horizontal Displacement - Specimen No. US-5

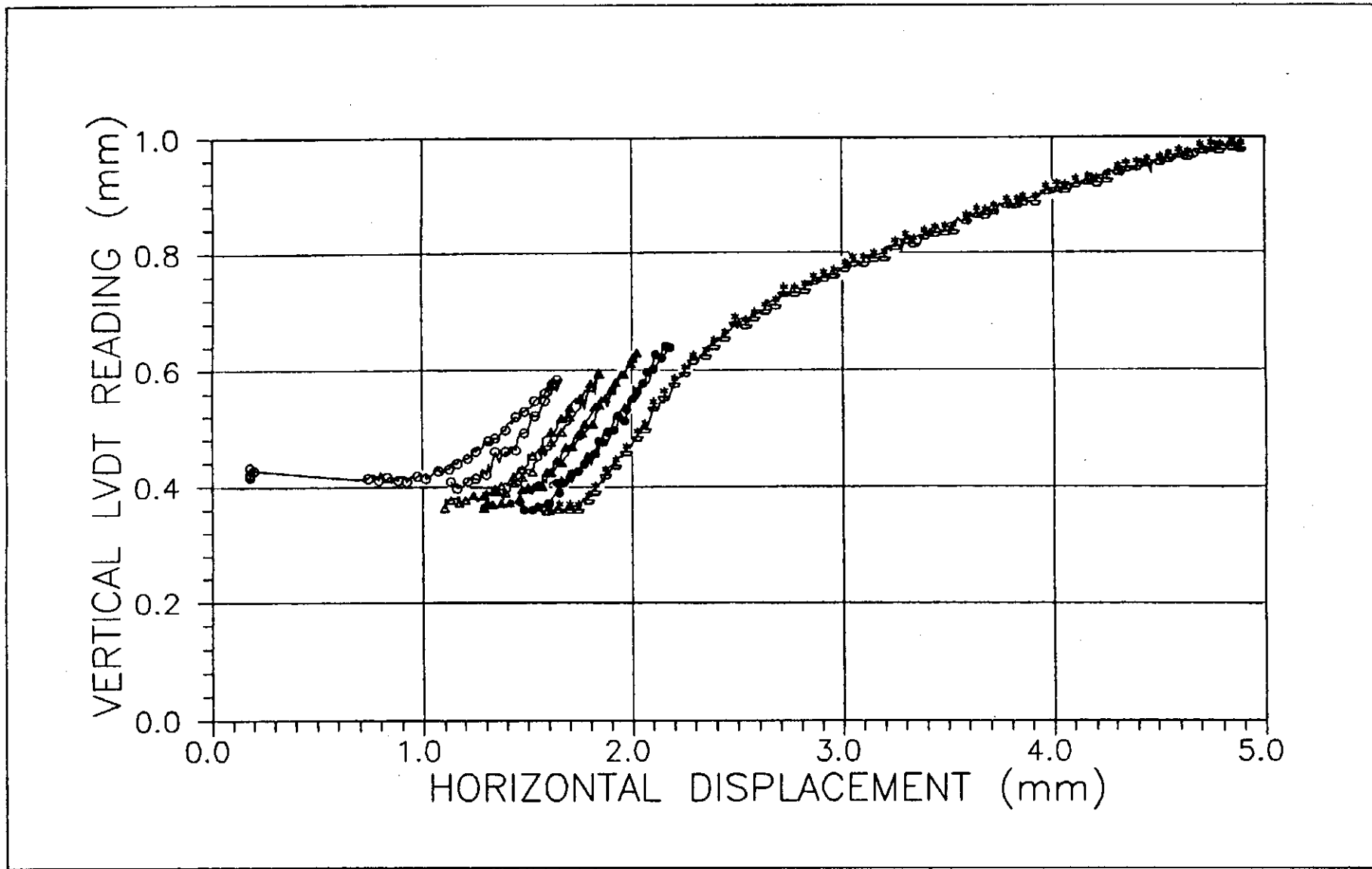


Figure 76b - Vertical Deflection versus Horizontal Displacement - Specimen No. US-5

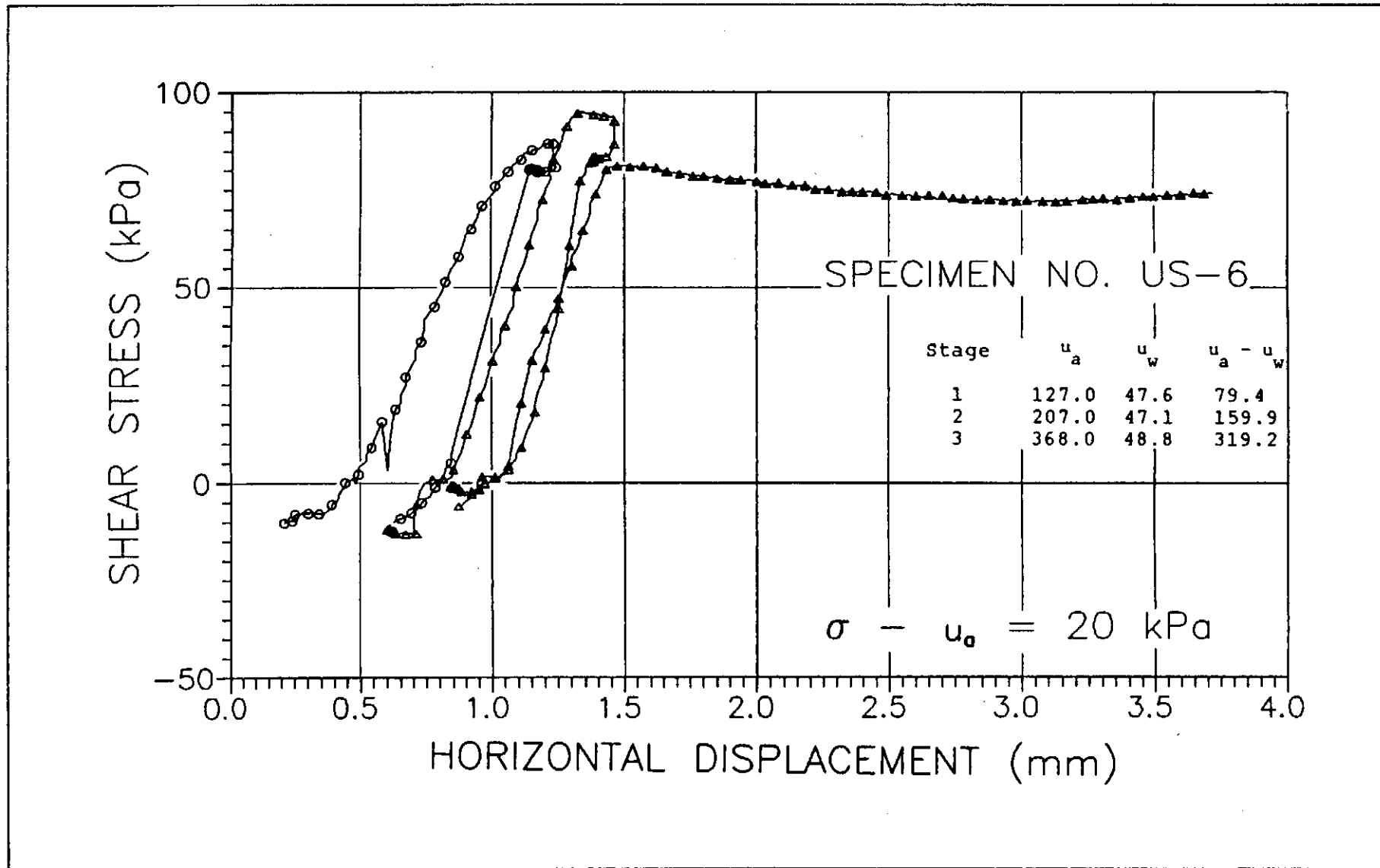


Figure 77a - Shear Stress versus Horizontal Displacement - Specimen No. US-6

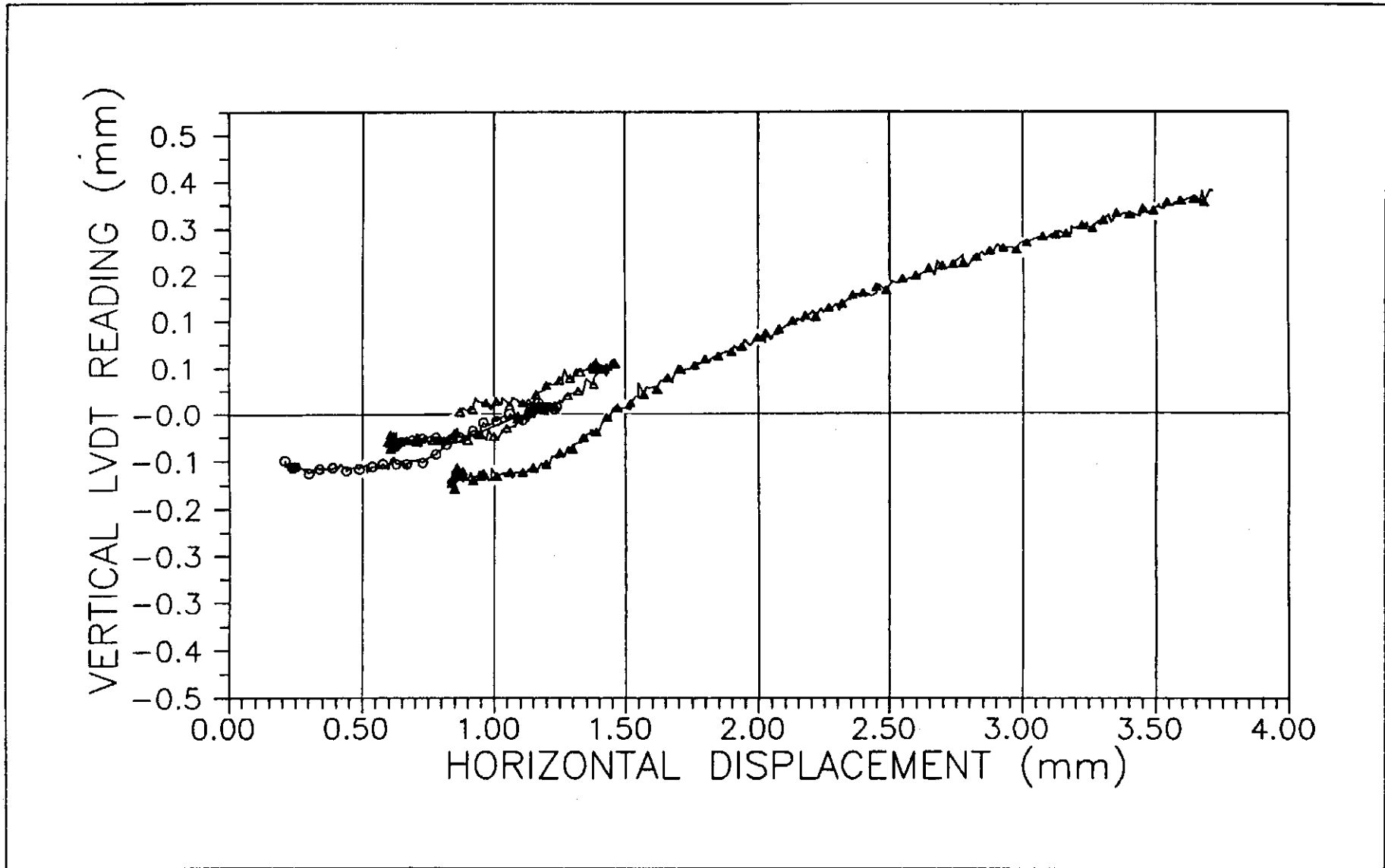


Figure 77b - Vertical Deflection versus Horizontal Displacement - Specimen No. US-6

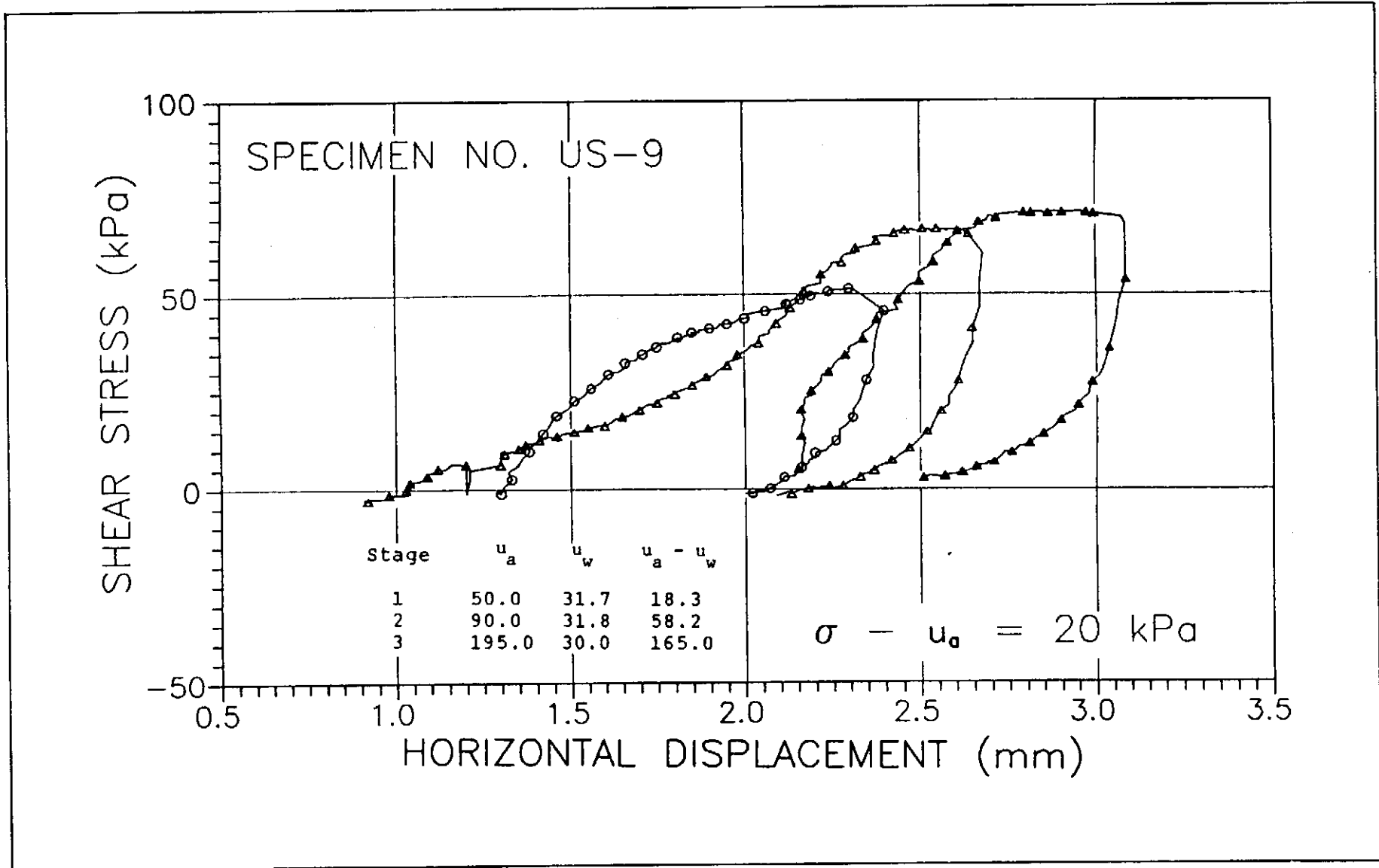


Figure 78a - Shear Stress versus Horizontal Displacement - Specimen No. US-9

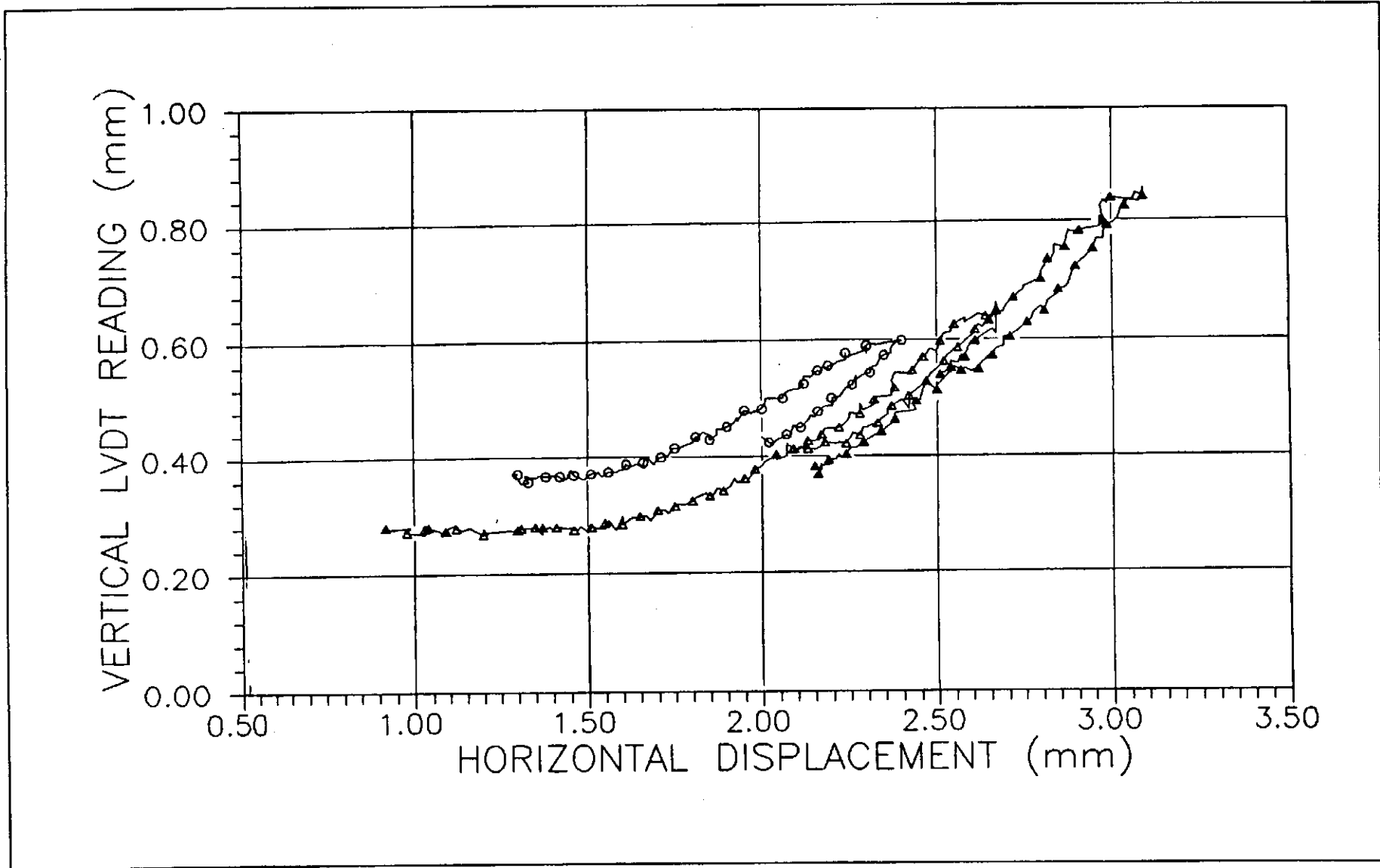


Figure 78b - Vertical Deflection versus Horizontal Displacement - Specimen No. US-9

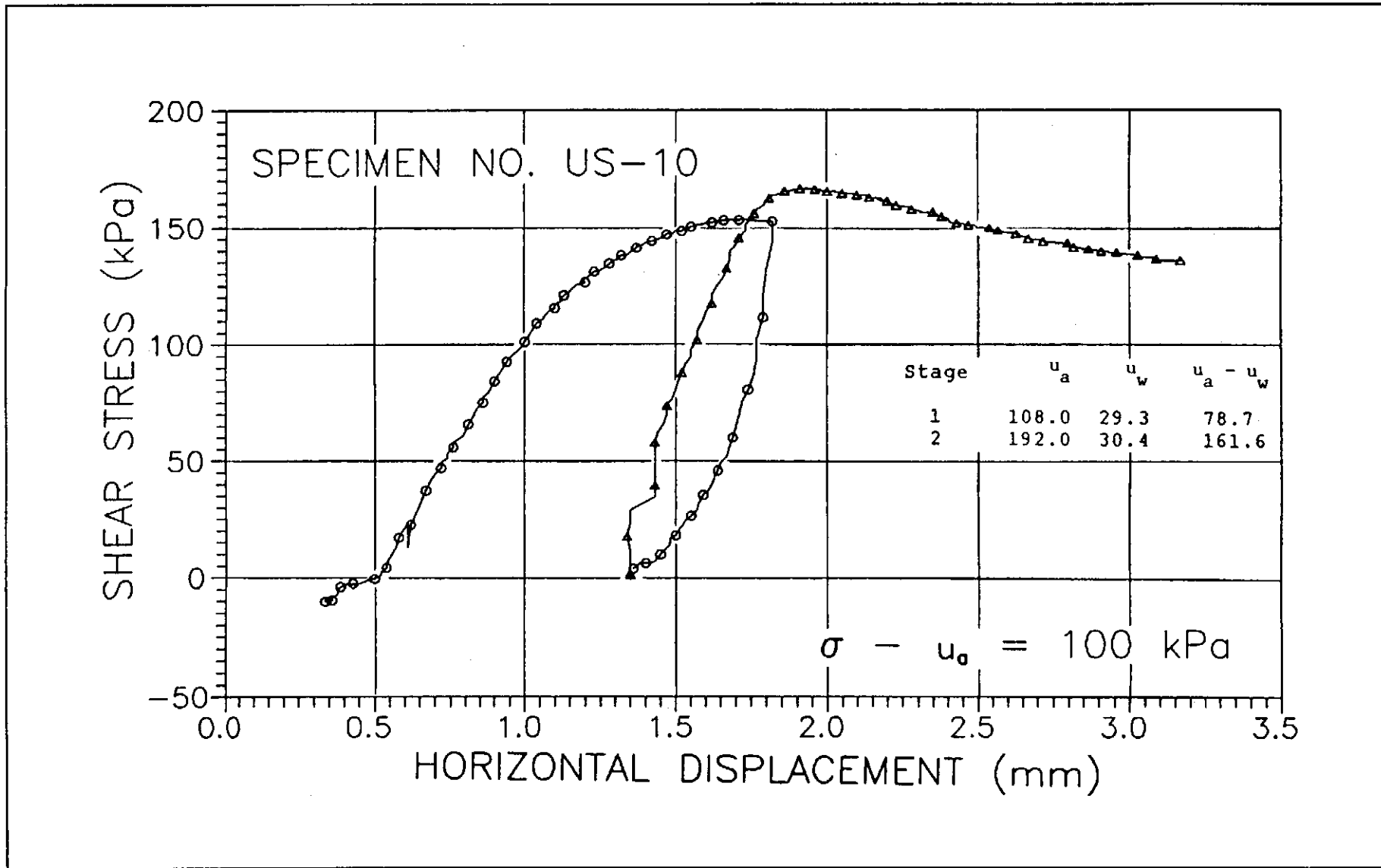


Figure 79a - Shear Stress versus Horizontal Displacement - Specimen No. US-10

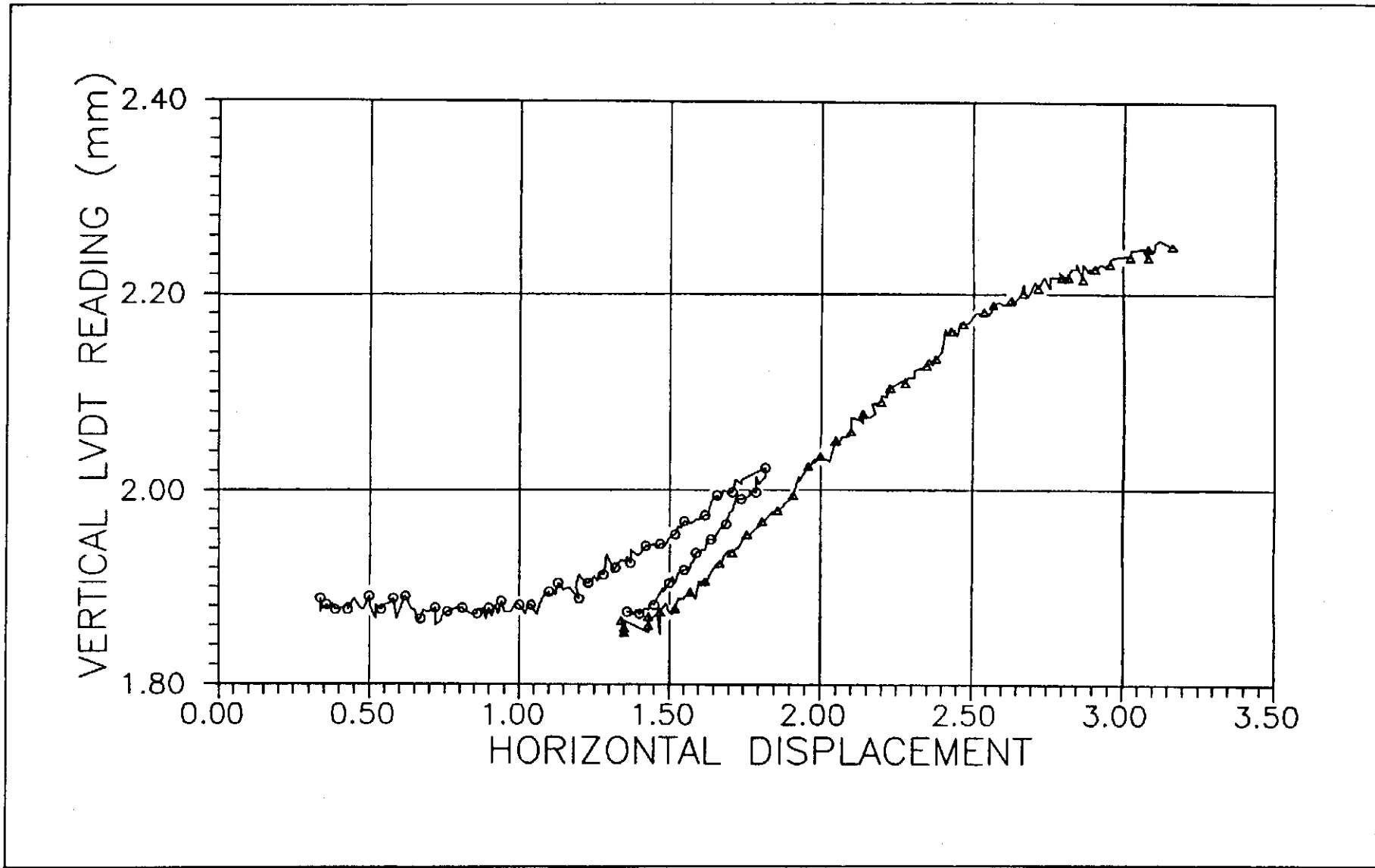


Figure 79b - Vertical Deflection versus Horizontal Displacement - Specimen No. US-10

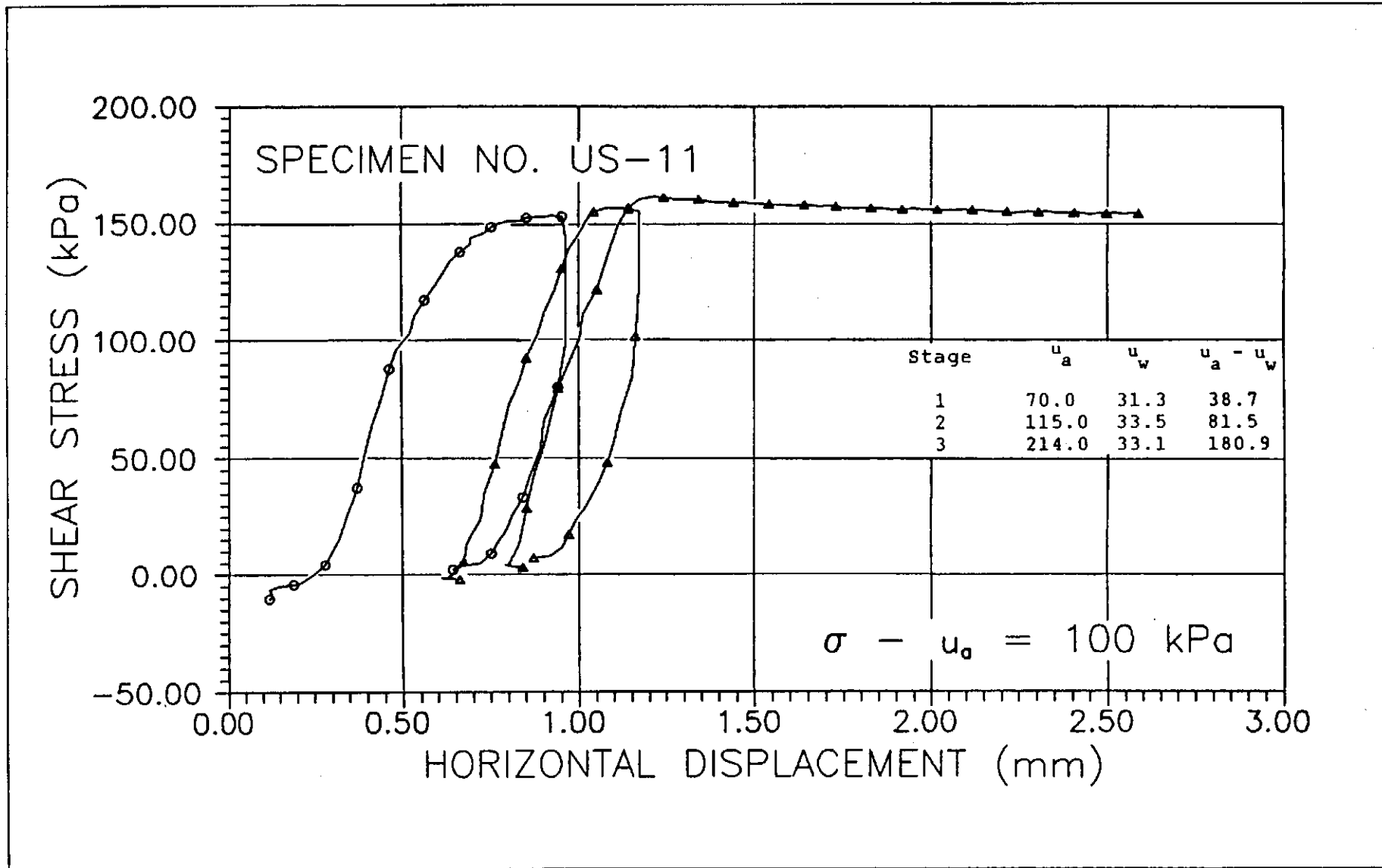


Figure 80a - Shear Stress versus Horizontal Displacement - Specimen No. US-11

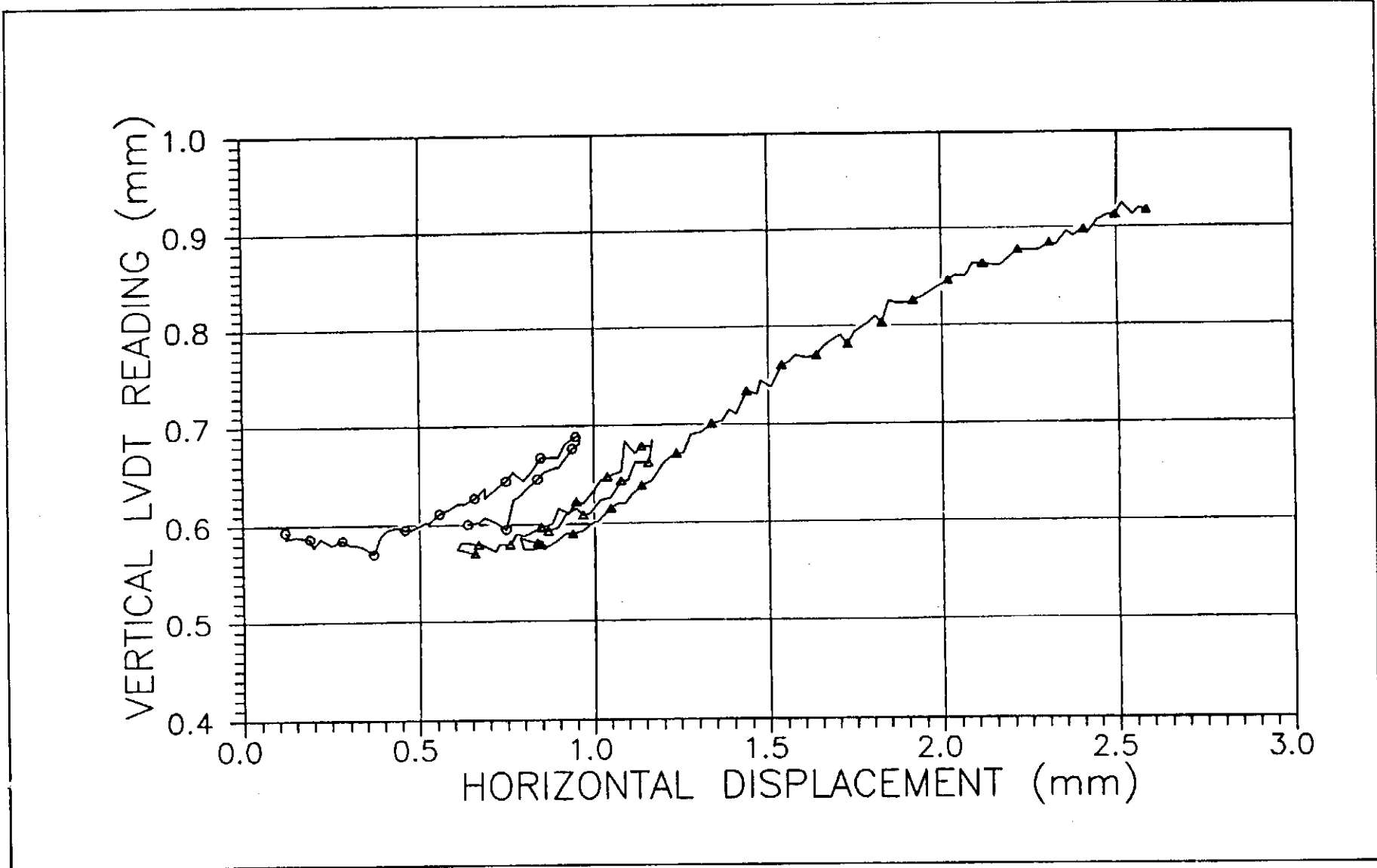


Figure 80b - Vertical Deflection versus Horizontal Displacement - Specimen No. US-11

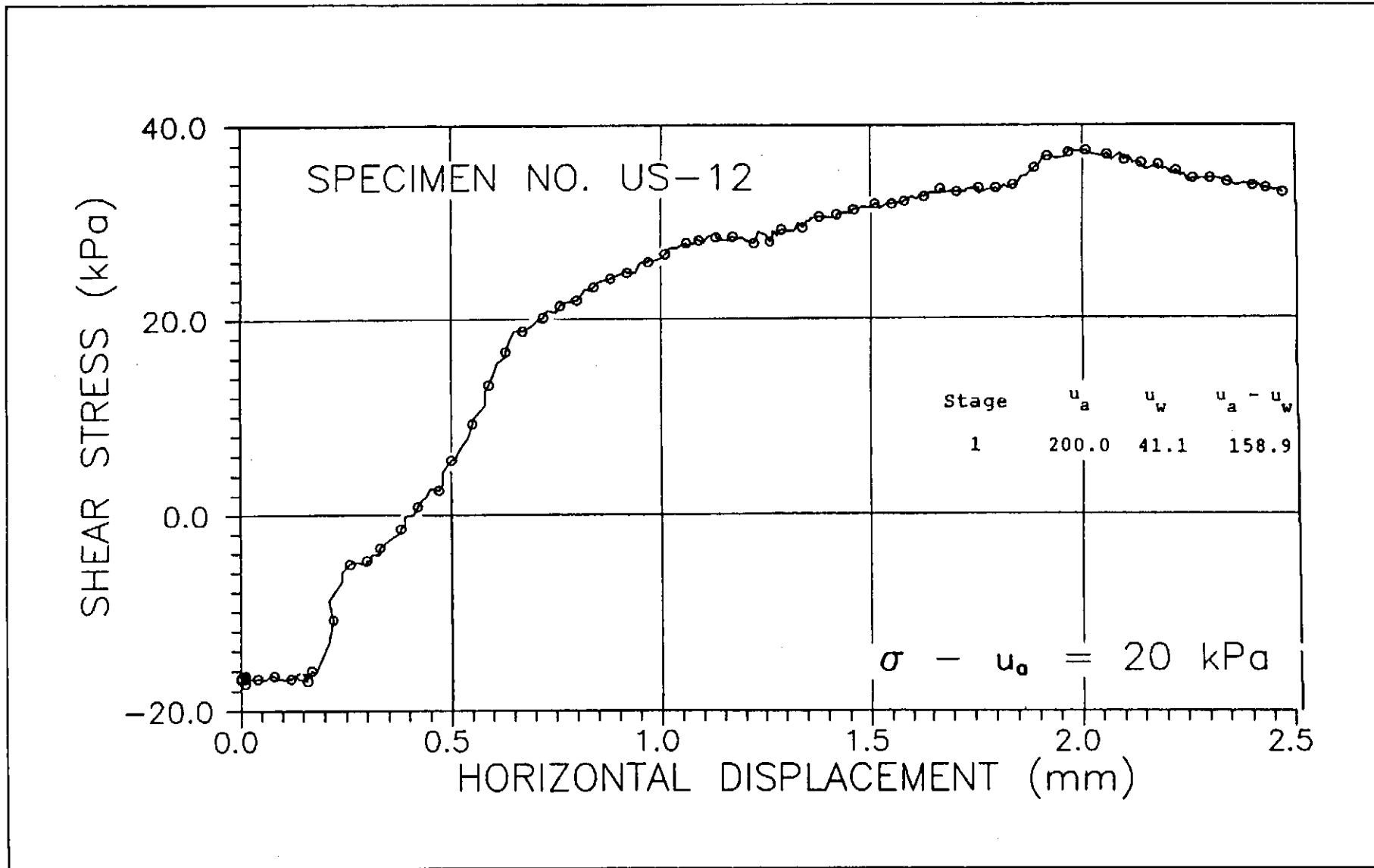


Figure 81a - Shear Stress versus Horizontal Displacement - Specimen No. US-12

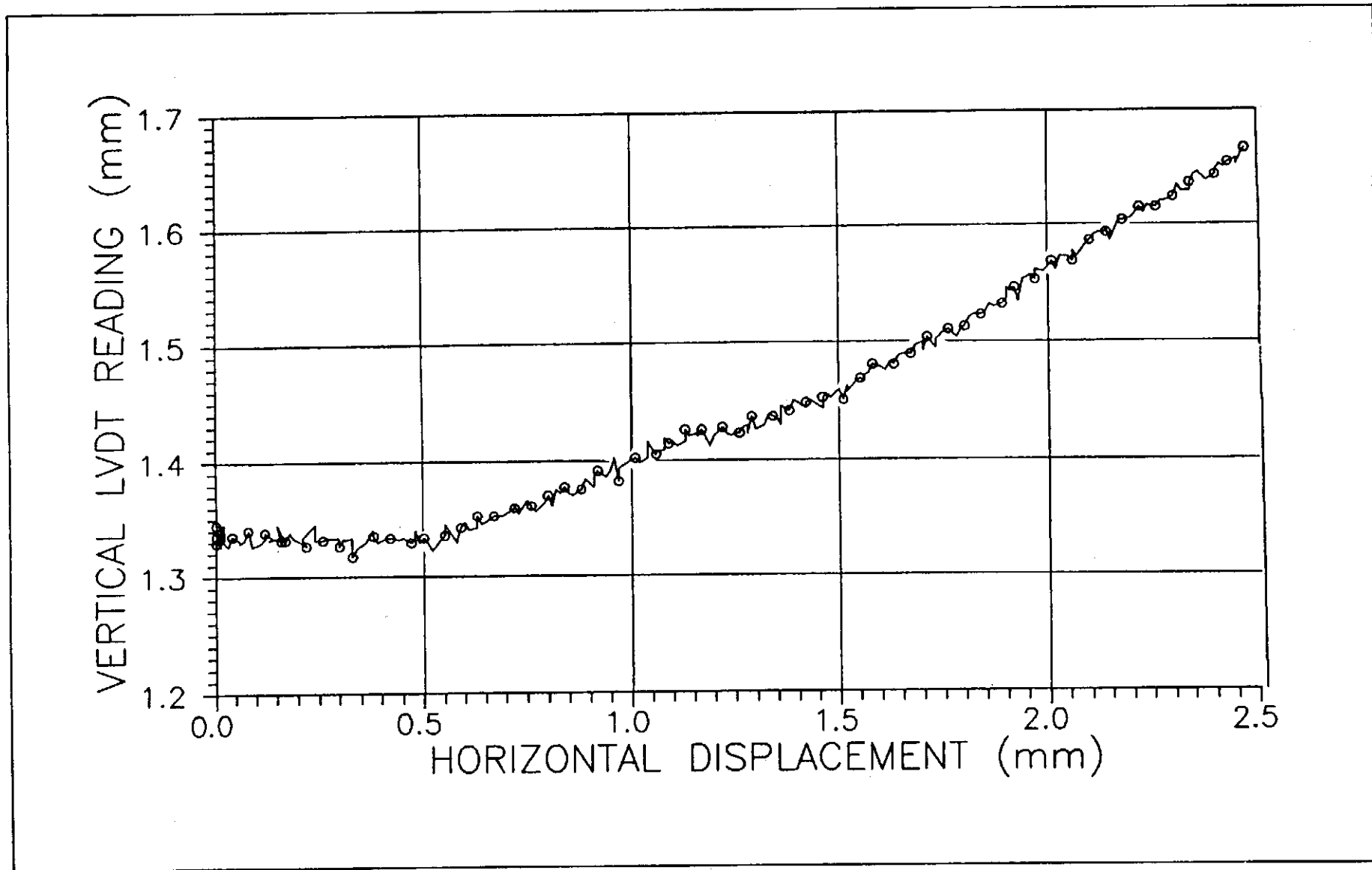


Figure 81b - Vertical Deflection versus Horizontal Displacement - Specimen No. US-12

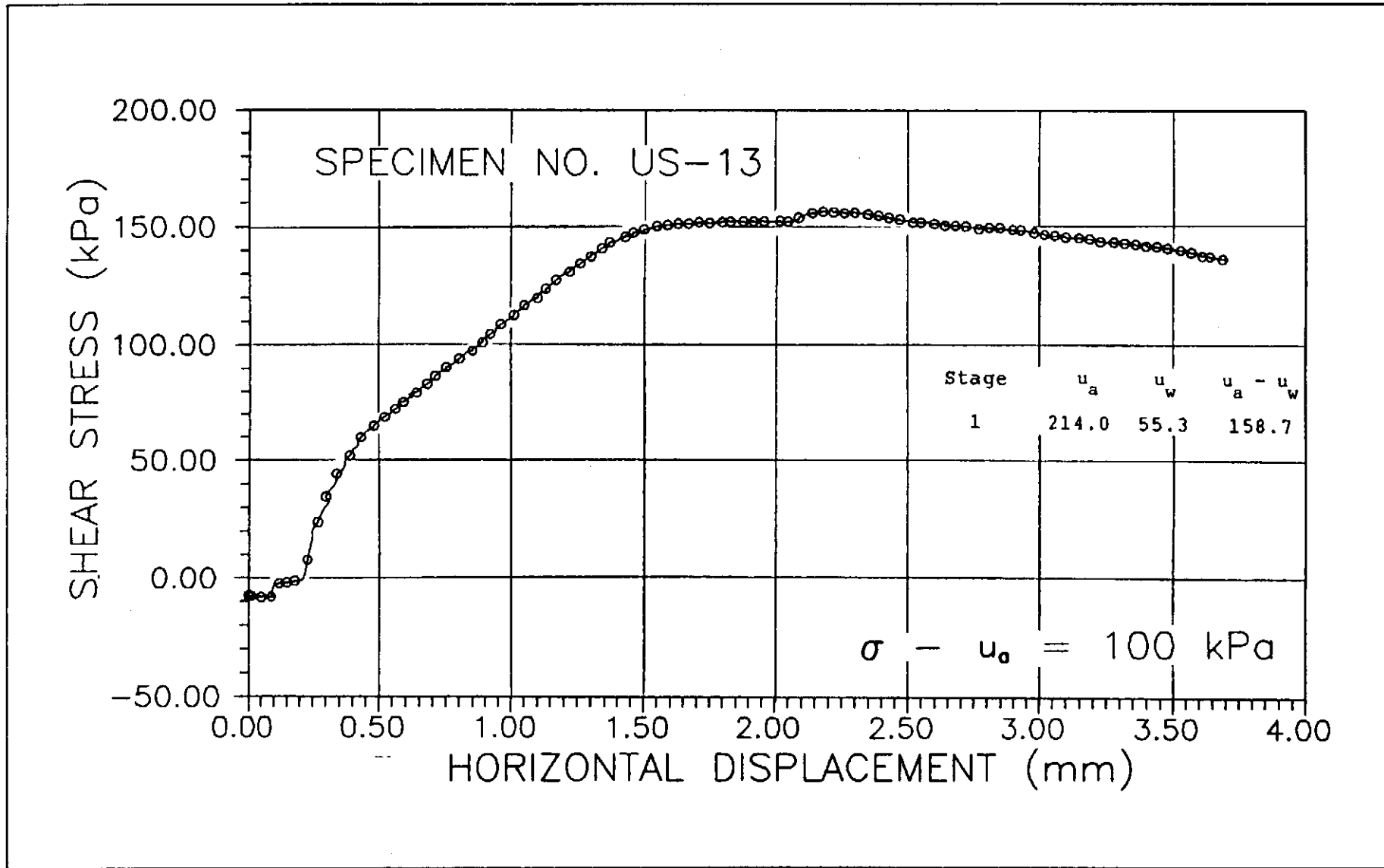


Figure 82a - Shear Stress versus Horizontal Displacement - Specimen No. US-13

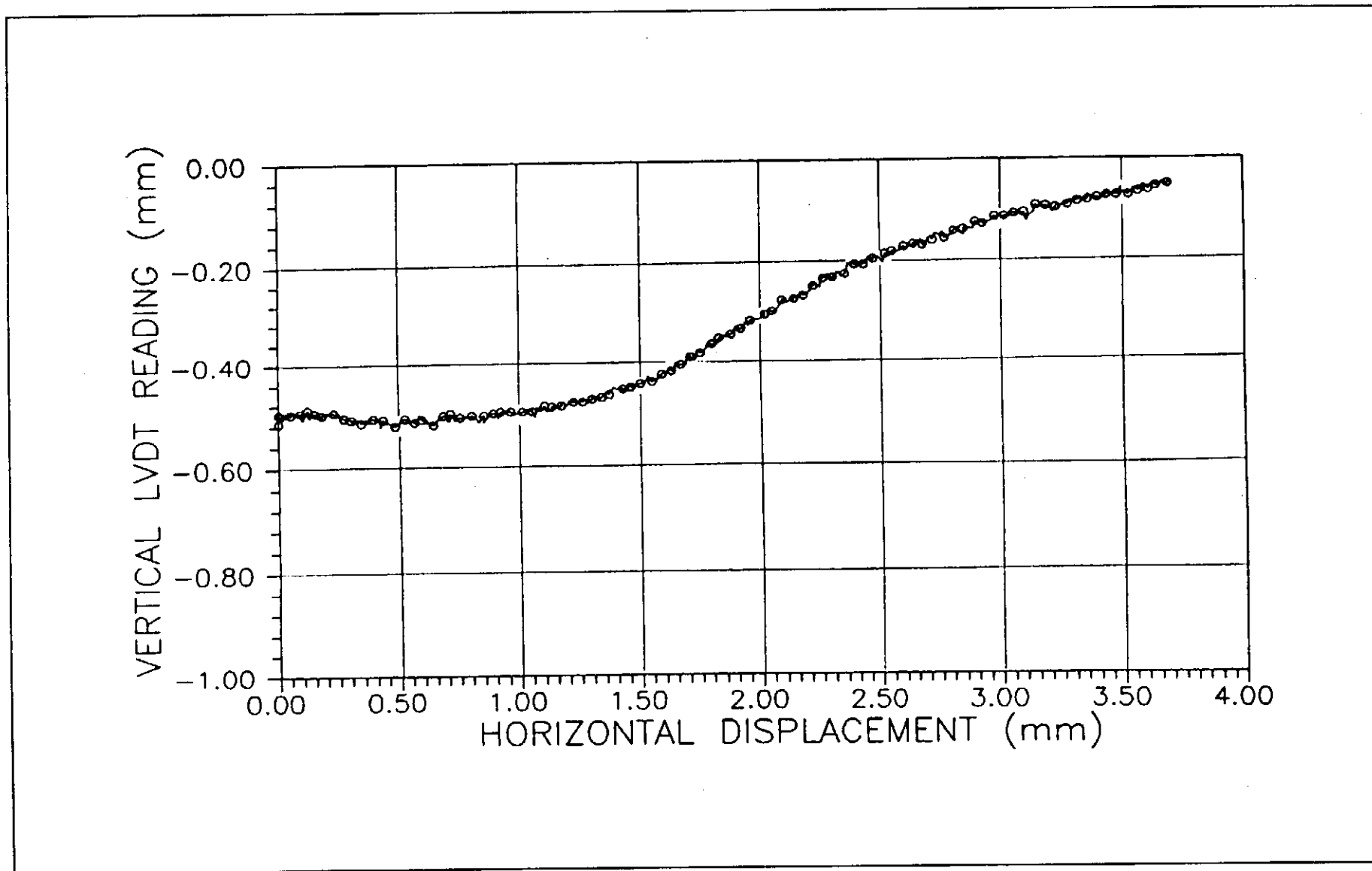


Figure 82b - Vertical Deflection versus Horizontal Displacement - Specimen No. US-13

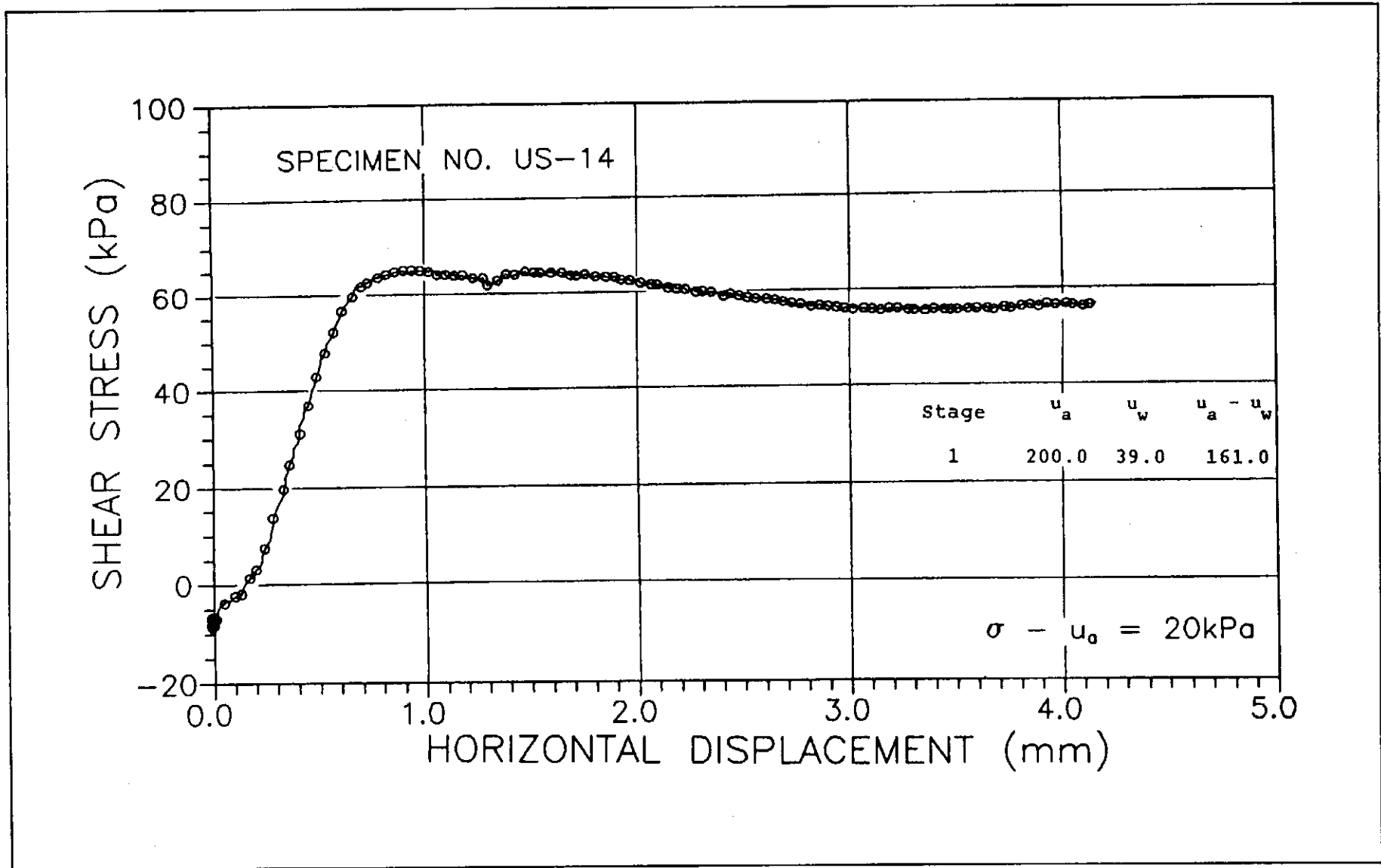


Figure 83a - Shear Stress versus Horizontal Displacement - Specimen No. US-14

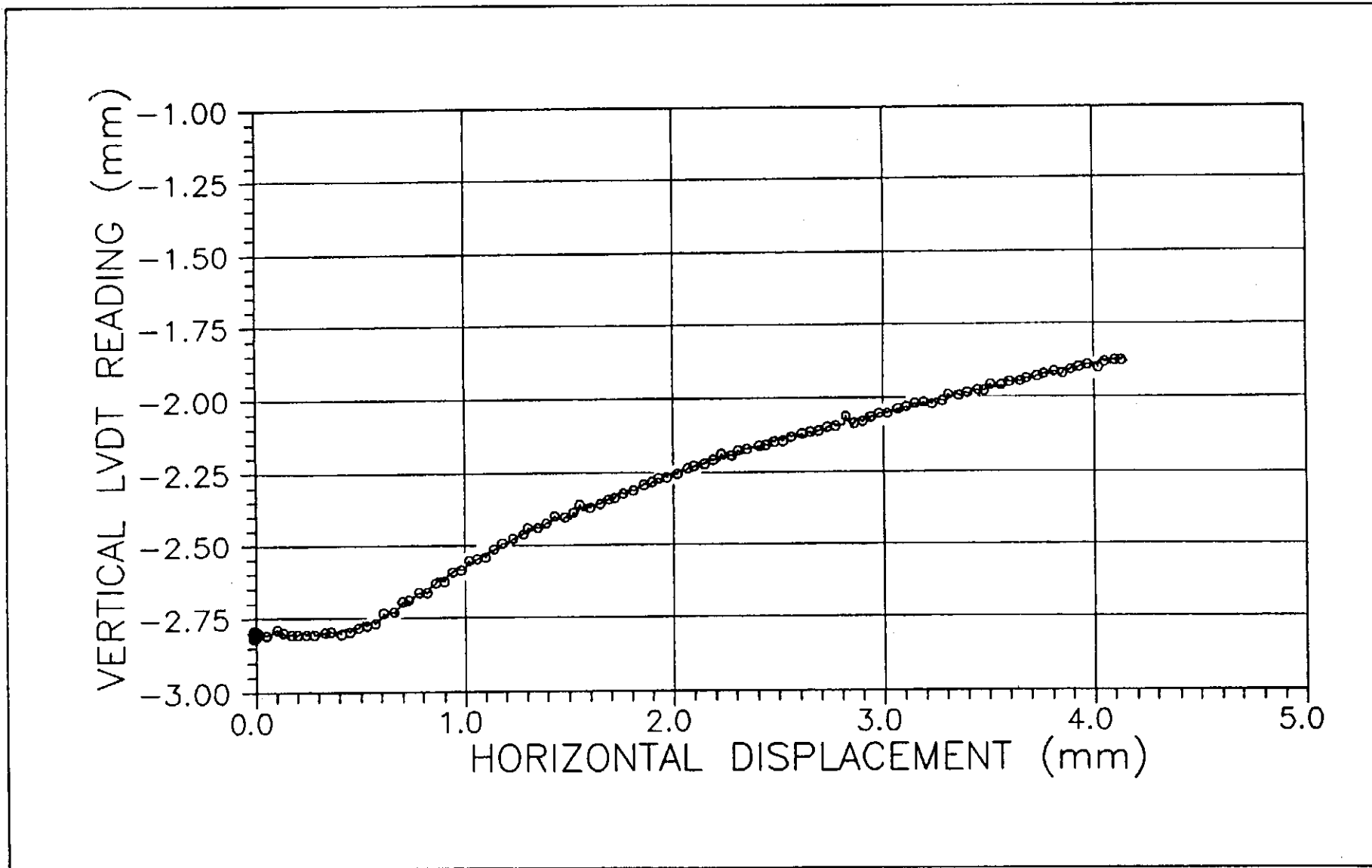


Figure 83b - Vertical Deflection versus Horizontal Displacement - Specimen No. US-14

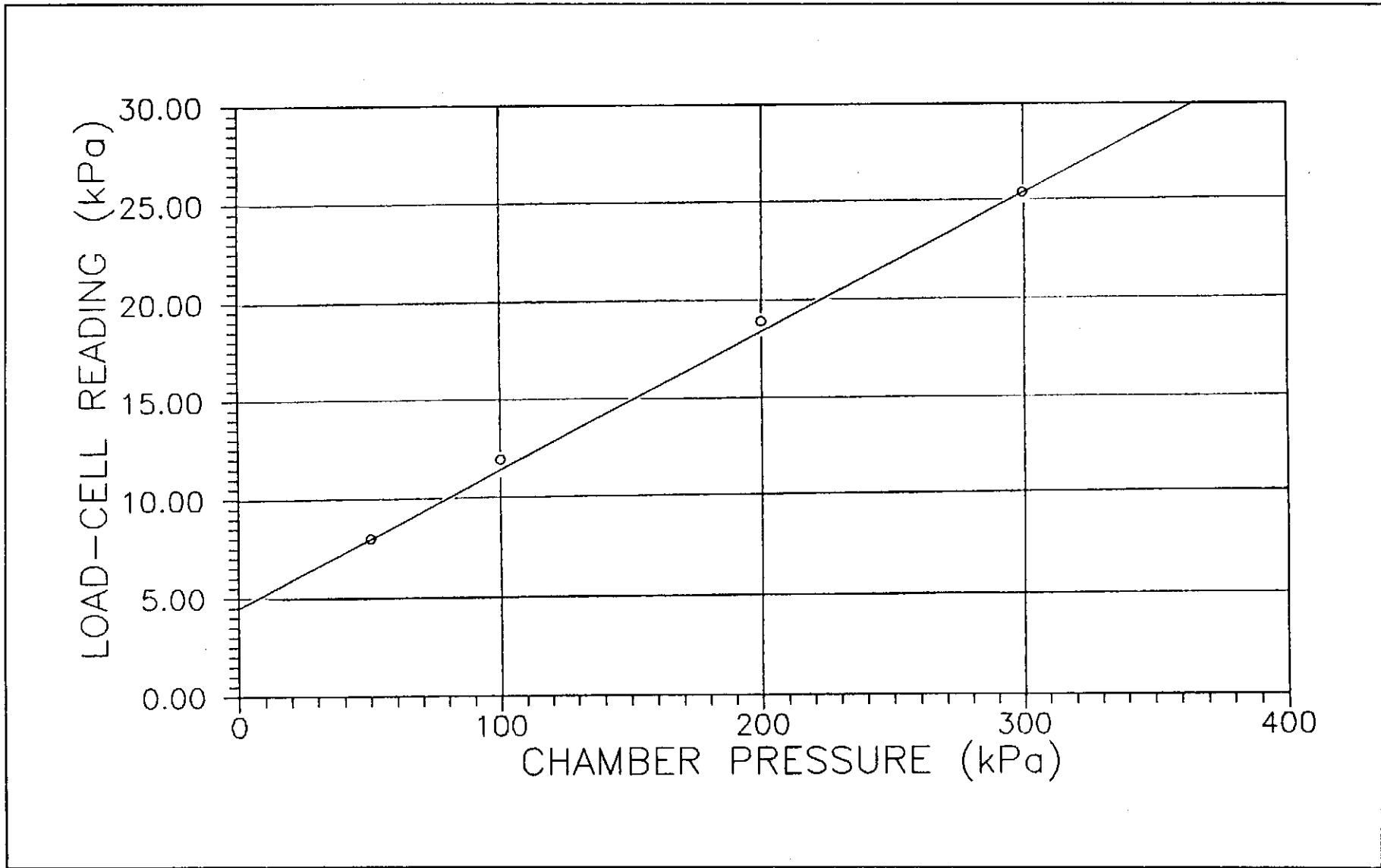


Figure 84a - Correction for Chamber Pressures on Load-cell Reading

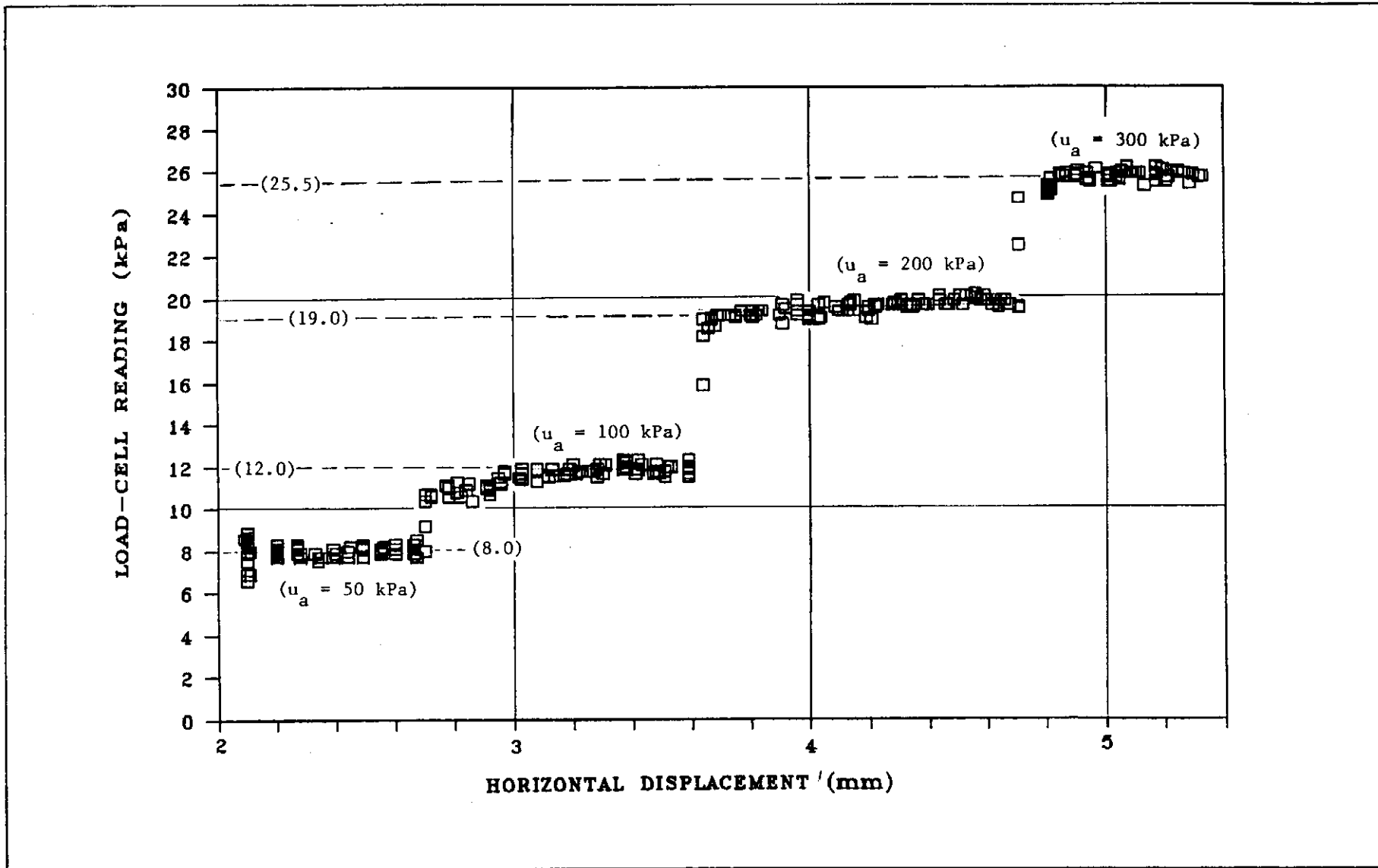


Figure 84b - Load-cell Readings with Respect to Shear Displacement at Various Chamber Pressures

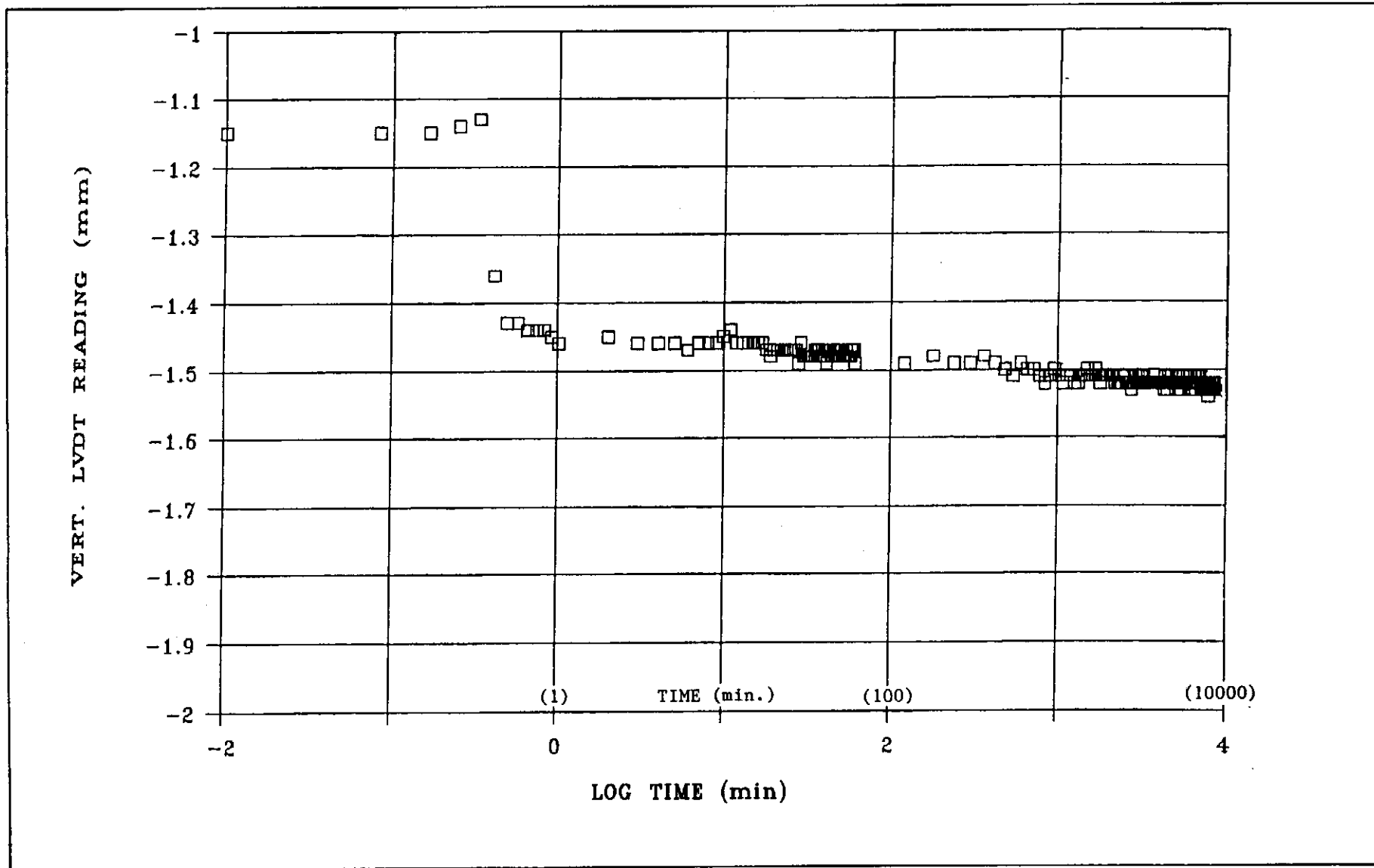


Figure 85a - Vertical Deflection with Time during Pressures Equilibration for Specimen No. US-1, Stage 1

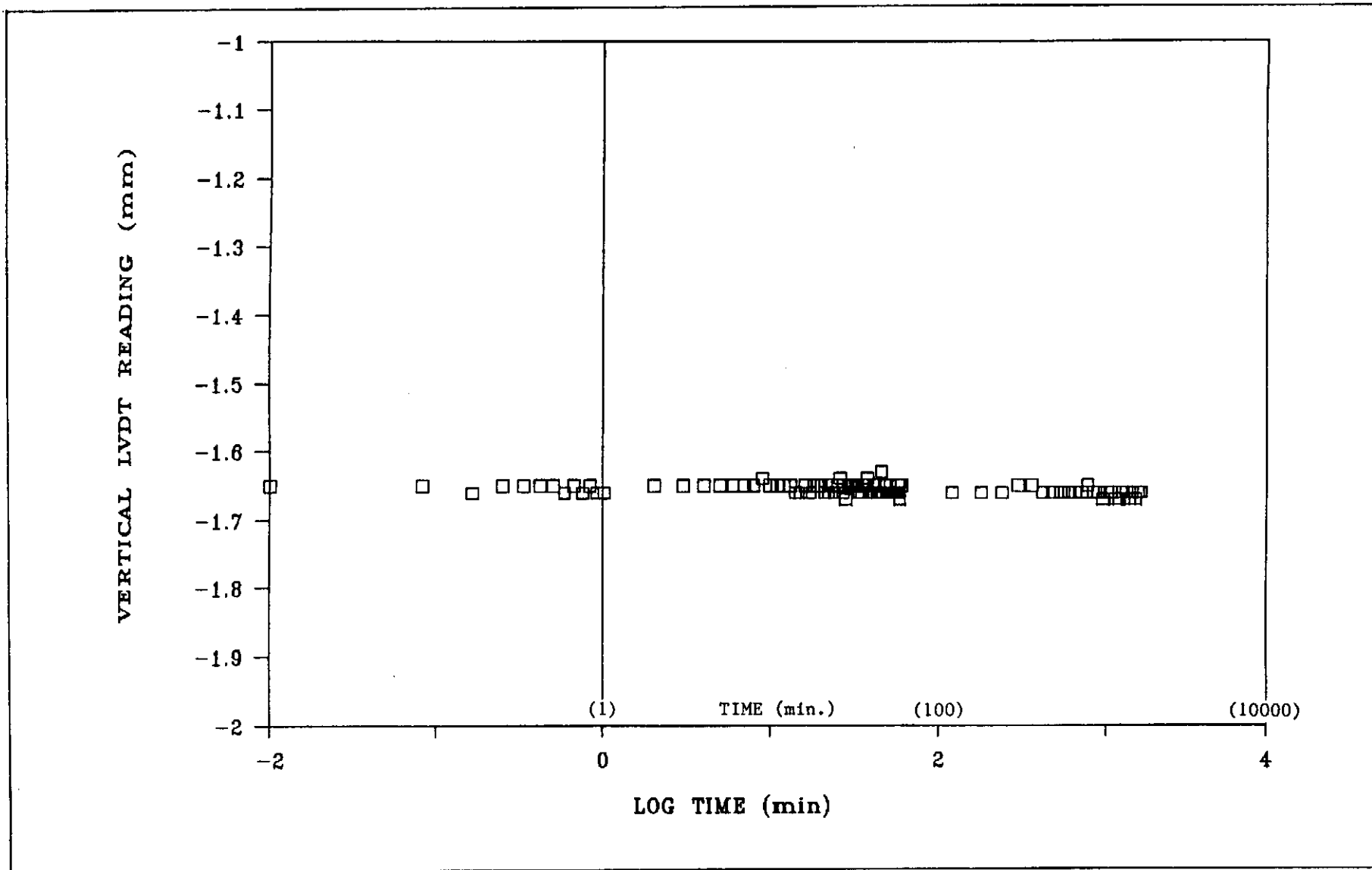


Figure 85b - Vertical Deflection with Time during Pressures Equilibration for Specimen No. US-1, Stage 2

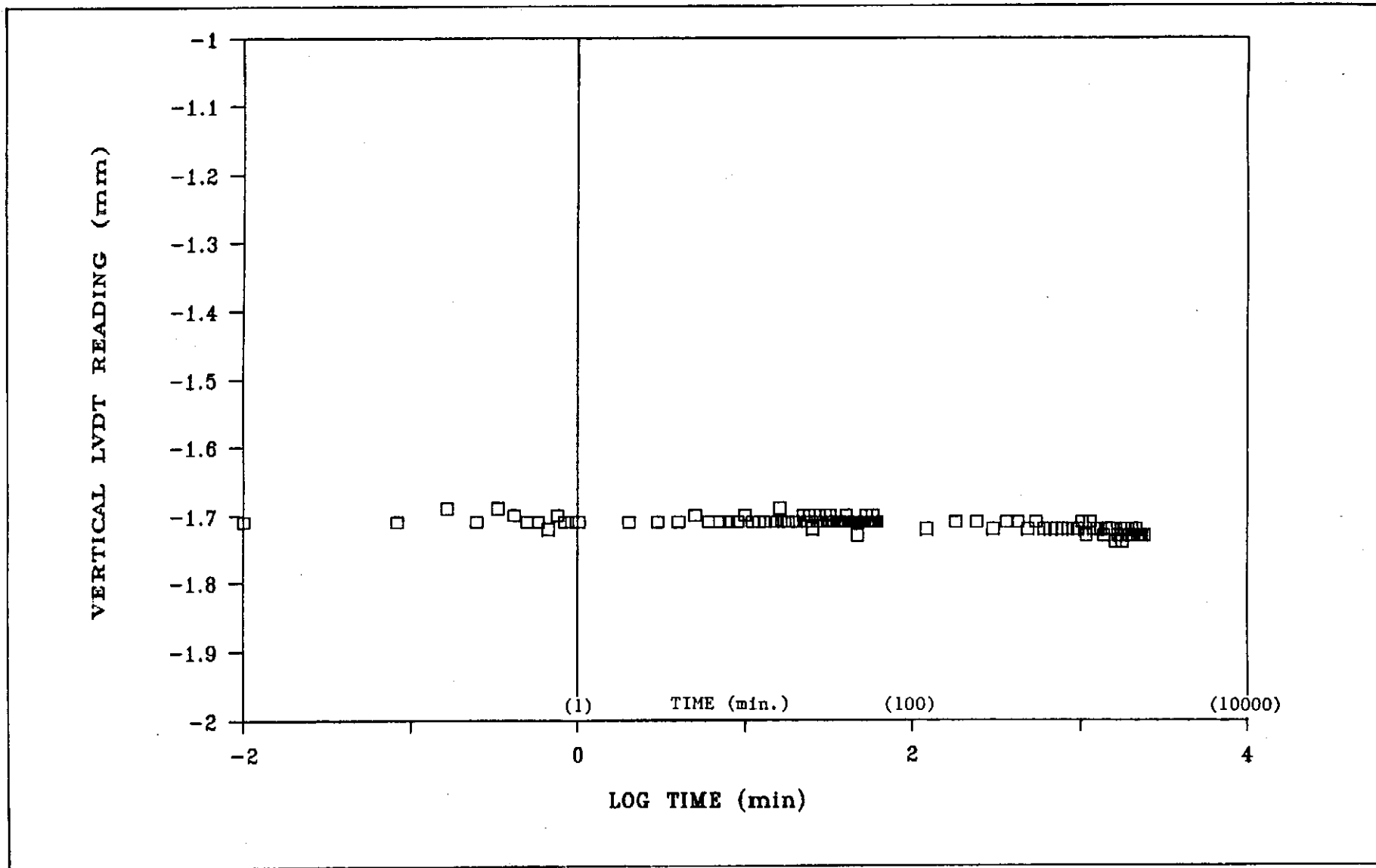


Figure 85c - Vertical Deflection with Time during Pressures Equilibration for Specimen No. US-1, Stage 3

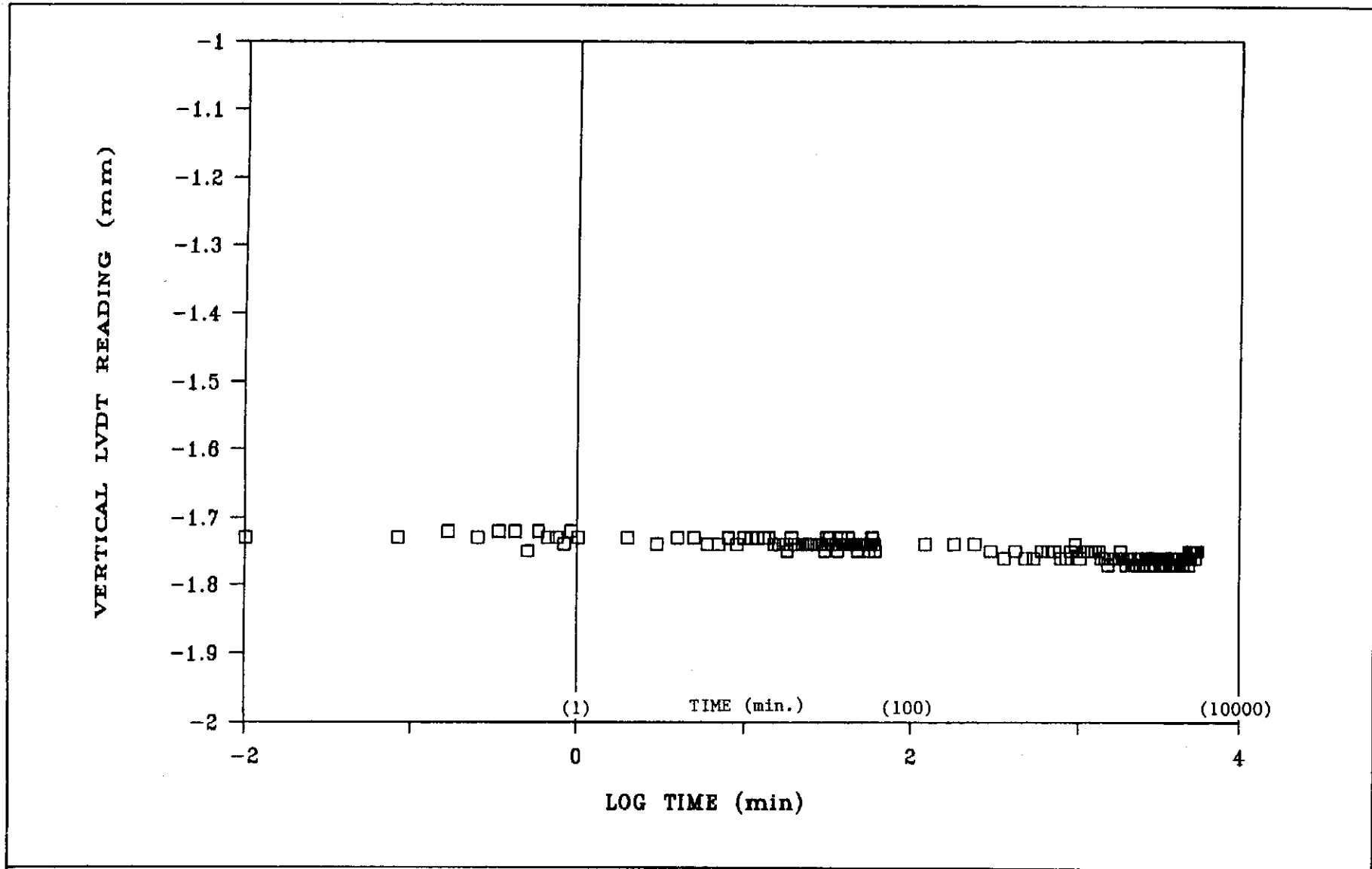


Figure 85d - Vertical Deflection with Time during Pressures Equilibration for Specimen No. US-1, Stage 4

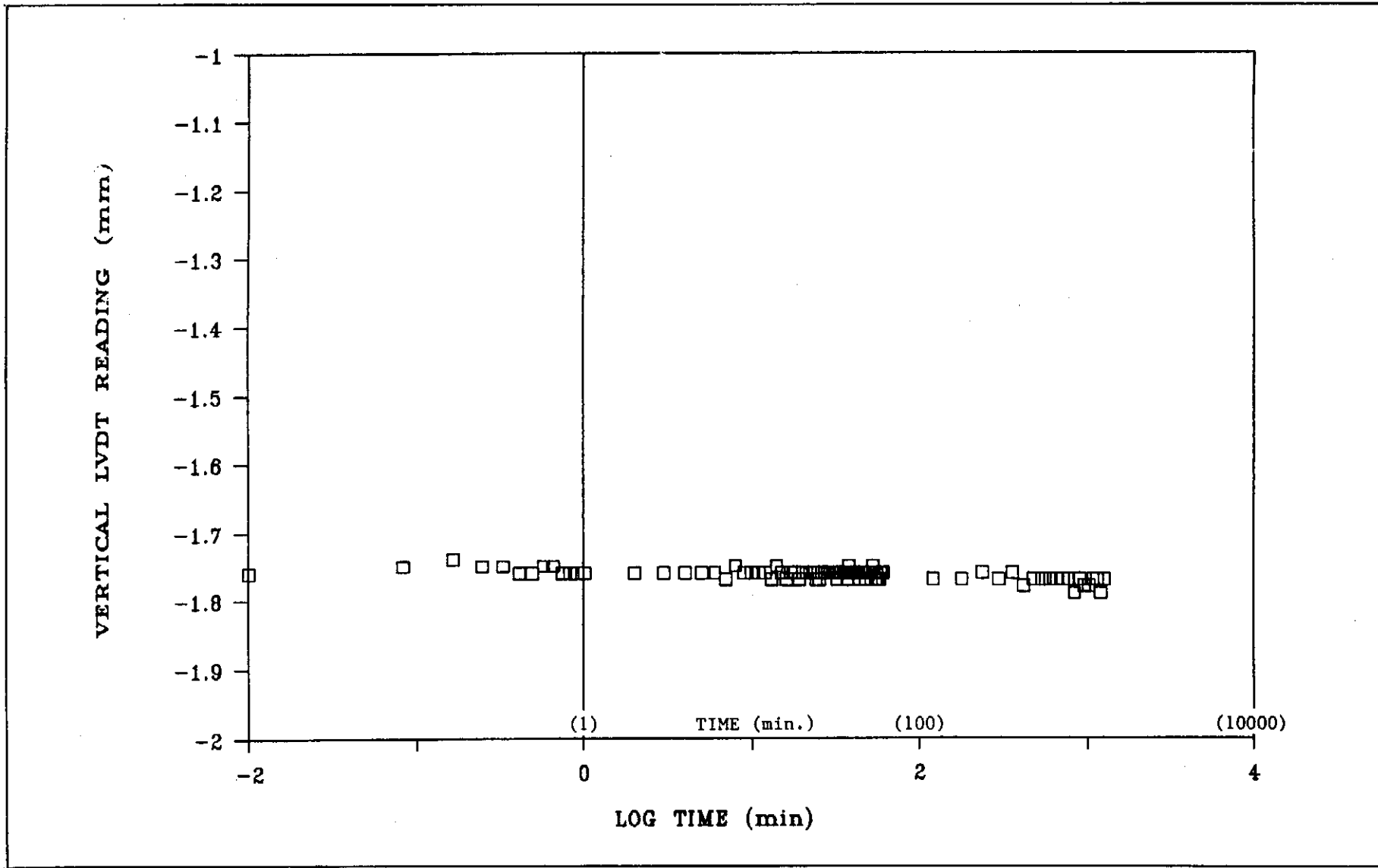


Figure 85e - Vertical Deflection with Time during Pressures Equilibration for Specimen No. US-1, Stage 5

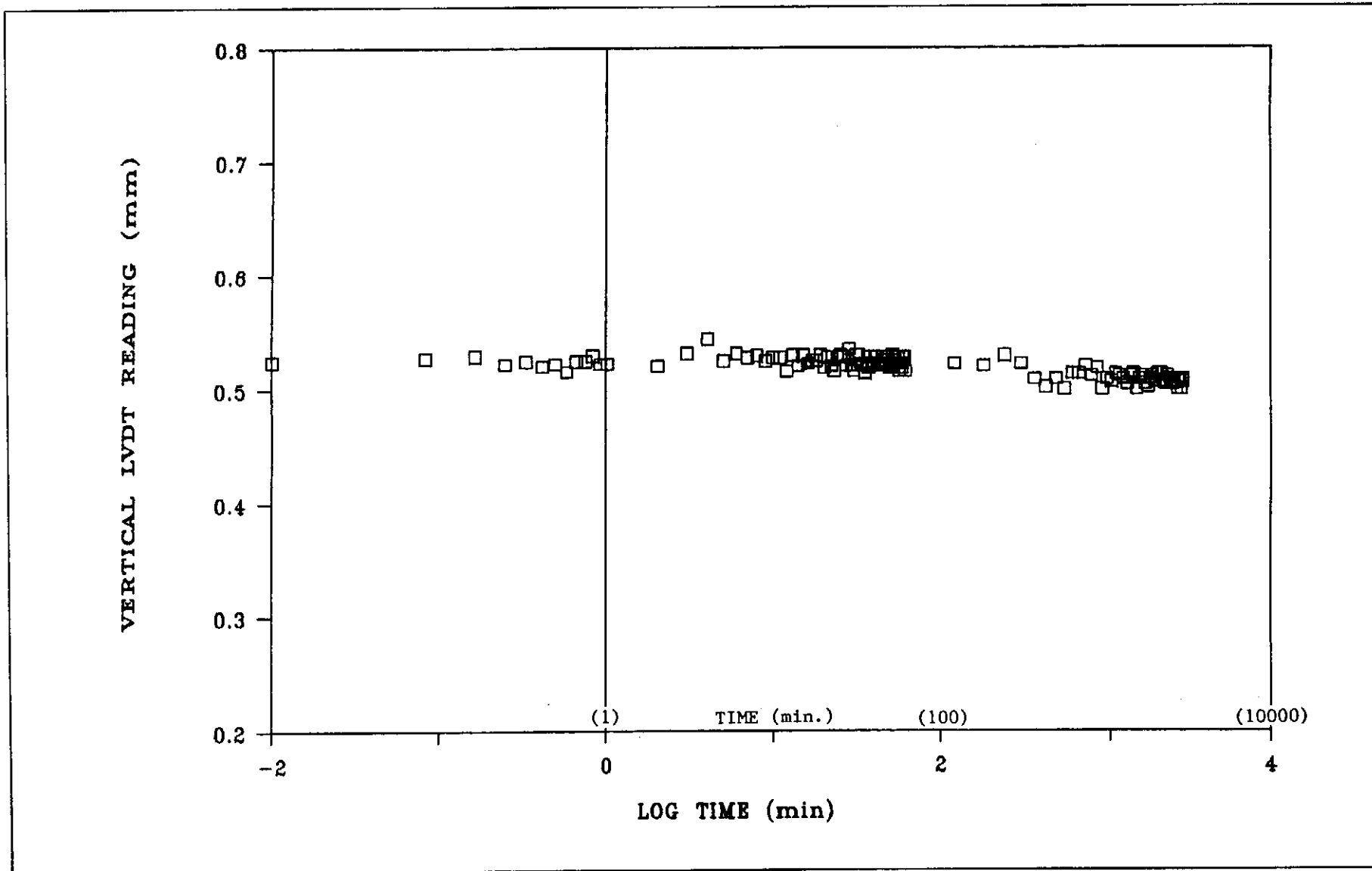


Figure 86a - Vertical Deflection with Time during Pressures Equilibration for Specimen No. US-3, Stage 1

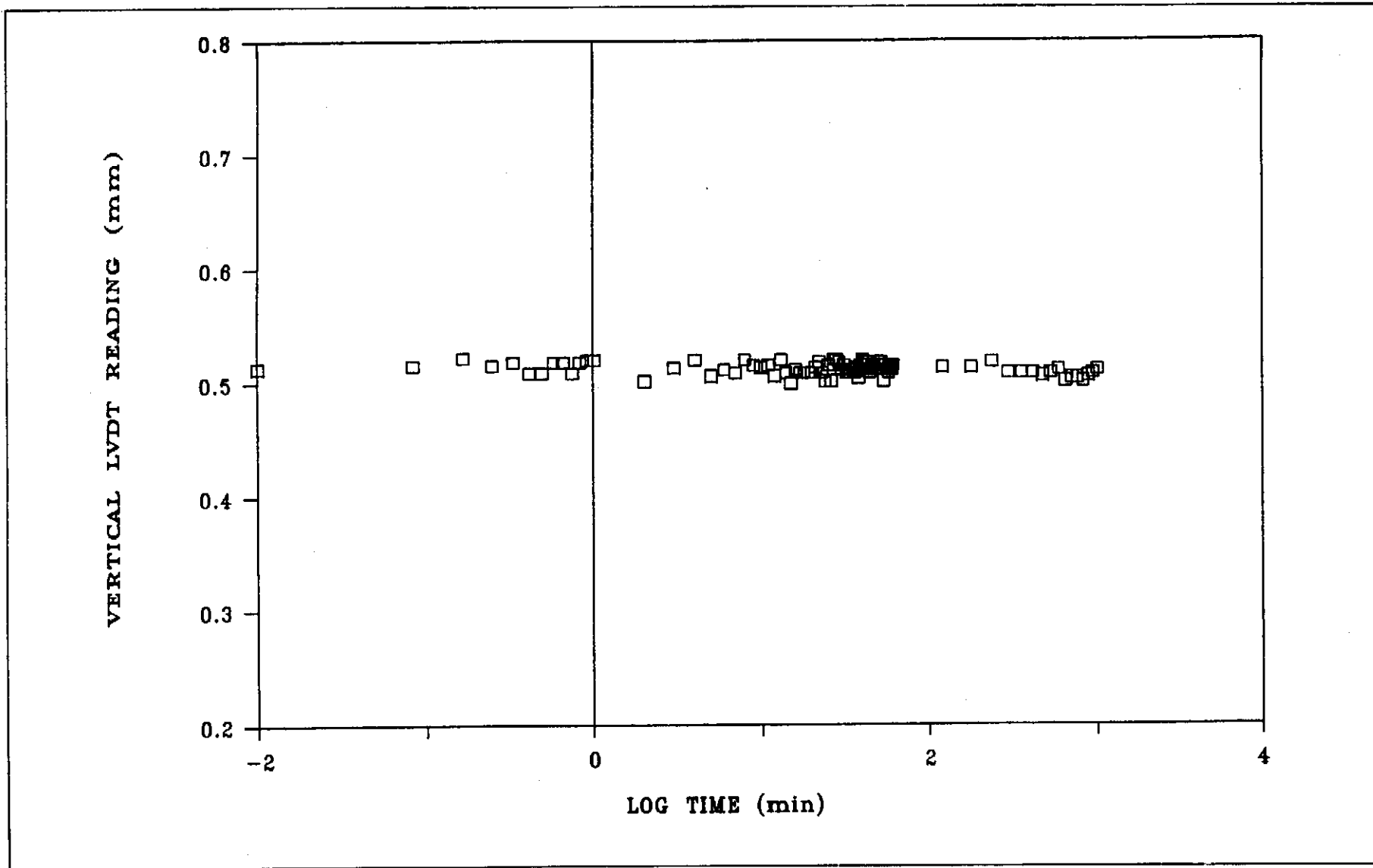


Figure 86b - Vertical Deflection with Time during Pressures Equilibration for Specimen No. US-3, Stage 2

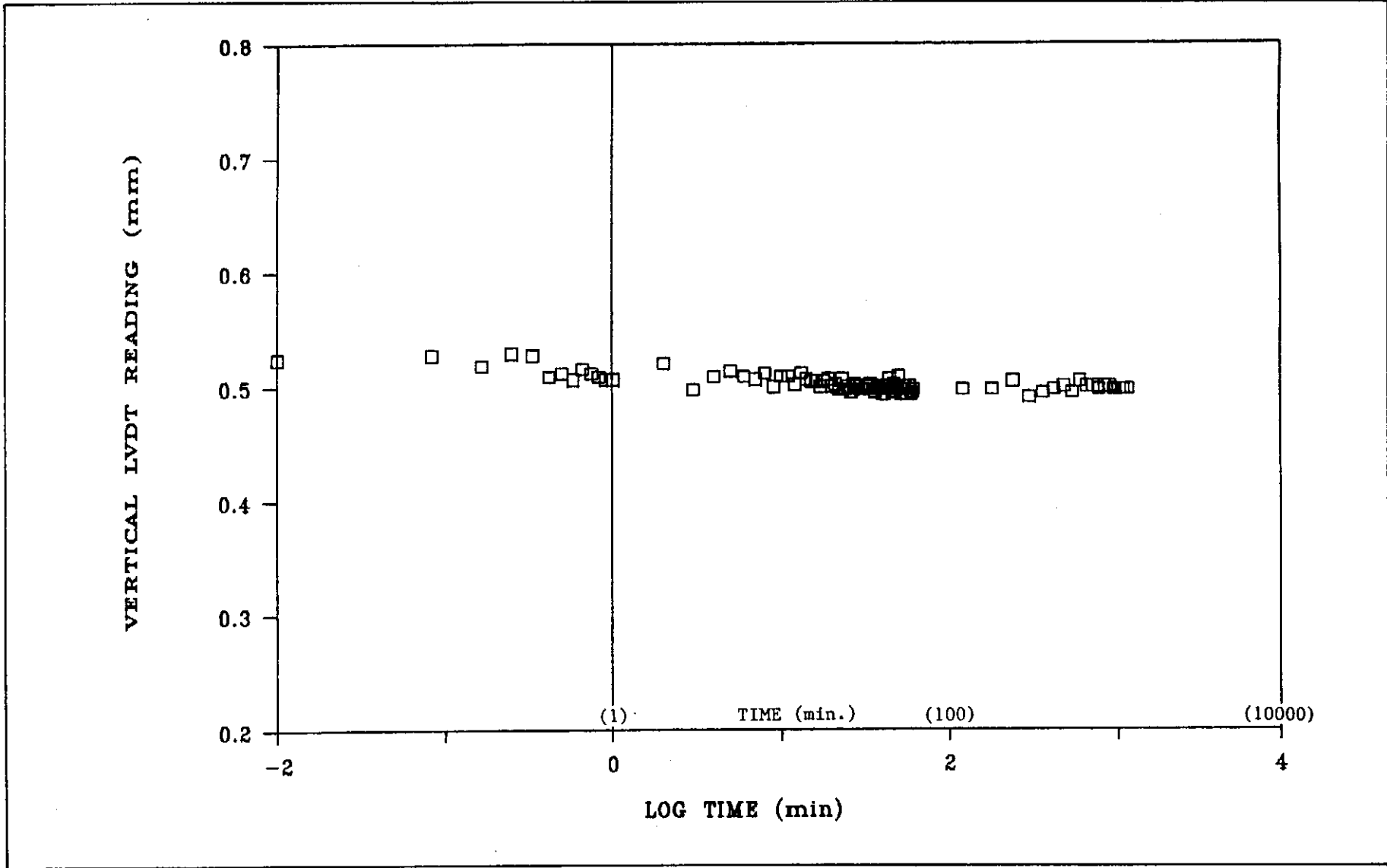


Figure 86c - Vertical Deflection with Time during Pressures Equilibration for Specimen No. US-3, Stage 3

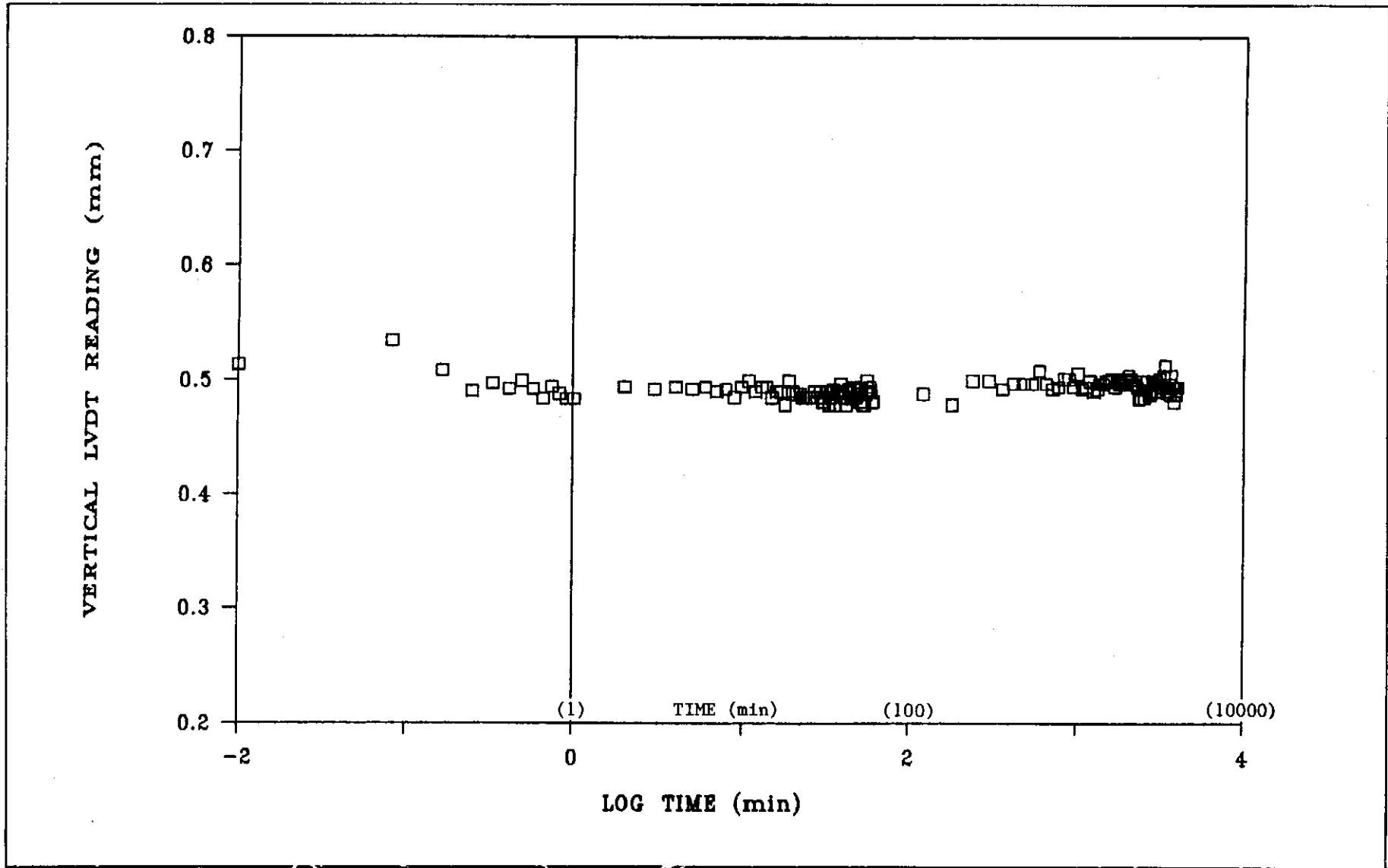


Figure 86d - Vertical Deflection with Time during Pressures Equilibration for Specimen No. US-3, Stage 4

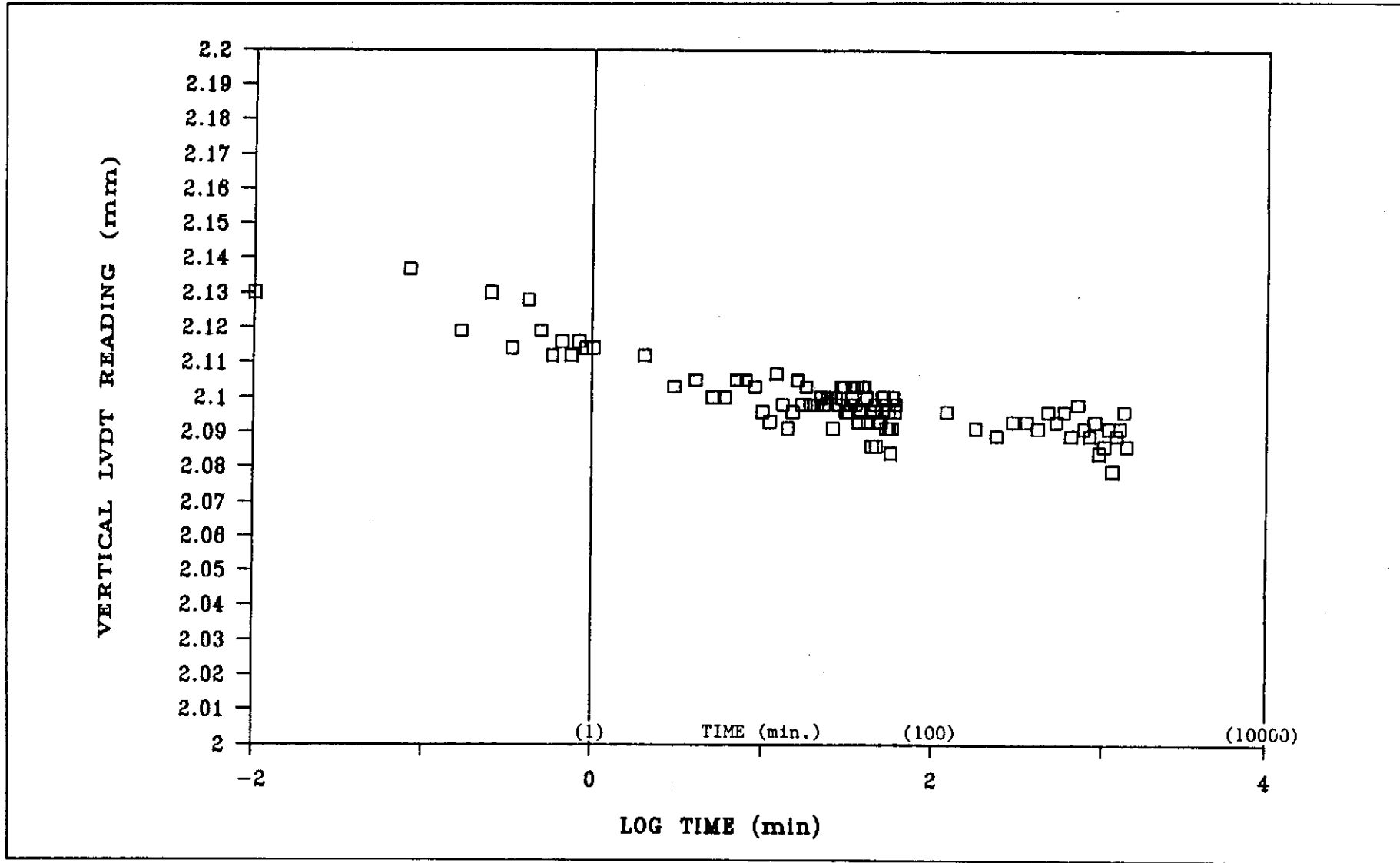


Figure 87a - Vertical Deflection with Time during Pressures Equilibration for Specimen No. US-4, Stage 1

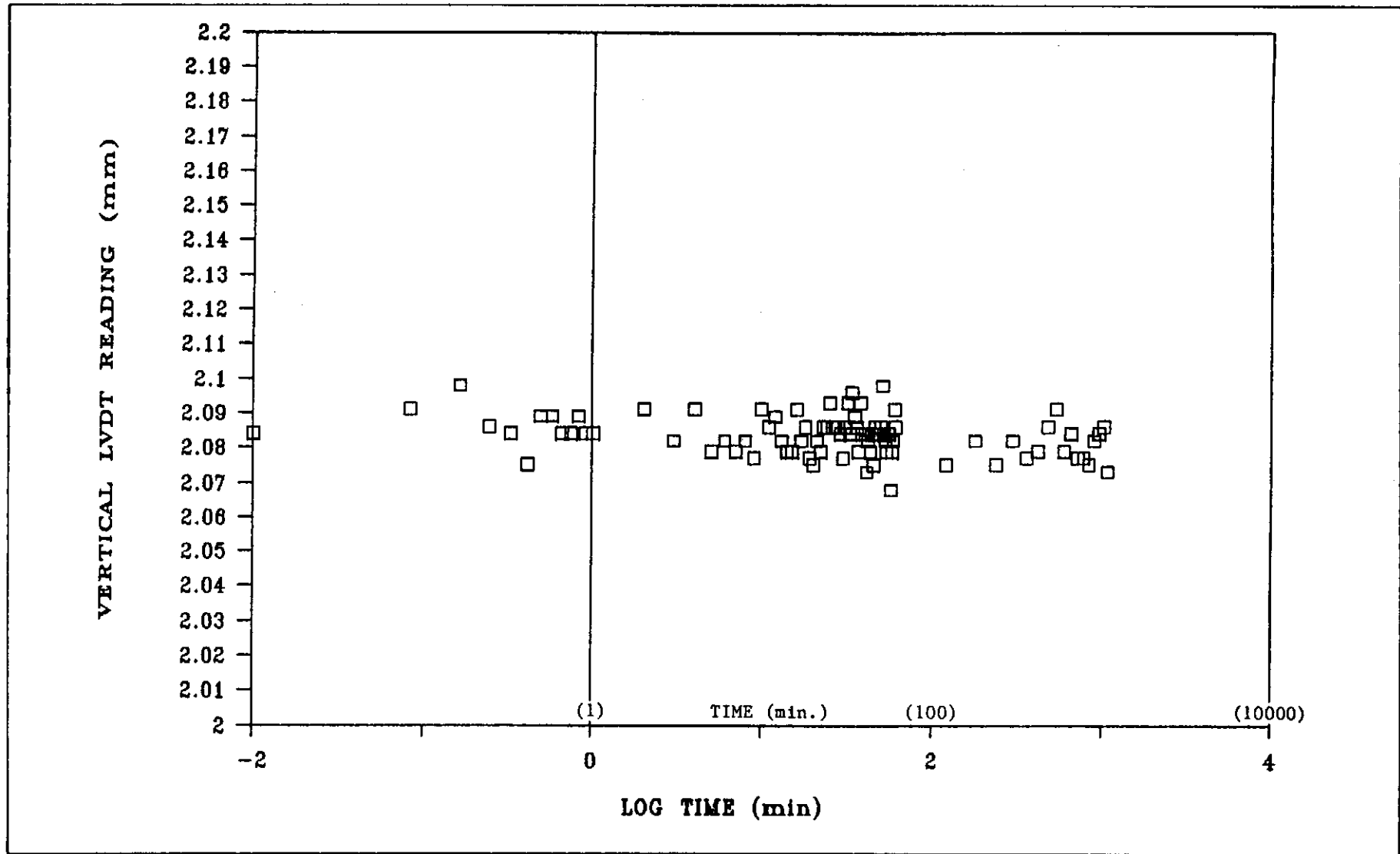


Figure 87b - Vertical Deflection with Time during Pressures Equilibration for Specimen No. US-4, Stage 2

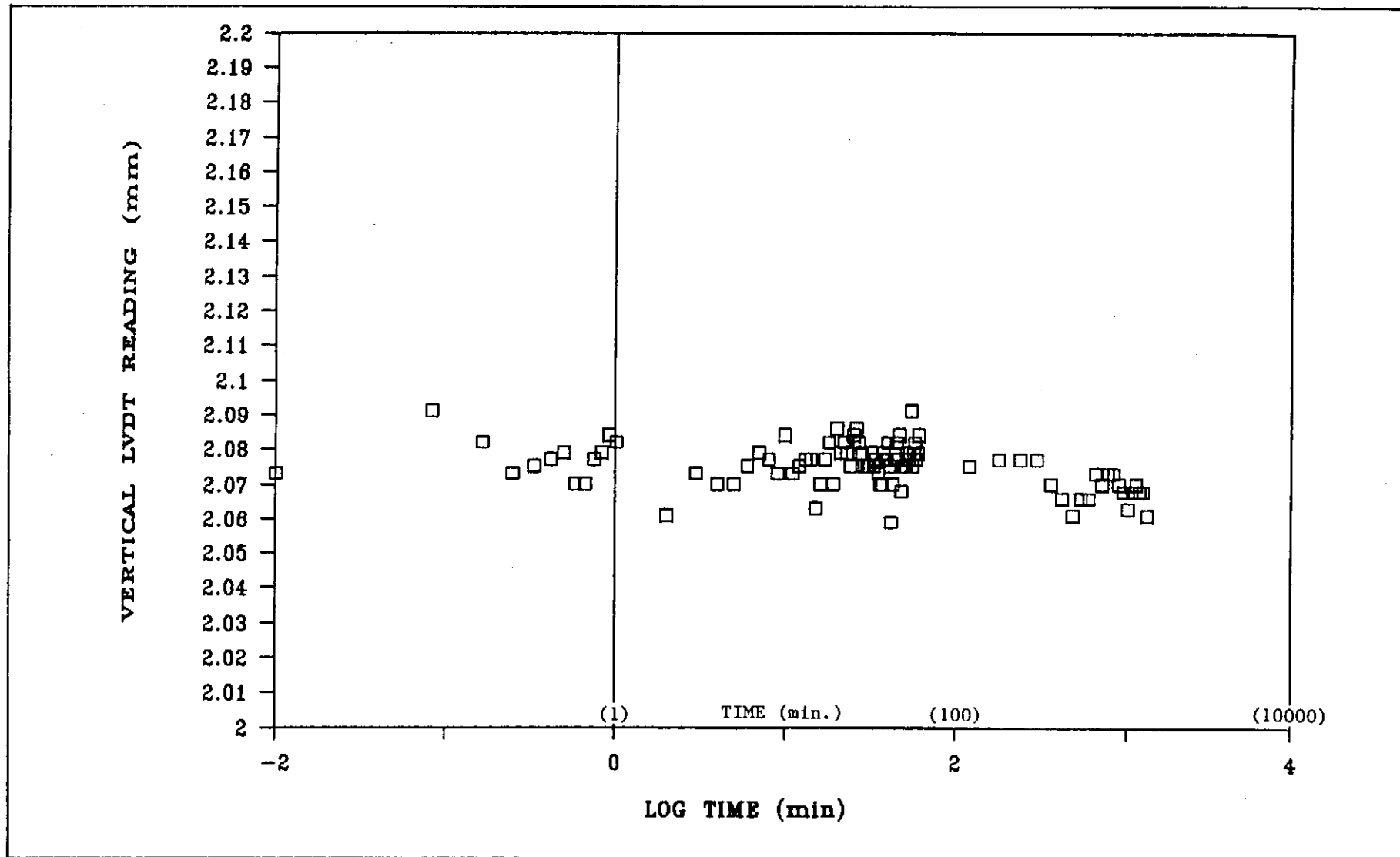


Figure 87c - Vertical Deflection with Time during Pressures Equilibration for Specimen No. US-4, Stage 3

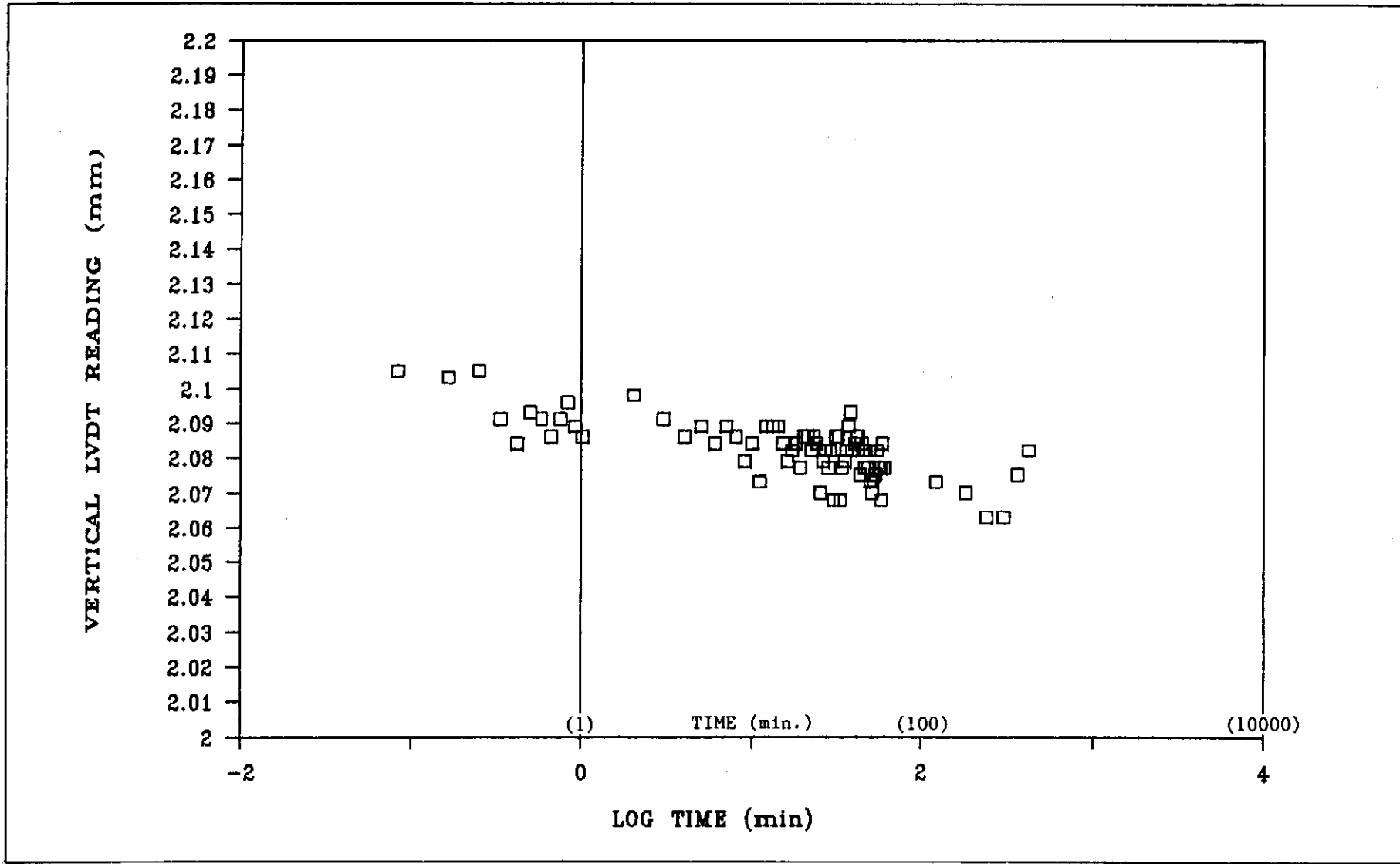


Figure 87e - Vertical Deflection with Time during Pressures Equilibration for Specimen No. US-4, Stage 5

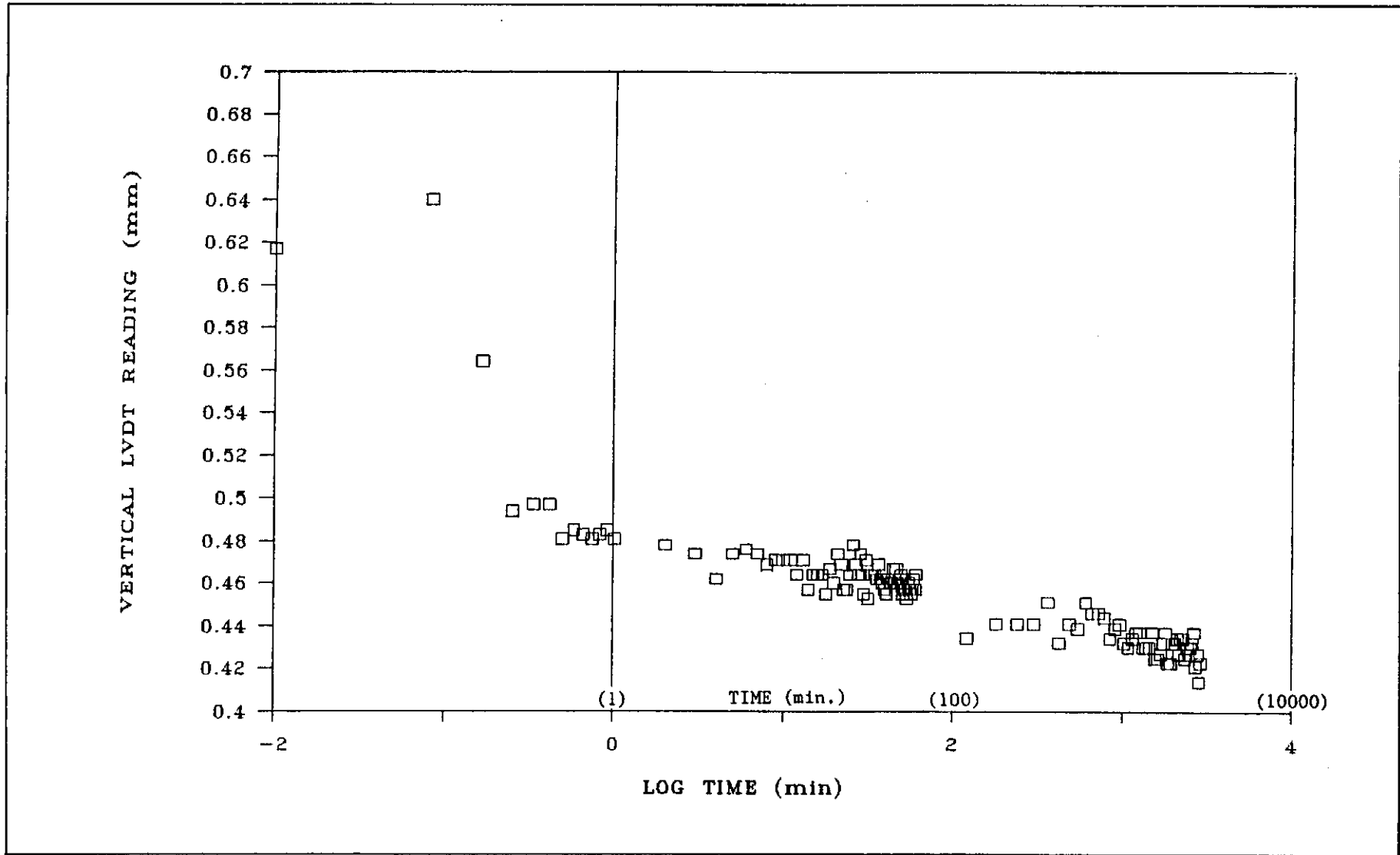


Figure 88a - Vertical Deflection with Time during Pressures Equilibration for Specimen No. US-5, Stage 1

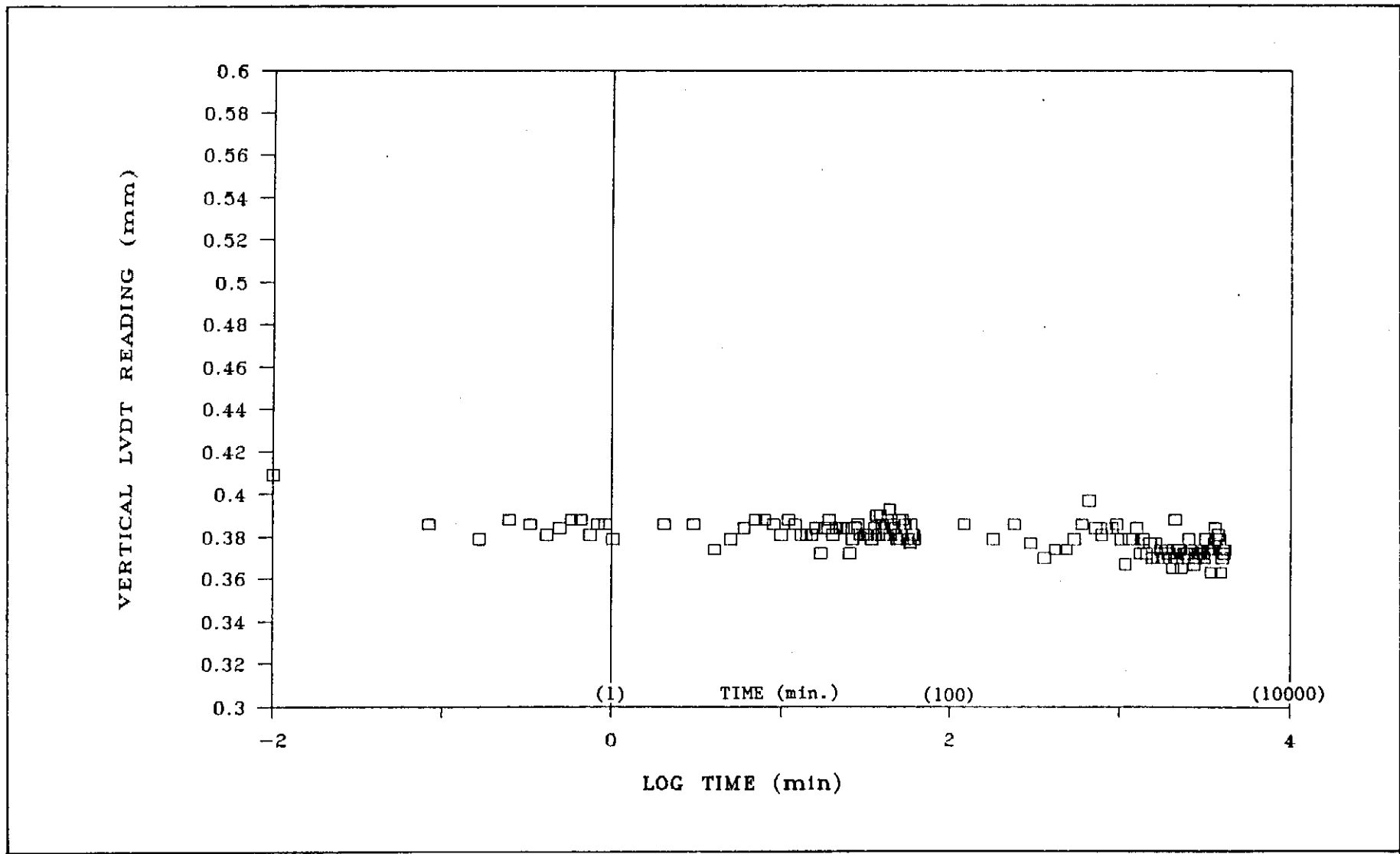


Figure 88b - Vertical Deflection with Time during Pressures Equilibration for Specimen No. US-5, Stage 2

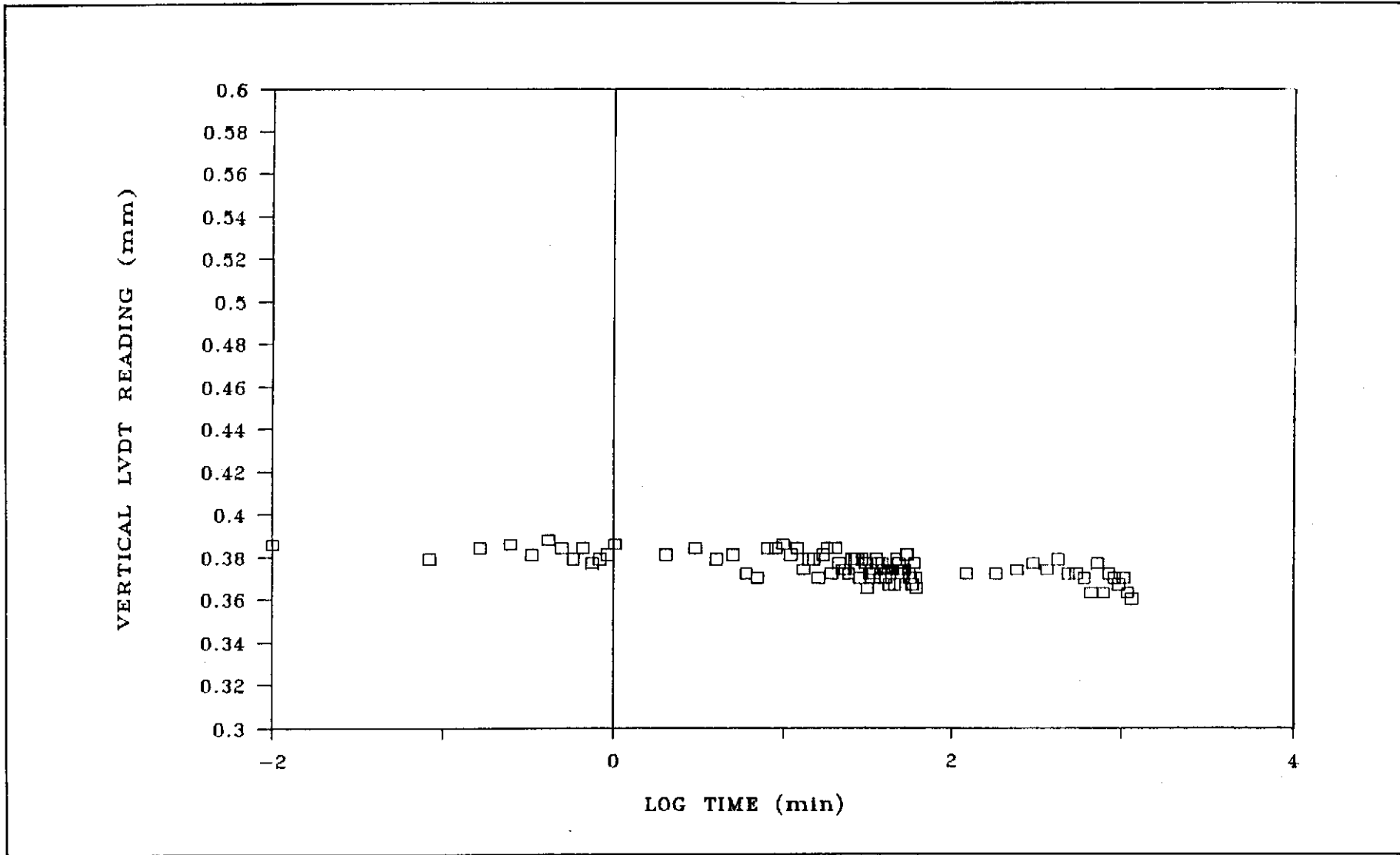


Figure 88c - Vertical Deflection with Time during Pressures Equilibration for Specimen No. US-5, Stage 3

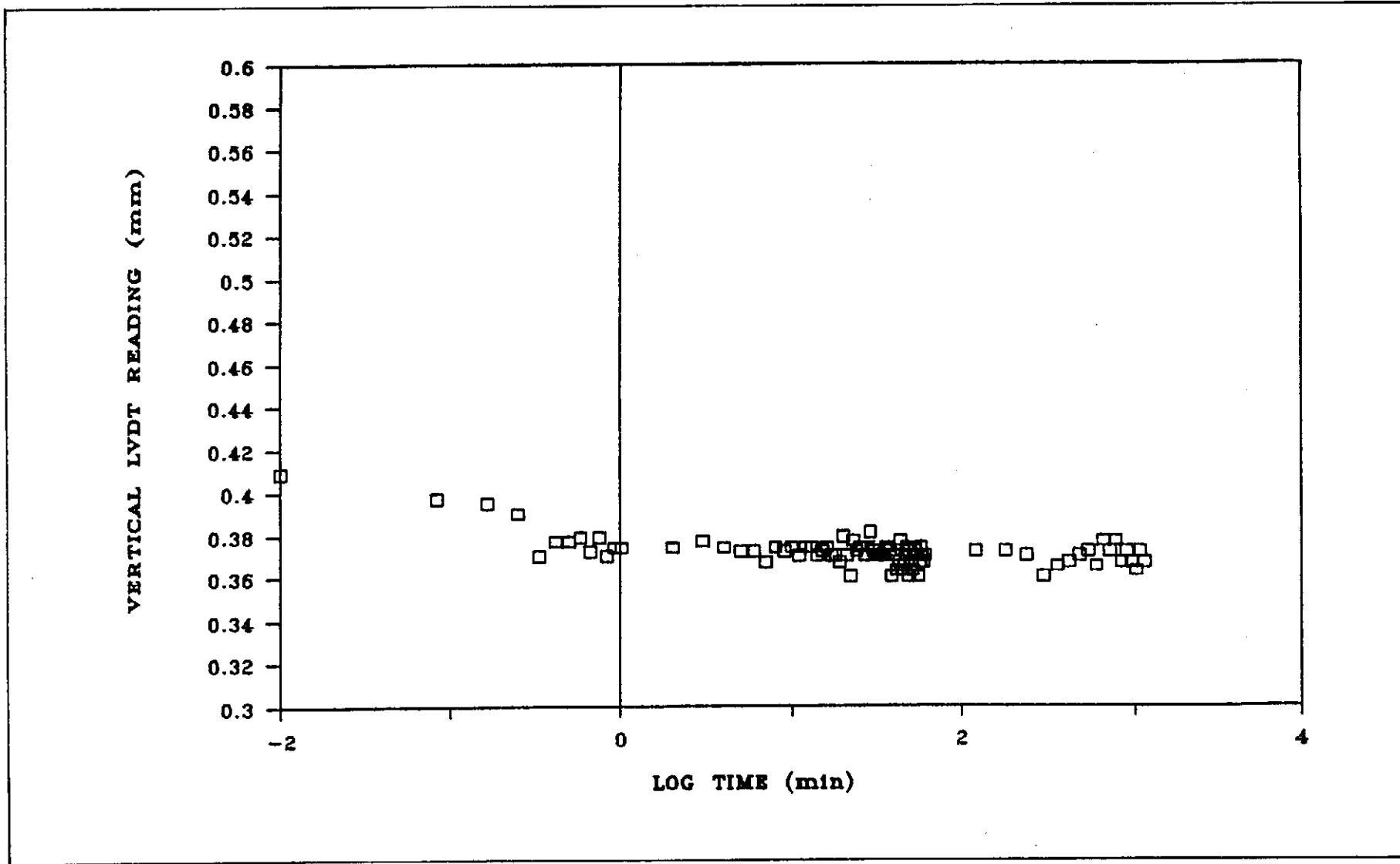


Figure 88d - Vertical Deflection with Time during Pressures Equilibration for Specimen No. US-5, Stage 4

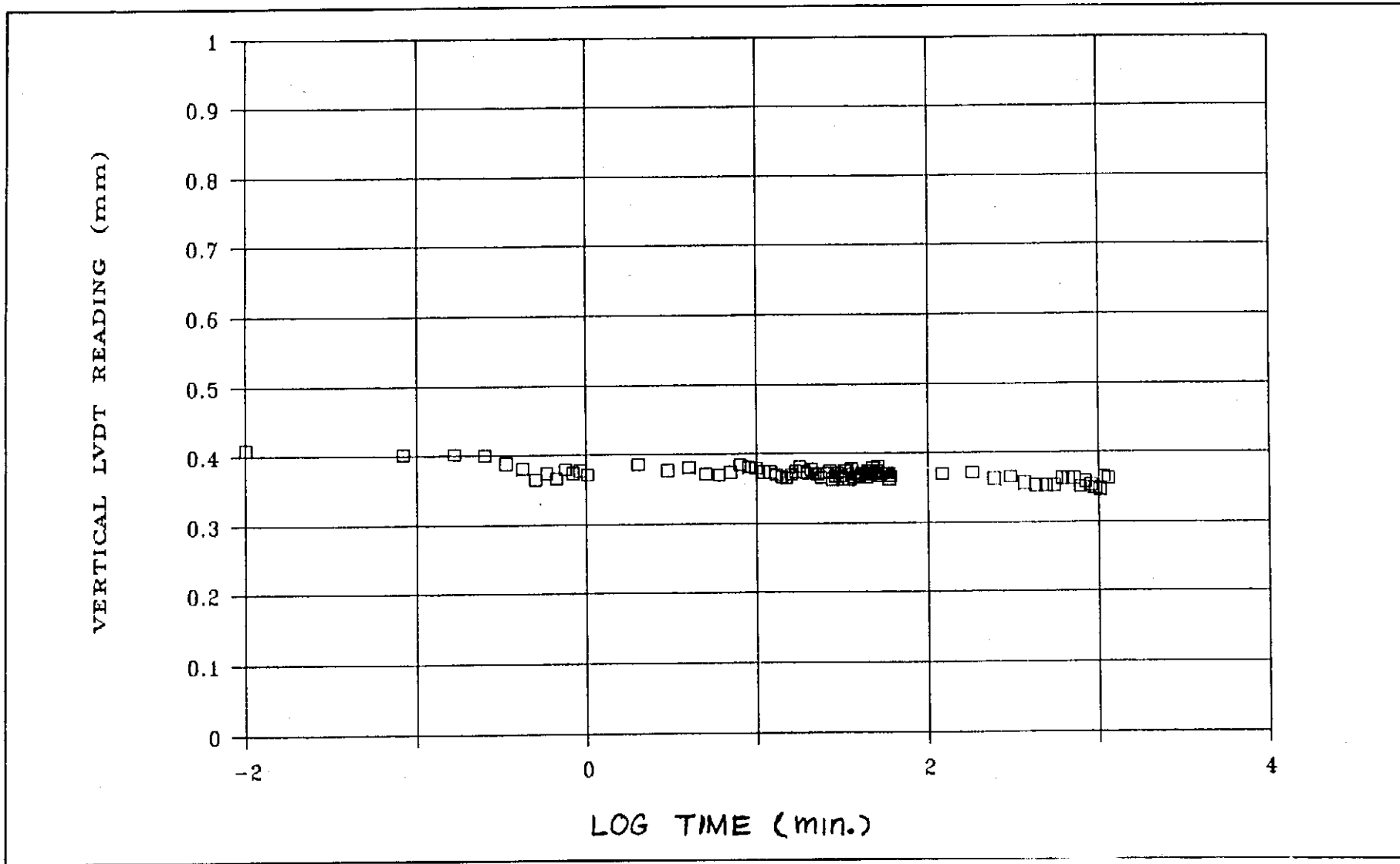


Figure 88e - Vertical Deflection with Time during Pressures Equilibration for Specimen No. US-5, Stage 5

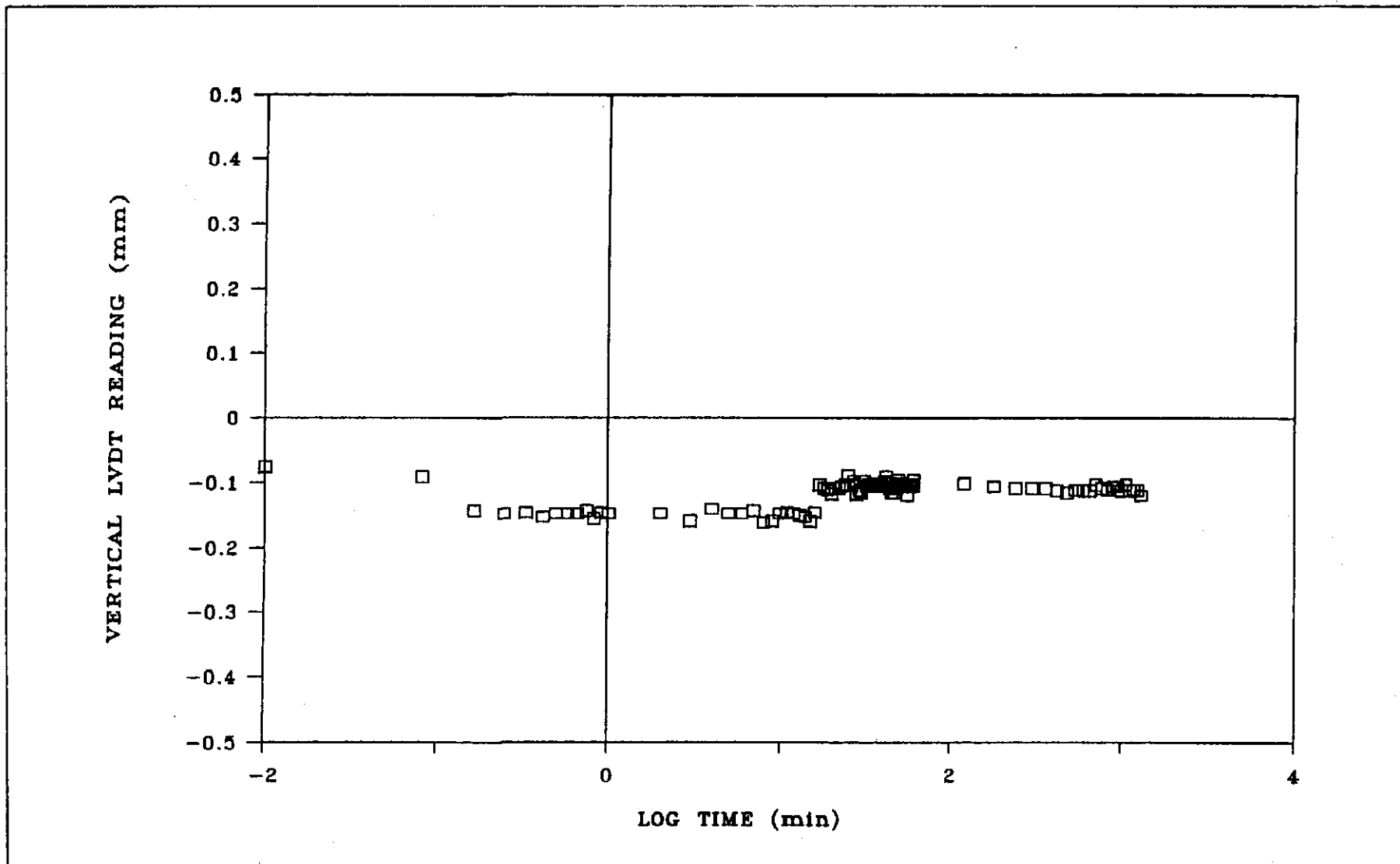


Figure 89a - Vertical Deflection with Time during Pressures Equilibration for Specimen No. US-6, Stage 1

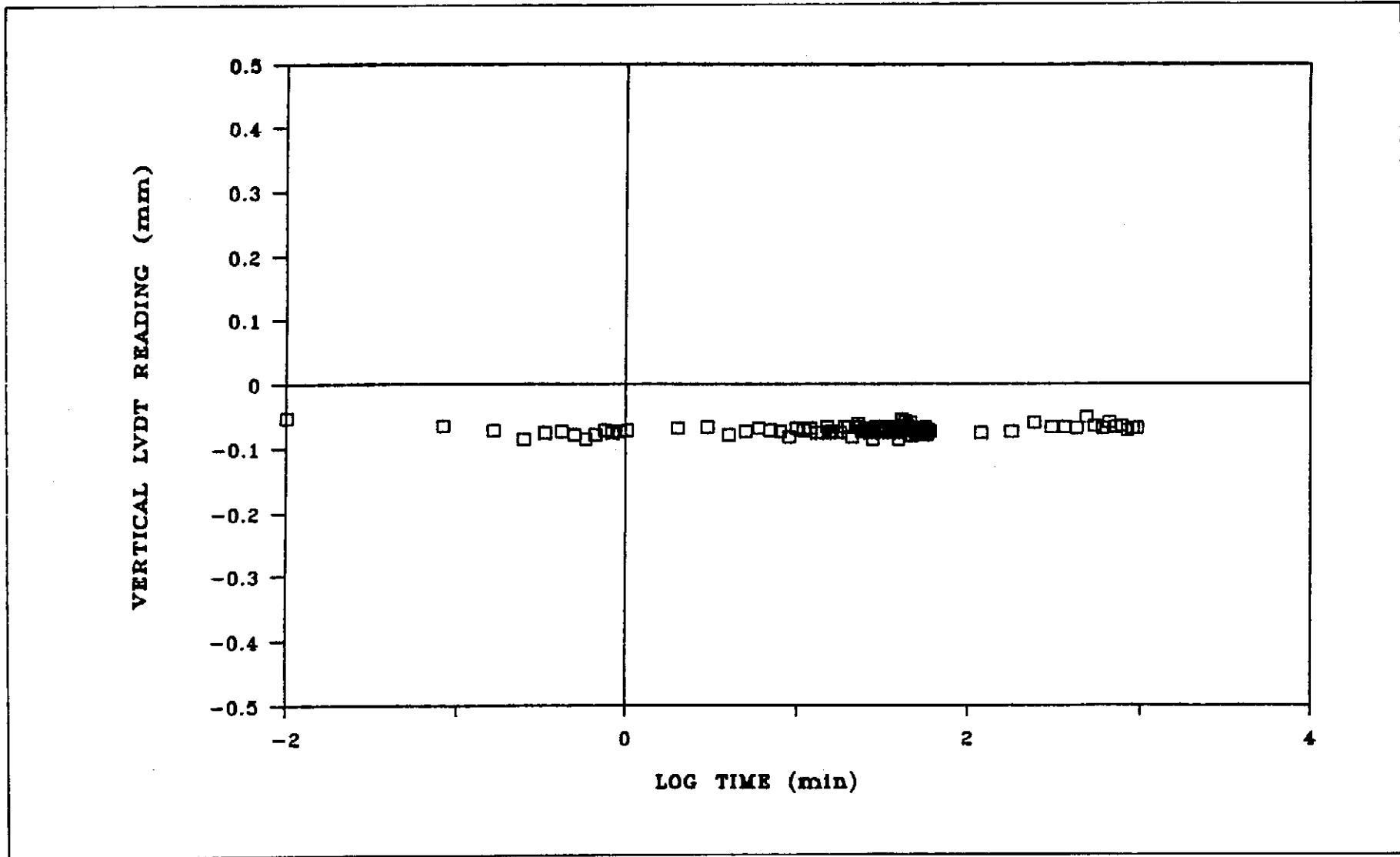


Figure 89b - Vertical Deflection with Time during Pressures Equilibration for Specimen No. US-6, Stage 2

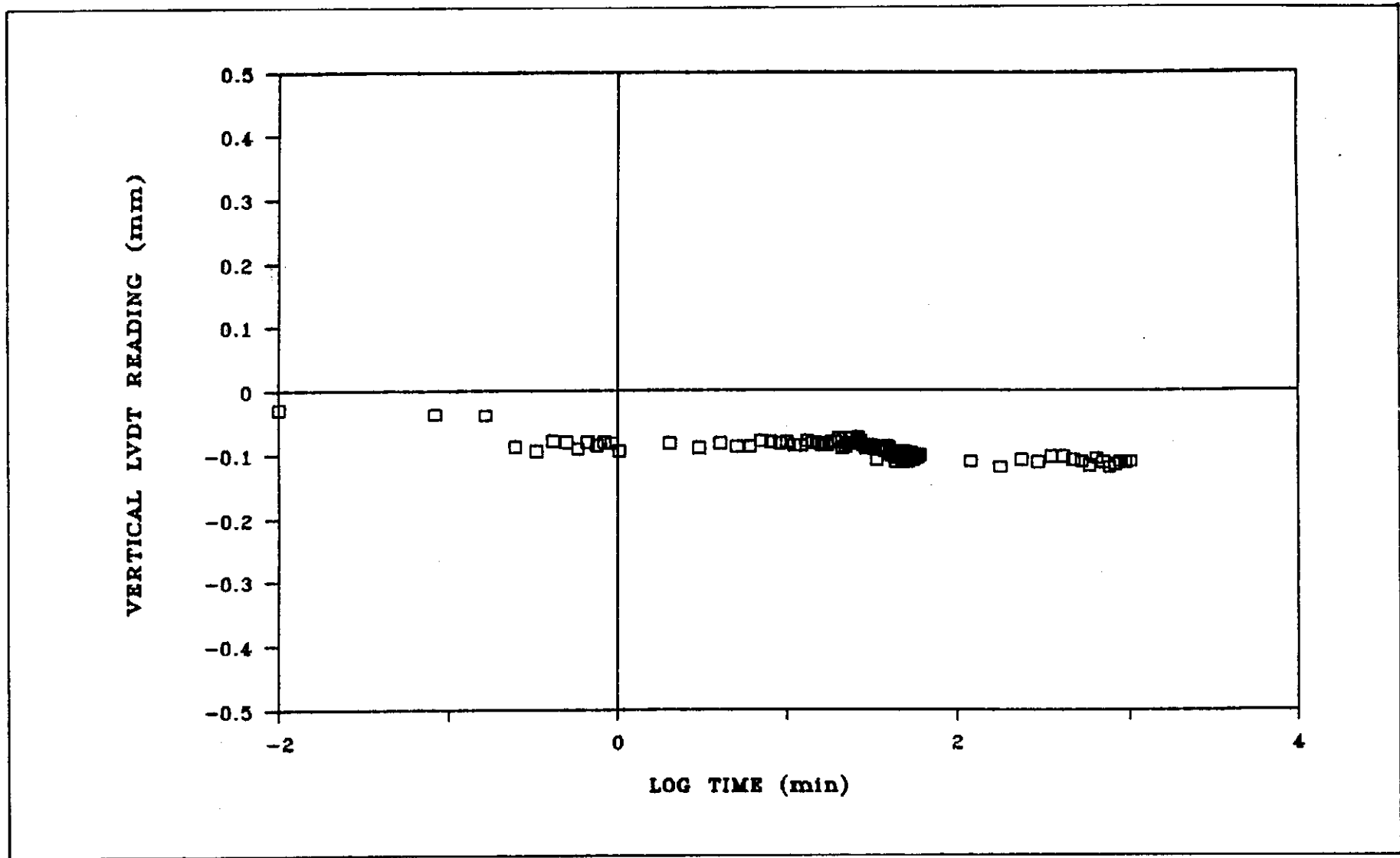


Figure 89c - Vertical Deflection with Time during Pressures Equilibration for Specimen No. US-6, Stage 3

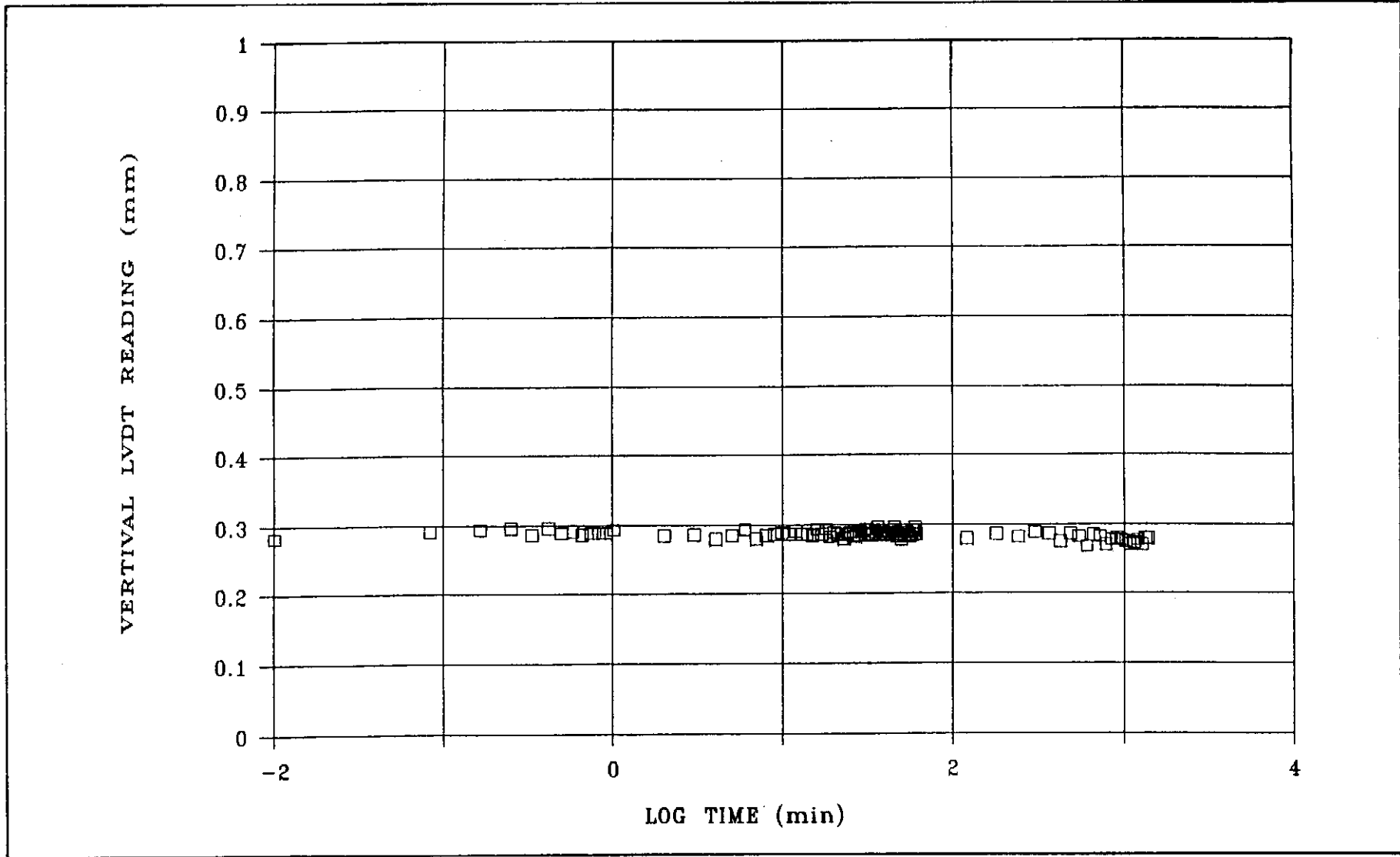


Figure 90a - Vertical Deflection with Time during Pressures Equilibration for Specimen No. US-9, Stage 2

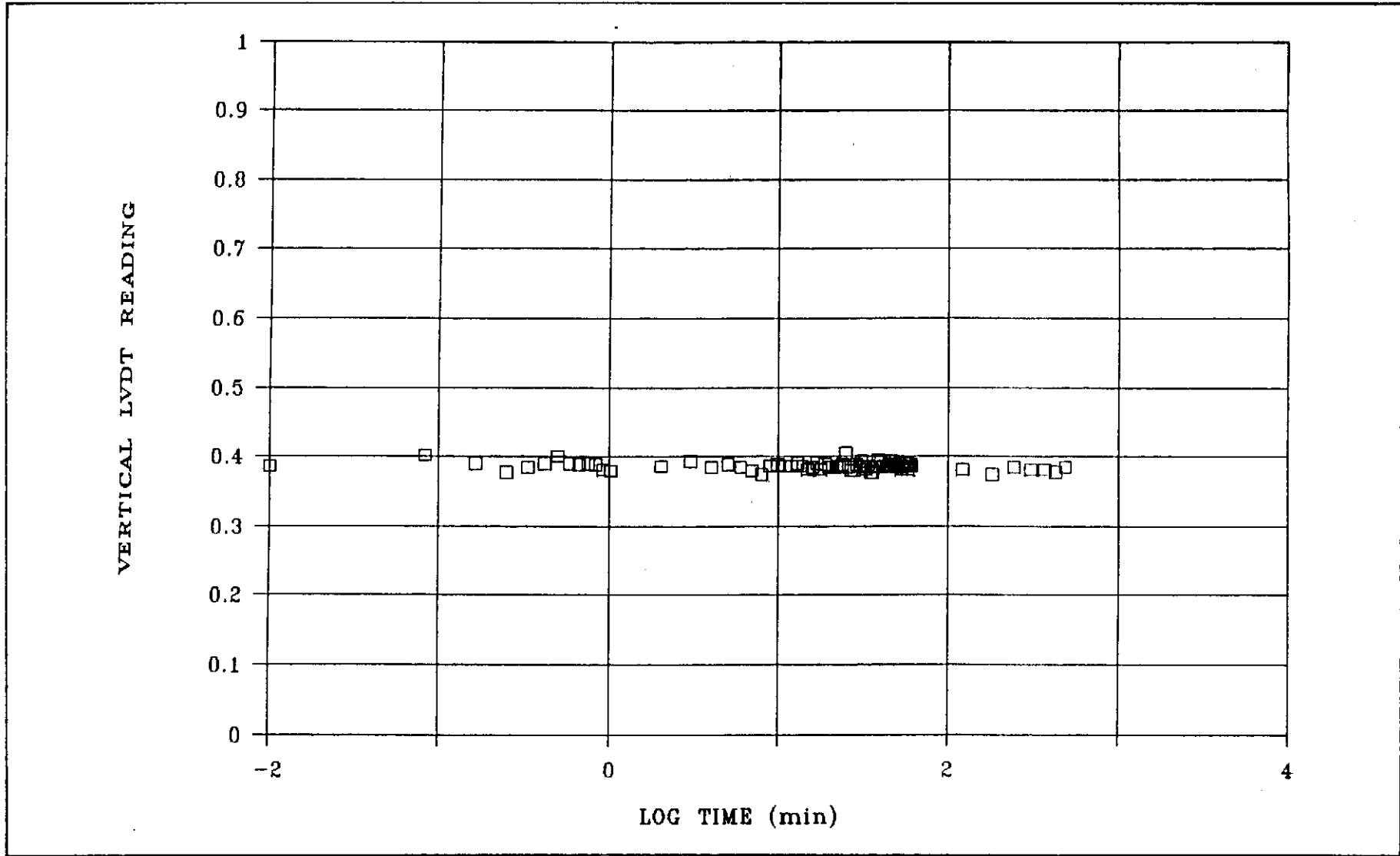


Figure 90b - Vertical Deflection with Time during Pressures Equilibration for Specimen No. US-9, Stage 3

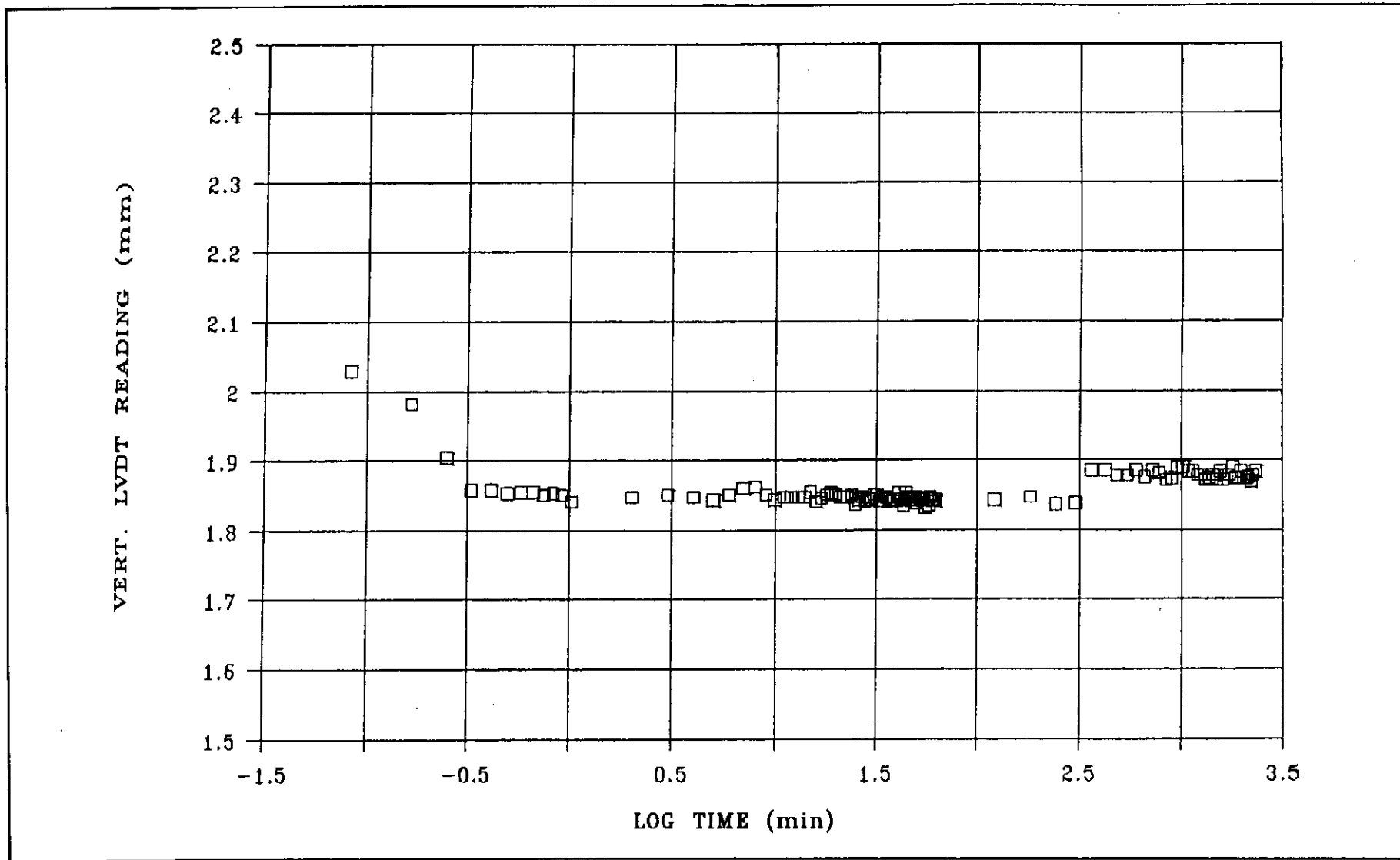


Figure 91a - Vertical Deflection with Time during Pressures Equilibration for Specimen No. US-10, Stage 1

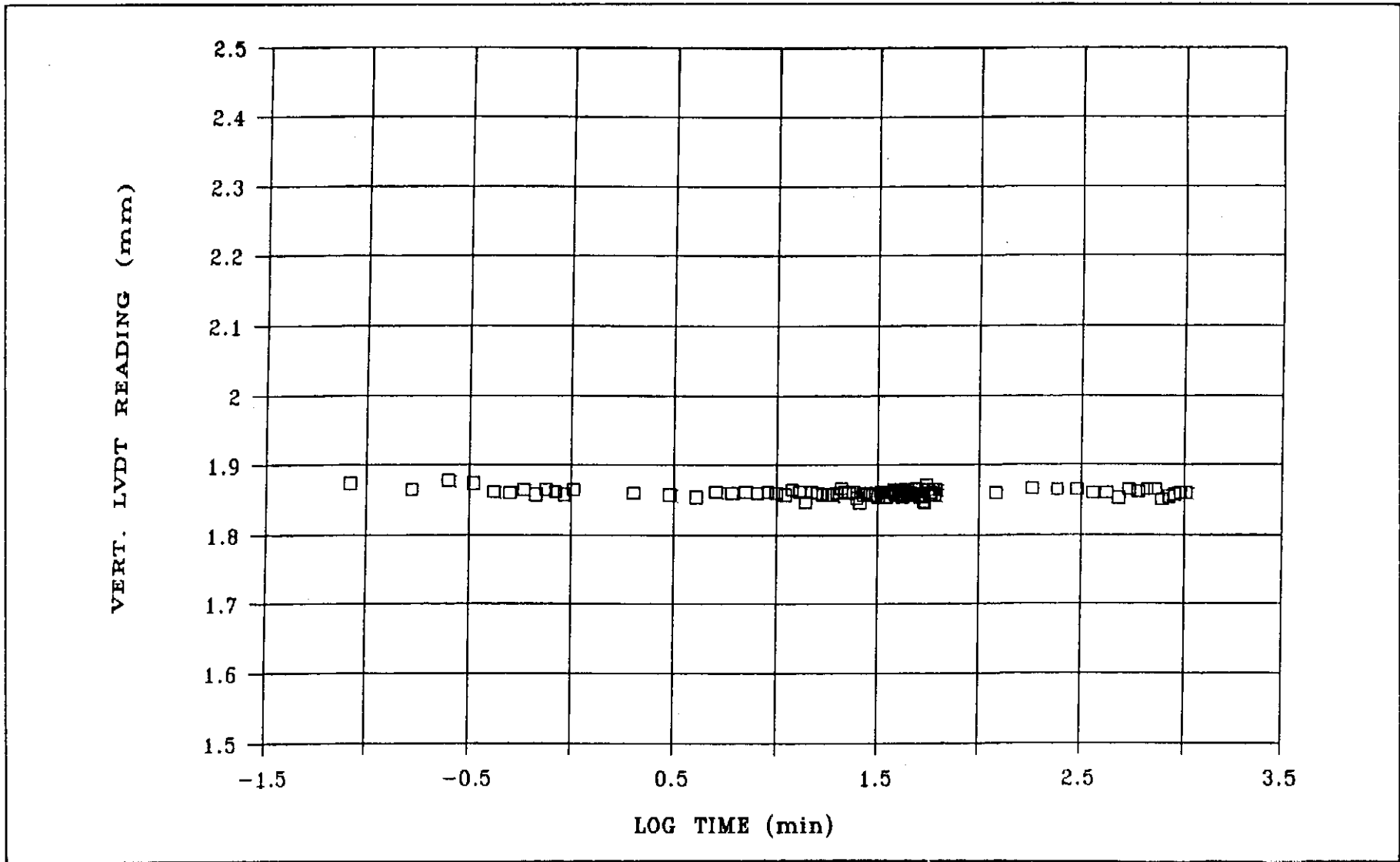


Figure 91b - Vertical Deflection with Time during Pressures Equilibration for Specimen No. US-10, Stage 2

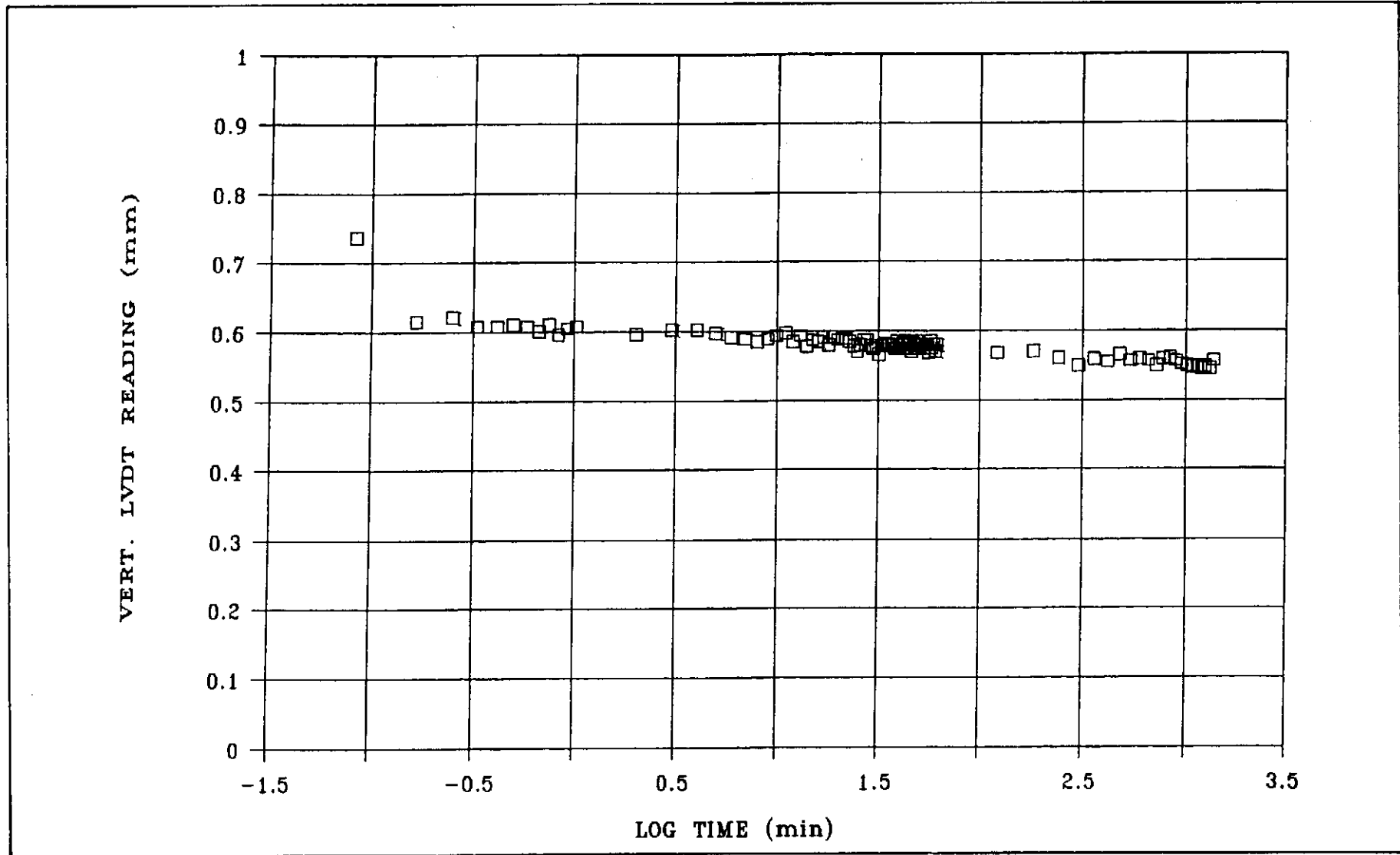


Figure 92a - Vertical Deflection with Time during Pressures Equilibration for Specimen No. US-11, Stage 1

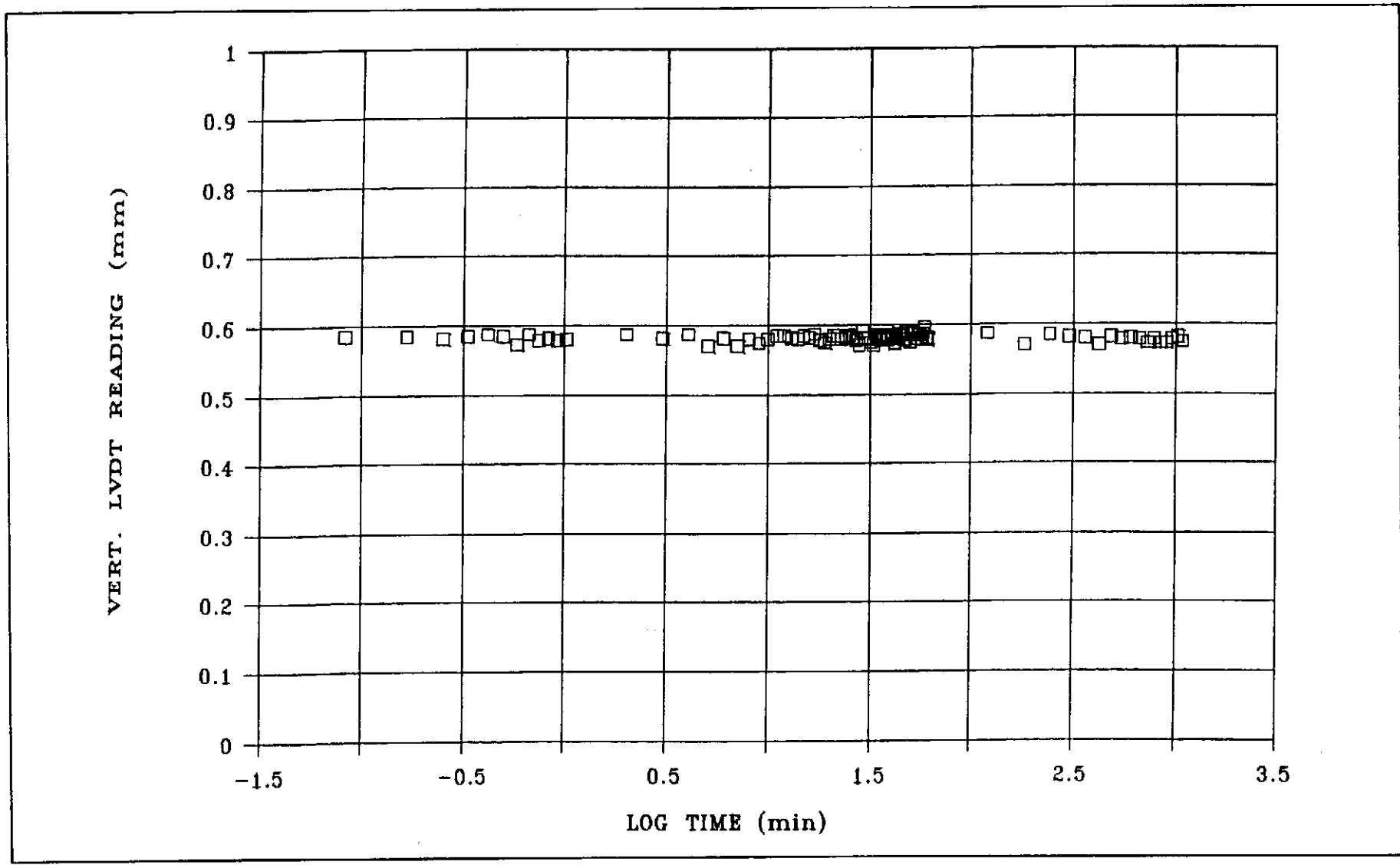


Figure 92b - Vertical Deflection with Time during Pressures Equilibration for Specimen No. US-11, Stage 2

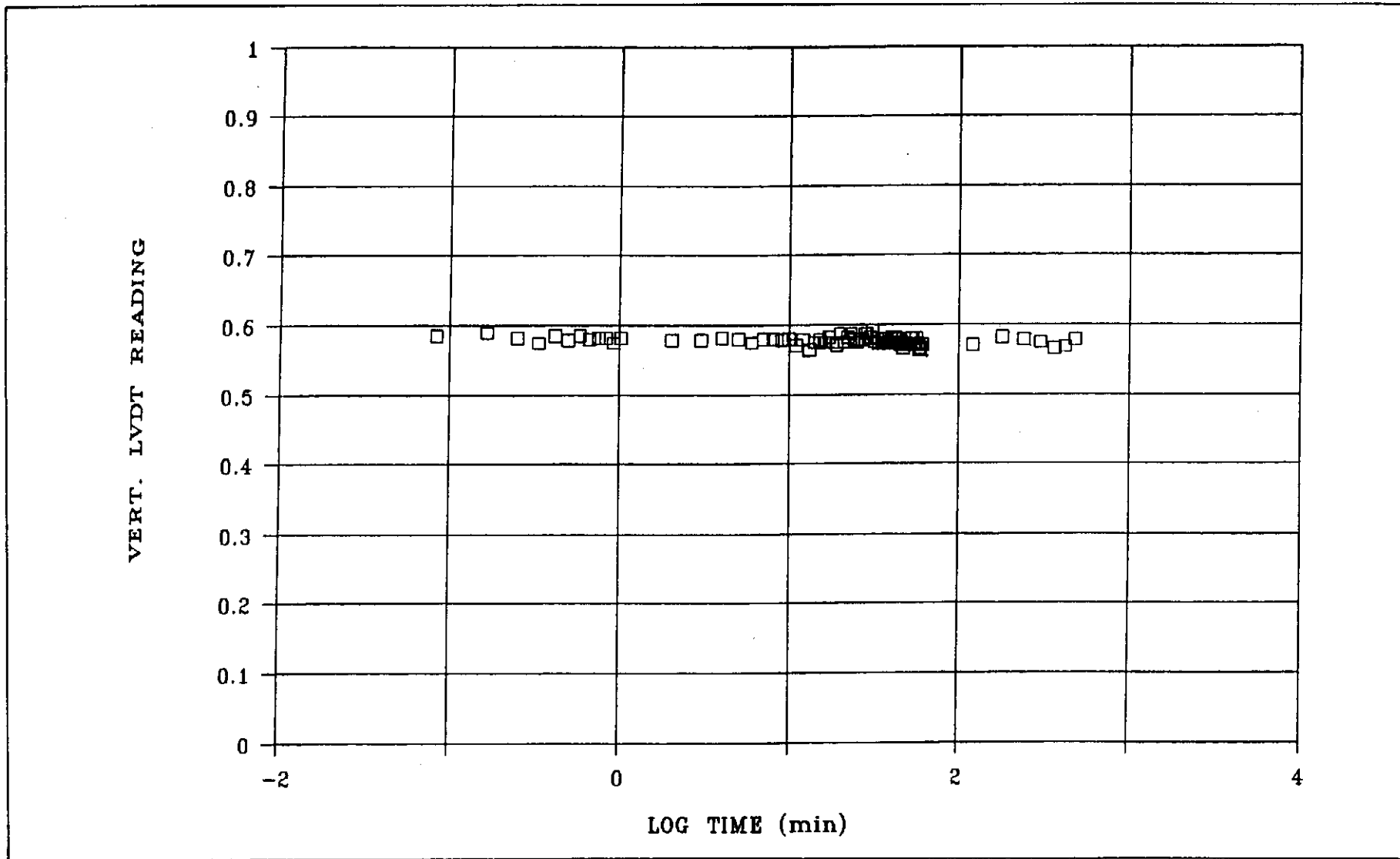


Figure 92c - Vertical Deflection with Time during Pressures Equilibration for Specimen No. US-11, Stage 3

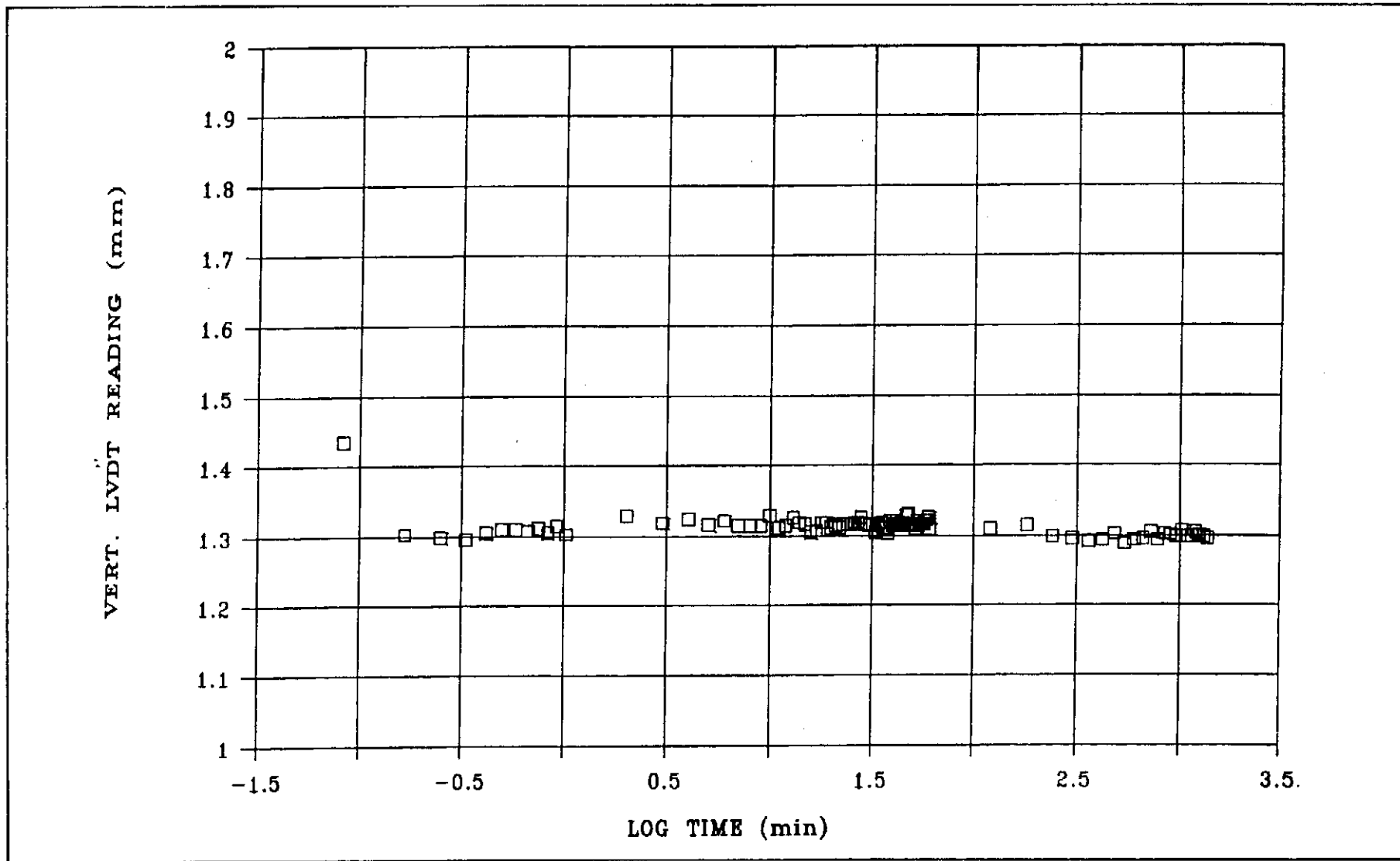


Figure 93 - Vertical Deflection with Time during Pressures Equilibration for Specimen No. US-12, Stage 1

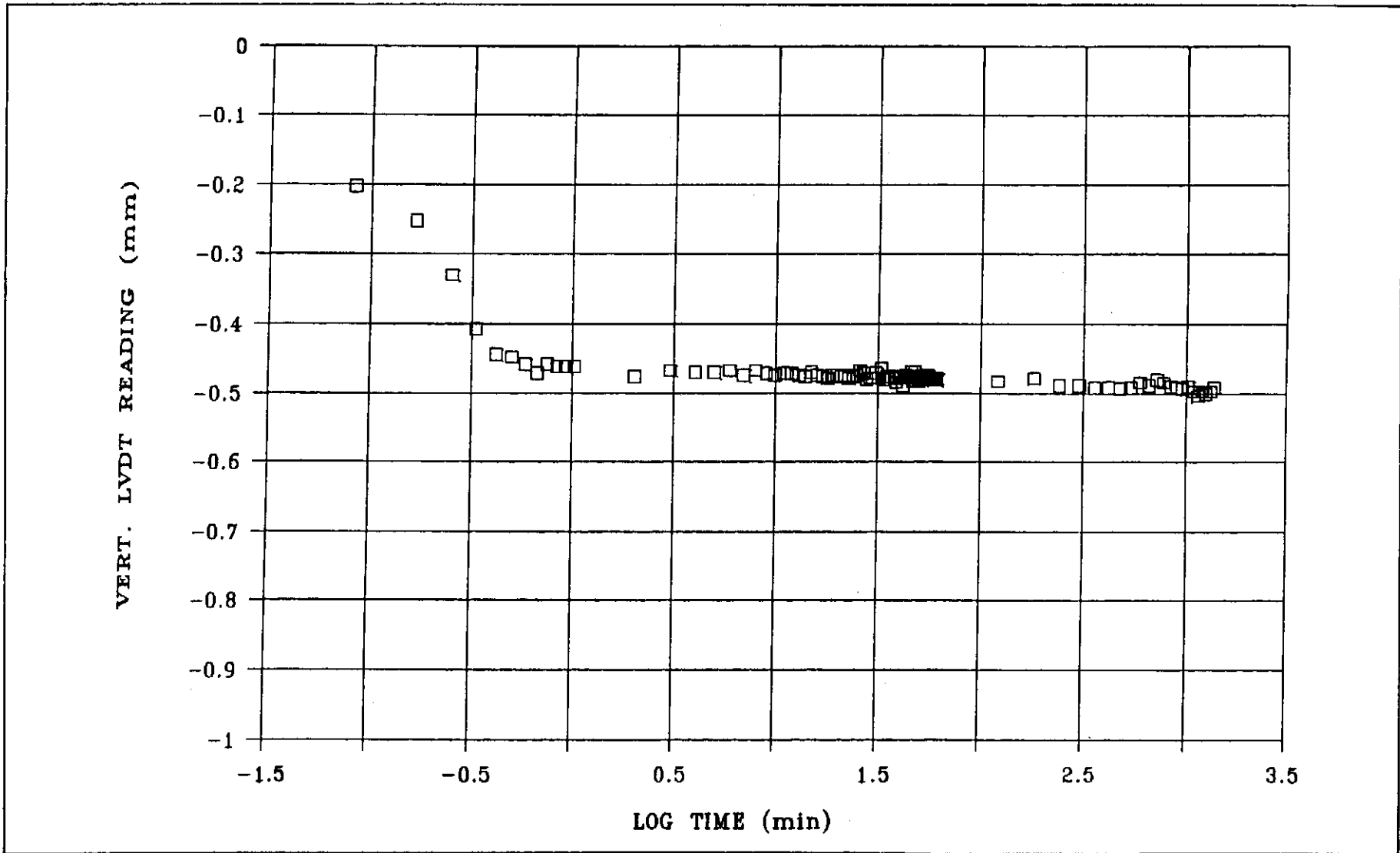


Figure 94 - Vertical Deflection with Time during Pressures Equilibration for Specimen No. US-13, Stage 1

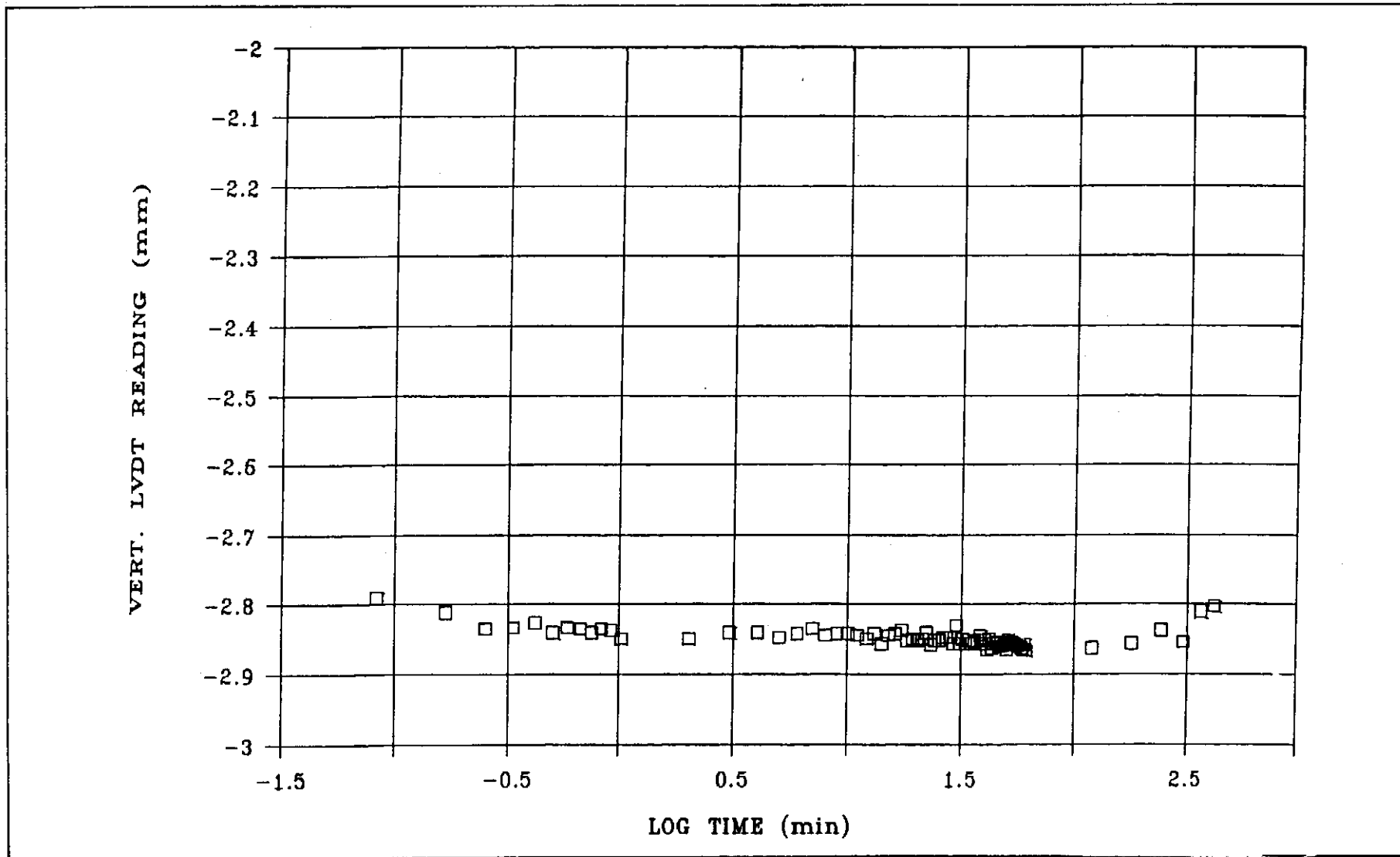


Figure 95 - Vertical Deflection with Time during Pressures Equilibration for Specimen No. US-14, Stage 1

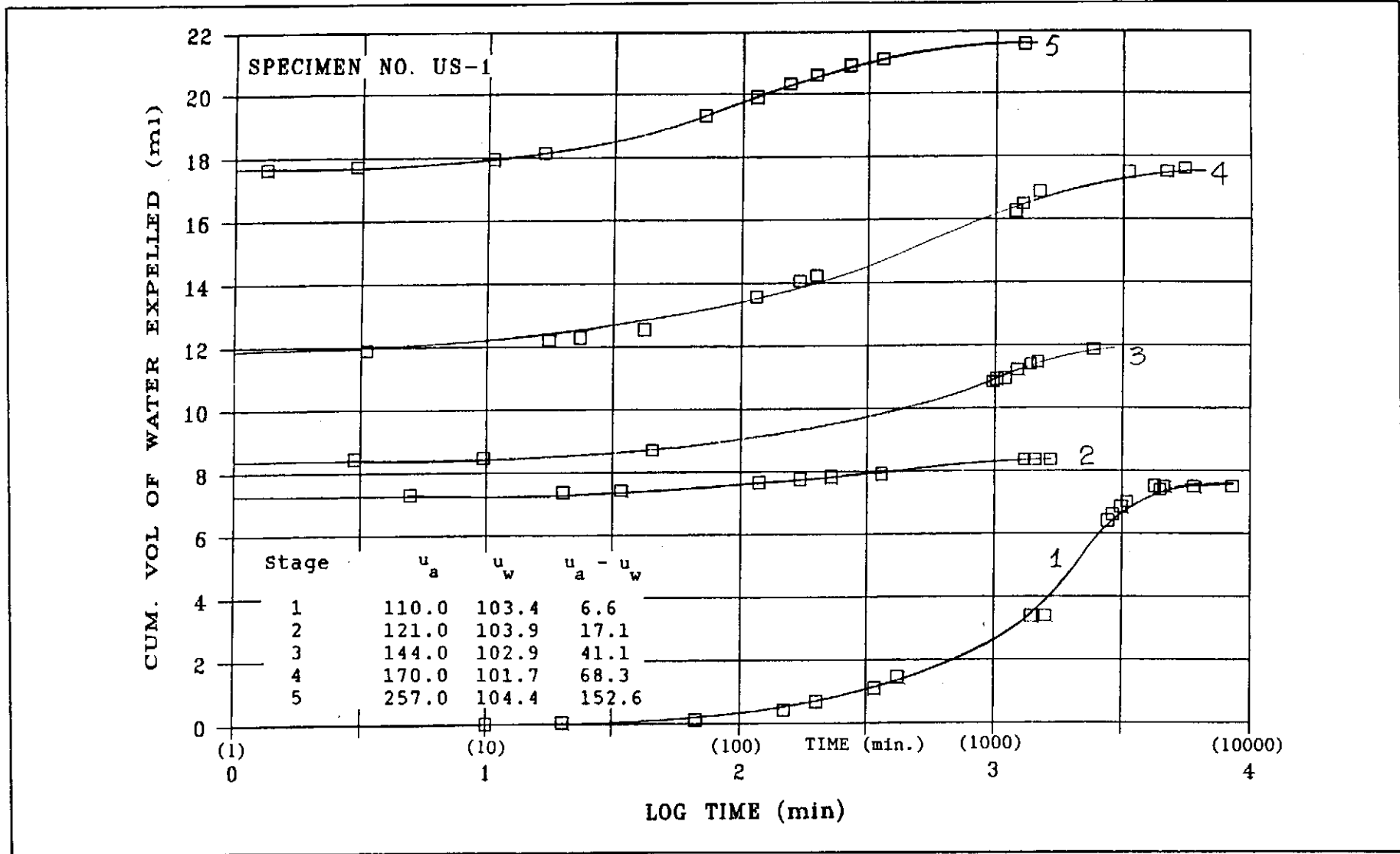


Figure 96 - Movement of Water from Specimen during Suction Equilibration for Specimen No. US-1

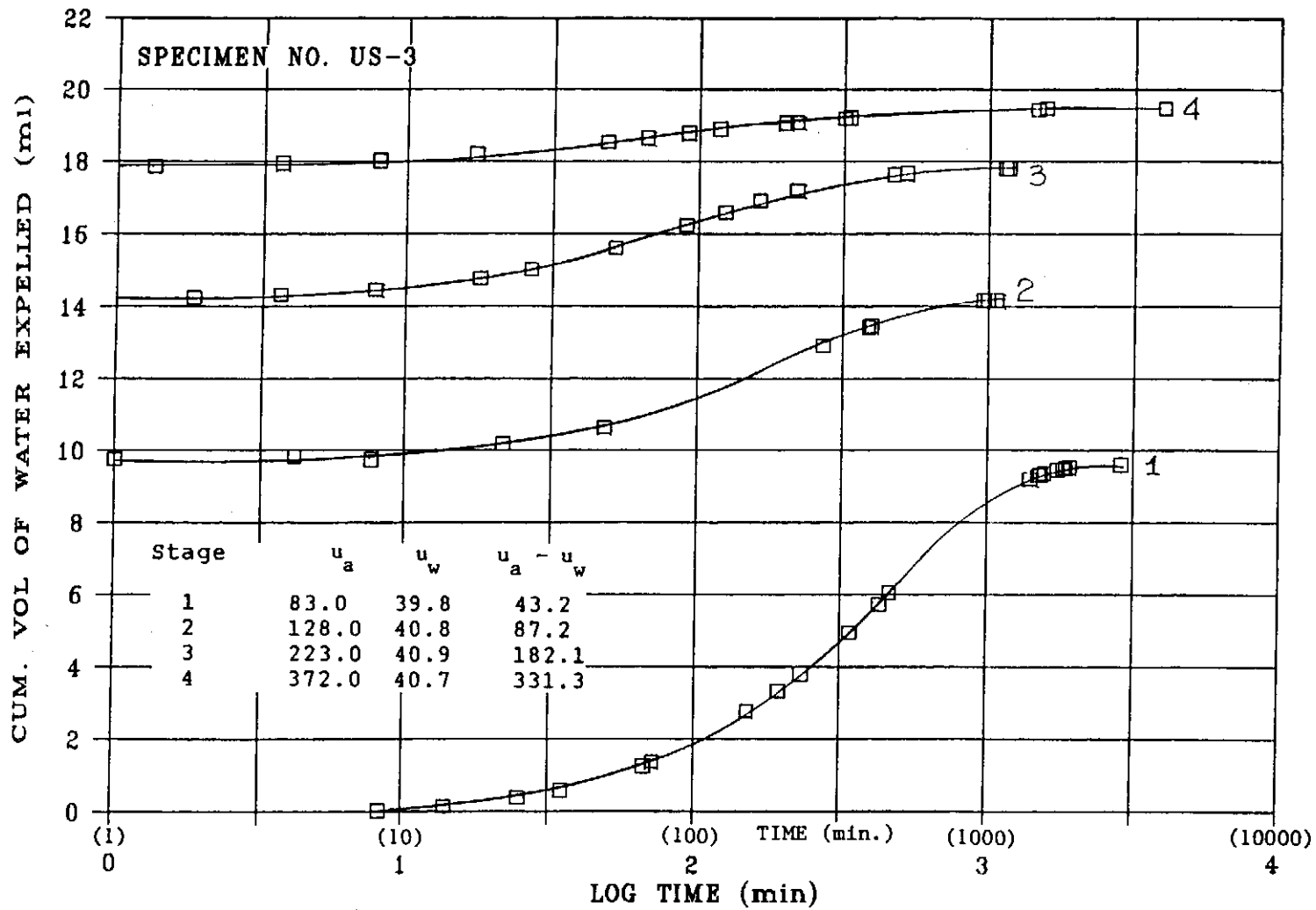


Figure 97 - Movement of Water from Specimen during Suction Equilibration for Specimen No. US-3

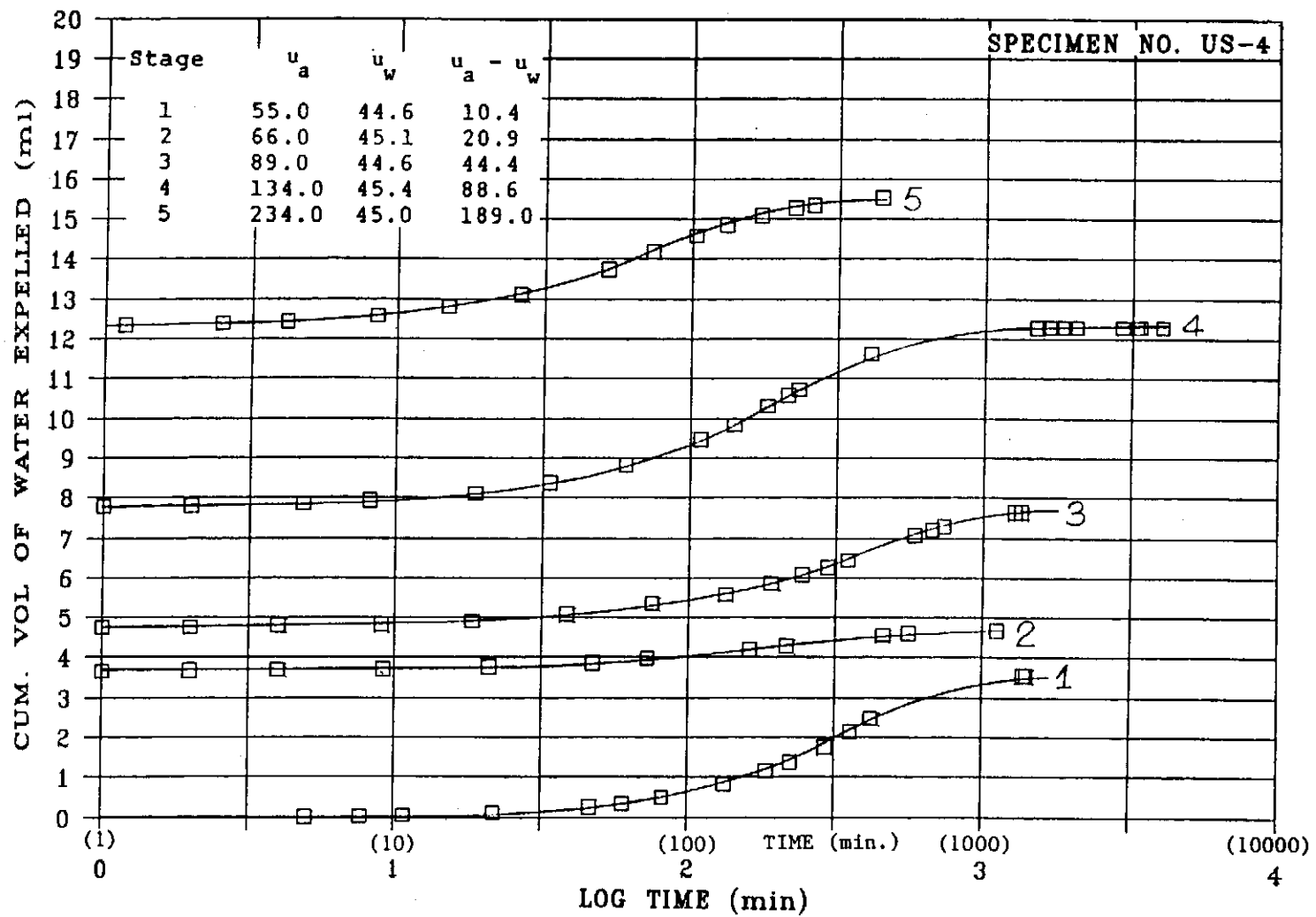


Figure 98 - Movement of Water from Specimen during Suction Equilibration for Specimen No. US-4

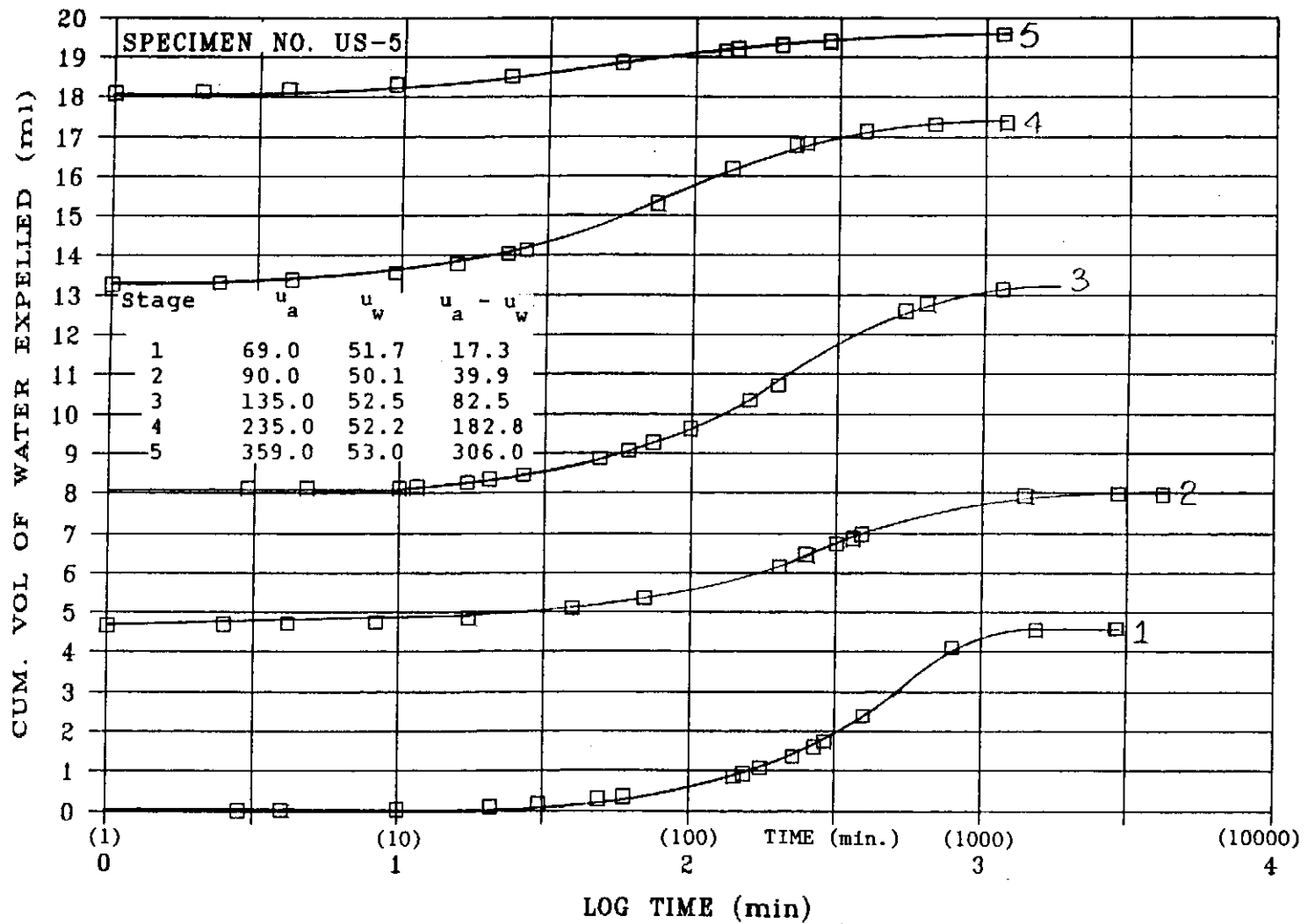


Figure 99 - Movement of Water from Specimen during Suction Equilibration for Specimen No. US-5

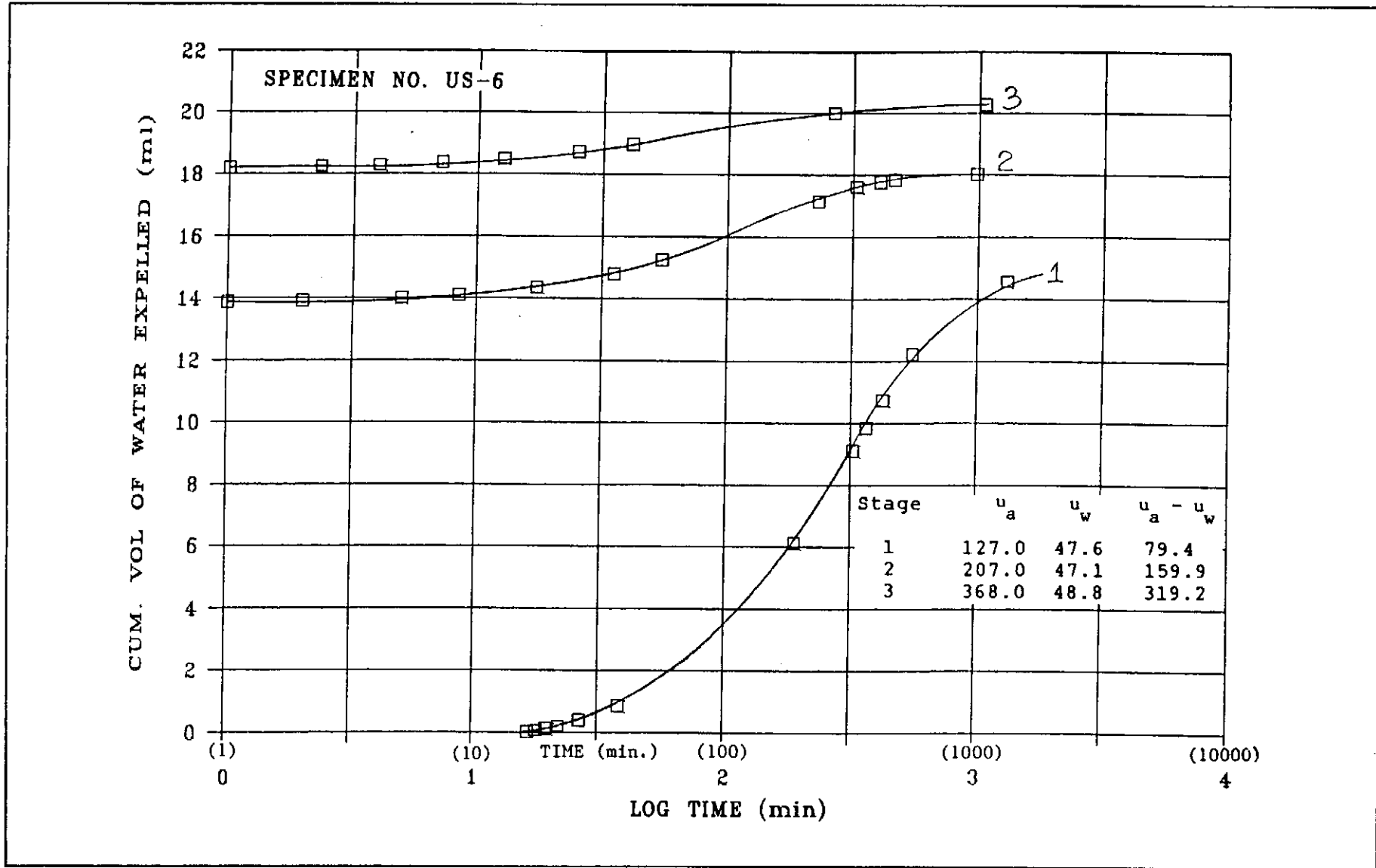


Figure 100 - Movement of Water from Specimen during Suction Equilibration for Specimen No. US-6

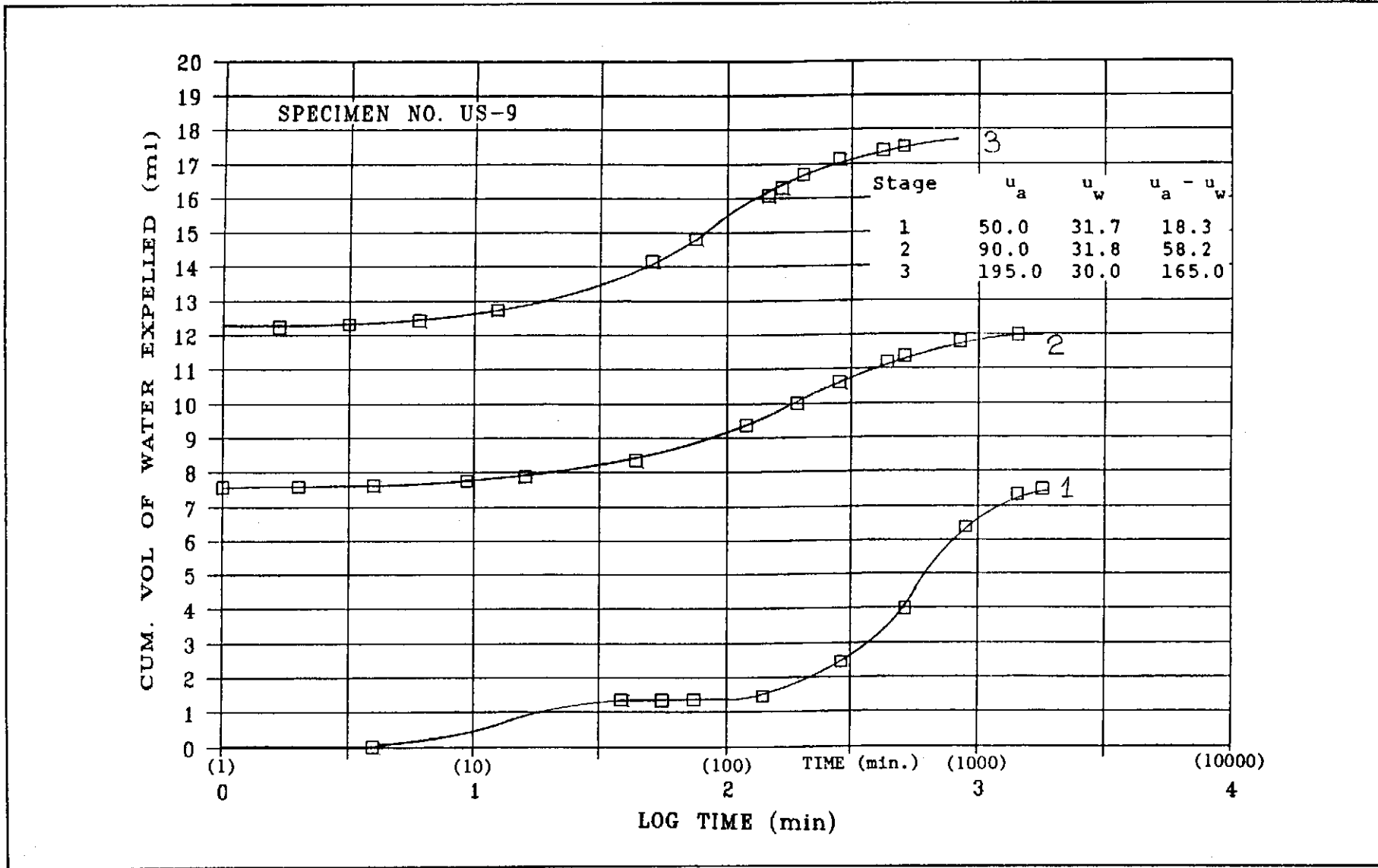


Figure 101 - Movement of Water from Specimen during Suction Equilibration for Specimen No. US-9

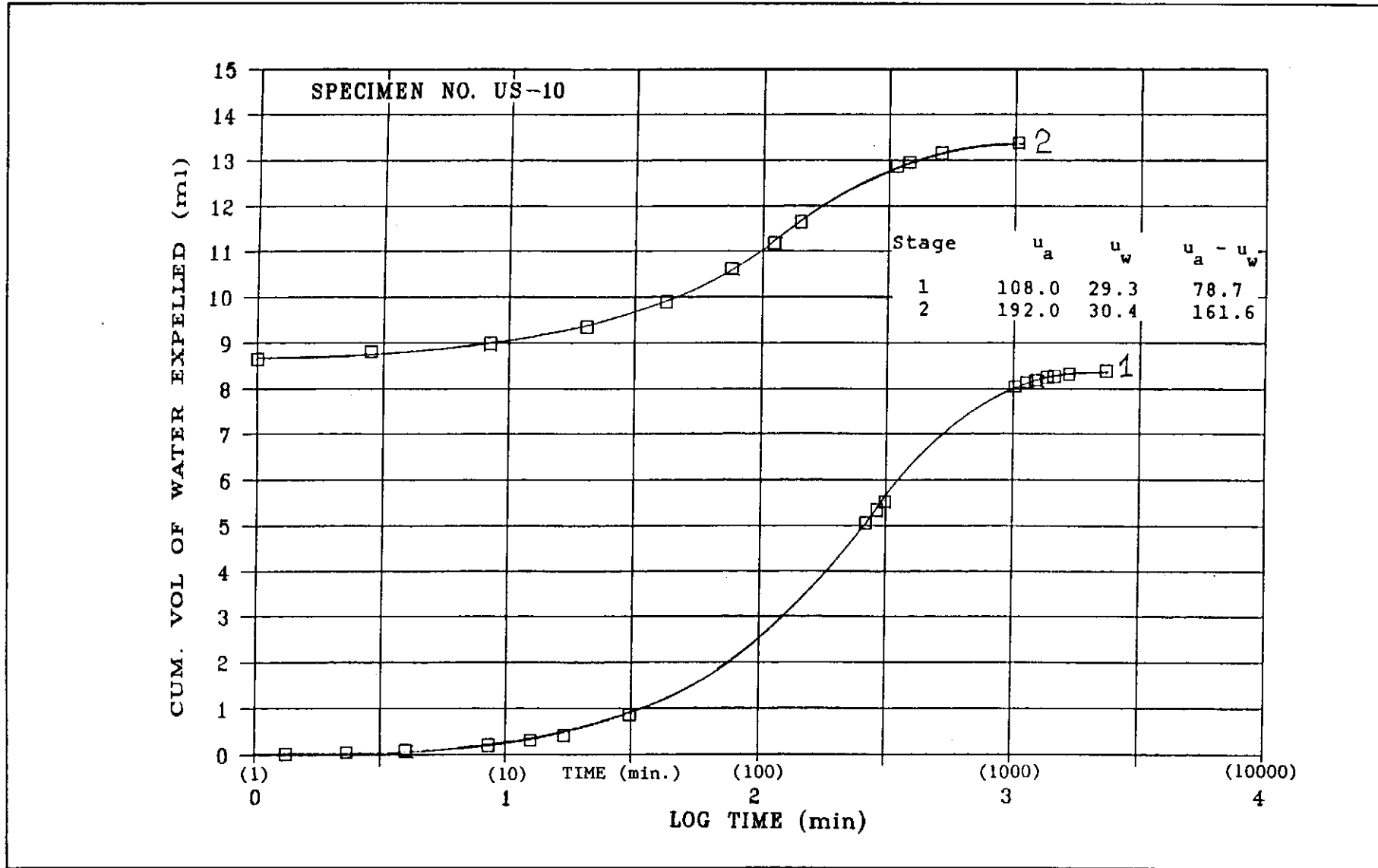


Figure 102 - Movement of Water from Specimen during Suction Equilibration for Specimen No. US-10

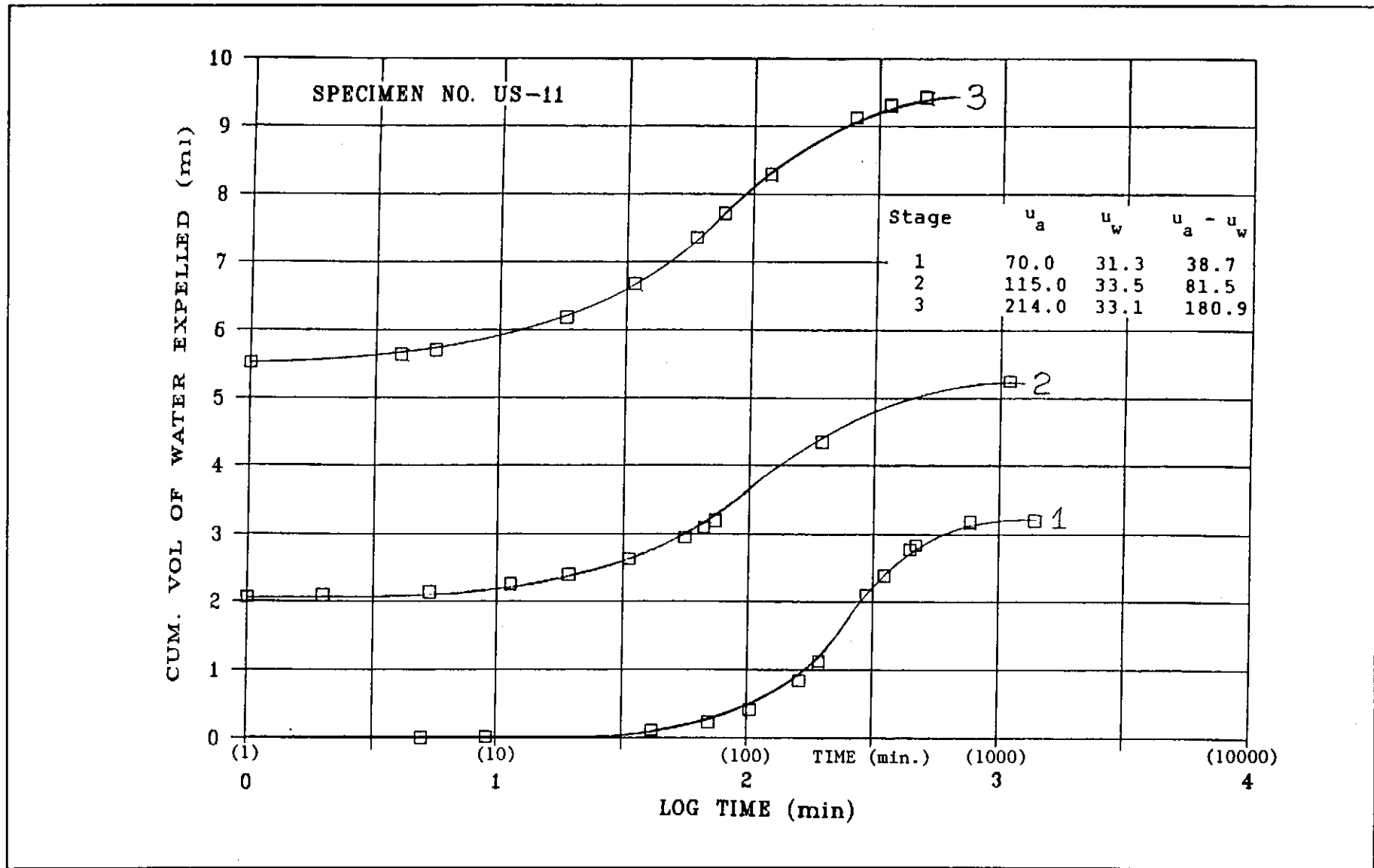


Figure 103 - Movement of Water from Specimen during Suction Equilibration for Specimen No. US-11

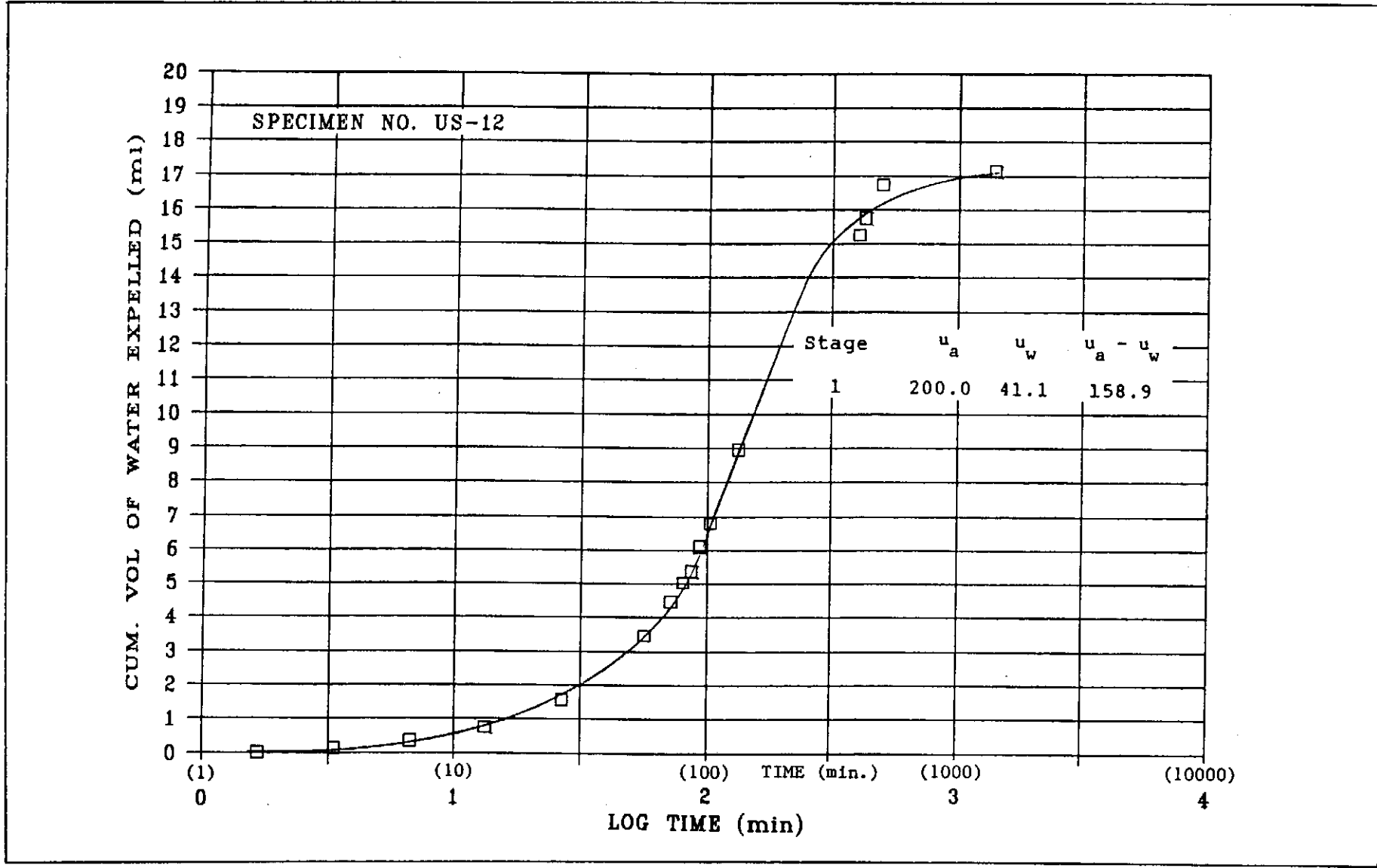


Figure 104 - Movement of Water from Specimen during Suction Equilibration for Specimen No. US-12

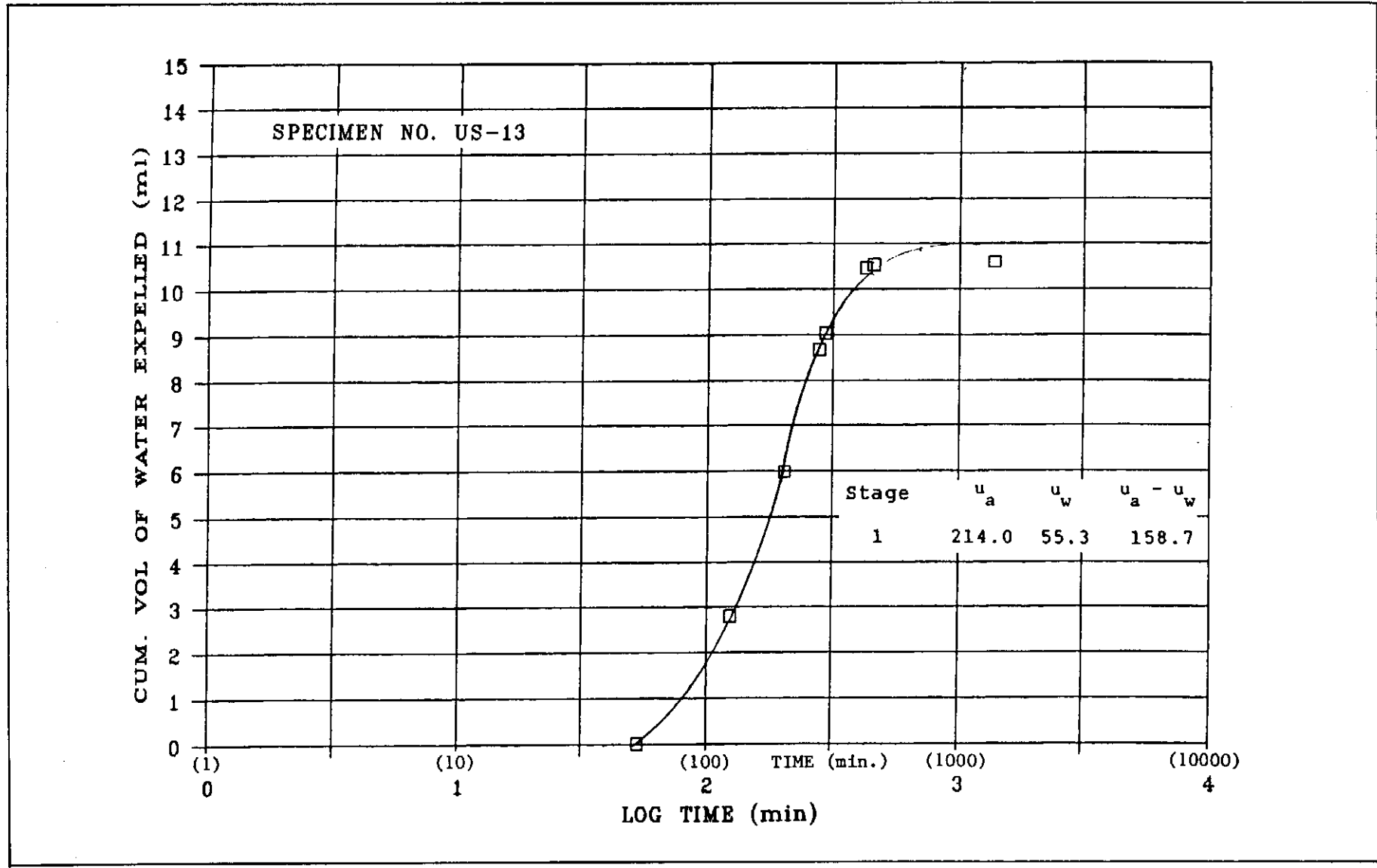


Figure 105 - Movement of Water from Specimen during Suction Equilibration for Specimen No. US-13

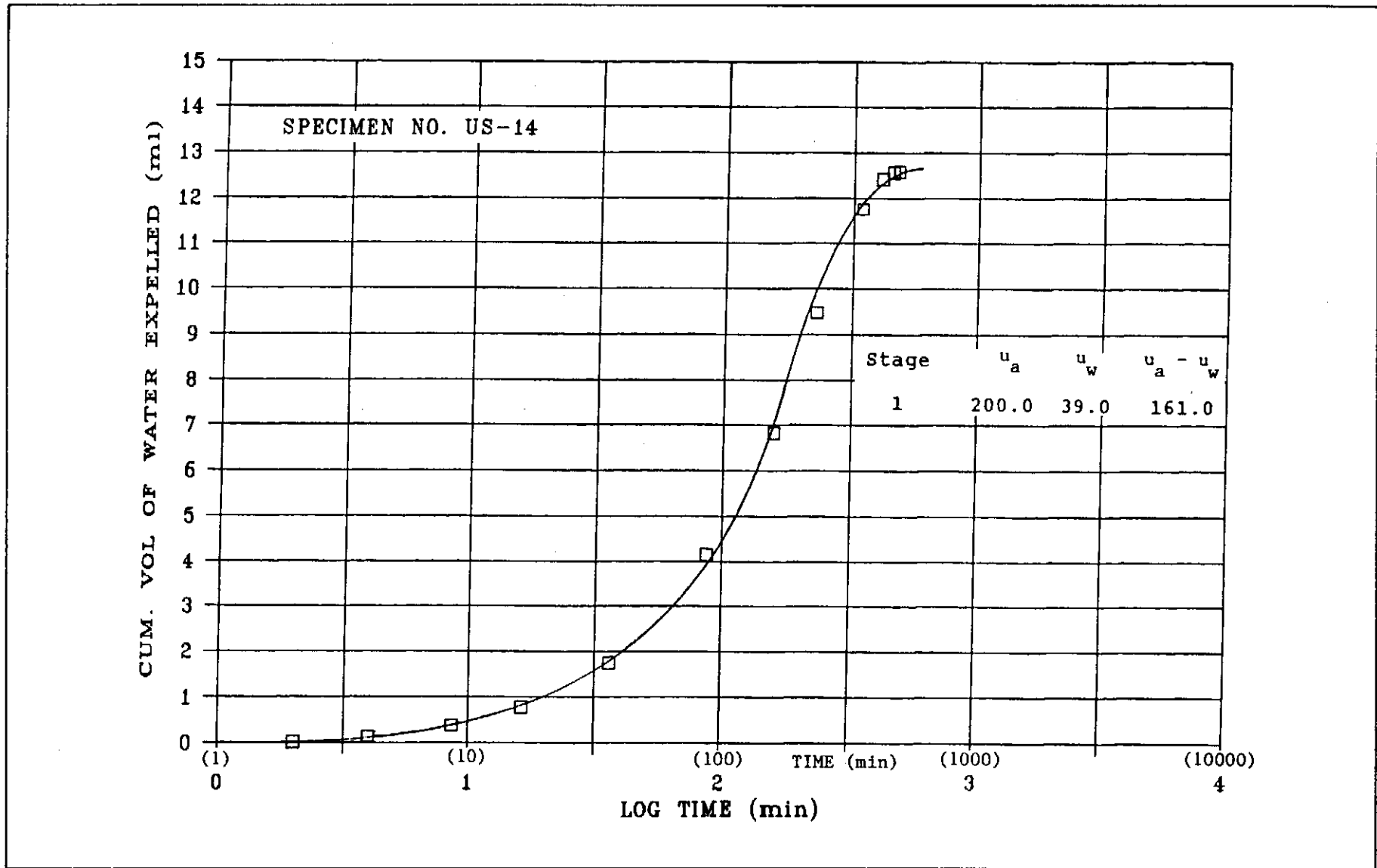


Figure 106 - Movement of Water from Specimen during Suction Equilibration for Specimen No. US-14

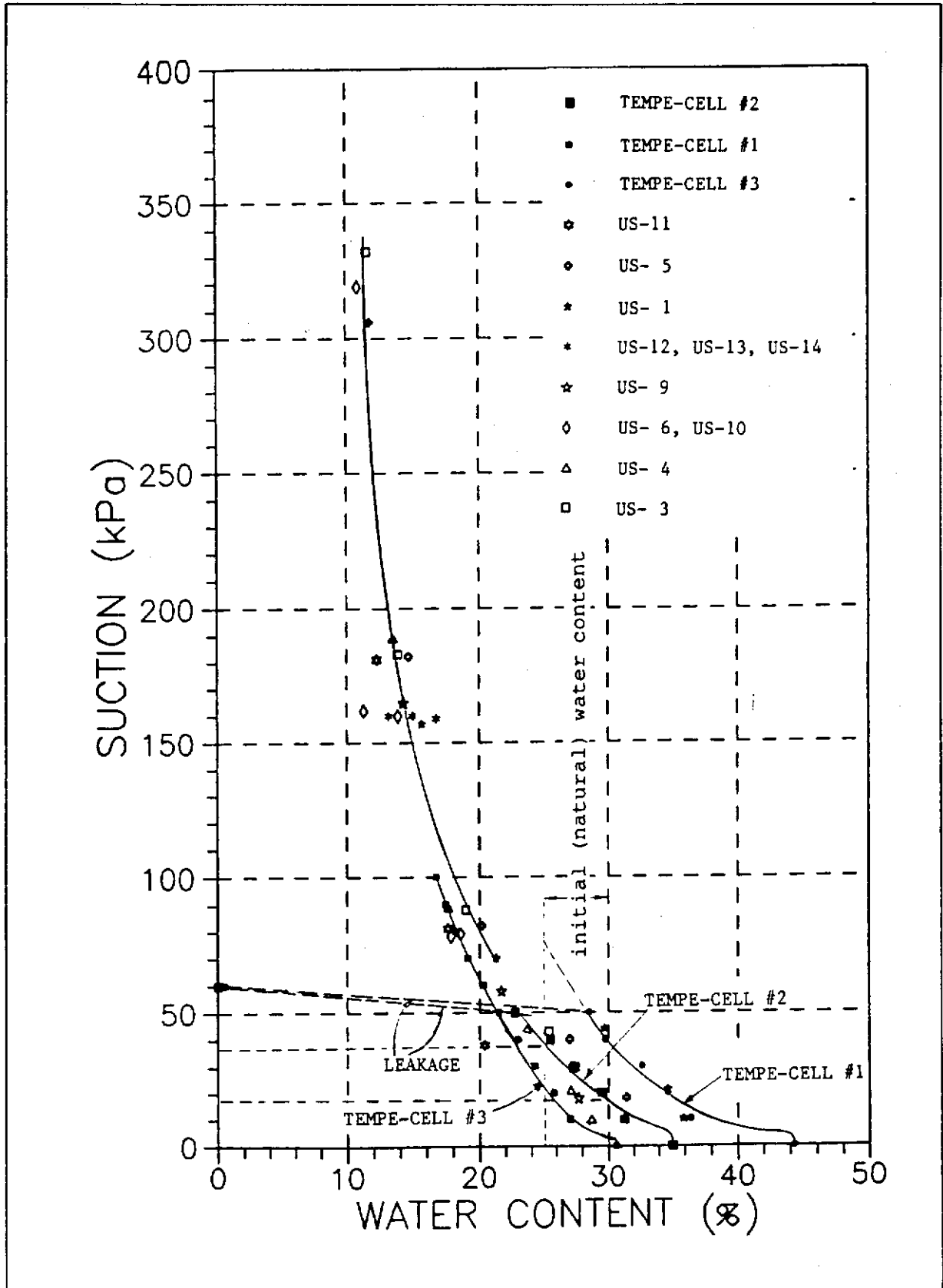


Figure 107 - Suction versus Water Content Relationship of Direct Shear Test Specimens in Main Test Program and of Tempe-cell Specimens

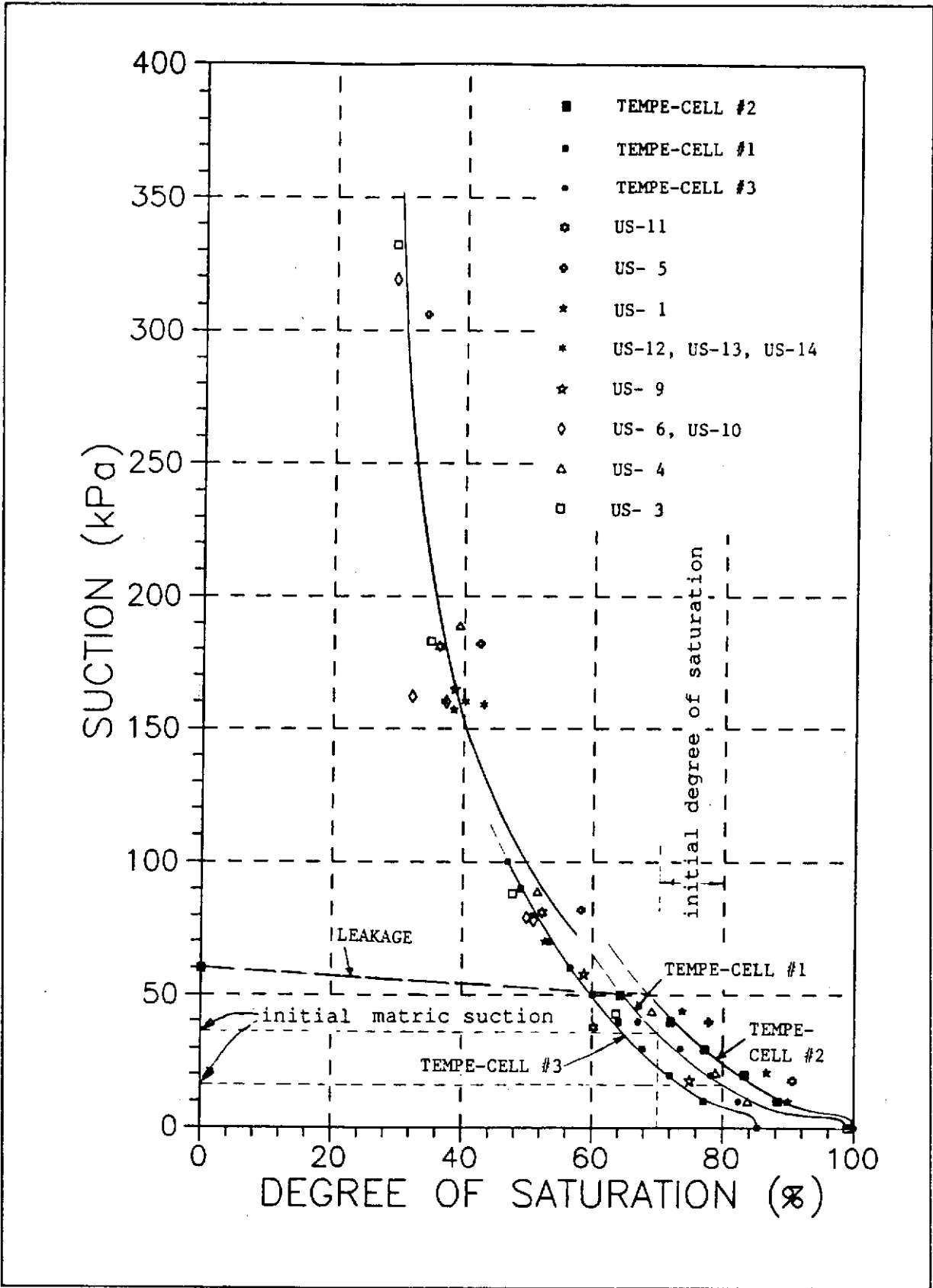


Figure 108 - Suction versus Degree of Saturation Relationship of Direct Shear Test Specimens in Main Test Program and of Tempe-cell Specimens

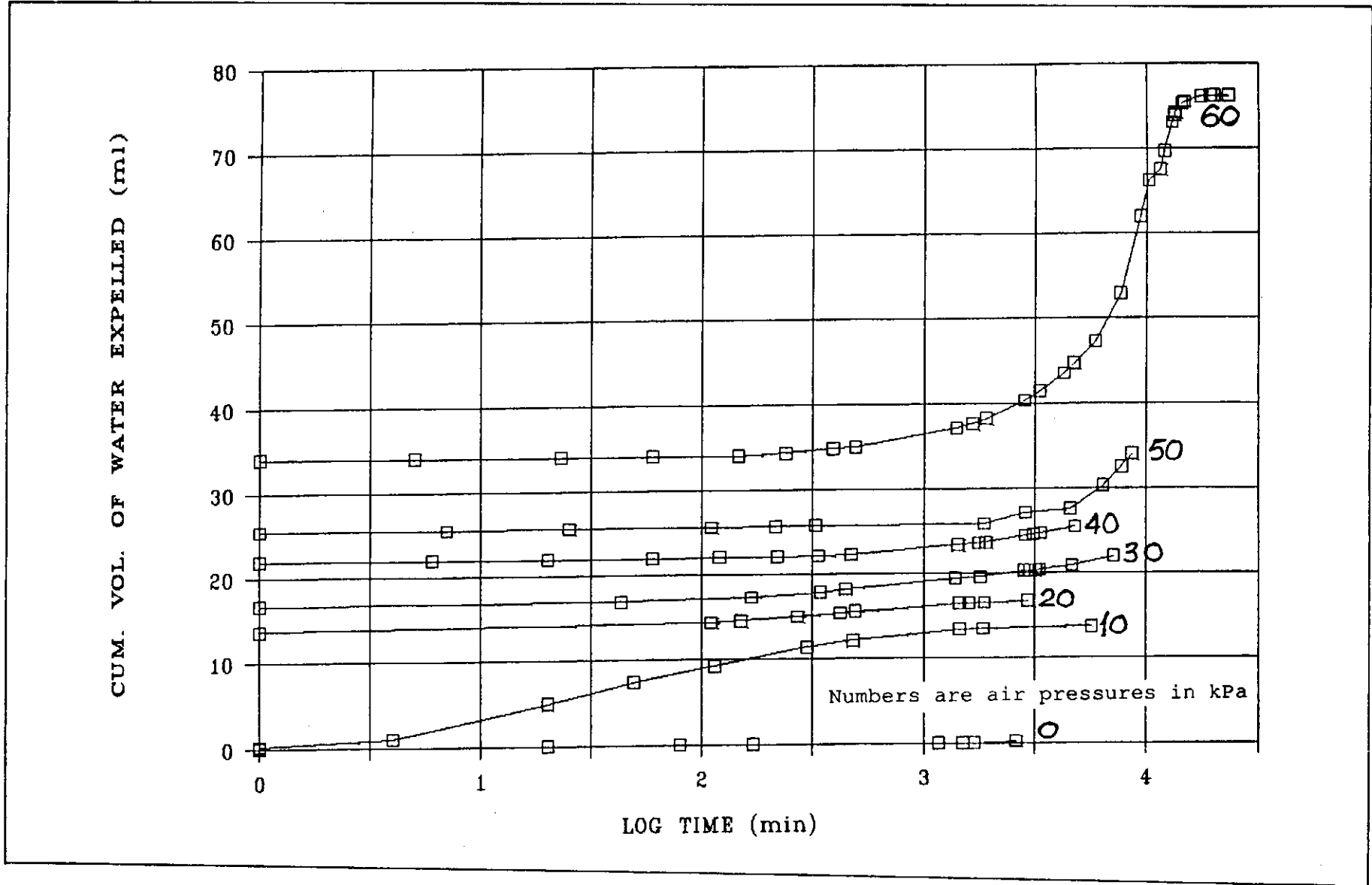


Figure 109 - Results of Tempe-cell Test No. 1

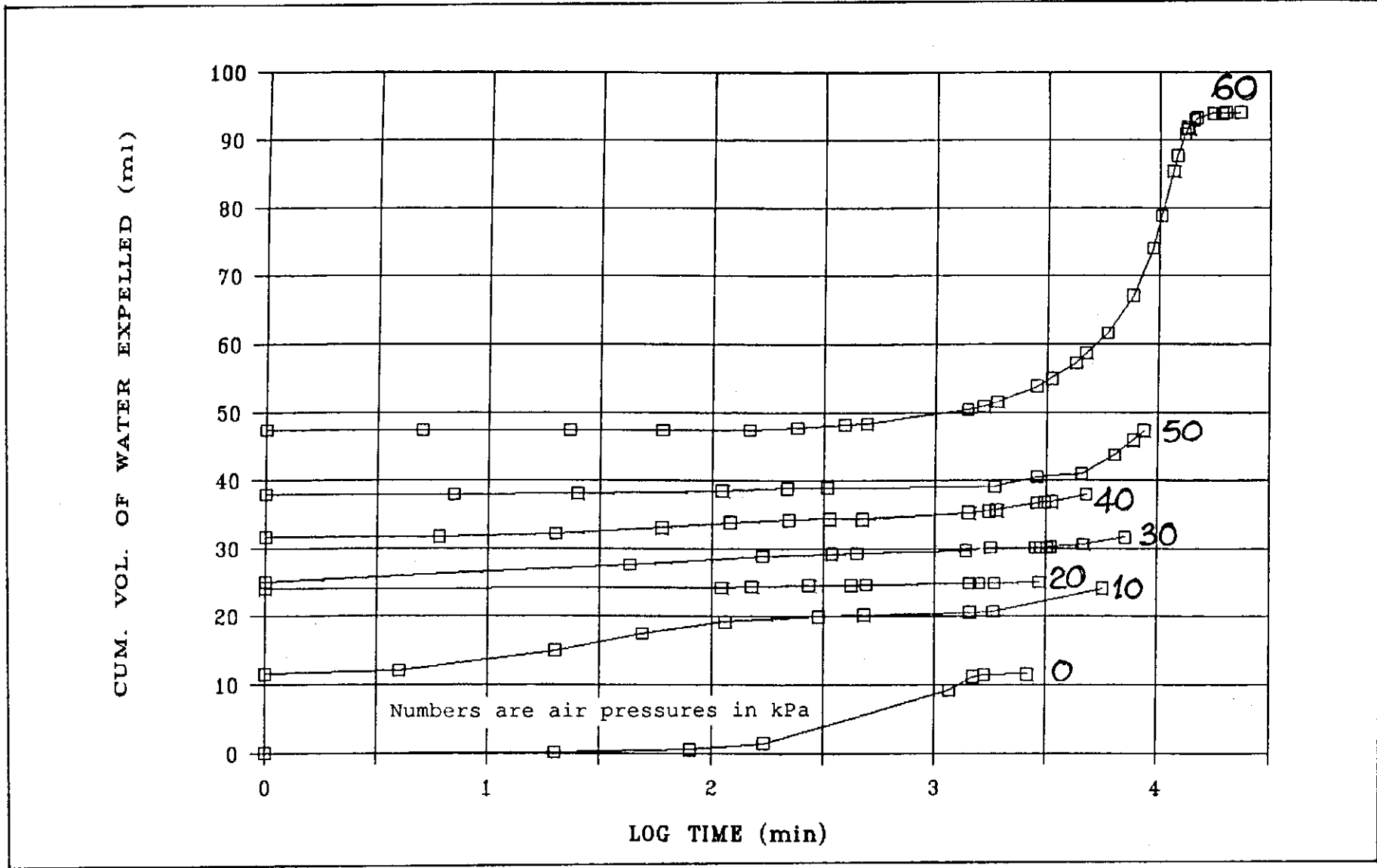


Figure 110 - Results of Tempe-cell Test No. 2

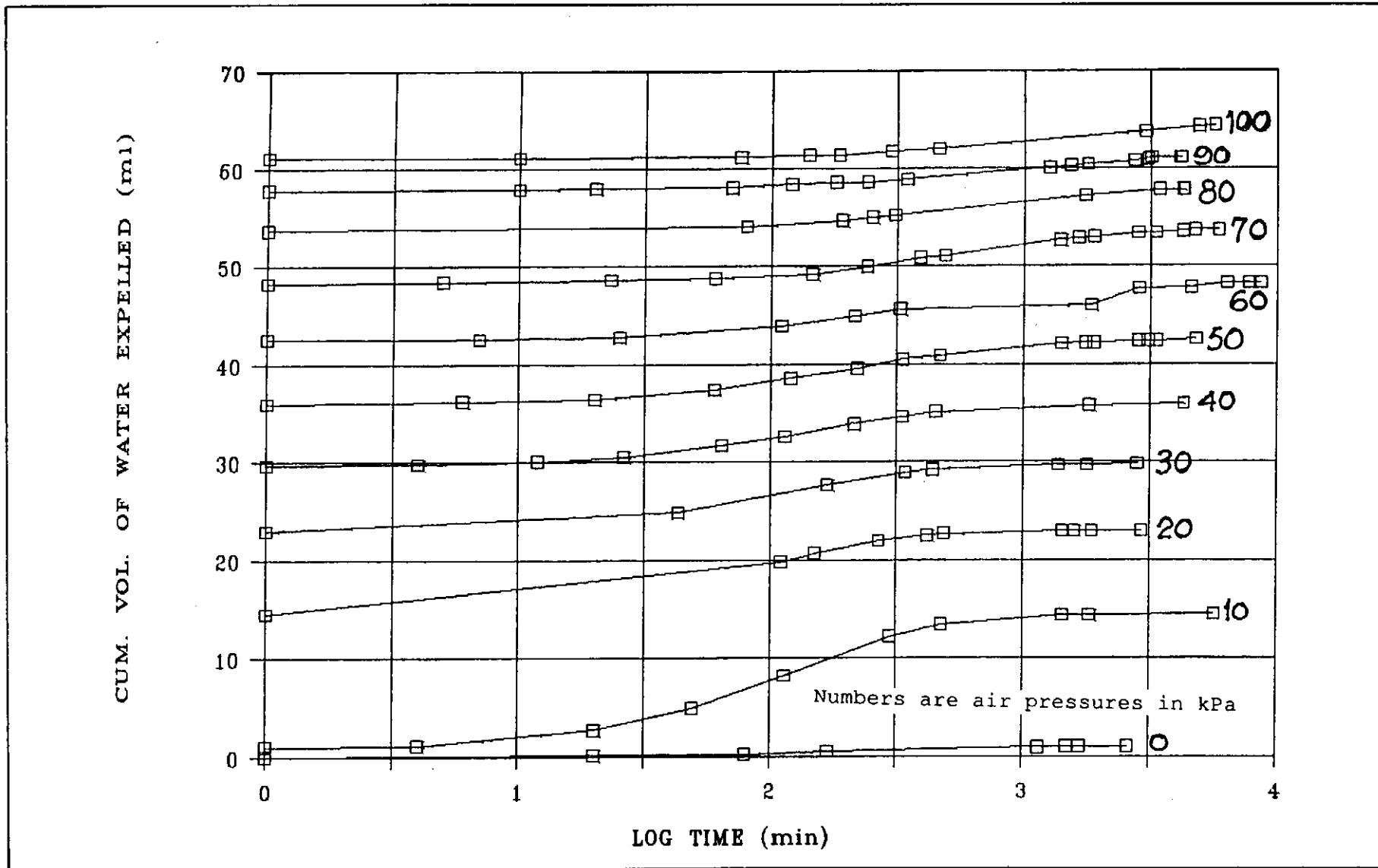


Figure 111 - Results of Tempe-cell Test No. 3

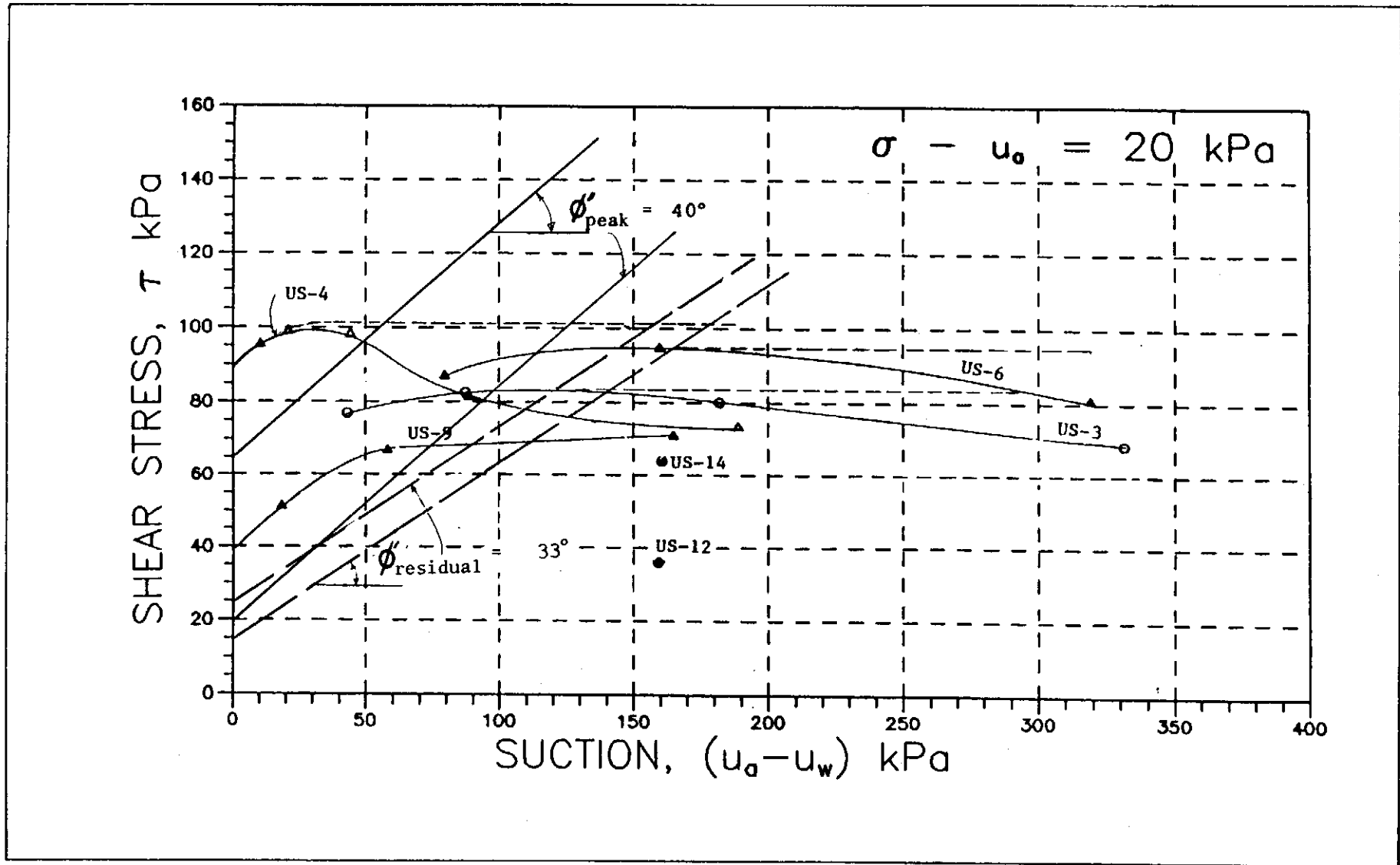


Figure 112 - Shear Stress versus Matric Suction Relationship of Fine Ash Tuff as Obtained from Direct Shear Tests at Various Applied Matric Suctions and a Constant Net Normal Stress of 20 kPa

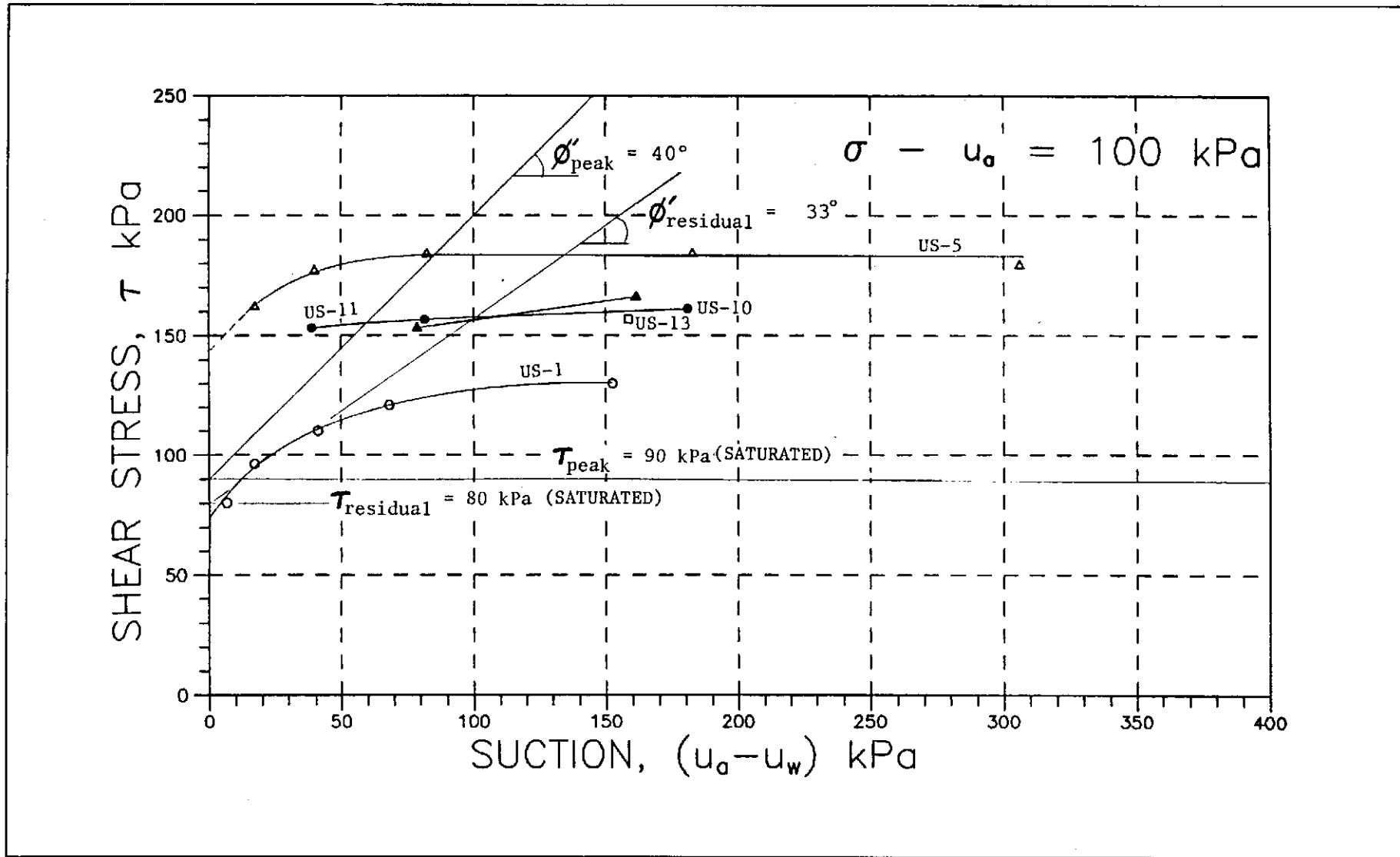


Figure 113 - Shear Stress versus Matric Suction Relationship of Fine Ash Tuff as Obtained from Direct Shear Tests at Various Applied Matric Suctions and a Constant Net Normal Stress of 100 kPa

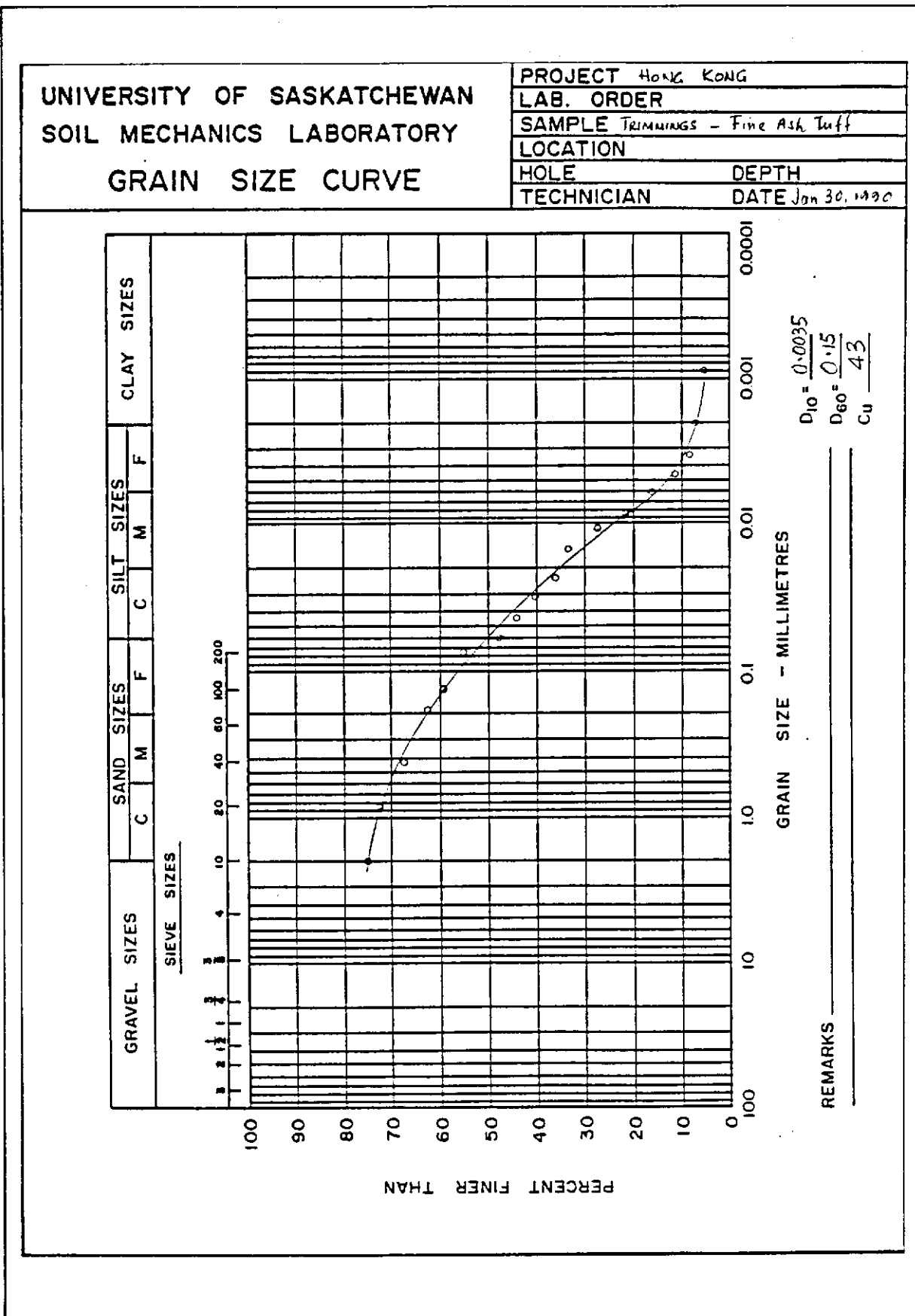
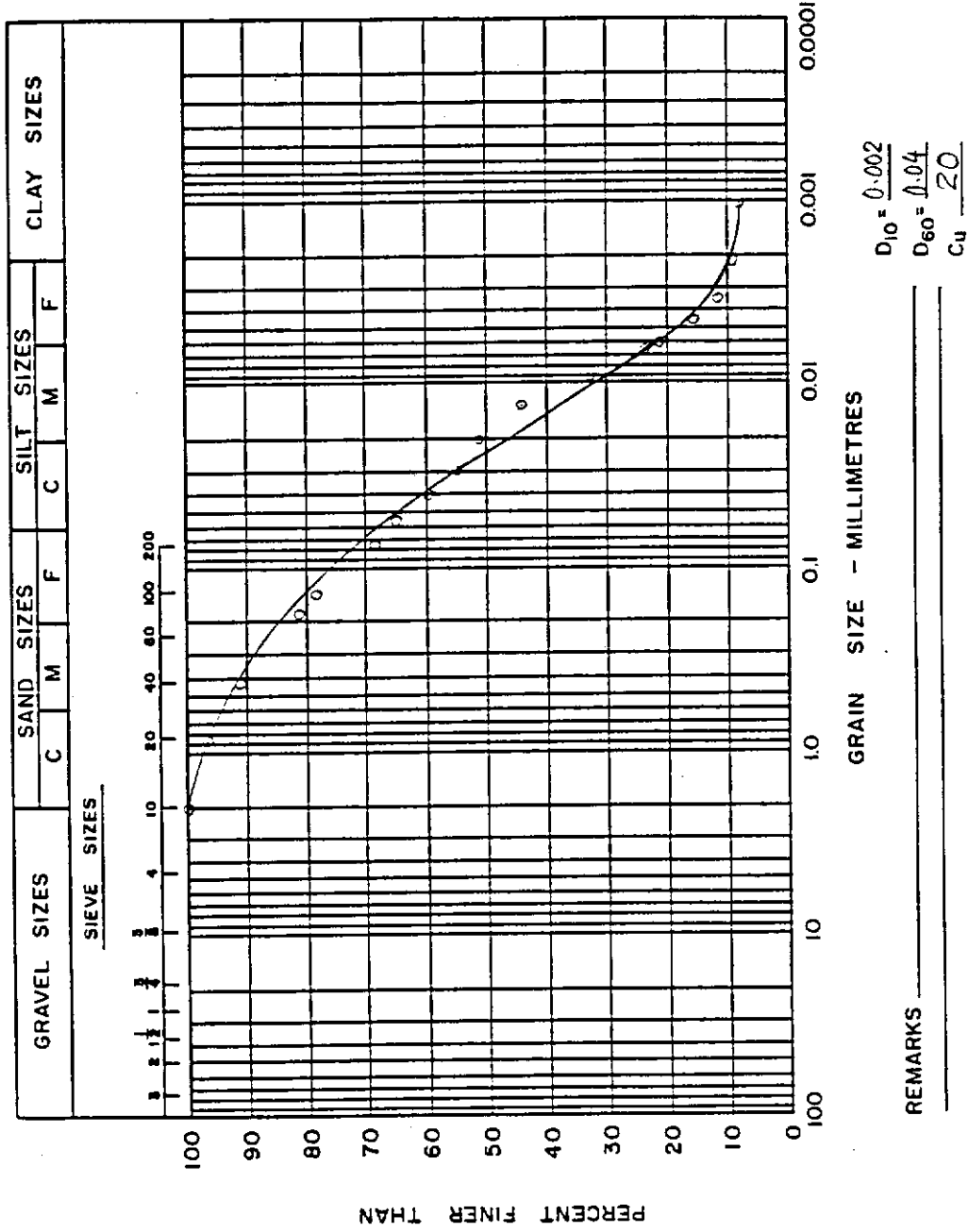


Figure 114 - Grain Size Distribution of Specimen Trimmings

UNIVERSITY OF SASKATCHEWAN
SOIL MECHANICS LABORATORY
GRAIN SIZE CURVE

PROJECT HONG KONG
LAB. ORDER
SAMPLE P2
LOCATION
HOLE DEPTH
TECHNICIAN DATE Jan 30, 1990



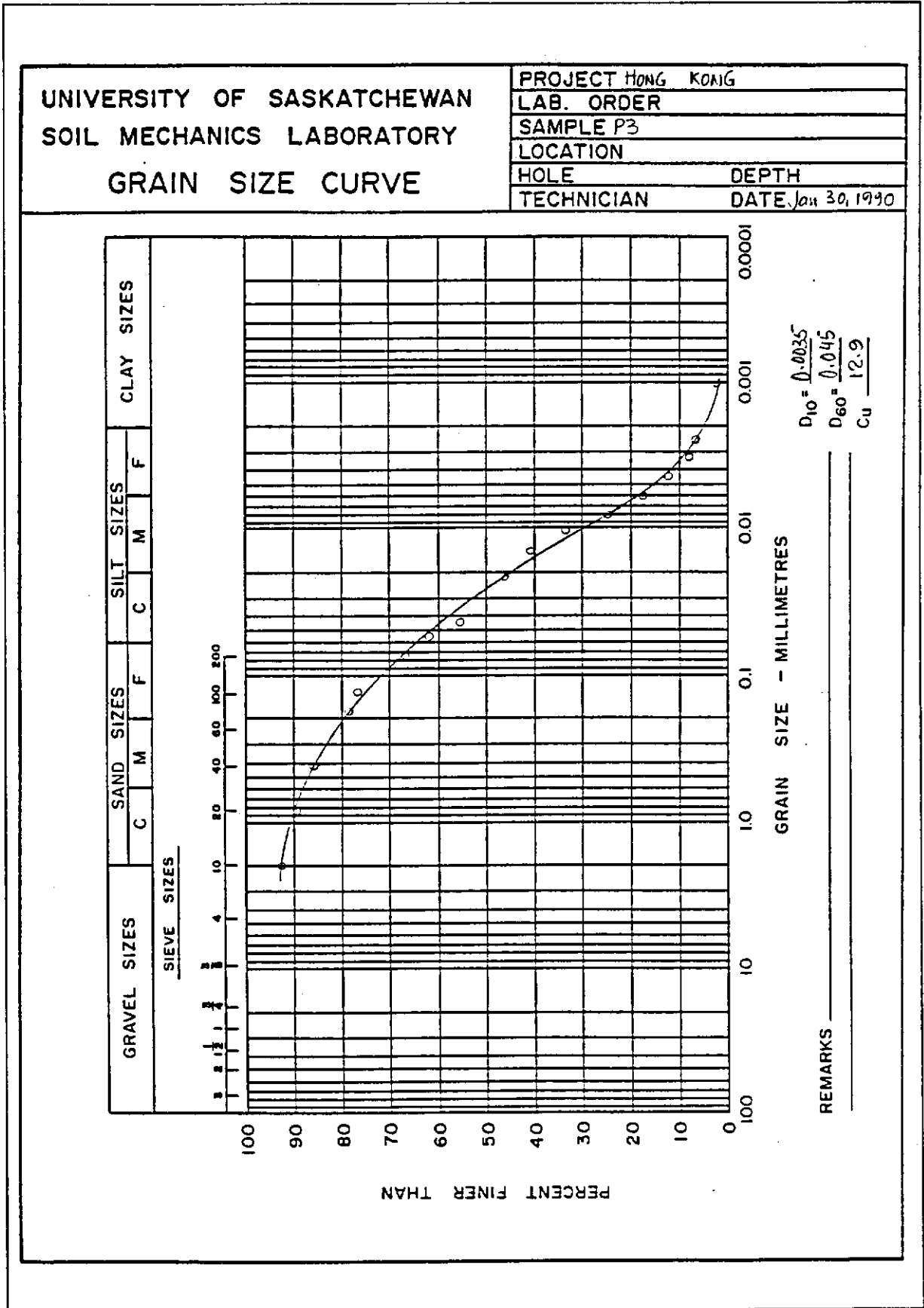


Figure 116 - Grain Size Distributions of Specimen No. P3

APPENDIX A

**TUFF SAMPLING SITE AND DESCRIPTION OF SAMPLES
(T.Y. Irfan)**

CONTENTS

	Page No.
TITLE PAGE	220
CONTENTS	221
A1. INTRODUCTION	222
A2. SITE DESCRIPTION	222
A3. GEOLOGICAL SETTING	222
A4. WEATHERING	222
A5. SAMPLING	223
A6. SAMPLE DESCRIPTIONS	223
A7. REFERENCES	225
LIST OF FIGURES	226
LIST OF PLATES	232

A1. INTRODUCTION

A research project consisting of a study of direct shear testing of a selected 'undisturbed' Hong Kong Soil under various applied suctions with a view to quantifying the effect of matric suction on the shear strength of the soil is to be carried out by Prof. F.R. Fredlund of University of Saskatchewan on behalf of the Geotechnical Control Office.

The soil chosen to be tested is a completely decomposed fine ash tuff from the Junk Bay area, Hong Kong. This report gives a brief description of the geology and weathering characteristics of the sampling site and the three block samples selected from a trial pit on the site.

A2. SITE DESCRIPTION

The sampling site is located at an elevation of about 130 mPD, on the mid-slopes of Tai Sheung Tok hill (elevation 400 mPD), west of the Tseung Kwan O (Junk Bay) new town, New Territories, Hong Kong (Figures A1 and A2, Plates A1 and A2). The block samples were collected from a trial pit excavated on the small cut slope adjoining a minor access road, off Tsui Lam road.

The average gradient of the natural hillside in the immediate vicinity of the sampling site is 25° to 30°. A minor side valley running in an approximately W-E direction is present to the north of the site. The hillside is densely vegetated with shrubs, short trees and long grass.

A3. GEOLOGICAL SETTING

The site is shown to be underlain by volcanic rocks of the Ap Lei Chau Formation (JAC) belonging to the Repulse Bay Volcanic Group of Upper Jurassic age on the recently published geological map (GCO, 1986). The Ap Lei Chau formation is dominantly composed of fine ash vitric tuffs which may locally contain eutaxitic layers (layered flow deposits). A more detailed account of this formation and the petrological characteristics is given by Strange and Shaw (1986).

An examination of rock outcrops and observations in the trial pit excavations indicate that the main rock type in the sampling site is a fine ash vitric tuff with scattered crystals and occasional lapilli. The fine ash tuff is dark grey coloured when fresh with up to 20% crystals of feldspars and some quartz in a very fine grained devitrified glass matrix. Most crystals are less than 1 mm in size, but occasionally up to 2 mm.

A4. WEATHERING

The weathering profile is very variable, but generally thin in the vicinity of the site (Figure A3, Plates A3 and A4). Moderately weathered rock (BS 5930: 1981) overlain by a thin layer of transported soil (colluvium) is exposed on the cut slope, a few metres north of

the sampling location (Plate A3). Almost fresh rock outcrops can also be seen on the reservoir cutting to the south of the site (Plate A1).

At the sampling location itself, at least 5 m of residual soil and completely weathered volcanic rock is present underneath a colluvium cover of 0.8 m (Figure 3). A gradual transition from residual soil (i.e. soil with no original rock fabric) to completely weathered rock exists at this location. Colluvium thickens to over 2.5 m towards the minor drainage channel on the south. The colluvium thickness also increases towards the natural drainage channel at the northern portion of the site. A second trial pit opened on the natural hillside above the cutting showed at least 2.5 m of colluvium underlain by completely weathered tuff containing pockets of residual soil.

The true residual soil under the colluvium is patchily developed (or removed by erosion?), up to 1 m thick and is mottled brown and yellowish brown in colour. Very little or no original volcanic rock fabric is present in this zone. The percentage of volcanic rock fabric increases gradually in the zone termed as "transition residual soil" and short, discontinuous relict discontinuities may be present. The completely weathered rock (also known as saprolite) from which the block samples were collected, may contain small pockets or thin bands of residual soil (e.g. sample no. JB-3). This zone is mottled reddish brown and yellowish grey in colour. Yellowish grey colour increases with depth. The soil contains closely to very closely spaced, mostly sub-vertical, relict joints with a spacing of 20 to 80 mm. In addition, a branched network of very closely spaced (less than 20 mm) irregular fractures are also present (legacy of original rock fabric?). The relict joints may contain coatings or thin infillings of black silty material (MnO_2 ?). White clayey kaolin (?) veins are present along some of the discontinuities.

Plates A1 to A4 show the general views of the sampling site and the weathering characteristics along the access road in the vicinity of the sampling location.

A5. SAMPLING

Hand trimmed block samples, approximately 300 x 300 x 300 mm size, were taken from a trial pit excavated on the cut slope in a location where the soil profile was the thickest. The block samples were covered by aluminium foil, the gap between the box (400 x 400 x 400 mm in size) and the sample was filled with a solution of quick setting polyurethane. Plates A5 to A8 show a sequence of the sampling operations. Figure A4 shows a sketch cross-section across the sampling location and Figure A5 gives a simplified log of the trial pits and the sample locations.

A6. SAMPLE DESCRIPTIONS

The block samples were selected within a depth of 1.6 to 1.8 m and in close proximity to each other in the trial pit to ensure sample uniformity. They were selected from the completely weathered volcanic rock zone and would broadly be described as "completely decomposed" or grade V rock by the decomposition grade classification recommended by Geoguide 3 (GCO, 1988). A close examination of block samples after trimming showed that

variations in terms of soil fabric and discontinuity properties amongst the samples and also across each sample; related to process of weathering and original rock properties.

A detailed description of each of the block samples is given below. Plates A9 to A14 show the block samples after trimming. Face A is upslope face in all the samples.

<u>Sample No.</u>	<u>Decomposition Grade (GCO, 1988)</u>	<u>Location</u>	<u>Description of Block Sample</u>
JB-1	V	1.8 m depth in trial pit TP1	Reddish brown with patches of yellowish grey, Completely Decomposed Fine Ash Tuff with very closely spaced, black MnO ₂ coated/infilled relict joints. There are small patches without volcanic rock fabric (deep reddish brown in colour) (Clayey Sandy Silt). Plate A9.
JB-2	V	1.6 m depth in trial pit TP1	Mottled yellowish grey and reddish brown (increasing in yellowish grey towards the base), Completely Decomposed Fine Ash Tuff, with very closely spaced, black MnO ₂ coated/infilled relict joints. There are small patches without volcanic rock fabric (deep reddish brown in colour), generally more porous. May contain thin kaolin veins/infillings (Clayey Sandy Silt). Plate A10.
JB-3	V	1.6 m depth in trial pit TP1 (adjacent to JB-2)	Yellowish grey with patches of reddish brown, Completely Decomposed Fine Ash Tuff, with very closely spaced black MnO ₂ coated/infilled relict joints. There are small patches without volcanic rock fabric, particularly near the top surface. One or two joints contain, deep reddish brown coloured porous material, up to 20-30 mm thick, with lost volcanic rock fabric (Plates A11, A12 & A13). There is a thin kaolin vein on face D.

In general, the feldspar megacrysts are powdery to gritty, sometimes hard, in all the block samples indicating that the decomposition is not intense. The clay content of the soil is small, most of the material is silt size. Feldspars show more intense decomposition adjacent to kaolin veins in kaolinized patches (effect of hydrothermal alteration by a granite at depth). The sample JB1 is slightly more intensely decomposed than the other two samples. It also contains a higher amount of no fabric areas. The relict discontinuities are generally subvertical to vertical and parallel to face A in all the samples. In addition, there are more closely spaced irregular network of "fractures" in the soil.

A7. REFERENCES

- GCO (1986). Hong Kong and Kowloon : solid and superficial geology. "Hong Kong Geological Series HGM 20", Sheet 11, 1:20 000.
- GCO (1988). "Guide to Rock and Soil Descriptions (Geoguide 3)". Geotechnical Control Office, Hong Kong, 189 p.
- Strange & Shaw (1986). "Geology of Hong Kong Island and Kowloon". Geotechnical Control Office, 134 p. (Hong Kong Geological Survey Memoir No. 2).

LIST OF FIGURES

Figure No.		Page No.
A1	Location Map 1:100 000 Scale	227
A2	Location Map 1:1 000 Scale	228
A3	A Sketch of Weathering Profile in the Immediate Vicinity of the Sampling Location	229
A4	Sketch Cross-section across the Sampling Location	230
A5	A Simplified Log (Face A) of the Trial Pit TP1 and the Sample Locations	231

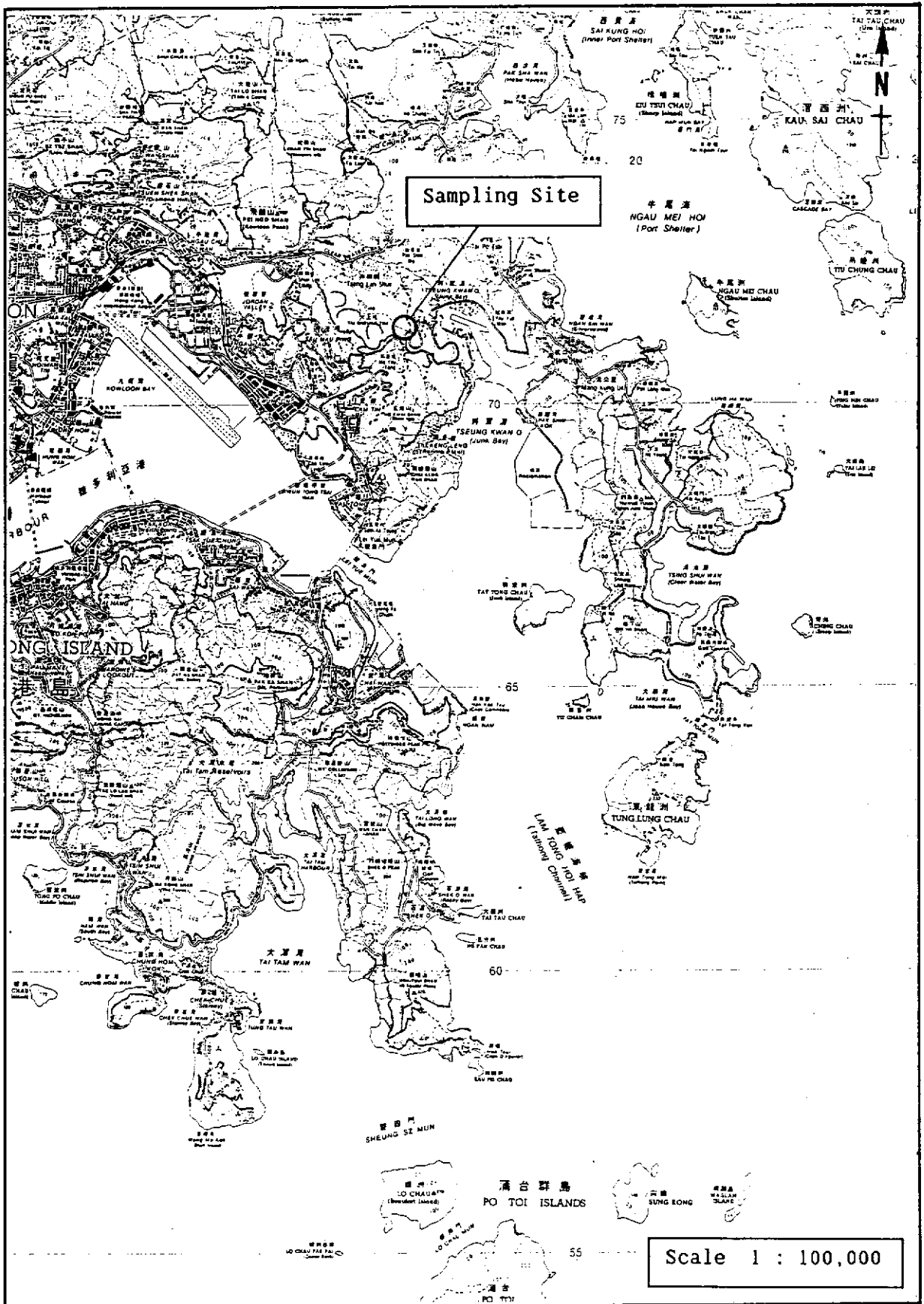


Figure A1 - Location Map 1 : 100 000 Scale

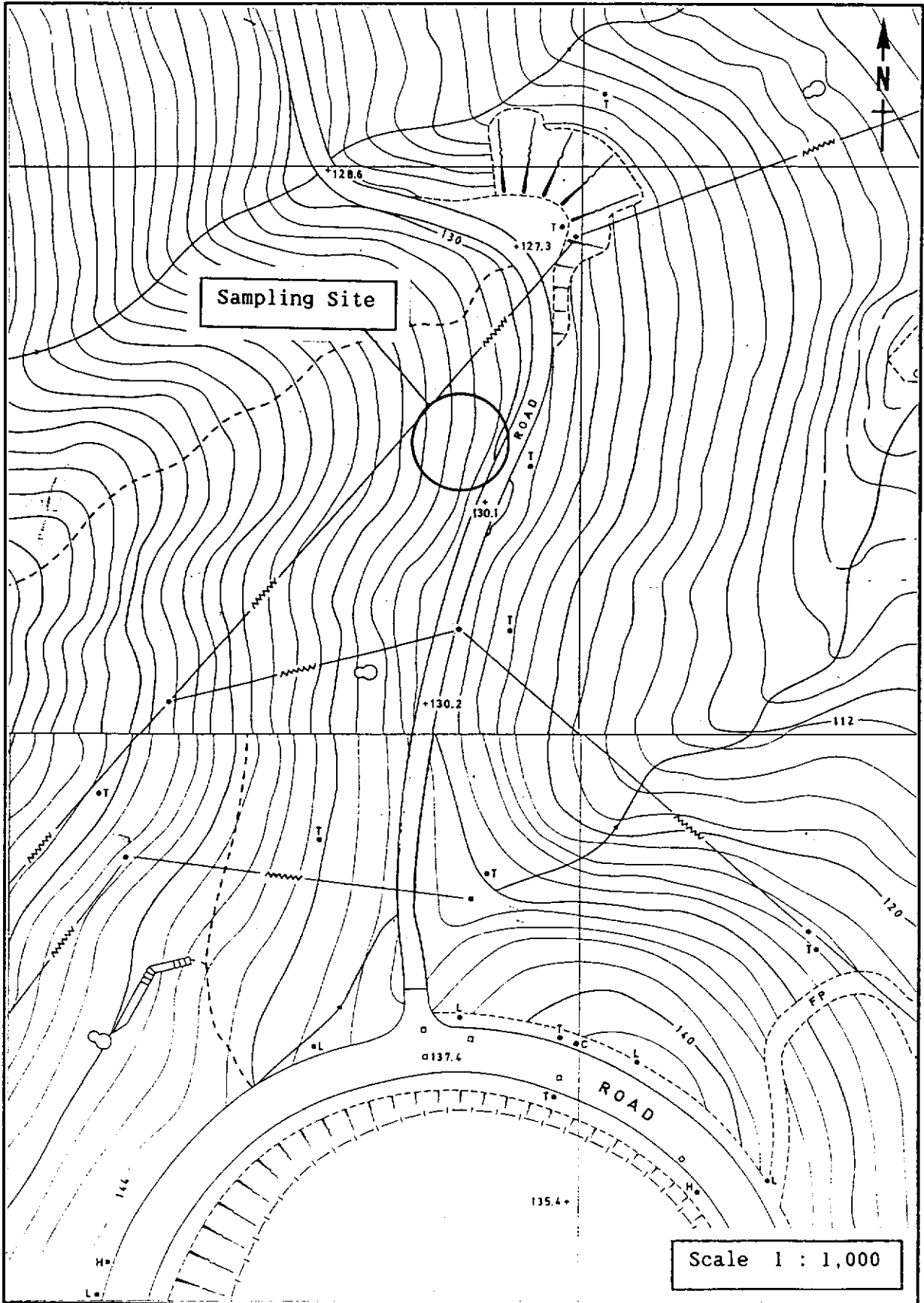


Figure A2 - Location Map 1 : 1 000 Scale

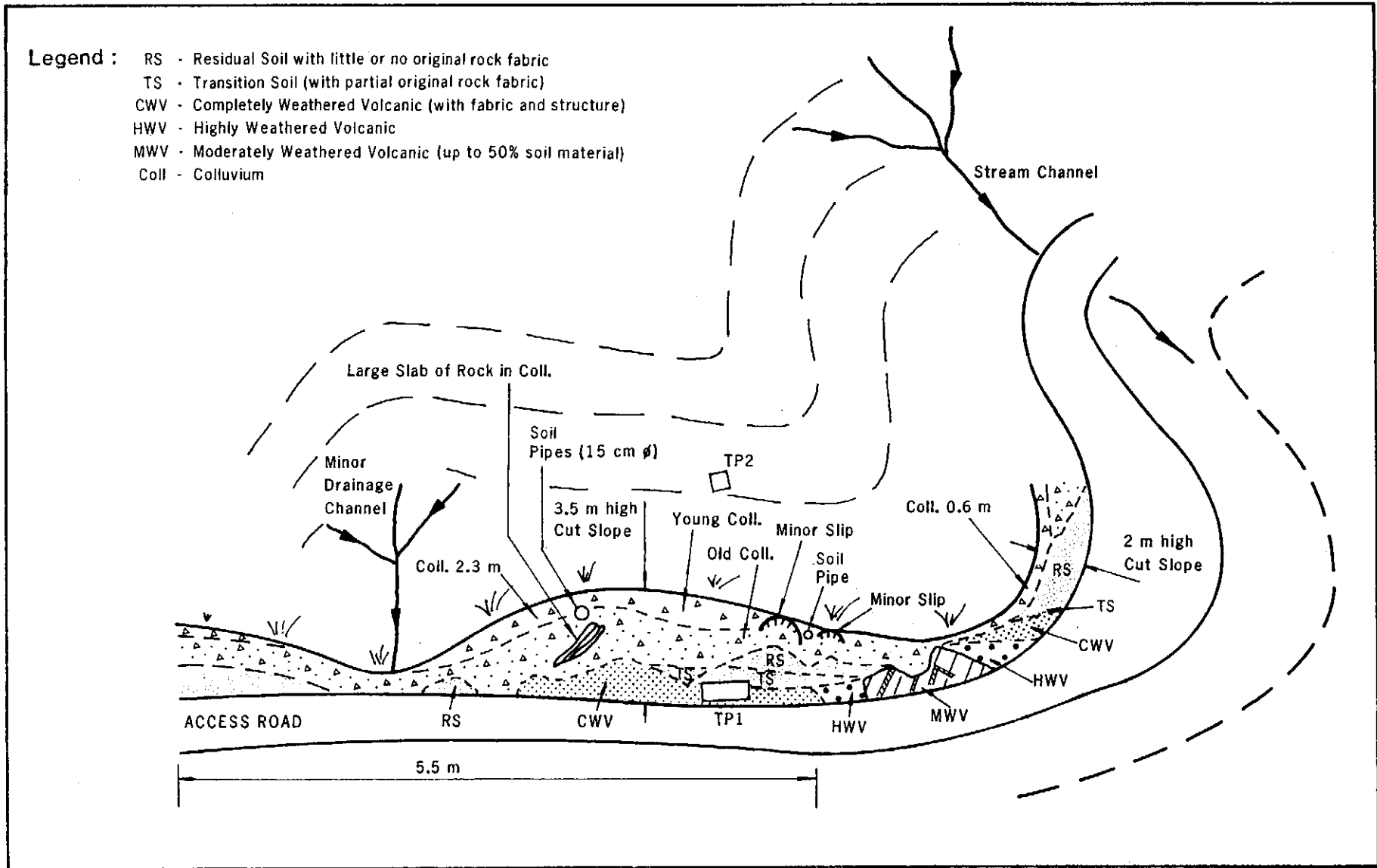


Figure A3 - A Sketch of Weathering Profile in the Immediate Vicinity of the Sampling Location

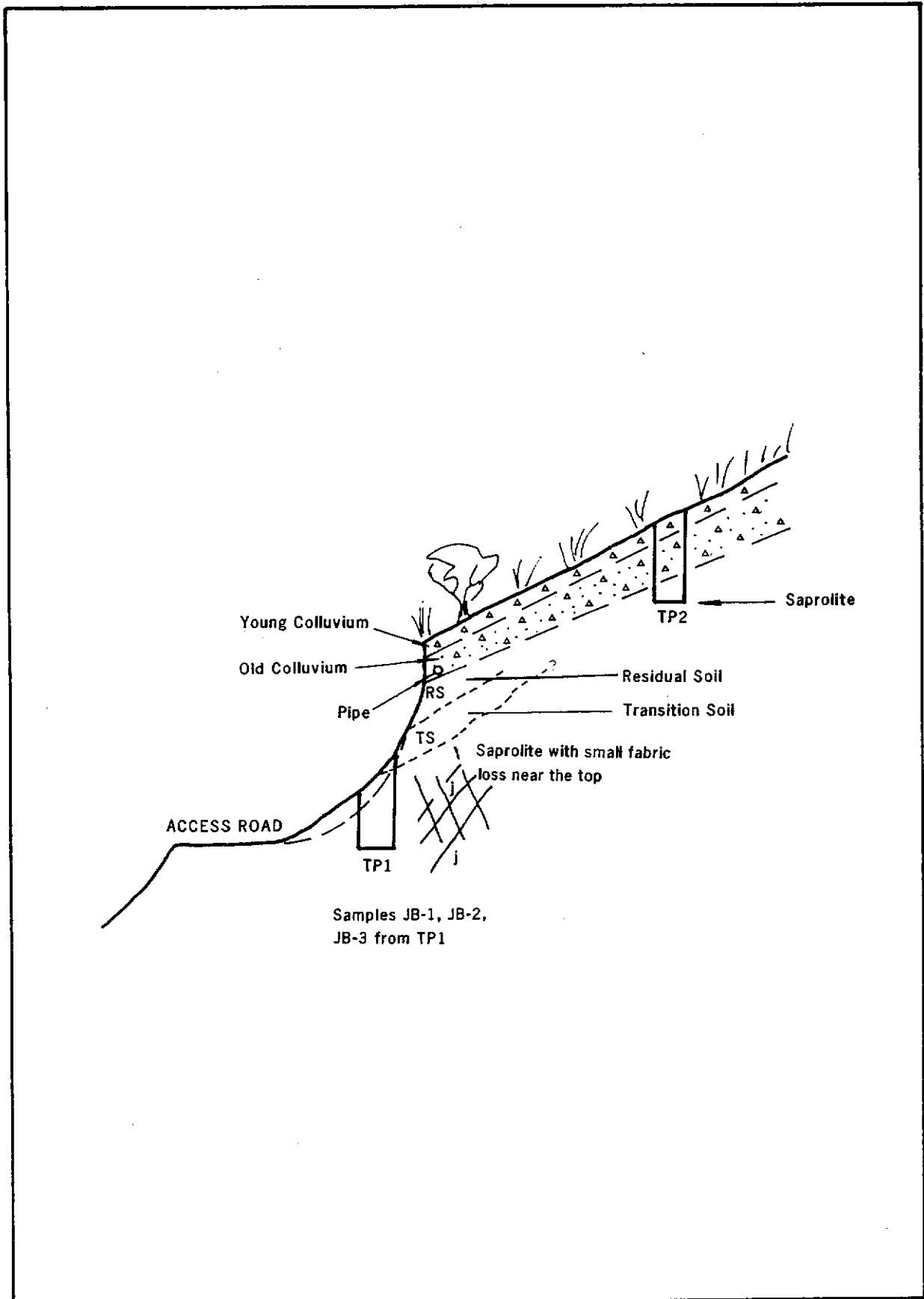


Figure A4 - Sketch Cross-section Across the Sampling Location

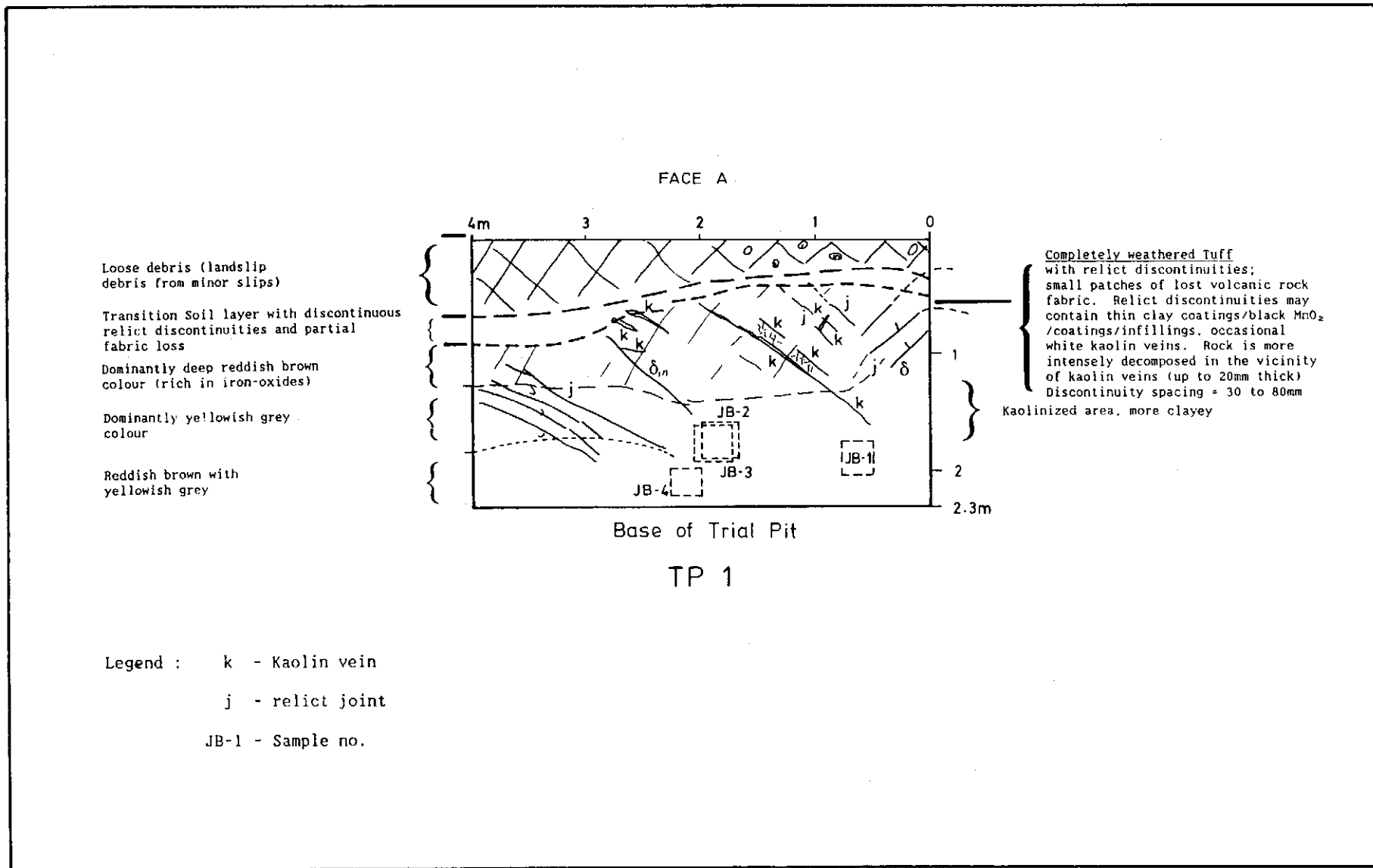


Figure A5 - A Simplified Log (Face A) of the Trial Pit TP1 and the Sample Locations

LIST OF PLATES

Plate No.		Page No.
A1	General View of the Sampling Site on the Mid-slopes of Tai Sheung Tok Hill	233
A2	The Sampling Site	234
A3	Rock Outcrops North of the Sampling Location	235
A4	The Trial Pit Location and the Weathering Profile	236
A5	Sampling Operation - Hand Trimming of Block Sample	237
A6	Sampling Operation - Hand Trimmed Sample before Covering by Aluminium Foil	237
A7	Sampling Operation - Sample Box in Place	238
A8	Sampling Operation - Polyurethane Covered Sample in Box	238
A9	Sample JB-1 and Faces A & D of the Trial Pit TP1	239
A10	Sample JB-2	239
A11	Sample JB-3	240
A12	Sample JB-3, Bottom of the Sample	240
A13	Sample JB-3, a Close-up of the Area of No Volcanic Fabric (Deep Reddish Brown Coloured)	241
A14	Sample JB-3, Face B	241



Plate A1 - General View of the Sampling Site on the Mid-slope of Tai Sheung Tok Hill



Plate A2 - The Sampling Site



Plate A3 - Rock Outcrop North of the Sampling Location



Plate A4 - The Trial Pit Location and the Weathering Profile



Plate A5 - Sampling Operation - Hand Trimming of Block Sample



Plate A6 - Sampling Operation - Hand Trimmed Sample Before Covering by Aluminium Foil



Plate A7 - Sampling Operation - Sample Box in Place



Plate A8 - Sampling Operation - Polyurethane Covered Sample in Box

Plate A9 -
Sample JB-1 and Faces A & D of
the Trial Pit TP1



Plate A10 - Sample JB-2



Plate A11 - Sample JB-3

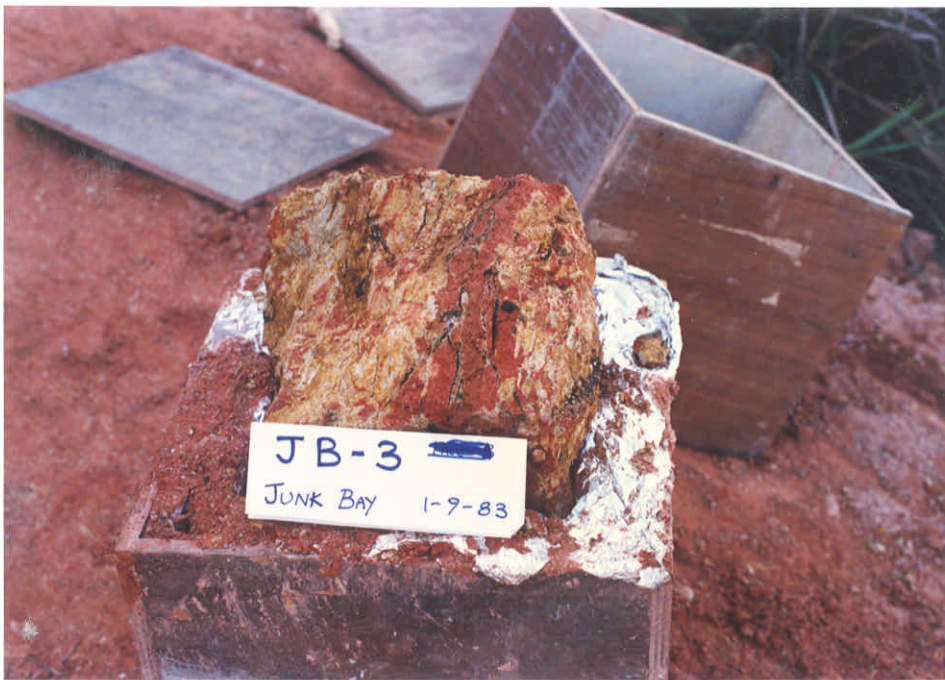


Plate A12 - Sample JB-3, Bottom of the Sample

Plate A13 -
Sample JB-3, A Close-up of the
Area of No Volcanic Fabric
(Deep Reddish Brown Coloured)



Plate A14 - Sample JB-3, Face B